INVESTIGATION OF TWO-PHASE FLOW BEHAVIOR AND PATTERNS IN HORIZONTAL AND VERTICAL PIPES

MOHAMAD ARDAN BIN ZUBIR

FACULTY OF ENGINEERING
UNIVERSITY OF MALAYA
KUALA LUMPUR

2015

INVESTIGATION OF TWO-PHASE FLOW BEHAVIOR AND PATTERNS IN HORIZONTAL AND VERTICAL PIPE

MOHAMAD ARDAN BIN ZUBIR

THESIS SUBMITTED IN FULFILMENT OF THE
REQUIREMENTS FOR THE DEGREE OF
MASTER OF ENGINEERING SCIENCE

FACULTY OF ENGINEERING
UNIVERSITY OF MALAYA
KUALA LUMPUR

2015

ABSTRACT

Two-phase flow takes place in a wide range of application in the industry. Basic research related to two-phase flow such as flow pattern and void fraction is very useful in contributing to design for optimized the system. This research analyzed the behavior and pattern of the two-phase air- water flow in the pipes. The relationships of the pipe diameter with the flow behavior and the aspect ratio, L/D of the pipe are examined. Three different pipes sizes of 21.0-mm, 47.0-mm and 95.0-mm inner diameters with length of 3 meter are used in this experiment. The flows are upward vertically positioned and horizontal which are supported by a steel frame and a close loop water system. The superficial velocities for the air and water flow are set between 0.02 to 2.0 m/s for air, and 0.02 to 3.0 m/s for water, depending on the size of the pipe. A high speed video camera is utilized to capture the flow patterns for different pipe orientations and flow velocities. All data were analyzed, tabulated and displayed in form of figures and graphs. The study continues by developing a measurement method to calculate the void fraction. A simple conductance probe device is designed using a ring shape sensor connected to the LABView data acquisition device. The result of the void fraction measurement in two-phase flow than compared with other related correlation. The diameter size and aspect ratio L/D of the pipes has significant impact on the flow patterns.

ABSTRAK

Aliran dua fasa melingkupi pelbagai penggunaan secara meluas di dalam industri. Penyelidikan asas berkaitan aliran dua fasa seperti corak aliran dan ruang kosong adalah sangat berguna di dalam merekabentuk yang menyumbang kepada mengoptimakan sistem. Penyelidikan ini telah mengkaji tentang sifat dan corak aliran dua fasa yang bergerak didalam paip. Perhubungan diameter paip dengan sifat aliran dan juga nisbah L/D paip juga dikaji. Tiga paip yang berlainan saiz iaitu diameter dalam 21.0-mm, 47.0-mm dan 95.0-mm dan 3 meter panjang setiap satu digunakan di dalam kajian ini. Arah aliran adalah aliran bergerak menegak keatas dan juga aliran melintang didalam paip yang disokong oleh struktur besi dan juga sistem aliran air tertutup. Kelajuan nyata bagi udara dan air diantara 0.02 hingga 2.0 m/s untuk udara dan 0.02 hingga 3.0 m/s bagi air bergantung kepada saiz paip. Kamera video berkelajuan tinggi digunakan untuk mengambil gambar corak aliran di dalam posisi dan kelajuan berlainan. Kesemua data kemudiannya dianalisis dan disusun untuk dibentangkan di dalam bentuk gambarrajah dan graf. Kajian diteruskan dengan membina kaedah pengukuran bagi mengira pecahan kosong. Alatan konduktor yang ringkas direka menggunakan sensor berbentuk cincin yang disambung kepada alatan pengumpulan data yang dijana menerusi perisian LabView. Hasil kajian pengukuran pecahan kosong dalam aliran dua fasa kemudiannya di bandingkan dengan persamaan lain ynag berkaitan. Diameter paip dan nisbah L\D memberi kesan kepada corak aliran bagi aliran dua fasa.

ACKNOWLEDGEMENT

First of all thanks to Allah for giving me good health and clear mind which enable me to complete the research project. With this opportunity, I would like to express my gratitude to my supervisor, Dr. Rahizar Ramli and also Dr. Zamri for their constant guidance. Greatly thanks to University Malaya and University Malaya staff for supporting my study and provide a grant for my research. Also special thanks to the people that helping me for this research especially a technician, Mohd Asri Ismail and related undergraduate students.

TABLE OF CONTENTS

APPENDICES

LIST OF FIGURES

LIST OF FIGURES

LIST OF FIGURES

LIST OF FIGURES

LIST OF TABLES

LIST OF TABLES

NOMENCLATURE

W_L	mass flow of liquid density
W_G	mass flow of gas density
ρ_L	liquid density, kg/m^3
ρ_G	gas density, kg/m^3
L	length, m
D	diameter, m
A	cross sectional area, m^2
A_L	cross sectional area occupied by liquid phase, m^2
A_G	cross sectional area occupied by gas phase, m^2
u_L	liquid mean velocity, m/s
u_G	gas mean velocity, m/s
α	void fraction
j	superficial velocity, m/s
j_L	water superficial velocity, m/s
j_G	air superficial velocity, m/s
V_L	liquid phase voltage, V
V_{LG}	gas-liquid phase voltage, V
Q	flow rate, m^3/s
Q_L	liquid flow rate, m^3/s
Q_G	gas flow rate, m^3/s
η	hold-up
RTP	electric resistance of two-phase flow
RG	electric resistance of gas phase

RL	electric resistance of liquid phase
I_0	constant current supplied
α	void fraction
V_L	liquid phase voltage drop, V
V_{TP}	gas-liquid phase voltage drop, V
L/D	ratio of length over diameter
CECM	constant electric current method
ID	inner diameter
α_{means}	actual void fraction
α_{pred}	prediction void fraction
ε	error
s	deviation

Chapter 1: Introduction

1.1 Background

Two-phase flow occurs in a wide range of applications in industrial plants, boilers and nuclear reactors. Some of other applications of a two-phase flow exist in cooling systems or in small space such as in electronic equipment. The fundamental information such as flow pattern, void fraction, phase distribution and pressure loss are all important parameters in designing a two-phase flow system. This research can contributed to reach the economic designs, optimization of operating conditions and assessment of safety factor. The outcome of two-phase flow studies can contribute to a lot of application especially in industrial plants, medical appliances and cooling system applications. For further research, the two-phase flow study can be applied in a boiling condition with the existence of heat into the flow.

The studies of the two-phase flow can be divided into two main systems, non-heated and heated systems. For a heated system, an example of this trend is shown by the history of the development of boilers and condensers for power-generating plant. In the nineteenth and early twentieth century these components designed on basis of empirical relationships derived from experience and the problems were mainly associated with materials, which set severe limits to their capabilities. Efficiency was not a predominating factor and the fuel consumptions were very high compared with modern figures (Butterworth and Hewitt, 1977).

In general, the need for information arises from three sources. First there is the need of designers for detailed information in order to optimize their designs of product which is competitive in today's market. This type of requirement leads to detailed

quantitative studies, for example, the heat transfer coefficient or two-phase pressure drop. A second requirement is the need of plant operators to decide on the optimum operating conditions or, in a less fortunate situation, require faults diagnosing which have already occurred owing to departure from the ideal condition. The solution to this type of problem may involve an experimental investigation of particular geometry or two-phase flow regime which has not previously studied. Finally, the safety of the plant operation needs to be considered and in some cases it is necessary to know the maximum safe operating limits with precision (Hlang et al, 1999).

1.2 Two Phase Flow and Flow Pattern

Multiphase flow is characterized by the existence of interfaces between many phases in the flowing system and discontinuities of associated properties between each phase. Multiphase flow is the term used when there is more than one phase of substance co-exists within the flow and as a result of interaction between each phase boundary. Gases, liquid and solid are the basic phases in the multiphase flow. The numbers of phase partner in the multiphase flow have been observed either all gas-liquid-solid interaction of flow or between two phases such as in gas-liquid, liquid-solid and gas-solid interaction. For the interaction that occurs just between two phases either gas-liquid, liquid-solid or gas-solid interaction, this type of interactions is usually called a two-phase flow. Two-phase flow is the most usual phenomenon occurs in our life which is in nature system or the system that is made by humans. In engineering applications, gas-liquid two-phase flow is the most frequent phenomenon encountered in many engineering equipments involving piping system.

Two phase flow is a term covering the interacting flows of two phases substance either gas-solid mixture, gas-liquid mixture, liquid-solid mixture, or two-immiscible-liquids mixture. In fluid mechanics where fluid in the form of the gas and liquid substance, two phase flow are studied in a phase of gas and liquid with interfacing between the those two phases. Gas-liquid two phase flows are commonly found in many places mostly in the industrial processes and engineering applications.

Most of engineering equipments such as boilers, condensers and cooling systems consist of pipelines for the circulation system which carries a two-phase flow. Those equipments rely on the efficiency of water and gas flow during the operating time. The performance for that operating system relies on the performance of the flowing system of the two-phase flow. For the transportation mechanism in chemical processes such as petroleum and coals separation process are also served by two-phase flow. Two-phase flow also occurs naturally in our everyday life for example pouring water from a bottle, the drinking gas bubble in glass and water flow at the car wind screen.

It is evident that the two-phase flow applications takes place in a wide range of engineering equipments. The fluctuated flow behavior and non-uniform flow patterns give numerous predictions of prevailing two-phase flow regimes causing problems in transportation of two-phase flow in the pipeline of many engineering equipments. For example, the ‘slug flow’ and ‘churn flow’ in chapter 2.2.1 is said to have large pressure fluctuations which can damage the equipments. It gives an influence in heat and mass transfer mechanism in the system. Hence it is important to begin the first stage of analyzing the two-phase flow with the study of flow regimes to better understand the flow behavior.

There is a possibility that certain types of two-phase flow patterns and behaviors affect the equipment and influence its performance and efficiency (Abdulmouti, 2014). Thus the design of the pipeline system of the equipment becomes a priority to overcome this issue. The design priority includes the measurement of safe length of flowing part, diameter of the pipeline system, the fluid characteristics and the fluid conditions. Safety assessment study is important in two-phase flow applications in order to avoid any failure to the system. A proper control system for the two-phase flow equipment such as controlling the flow velocity is required. The failure of the system to operate or perform effectively which is caused by extreme behavior of the two-phase flow may affect the system and become disastrous. It is possible to overcome these problems with the study of a wide range of flow conditions of both phases that is involved in a particular two-phase flow system. Hence, it is essential for engineers and machine operators to have sufficient knowledge regarding circumstances involving the two-phase flow.

Furthermore in the two-phase flow system, one of the main analyses that should be considered is the flow pattern or flow regime and the change of liquid film along the channel. The variations of the patterns are due to the subjective nature of flow conditions, such as pressure drop, droplet deposition and entrainment, and sometimes the effect from unexpected back flow during the flowing process. Many other definitions with a variety of names are given to some specific geometric of these flow patterns. The existence of different flow patterns and regimes in the gas-liquid two-phase flow is a normal phenomenon that occurs in a pipeline or tube containing the two-phase flow. The different patterns for the two-phase flow develop along the vertical tube from a bubbly flow to a slug flow as the concentration of the bubble is high and collision occurs between the disperse phase of the bubble. The churn flow regime is observed to be developed from the breakdown of liquid film from the slug flow when

the regime becomes unstable with the increase of the gas phase. Hence, a critical annular flow is when the gas phase concentrating at the centre of the pipe whiles the liquid flow on the pipe wall. Finally wispy annular flow is formed when the liquid flow rate is increased in the annular flow and developing more liquid droplet concentration in the gas core of annular flow (Butterworth and Hewitt, 1977).

The common practice to observe the two-phase flow data and classify the flow patterns is by visual observation and to plot the data as a two-dimensional flow-pattern map in terms of particular system parameters. Therefore, in order to accomplish a reliable design involving the two-phase gas-liquid flow systems such as pipe lines, evaporation and condensers, a prior knowledge of the flow-pattern is required.

In this research, the fundamental study of gas-liquid two-phase flow has been carried out by using the experiment set-up developed and observation method with guideline provided by literature study. Quantitative information such as flow rates of liquid and gas, phase superficial velocities, and the experiment results are tabulated with respective graph and the relation of these variables are analyzed.

1.3 Applications of Two-Phase Flow

Two-phase flow has various applications such as waves at sea to and blood flow in a blood vessel. Knowledge of two phase flow is very important for engineers in technical applications such as nuclear power plant, chemical industries, oil wells and pipelines. A study of two phase flow is essentially needed in the design and safety aspect of various components in industries. Therefore, it can be applied to increase its quality, increase the safety of the process, increase the efficiency of the productions and reduce the cost for the production and maintenance.

1.3.1 Industrial Application

The two-phase flow plays an important role and has a broad range of engineering applications in many industries. Power generation industries, oil and gas industries, and chemical processing industries are some of the examples involving the two-phase flow. In these industries, two-phase flow exists in their piping systems particularly in the refrigeration system, oil and gas mixture transport pipelines, steam generators, condensers, boilers, cooling towers and extraction and distillation processes.

There are two types of phase distribution which is the adiabatic systems, a system that has separate or mix phases flowing without any phase change occurs to the substance; and a diabatic system when phase changes occur. In the adiabatic systems, the phase mixing or phase separation process takes place without any heat transfer or phase change to the substance. The two-phase mixing substance stays separate with an interfacing between the phases. The examples of adiabatic system applications in pipeline are the systems that are used to transport the oil-gas mixtures, airlift pumps, and gas-pulverization of solid particles.

In other example, the conversion of heat energy transfer to the system is also involved during the operation. This type of process is a diabatic and it is enabled by the use of a working fluid. In this case, the heat is either being added to or being removed from the working fluid in two or more of the components and a phase-change occur during processes such as phase from liquid to gas or from gas to liquid. The examples of the two-phase flow in diabatic systems applications are such as boilers, steam generators, cooling tower and condenser in the power generation industries, air conditioning, evaporators and refrigeration systems.

Another case where two-phase flow is observed and critically involved is in cavitation. It is a common problem in pumping works, the pump is operating close to the vapor pressure and always happens where the pressure drops further inside the pump, normally locally near the vanes for the pump and phase change can occur from liquid to gas and present in the pump. A large pressure difference between the different phases will produce a big pressure impact to the vanes and produce cavitations. Similar effects can also occur on marine propellers. The detail designing of propellers need to take account of this problem. When the vapor bubble developed nearby the propeller and collapses, it can produce very large pressure spikes. The continuous pressure spike over time will cause damage on the propeller or turbine. Flows of this type must be well understood for the design of steam generators (steam-water flow), internal combustion engines, jet engines, condensers, cooling towers, extraction and distillation processes, refrigeration systems, and pipelines for transport of gas and oil mixtures.

1.3.2 Two Phase Flow in Power Plant

Two-phase flow has a massive engineering applications especially in the power generation, chemical, and oil industries. Historically, probably the most commonly study cases of two-phase flow are in large scale power system industries. Usually, coal or gas-fired power stations use very large boiler or steam generator to produce steam and then flowing into the turbine to generate electricity. In such cases, the water is pressurized using the high pressure circulating pump and transported via heated pipes inside the boiler, which then changes the water to steam. The design of boiler and its piping system require a detailed understanding of two-phase flow heat transfer, mass transfer and pressure drop behavior, which is significantly different from single-phase condition. In more critically conditions, nuclear reactor power system uses water to remove the heat from the reactor core and involves the two-phase flow system. A great

deal of study has been performed on the nature of two-phase flow in such cases, so that the estimation of the failure can be predicted and engineers can perform the “Design Against Failure” (DAF) in piping system that have a two-phase flow phenomenon such as, loss of pressure and loss-of-coolant accident (LOCA) as reported by Levy, 1999.

Some of the researches are related on the two-phase flow system that mostly involves in the steam generator system inside nuclear power industry. There are a few types of nuclear power plants in this world. The mostly used are a pressurized water reactor (PWR) and boiler water reactor (BWR) power plant. The difference of both PWR and BWR nuclear power plant are on the steam generating system. For both systems, there are involved a lot of piping system and therefore a lot of problems are involved to the two-phase flow activities inside the pipes. Implicitly, the study of two-phase flow gives a big impact in the nuclear power plant industries.

The knowledge of important information on the main components of a power plant unit, such as the reactor or turbine, briefly describe safety and essential auxiliary systems and a list of technical specifications of significant plant equipment give a big impact in running on the power plant. A detailed study on two-phase flow can be applied in many major parts in the power plant system from optimization of the output of the system to the most important work which is the safety operation.

1.3.3 Two-Phase Flow in Oil and Gas Pipeline Transport

In the oil and gas industries, pipelines function to transport various types of liquids, gasses and also some of solid particles. Therefore, multiphase and two-phase flow knowledge is vital in the oil and gas transporting piping system and during the oil and gas recovery process. In this case, the information and measurement data of multiphase flow and two-phase flow are really important in order to determine the

condition of the flowing fluid. Applying the flow-pattern dependent method study for gas-oil pipeline transport, one has to realize that it is limited to stationary flow. Some of the method need to ignore any development length needed for transport from one flow pattern to another and hence many assumptions need to be set in order to minimize the external effect in the analyses. Therefore, special care should be taken in designing short pipelines with strong undulations of which some wrong assumptions may lead to inaccuracies during the measurements and observations.

Gas void fraction (GVF) is a familiar term in the oil and gas industries and the wet gas measurement described as a subset of multiphase flow measurement. The liquid void fraction (LVF) is the proportional term to the GVF in the gas liquid two-phase flow. The gas void fraction measurement contributed an important parameter for the multiphase flow measurement also in the wet gas measurement. During the oil and gas transportation, the liquid fraction in these flow regimes may include oil, water, condensate and injected chemicals, possibly a hydrate inhibitor such as methanol gas. Some of the terms can be different and may give a different name depending on the industries or different places. In multiphase flow, where in some cases it is very difficult to predict when it involves the complex flow regime and they are dependent on many factors including fluid properties and topography of the flow. The transition regions are the regions exist on the transition state between these distinct regimes and they are difficult to be identified and classified.

It is therefore important to judge the type of flow in measurement of oil and gas industries. The correct data of the flow information will affect to the cost of the operation. The flow types and the quality of the flow through the meter need to be controlled to optimize the production and can be accurately managed operation. It is more critical it when involved the second of third parties during business when selling

or buying the oil and gas product through the pipelines. For example in the power generating industries buying the gas product from the oil company through pipelines, the flow of the gas need to be controlled using some specification before going through the metering system. The flow control knowledge such as minimum length of pipes, liquid pressure and temperature are really useful before measuring the volume of the flow (Dualstream II, Development of a new intelligent wet gas meter 1994-2000, Solartron ISA).

1.4 Problem Statement

Determination of the characteristic of liquid film in two-phase flow is important and useful in order to have a safe operation, increase performance and to save the operational cost for the equipment. The two-phase flow pattern and void fraction are difficult to measure in real industry application. The pipe that is used is a solid pipe, and not a transparent pipe. So, the actual type of flow pattern cannot be determined by a visual method. The flow pattern map gives an advantage to determine the flow pattern from the reading of gas and liquid superficial velocity.

The void fraction measurement using the special equipment like x-ray and tomography methods are quite expensive and not cost effective to measure in real times application. The new method such as the Constant Electric Current Method (CECM) gives an advantage to the industry to measure the real time void fraction reading with a low operational cost.

1.5 Objectives

The main purpose of this study is to investigate on the flow behavior and pattern of gas-liquid two-phase flow in pipe using an experimental approach. The more specific objectives are like the following:

1. To investigate the pattern of the two-phase air-water flow in a pipe and find the relationship between flow pattern and the velocity of the flow.
2. Find the relationship on the effect of aspect ratio L/D and diameter size of the pipes to the flow behavior.
3. To measure the void fraction in the two-phase flow in a pipe.

The contribution in this research centered on the determination of the flow behavior in pipes and helping in design the economic system and optimizing the operating condition. Meanwhile, the measurement using the Constant Electric Current Method (CECM), will introduce a new method to measure the void fraction.

1.6 Scope of Study

To achieve the objective of the study, the result output should be as below:

(i). A comprehensive analysis of the flow pattern in vertical and horizontal pipes with three pipes size of 21mm, 47mm and 95mm inner diameter, and using different air and water superficial velocity.

(ii). An analysis and observation on the effect of gas and water superficial velocity to the flow pattern.

(iii). An analysis on the effect of aspect ratio L/D of the pipe using a different pipe size with different air and water superficial velocities.

(iv). A comprehensive analysis to measure the void fraction using CECM method.

However, this research has a limitation on the experimentation equipment. The air and water supply have a maximum amount of supply that limits the supply of gas and liquid superficial velocity. The range of air superficial velocity is 0.05 m/s to 3.0 m/s and the range of water superficial velocity is 0.05 to 3.0 m/s.

Chapter 2: Literature Review

2.1 Fundamental of Two-Phase Flow

In fluid mechanics, two-phase flow is the phase that containing or the interacting flow between two phases either gas-solid, gas-liquid or liquid solid flow. The interface between the phases is influenced by the motion of the flow, (Butterworth and Hewit, 1977). Two-phase flow model refers to the way of examining the existing behavior and pattern of two-phase flow in certain condition. There are three ways the model of two-phase flow can be explored. They are laboratory experimental approach referring to industrial scales model equipped with suitable instrumentation, computational modeling method and theoretical calculation and correlation. Due to the complexity on analysis of two-phase flow, certain assumptions need to be made particularly to the boundary conditions. It will be easier to treat the two-phase flow as one-dimensional flow and learn the relationship continuity for single-phase and two-phase energy and momentum balances to analyze two-phase flow. The distribution of each phase respectively in the two-phase flow is really important to identify the characteristics of the flow. Basic information such as the two-phase flow void fraction, heat transfer, flow pattern, pressure loss and phase distribution are all related parameters in the study of two-phase flow.

Two-phase flow is commonly used in industrial plants, cooling system, and in some of the closed system. In real situation, there is no chance to observe a real mixture of two phase flow in a pipe. Although there are several methods to observe the flow in two-phase flow systems such as neutron beam, tomography and X-ray methods, the possibility of observing continuous flow is not cost efficient. Study relationships and correlations for two-phase flow will help to determine the flow characteristics of the

system. Thus, laboratory experiments can provide some valuable quantitative information of flow phenomena in two-phase system.

The contribution of the two-phase flow study is the requirement for optimization of operating conditions, economic designs and assessment of safety factors for the system. For the economic designs, related information and knowledge on two-phase flow is needed by designers to optimize the system or equipment design in the competitive market. Optimum operating conditions is the second contribution of the quantitative information from the study where the operators of the plant must decide and the requirements on related knowledge are needed to diagnose faults and to operate at maximum capacity. The solution to this type of problem may involve an experimental investigation of a particular geometry or two-phase flow regime which has not previously been studied, for example, the failure of boiler tubes due to flow stratification which may be corrected by flow changes. Moreover, the study of two-phase flow is necessary in the safety aspect, particularly in design and analysis. Knowing the maximum safe operating limits in plant operation is really important in order to balance the optimum operation condition and safety limit of the system. For example, in some critical condition such as nuclear reactors, the maximum heat absorbed from the fuel bundle must be carefully calculated and knowledge on the full range of operating conditions are required in order that the safety margins may be allowed (Shires, 1977).

One of the fundamental studies of gas-liquid two phase flow was reported in experimental study by Ide et al. (2006). This study concentrates on the characteristic of an air-water isothermal two-phase flow in mini channels. The experiment used the capillary tubes with inner diameter of 1 mm, 2.4 mm and 4.9 mm, also in capillary

rectangular channels with an aspect ratio of 1 to 9. The directions of flow were vertical upward, horizontal and vertical downward. The studies were based on the experience of fundamental research into the gas-liquid two-phase flows in circular tubes, the time varying holdup and the pressure loss. The effects of the tube diameter and aspect ratios of the channels on these flow parameters and the flow patterns were investigated. The correlations of the holdup and the frictional pressure drop were proposed.

The characteristics and phase distribution patterns of two-phase flow in vertical large diameter pipe have been experimentally and theoretically studied for various flow conditions by Shen et al. in 2005. The value of interfacial parameters such void fraction, Sauter mean diameter and pressure loss have been measured by using the optical probes and differential pressure transducer in a vertical upward air-water two-phase flow in a pipe with 0.2 m in inner diameter and 2.4 m in height. From the experiment, the phase distribution of flow pattern is divided into two basic patterns, called wall peak and core peak. By using the skewness concept, the two-phase-phase pattern have been quantitatively distinguished by comparisons of establishing of phase distribution pattern transition criterion and the empirical relation of transition from wall peak to core peak have been determined. The flow plugging phenomena in the low region of the test section at high superficial gas velocity conditions also has been studied in the vertical large diameter pipe.

2.2 Flow Pattern

The characteristic of two-phase flow is depends on the interface exist between two phase in gas-liquid flows and the interface have variety forms. The two-phase flow can be simplified by classifying by the types of interfacial distribution that called the flow regime or flow pattern. There are various forms of flow patterns in gas-liquid two-

phase flow in pipes. In vertical pipes, the common names of pattern including slug flow, bubbly flow, wispy annular flow, annular flow and churn flow; also intermediate flow patterns are frequently be faced. The horizontal flow have specific names such as stratified flow, bubbly flow, wavy flow, plug flow, slug flow and annular flow. The fundamental knowledge of flow pattern and flow transition are important to develop the numerical simulation of two-phase flow. The two-phase flows also involved the transfer of mass, energy and momentum between phases which are related to the velocity, viscosity and some others parameter such as temperature and pressure. The experimental studies can be performed to identify the flow pattern or flow regime.

The determination of flow pattern is essential in order to predict the characteristic of the flow, where it may contribute information to solve problems that occur in the two-phase flow system. Many factors must be taken into account in the two-phase flow system including the mass flow rate, type and size of channels, flow direction, phase properties and gravity factors. These factors influence the characteristic of the flow that give direct impact to the two-phase flow system. In this study, there are two flow conditions that are discussed and investigated experimentally where they are the vertical upward flow and horizontal flow in circular pipes, with different size of diameters.

Kim et al. (2001) set out a study on the void fraction, flow pattern and slug rising velocity, and a counter-current two-phase flow in a vertical round tube with wire coil inserts in through experimental studies. In this experiment, the flow pattern and slug rising velocity determined visually using a video camera. The void fraction is measured by a quick-closing valve method. Four kinds of coils with different pitches and diameter were used as insert on in order to produce induced disturbance into gas

liquid flows to enable the comparison of shape and motions of bubbles with those observed in a smooth tube without insert on the wire coil. From the result, the bubbly flow occurs in the low gas superficial velocity region in the wire-coil inserted tube, while the slug or churn/annular flow only appear in the smooth tube without insertion. Slug rise velocity in the wire-coil inserted tube is higher than that in the smooth tube. Experiments also showed that the modified mean flow velocity measured with core area, the slug rise velocity of the wire-coil tube insertion was agreed with Nicklin's correlation. At high gas superficial velocity, the void fraction in a wire-coil inserted tube was found to be lower than that in a smooth tube.

Taitel and Dukler (1976) produced a models to determine the flow regime transitions in two-phase gas-liquid flow. The flow patterns data is plotted in two-dimensional graph to locate the boundaries transition of two-phase gas liquid flow (Figure 2.1). The transition mechanism is fully based on physical concepts and predictive in that no flow regime transition used.

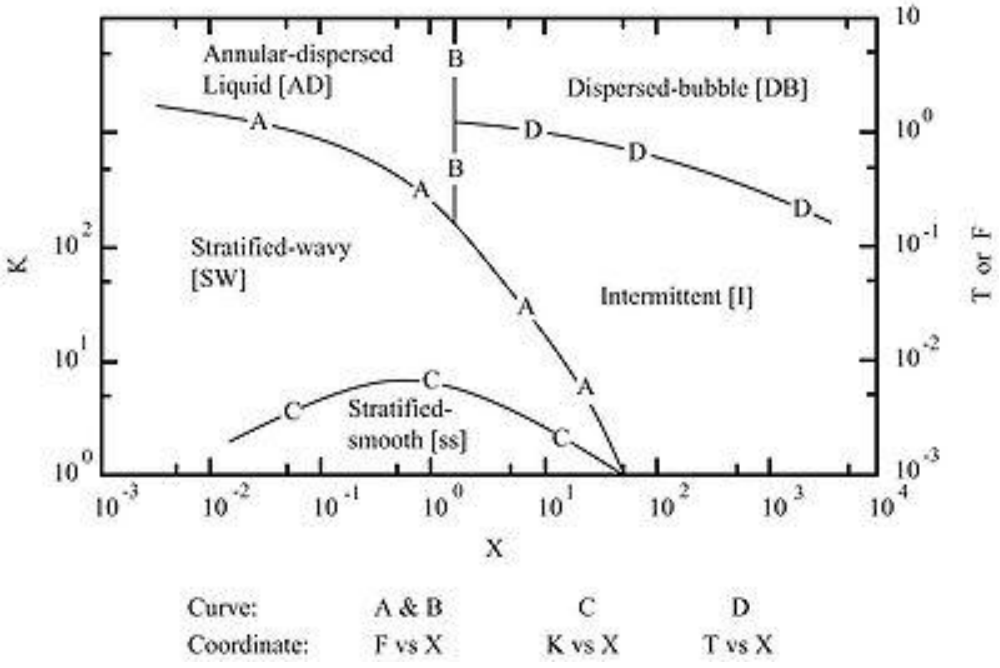

Figure 2.1: Flow mapping of horizontal flow patterns (Taitel and Dukler, 1996).

Ohnuki and Akimoto (2000) doing a research on the dependency of gas-liquid two-phase flow in a pipe scale. Experimental results show the transition characteristic of phase distribution and flow patterns in upward air-water two-phase flow along a large vertical pipe with an inner diameter of 0.2 m and the length of pipe diameter ratio, L/D 61/5. The study was conducted under air superficial velocities, varies from 0.03 m/s to 4.7 m/s and water superficial velocity varies from 0.06 m/s to 1.06 m/s. The axial differential pressure, phase distribution, bubble size and bubble and water velocity were measured while the flow pattern were observed. From the observation, there was no large bubble occur for the L/D ratio less than 20 but the small bubbles coalesce as same as in small scale pipe. The large bubbles only occur at L/D ratio above 20. The churn flow was dominant at large vertical pipe. Meanwhile, for small scale pipe with same condition, the pipe was dominated by the slug flow. The result showed that:

1. At low superficial velocity, small pipe have a wall-peak phase distribution. The core peak phase distribution occurs when some large eddied including bubble clusters fill up the pipe.
2. In large pipe, the large coalescent bubbles are flowed through the test section in form of churn bubbly flow and the type of phase distribution is a core peak. In small scale pipe, the Taylor bubbles or small bubble were flowing in form of gas-liquid mixtures region and the type of phase distribution is wall-peak.
3. In large vertical pipe, the size of wall-peak is lower even through the flow has the same bubble sizes. The radial velocity gradient of water and large turbulence dispersion force are the cause for the lower peak inside the test section Ohnuki and Akimoto, (2000).

2.2.1 Types of Flow Patterns in Vertical Pipes

The identifications of these flow pattern or regimes are required because of their significant influence on the characteristics of the flow. The flow patterns give a big impact on some behavior of the flow such as heat transfer conditions and pressure fluctuation. The classification of flow patterns types is useful but sometimes it becomes very subjective to define. A variety of names have been given by researchers but a suitable definition needs to be chosen for their relative generality of acceptance. Hewitt, (1979) have defined various flow pattern or regimes for co-current vertical upward flow of gas-liquid in a vertical pipe as follows:

a) Bubble flow

The gas phase is dispersed uniformly in the form of discrete bubbles in the continuous liquid phase inside the pipe. The size of the bubbles may vary in size and shape but they are mostly nearly spherical shapes and their diameters are much smaller than the diameter of the pipe itself.

b) Bubbly-Slug Flow

This is the pattern where there are non-uniform distributions of the concentration of small bubbles in the flow direction inside the pipe and a number of small bubble increase inside the flow. The small bubbles then coalesce with each other and occur in the part of high bubble concentration forming a spherically capped bubble.

c) Slug Flow

When increasing the gas flow, the proximity of the bubbles is very close and the percentage of the bubbles to collide and coalesce is really high. The bubbles will form a larger bubble, which the bubble diameter is similar to the pipe diameter. The bubble

shape is similar to a bullet with hemispherical nose with a blunt tail end. This type of bubble has their own characteristics and known as Taylor bubbles. Taylor bubbles is a type of gas-liquid flow pattern that consists of elongated bubbles, separated by liquid slugs and may contain small bubbles. It is surrounded by a thin liquid film that separated the bubble and the pipe wall. The direction of Taylor bubble may flow downward because of gravity, even though the net flow of fluid is upward.

d) Churn Flow

The structure of the flow becomes unstable when the velocity of the flow is further increased. The liquid motion is moving oscillatory up and down but still in an upward flow. The Taylor bubble become unstable flow regime as a result of the relative parity of the gravity and shear forces acting in opposing directions on the thin liquid film of liquid. The continuity of the liquid slug flow is dramatically destroyed. This characteristic of flow pattern is the intermediate regime between the slug flow and annular flow regimes. The churn flow in some cases may not develop at all for example in a small diameter tubes. The flow just passes directly from slug flow to annular flow regime. In some situations, churn flow need to be avoided in two-phase flow piping system. The mass of the slugs may destruct on the piping system such as those from a reboiler back to a distillation column or in refrigerant piping networks.

e) Annular Flow

Annular flow is where there is a gas flowing at the core of the pipe, while the liquid film flowing on the wall of the pipe. Once the interfacial shear of the high velocity gas on the liquid film becomes dominant over gravity force, the liquid is expelled from the center of the pipe and flows as a thin film on the wall and forming an annular ring of liquid, while the gas flows as a continuous phase up the center of the

pipe. A high frequency of waves and ripples disturbed the flow at the interfacial of gas core and liquid film inside the pipe. A small droplet of liquid may entrained at the gas core and may increase when increasing the flow rate. This type of flow regime is particularly stable mostly is a desired flow pattern for two-phase flows in pipe.

f) Wispy Annular Flow

The liquid droplet concentration in the gas core of annular flow will increase as the increasing liquid flow rate from the annular. The wispy condition will appear at the gas core when droplet coalesced with each other. This flow pattern and characteristic just happen at high mass velocity of two-phase flow.

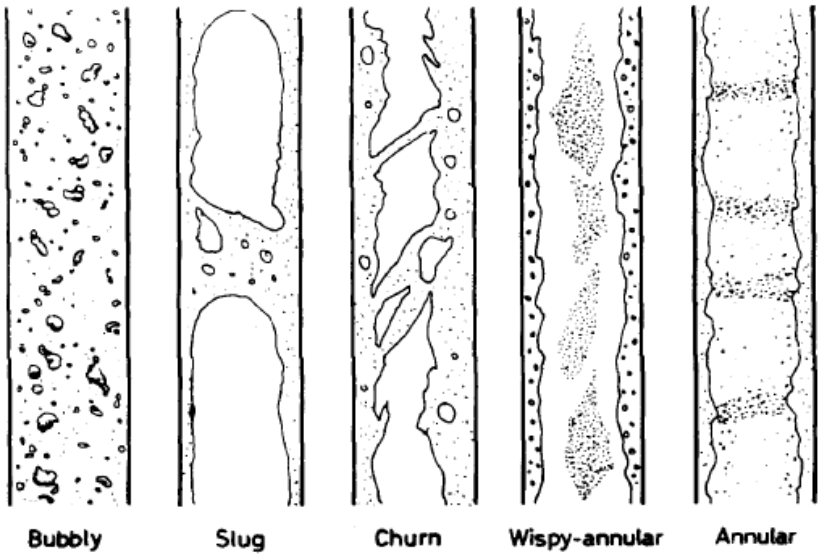

Figure 2.2: Vertical gas-liquid two-phase flow pattern (Collier and Thome, 1996).

2.2.2 Types of Flow Pattern in Horizontal Pipes

The flow patterns of two phase flow in horizontal flows are a bit similar to the flow pattern for the vertical upward flows as discussed in the previous section. The differences between the horizontal flows and vertical upward flows are affected by the gravity. The buoyancy gives a difference effect between the horizontal and vertical upward flow. In this case, the flow pattern will have a separation line between the gas and liquid flow where the liquid will flow to the bottom part of the pipe and the gas will flow to the upper part of the pipe due to the their buoyancy. The flow pattern for two-phase flow of gas and liquid in a horizontal pipe is shown in figure 2.3 and categorized by (Wolverine Tube, Inc., 2007) as follows:

a) Bubbly flow

The bubbly flows are clarified when the bubbles of gas dispersed and flow through the liquid with high concentration of bubble normally at high liquid velocity. After a certain length in the pipe, the bubble will move to the upper half caused by buoyancy effect. The shear force will make the bubble tent to disperse uniformly inside the pipe

b) Stratified flow

Stratified flows are clarified when the liquid and gas have a complete separation of their phase. This pattern happens at low gas and liquid velocity. The gas will flow at the upper part of the pipe while the liquid will flow at the bottom part of the pipe and have an undisturbed horizontal interface. At low liquid and gas velocities, complete separation of the two phases occurs. Hence the liquid and gas are fully stratified in this regime.

c) Stratified-wavy flow

Stratified-wavy flows happen when the gas velocity increases in the stratified flow. The waves are formed on the interface between gas and liquid flow in the direction of the flow. The wave amplitude depends on the velocity of the flow and the maximum amplitude will not reach the top part of the pipe. The thin liquid films will leave the pipe wall after wave flow through the pipe.

d) Intermittent flow

When the interfacial wave's amplitude become larger enough and reaches the top of the pipe, the flow regime will change either a slug flow or a plug flow. The pattern normally occurs when further increasing of the gas velocity. The large amplitude waves will wash up the top of the pipe with some smaller wave between that. Large amplitude waves contain entrained bubbles. The top wall is nearly continuously wetted by the large amplitude waves and the thin liquid film left behind. Intermittent flow is also a composite of the plug and slug flow regimes. These subcategories are characterized as plug and slug flow.

e) Plug flow

The plug flow sometime called an elongated gas bubble flow where the length of the bubble is much longer then a normal bubble. It moves at the upper part of the pipe meanwhile the liquid phase is continuous flow along the bottom of the pipe. The diameter of the elongated bubble is smaller compared to the diameter to the pipe. Between the elongated bubbles are separated by liquid plugs. Sometimes the plug flow is called the elongated bubble flow.

f) Slug flow

Slug flow is a continuous pattern from the plug flow when increasing the gas velocities. When the waves in wavy or plug flow grow big enough to touch the upper parts of the pipe, then the slug flow pattern is entered. The diameters in the elongated bubbles become larger and finally have the same diameter as the pipe diameter. Sometimes the slug flow can also be described as a large amplitude wave flow. The elongated bubbles are separates by a liquid slug flow.

g) Annular flow

Annular flow occurs at a very high gas flow velocity. Even with further increasing of gas flow rates, the liquid forms a continuous annular film around the parameter of the pipe. Similar with the vertical flow, the liquid films are formed around the pipe with the thickness of the liquid film thicker at the bottom than the top. There are small amplitude waves flowing on the interface between liquid and gas core inside the pipe. Some of the liquid droplet may disperse in the gas core inside the flow.

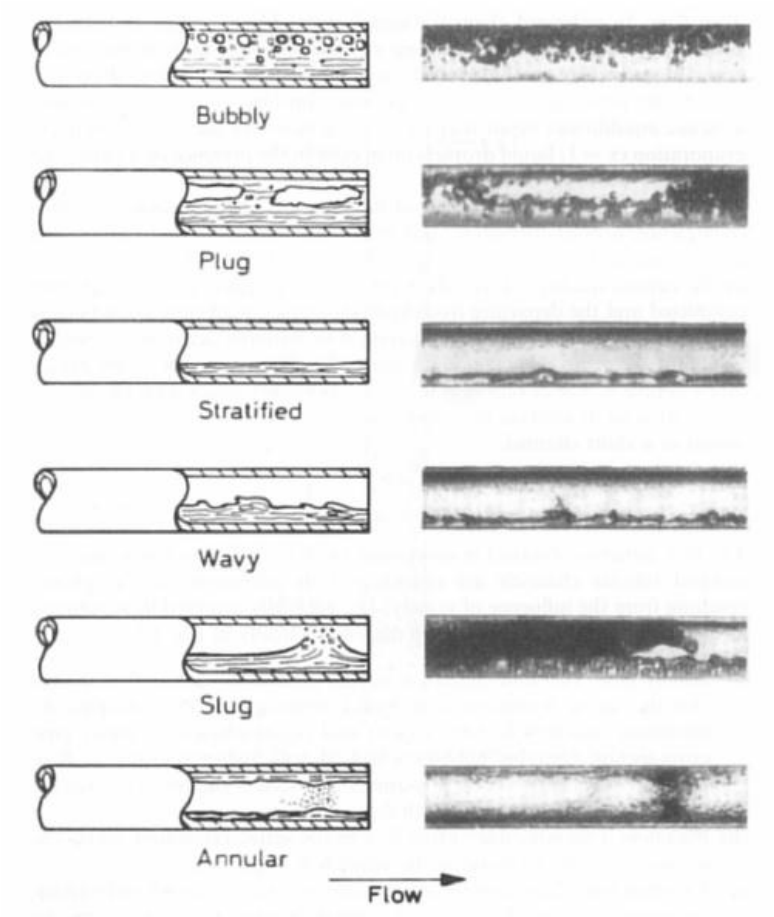

Figure 2.3: Horizontal gas-liquid two-phase flow pattern (Collier and Thome, 1996).

2.2.3 Flow Pattern Transition

The flow pattern transition is the phenomena which is the transition from one pattern to other pattern. The example of the transition of the flow pattern is from the change of slug to churn flow in vertical upward flow or from the plug to slug flow in the horizontal flow.

The flow pattern transitions are related to a few factors such as the pipe size, flow velocity, length of the pipe and the flow condition such as temperature and pressure. The external factor such as vibration can affect the pattern of the flow as well.

2.3 Void Fraction

Void fraction experiment is an experiment to measure the ratio of the gas phase (the voids) volume in the tube or pipe to the total volume of the pipe. Consider an adiabatic case; a mass flow W_L of liquid density ρ_L and a mass flow W_G of gas density ρ_G are flowing upwards in a vertical pipe or in the horizontal flow of length L with diameter D and cross sectional area A. Then by assuming that equilibrium has been achieved and that the liquid mean velocity u_L and the gas mean velocity u_G including the cross sectional area occupied by the liquid A_L and the gas A_G remain constant, the void fraction can be defined by the following figures and equations (Butterworth and Hewitt, 1977).

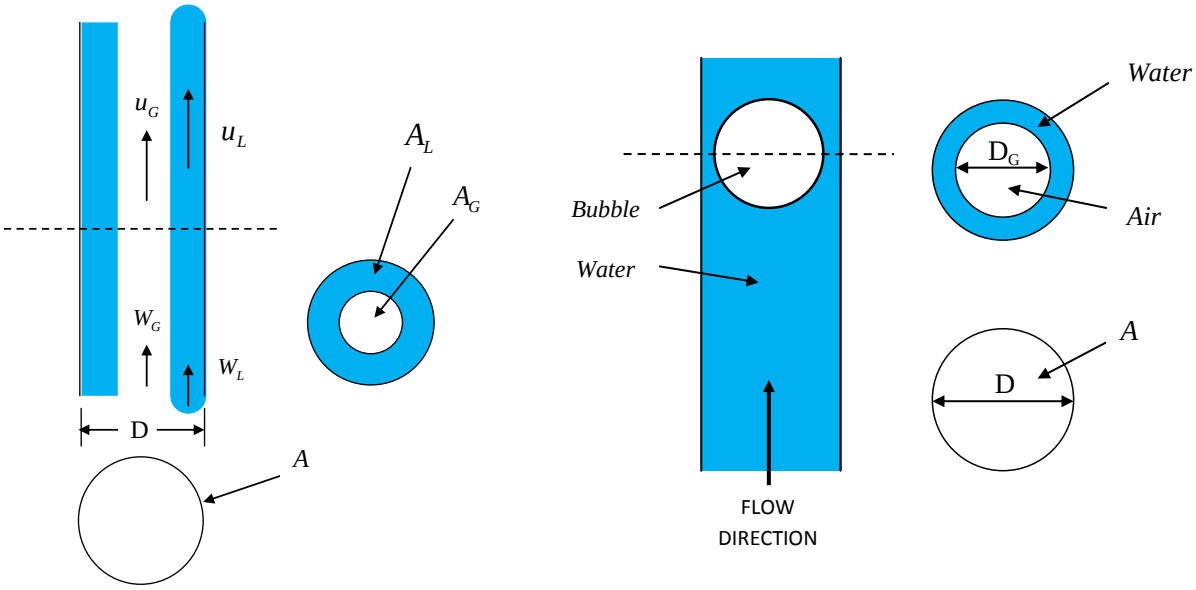

Figure 2.4: Fundamental of void fraction measurement

$$\alpha = \frac{A_G}{A} = \frac{1}{\left\{1 + \frac{W_L}{W_G}\frac{\rho_G}{\rho_L}\frac{u_G}{u_L}\right\}} \tag{2.1}$$

or simply,

$$\alpha = \frac{A_G}{A} = \left(\frac{D_G}{D}\right)^2 \tag{2.2}$$

2.3.1 Measurement Techniques of Void Fraction

Visual Observation

There are several techniques that have been developed and used to observe the flow patterns. The common and simple methods to get the information of flow pattern by using the visual observation or techniques of the flow. Taylor and Hewitt (1970) used the visual observation technique to observe the flow pattern inside the tube. A high-speed photography technique is required in order to visualize the high velocity flows. The major disadvantages of the visual observation technique is that as the light passes through the flow it was subjected to a complex series of refractions, thus the produced images are often confusing, making it difficult to interpret the flow pattern information. For the photo visualization technique, a high technology camera that has high shutter speeds required. Meanwhile, for video visualization technique, a high frame rate video capture is essential. A good lighting system is vital during the visual observation to capture high quality pictures or videos.

X-radiography

X-radiography technique has been developed in order to overcome the refractions issue in visual observation. X-ray images can offer more useful information on the nature of the flow. The images produced from the x-radiography depend only on absorption and more information on the flow characteristic can be acquired from the images. It was developed by Jones and Zuber (1975). The X-ray beam passed through the flow and the intensity result is determined by the detector. The output signal as a function of time is measured from the instantaneous void fraction and the probability density is used as a function for void fraction determination.

A flow visualization based on X-ray imaging was developed by Heindel et al., (2007). The experiment is to study, characterize and measure various flow characteristic in large vertical systems that have internal diameter of up to 32 cm and are as tall as 4m. The X-ray radiography and stereography imaging was provided by the facility to visualize and time-resolve 3D flow structure in multiphase and opaque fluid flows at up to 60 frames per second. The film radiography in their work are digitalized using a digital detector that uses direct electronic capture of the X-ray intensity.

Neutron Radiography (NR)

Neutron radiography (NR) technique is another method to measure and visualize the two-phase flow and void fraction. Mishima (1997) have measured the void fraction using neutron radiography and image processing technique. The test ran at high frame-rate NR with a steady thermal neutron beam and used the latest technology for neutron source, scintillator, high-speed video and image intensifier. Long recording time, high-frame-rate imaging and unnecessary triggering signal system were used. The recording speeds were at 250, 500 and 1000 frames per second, visualizing an air-water two-phase flow in a metallic pipe. The beam was attenuated in proportion to the water layer thickness along its path and the neutron beam projects the image of two-phase flow after the neutron beam penetrated the two-phase flow in the test section. The neutron beam delivered the image of two-phase flow and then changed into an optical image by the scintillator. Better image was produced by using the image intensifier from the luminous intensity of the optical image and then magnified using a telephotographic lens. Those images were captured again using a high-speed video camera and the quality was improved by using an image processing system.

Conductance Probes

Other common method to measure the void fraction is by using the resistance probes. These types of measurement method were used by Delhaye and Chevrier (1966), Malnes (1966) and Serizawa (1974). The tube wall is connected to the full insulated needle probe except its tip through the fluid. The conductance between the needle probe and the wall varies depending on the phase of the flow which is either in gas phase or liquid phase.

The conductance probes technique was also developed and used by Fiori et al. (1967), to characterize the flow pattern. The flow pattern characteristic is then obtained by displaying the response captured from the flow on the oscilloscope. This method has some disadvantages and does not provide accurate information as the contacts between the needle probe and the flow can occur in all flow patterns and therefore very difficult to determine the type of the pattern.

Another conductance method void fraction measurement was done by Fossa (1998), which used a ring-shaped and plate electrodes for measuring the conductance of gas-liquid mixtures in pipes. The device set up consists of electrode pairs placed on the internal wall of a cylindrical test duct, flush to the pipe surface. A.C. carried voltage with 20 kHz frequency was supplied across each pair of electrodes and then converted to D.C signal to get the liquid fraction values.

Electrical Resistance Tomography (ERT)

The Electrical Resistance Tomography (ERT) is one of the advanced methods nowadays that are used in monitoring the flow pattern. The ERT not only can produce the conductivity images, but also being able to measure some flow parameter. Yixin et

al. (2000) have done a research in applying the Electrical Resistance Tomography system to monitor the gas liquid two-phase flow in horizontal pipes. Sixteen titanium electrodes were flush-mounted on the inner sensor wall with equal space. The electrode is used to inject current into the sensing field and also to transfer the responded potential. The voltage data was collected using the data acquisition system.

Electrical Capacitance Tomography (ECT)

The other method that quite similar to ERT is the Electrical Capacitance Tomography (ECT). The ECT is a technique for obtaining information about the distribution of difference phase component of two-phase flow of closed pipes by measuring variations in the dielectric properties of the material. The usual information obtainable includes the measurement of the void fraction and velocities for two-phase flow and the cross-sectional images of the pipe. A basic Electrical Capacitance Tomography system are consist of a capacitance measuring unit, a capacitance sensor and a control computer. Rząsa, (2008) was done the measurement method of horizontal two-phase flow experimental using the optical and capacitance tomography. Five projections were used at the tested object for optical tomography system. Meanwhile the luminous intensity measurement changed into discrete signal (0 or 1) by using the optical sensors.

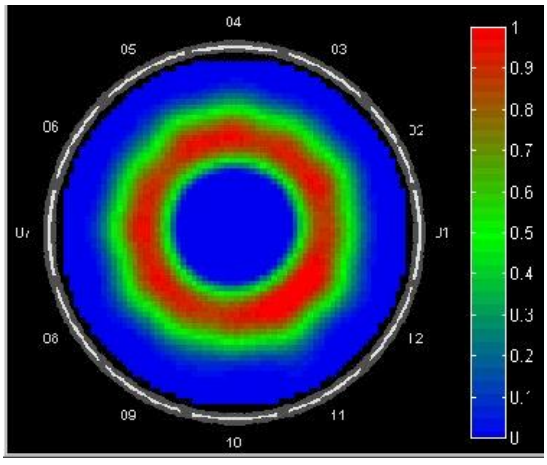

Figure 2.5: The example of Electrical Capacitance Tomography (ECT)

Fiber Optic Reflectometer (FOR)

Ho-Joon et al. (2008) has developed the fiber optic reflectometer (FOR) technique to observe and measure the bubble velocity, void fraction and the bubble diameter in the multiphase flow system. The study investigated the feasibility of the technique using the single fiber probe. The bubble surface determined the interface from the scattered signal with the Fresnel reflection signal from the tip of the optical fiber. The information obtained from the reflected signal before the fiber tip touches the bubble surface. The reflected signal from both the front and rear end of the bubble gives information on the velocity of the bubble. The bubble diameter can be determined by analyzing signal of the bubble from the velocity information whether the bubble is spherical or have minor axes if the bubbles are in ellipsoidal shape. The Ho-Joon Et al. (2008) is a good method to measure the void fraction, however this study is focused on a bubble flow pattern in the pipe.

All of the measuring techniques are good to measure a void fraction. However, all the measuring techniques have a limitations and weaknesses in measuring the void fraction. The common resistance probes method used by Delhaye and Chevrier (1966), Malnes (1966) and Serizawa (1974) is a simple method to measure the void fraction. This technique is easy to setup and not expensive. This resistance probes method has a potential to improve in measuring method to make it perfect. The Electrical Resistance Tomography (ERT) by Yixin et al. (2000) and Electrical Capacitance Tomography (ECT) by Rząsa, (2008) shows a good measuring technique to measure the void fraction. This technique required a complicated setup and expensive to use in a real application. The Ho-Joon Et al. (2008) is a good method to measure the void fraction, however in his study is only focused on a bubble flow.

2.3.2 Homogeneous Flow Model

In a one-dimensional flow assumption, void fraction α is defined as the fraction of flow area occupied by the gas phase:

$$\alpha = \frac{A_G}{A} \tag{2.3a}$$

$$1-\alpha = \frac{A_L}{A} \tag{2.3b}$$

The position of the two phases is not a concern in this model. The gas flow rate W_G is given by:

$$W_G = Wx = \rho_G u_G \alpha A \tag{2.4}$$

Similarly, for the liquid phase:

$$W_L = W(1-x) = \rho_L u_L (1-\alpha) A \tag{2.5}$$

Slip ratio, K is defined as the ratio of the gas velocity to liquid velocity. It is normally greater than unity which means u_G is usually greater than u_L.

$$K = \frac{u_G}{u_L} = \left(\frac{x}{1-x}\right)\left(\frac{1-\alpha}{\alpha}\right)\frac{\rho_L}{\rho_G} \tag{2.6}$$

From the equation (2.4), the void fraction can be determined as follows:

$$\alpha = \frac{1}{\left\{1 + K\left(\frac{1-x}{x}\right)\frac{\rho_G}{\rho_L}\right\}} \tag{2.7}$$

Suppose that there is no slip between the phases, K=1, equation (2.7) becomes:

$$\alpha = \frac{1}{\left\{1 + \left(\frac{1-x}{x}\right)\frac{\rho_G}{\rho_L}\right\}} \tag{2.8}$$

Now, the volumetric quality β is the volumetric flow of gas divided by the total volumetric flow, i.e.

$$\beta = \frac{Q_G}{Q_L + Q_G} \tag{2.9}$$

where Q_g and Q_L are the gas and liquid volumetric flows respectively. Substituting

$$Q_G = \frac{xW}{\rho_G} \tag{2.10a}$$

and

$$Q_L = \frac{(1-x)W}{\rho_L} \tag{2.10b}$$

into equation (2.7) gives

$$\beta = \frac{1}{\left\{1 + \left(\frac{1-x}{x}\right)\frac{\rho_G}{\rho_L}\right\}} \tag{2.11}$$

Hence,

$$\alpha = \beta \quad \text{, if } K = 1 \tag{2.12}$$

.

Since we can expect no slip when the two phases are flowing as a homogenous mixture, the no-slip condition is often referred to as ‘homogenous flow’.

2.3.3 Drift-Flux Two-Phase Flow Models

Drift-flux models have been used in thermal-hydraulic analysis codes in the nuclear and other industries to analyze behavior of systems during a wide variety of transient conditions. Drift-flux models are based on correlations to compute the void fraction distribution and slip in two-phase flow and it is needed to obtain the relative velocity

between the phases. In general, most of the drift-flux models correlations are based on work by Zuber and Findlay (1965).

In the drift flux model, void fraction α is a function of the total velocity and superficial gas velocities, *j* and *jG*, a phase distribution parameter C_o and a drift velocity v_{gj}.

$$\alpha = \frac{j_G}{C_o j + v_{gj}} \tag{2.13}$$

The superficial velocities for gas and liquid can be defined as the volumetric flow rate of each phase divided by the cross-sectional area of the channel.

For superficial gas velocity, j_G :

$$j_G = \frac{Q_g}{A} \tag{2.14a}$$

For superficial liquid velocity, j_L :

$$j_L = \frac{Q_L}{A} \tag{2.14b}$$

A study of the performance of void fraction correlations based on the Findlay-Zuber drift-flux model was done by Coddington and Macian (2002). There are 13 correlations that able to perform well for wide range of experimental conditions used in the assessment. The setup pressure and mass fluxes of these experimentations range from 0.1 to 15 MPa and from 1 to 2000 $kgm^{-2}s^{-1}$.

According to the assessment, five of the correlations yielded good predictions over the whole range of void fractions for rod bundle and tube data source. Furthermore,

among the five, two of the good prediction came from the system analysis codes. The correlations are Bestion (1985) and Chexal-Lellouche correlations (1992).

Table 2.1: The average error and deviation for Bestion, Toshiba and Chexal Lellouche void fraction correlations.

Correlation	Year	Data Source	Average error, ε	Deviation, s
Bestion	1985	Rod Bundle + Tube	0.018	0.088
Chexal-Lellouche	1992	Rod Bundle + Tube	-0.017	0.078
Toshiba	1989	Rod Bundle	0.019	0.103

The absolute error, average error and deviation are calculated using the following equations:

$$\varepsilon = \alpha_{means} - \alpha_{pred} \tag{2.15a}$$

$$\bar{\varepsilon} = \frac{1}{n}\sum_{i=1}^{n} \varepsilon_i \tag{2.15b}$$

$$s = \sqrt{\frac{\sum_{i=1}^{n} (s_i - \bar{\varepsilon})^2}{n-1}} \tag{2.15c}$$

Both of the correlation gives a good prediction of void fraction. The Bestion drift-flux correlation yields very good results for most of the experiment despite the simplicity of the correlation. On the other hand, the Chexal-Lellouche drift-flux correlation was complex requiring iterative solution but with no significant improvement compared to the Bestion's. The following formula describes the Bestion drift-flux correlation.

$$\alpha = \frac{j_G}{C_o j + v_{gj}} \tag{2.16a}$$

where

$$C_o = 1 \qquad \text{and} \qquad v_{gj} = 0.188\sqrt{\frac{g d_h \Delta p}{p_g}} \tag{2.16b}$$

The other best correlation prediction performance is by Toshiba (1989). The correlation is found by Mooroka et al. (1989). The performance of the correlation prediction was done by Melkamu et al. (2006). Toshiba's correlation shows best prediction capability in the inclined and vertical flow and also performs well among the top correlation for the horizontal flow. Therefore, Toshiba correlation is worth to be used as a general correlation for prediction of void fraction. The following formula is the Toshiba correlation of void fraction prediction.

$$\alpha = \frac{j_G}{C_o j + v_{g_j}} \tag{2.17a}$$

where

$$C_o = \frac{j_G}{j}\left(1+\left(\frac{j}{j_G}-1\right)^{(pg/pl)^{0.1}}\right) \text{ and } v_{gj} = 2.9\left(\frac{g\sigma_h \Delta\rho}{\rho_G}\right) \tag{2.17b}$$

Mishima and Hibiki (1996), carried out an experiment by using the inner diameters of the capillary tubes sizing from 1 to 4 mm. The void fraction was correlated well by the drift flux model with zero drift velocity. A new equation for the distribution parameter was developed based on the tube diameter as the function.

In another experiment by Triplett et al. (1998), void fractions were estimated by analyzing photographs taken during the experiments at the test section. The experiment was run by using the transparent circular microchannels with inner diameters of 1.1 and 1.45 mm. The range of the gas and liquid superficial velocities were varied between 0.02-80 m/s and 0.02-8 m/s, respectively. Each void fraction photograph covered a 6 mm-long segment of the test section.

The measured void fractions were compared with several existing correlations. Basically, the void fraction increases with increasing superficial gas velocity, j_G for constant superficial liquid velocity, j_L and decreases with increasing j_L for constant j_G. The deviations can overcome the problem that occurred by the difficulty and uncertainty associated with the calculation of void fractions using photographs. The homogeneous flow model provides a useful prediction of the channel void fraction at low j_G value corresponding to bubbly and slug two-phase flow patterns. The homogeneous model for the prediction of void fraction for churn and annular flow are still difficult to interpret due to the interphase slip between separation of the liquid and gas phases.

The agreement between the experimental data and the correlation of Chexal et al. (1997) is good for bubbly and slug flow patterns and at high j_L values and is comparable with the predictions of the homogeneous model. At lower j_L values, the correlation of Chexal et al. appears to over predict the void fractions in churn and annular flow patterns significantly although with margins notably smaller than the over prediction margins associated with the homogeneous model.

In other predictions of the Lockhart-Martinelli-Butterworth correlation (Butterworth, 1975) and the CISE correlation (Premoli et al., 1971), both correlations predicted well for the void fractions in bubbly and slug flow patterns representing high j_L, and they both over predict for churn and annular flow patterns.

From the results, for bubbly and slug flow patterns, the homogeneous flow model overall provided the most accurate prediction of the channel void fraction. Other

correlations however, all satisfactorily agreed with data for the latter flow patterns except when j_L was very low where the latter correlations significantly under predicted the measured void fractions. These under prediction of void fractions are likely to be due to the differences between two-phase flows patterns in large channels and capillaries.

2.4 Constant Electric Current Method

In the real application, two phases of liquid film flowing with high speed gas flow in various applications in the industrial equipment. Determination of the characteristic of liquid film in two-phase flow is important and useful to have a safe operation, increase performance and to save the operational cost for the equipments. However, the two phase flow phenomena cannot be seen in the actual condition through the pipe or tube. As discussed previously, the flow pattern and the void fraction just can be determined using special equipment like x-ray method through the pipe, which is not a cost effective.

The surface of the liquid film in two phase flow is usually accompanied by various kinds of flow regime complicated wave and that thickness is changed with time and position. The interface of the flow conditions in the two phase flow will affect the flow pattern of liquid film, the shear stress on the surface, bubble development condition and the liquid film breakdown in the flow. In order to accumulate the information of liquid film in real time, a suitable method is needed and one of the methods is Constant Electric Current Method (CECM). A simple method like CECM can be applied in the industrial equipment with a low cost budget and with continuous real time observation.

In this case, a good construction of the sensor is essential, such as size, which also included the space between a pair of sensor electrodes and the amount of voltage supplied to them. If the electrodes are mounted flush with the surface of the channel, two phase flow is not disturbed, and formation of other type of flow patterns can be avoided. In the usual conductance method, some common problems that always occur are such as:

1. The output from the sensor electrodes related to the size of film thickness caused by the constant power supply, is not suitable for measuring the fluctuating film thickness.
2. The current density is not uniform inside the pipe and dependent on the radial location of the gas phase.
3. The output has a possibility to saturate if the distance between two sensors is small compared with the film thickness. (Fukano, 1998)

Work by Fukano in 1998, Constant Electric Current Method (CECM) was developed and it is based on the supply of constant current power sources, which is connected to two types of electrodes. One of the electrodes is used for supplying electric power and the second electrode is for detecting voltage fluctuation during two-phase flow bringing the information of hold-up or film thickness and can be used to compute the void fraction. The main difference between the CECM methods compared with the conventional conduction method is the output of the sensor is not affected by the radial location of the gas phase. The CECM is sensitive enough to detect the change of hold-up especially for the thin film thickness and the interaction among the electrodes is negligible.

Figure 2.6 shows the basic idea of the Constant Current Electric Method (CECM) by Fukano, 1998. In this method, in order to overcome the problems that occur in the conventional conductance methods, the power electrodes for CECM are separated from sensor electrodes and the distance between power electrodes must be larger than the objective measuring section which makes the current power supply become satisfactory uniform in the measuring section that is shown in figure 2.7.

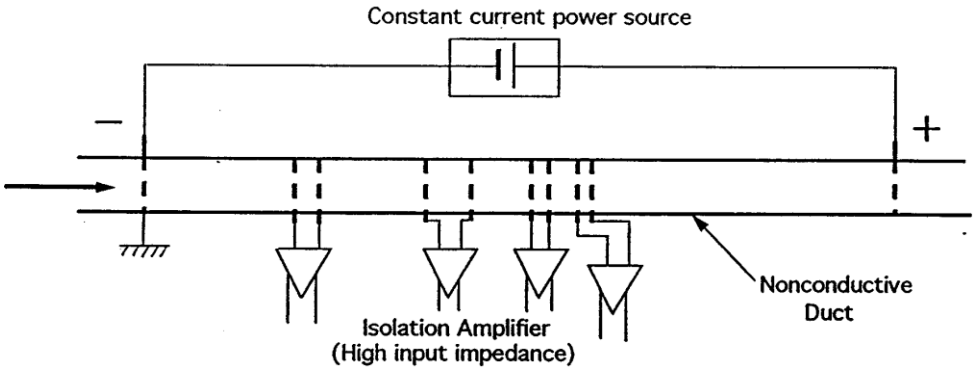

Figure 2.6: Basis Idea of Constant Electric Current Method (CECM) (Tohru Fukano, 1998)

The distribution of the electric current for CECM is uniform and not only related to the film thickness. The linearity of the reading output from the film thickness is quite good. CECM has high sensitivity to the film thickness especially for the liquid film flow. The interaction among the sensor is also negligible because of the high input-impedance amplifier. There is one power source needed even to measure many hold up at different locations. The electrodes are mounted to the surface of the pipe and do not disturb the flow of the two-phase flow. Therefore it has advantages in measuring the void fraction in any flow condition with high sensitivity of sensor that is able to detect the change of voltages constantly.

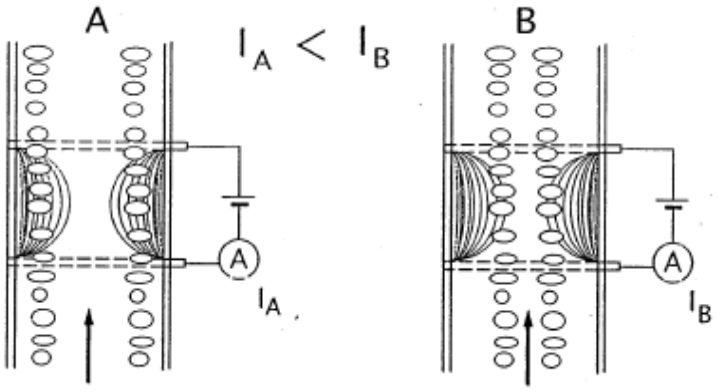

Figure 2.7: Equal output voltages in uniformly distributed electric current in the CECM independent of the location of the gas phase. (Fukano, 1998)

2.5 Other Factors That Affected the Two-Phase Flow

The two-phase flow results can be affected by internal or external factors. The effect of external factor can be neglected or controlled during the experiment. The internal factors that affected the experiment need to be determined and controlled. However, some of the internal factors were difficult to control and have a limitation on the experiment equipment. Mostly, the internal factors that affected the two-phase flow can be observed and determined only by conducting the experiment.

2.5.1 Vibration

The vibration gave an impact to the flow pattern of two-phase flow. From the observation, the vibration was increased the rate of coalesces for the bubbles. The slug flow inclined to break down to form the churn flow. In normal situation, the vibration generates naturally from the two-phase flow system. The vibration that generates by high speed two-phase flow inside the system was called a flow-induced vibration. Flow-induced vibration was changed the void fraction profile from wall peak to core peak or to the transition. The phenomena will increase the distribution parameter in the drift flux model as reported by Hibiki and Ishii (1998).

2.5.2 Pipe Surface and Wettability

Pipe surface type, roughness and the wettability gave an impact to the flow pattern of two-phase flow. The pipe roughness affects the smoothness of the flow. The surface condition was shift the range of boundary for the flow pattern at certain pattern. The pipe wettability was another factor needed to be viewed before setting up the experiment. The pipe needs to be chosen before setting up the experiment. Pipe wettability can shifted the transition boundary for the flow pattern of two-phase flow. The mean void fraction also can be affected by the wettability of the pipe. The effect of pipe wettability to the frictional pressure loss is insignificant due to some experimental conditions, Takamasa et al. (2008).

2.5.3 Pipe Bending Effect and Disturbance

From the experiment results, the pipe bending gave an impact to the flow pattern of two-phase flow. The pipe bending mostly happens at the connection between the two sections of the pipe experiment. The improper connection between the sections directly showed the changes to the flow pattern after flowing through the bending parts. The flow pattern clearly changed after flowing through the bending pipes and developed a new pattern. The change of direction and turbulence phenomenon makes the flow become unstable and forming a new pattern. From the observation, the internal disturbance for the two-phase flow has disturbed the flow pattern. The result was agreed with Kim et al. (2001) where the flow pattern boundary for some patterns will shift or change with the existence of disturbances inside the pipe.

2.5.4 Gas and Liquid Distributions

Gas and liquid distribution gave an impact to the two-phase flow experiment. The experiment needs a uniform distribution of gas and liquid flows inside the pipe starting from the gas liquid mixer. The unbalanced distribution will cause the false reading of the result. The equipment setup need a proper design to ensure that the experiment will run according to the objective and agreed with Shen et al. (2005). The experiment facilities have a specific measurement and standard to achieve the best result.

2.5.5 Limitations of the Experiment

There were a few limitations on the equipment during the experiment of two-phase flow. The critical limitations related to the equipment were:

i. Water flow rate

The water was supplied to experimental loop by using the water pump. The maximum flow rate of the water depended on the specification of the water pump minus the head loss inside the experimental loop. The model of water pump used for this experiment was Foras SD200/2. The range of the volumetric flow rate was between 200-900 L/min. However, after connecting to the system, the maximum of water flow rate was less than 250 L/min. The ideal water flow rate needed for the experiment was 850.70 L/min for the superficial velocity of 2.0 m/s for biggest pipe, 95.0-mm diameter pipe. With the limitation of the water pump, the maximum superficial flow rate can be set up for 95.0-mm pipe was at 0.5 m/s with the flow rate of 212.67 L/min.

ii. Air flow rate

The air was supplied by the air compressor for the experimental loop. The model of the air compressor is Dancomair-Elgi CLISBY Series S with capacity of 180 liters and maximum pressure up to 8 bars. After connecting to the experiment loop, the maximum flow rate of air was up to 400 L/min or 1.0 m/s for the 95.0-mm inner diameter pipe. The ideal gas flow rate needed for the experiment was 850.70 L/min at the superficial velocity of 2.0 m/s for 95.0-mm diameter pipe. The air flow rate was also fluctuated depends on the gas pressure inside the compressor tank.

iii. Air and water flow rate measurement

The difficulty of controlling the air and water valve in order to get the desired volumetric flow rate has already been discussed in chapter 3.5.2. A fine adjustment of the flow rate was difficult to achieve by manual handy valve tuning. The only way was just to reduce the error by trying to maintain the volumetric flow rate as close as possible to the desired value.

iv. Water temperature

The water temperature affected the conductivity of the water since the water becomes less viscous and ions can move more easily at higher temperatures as discussed in chapter 3.5.2. The water temperature should be maintained at room temperature at 27 °C. However, the water temperature was increase after flowing inside the loop for a while. The temperature increase of the water was caused by the frictional force of the water flowing along the long pipes. In addition, the dissipation of the heat generated by the pump was also the factor of the increase in water temperature. The increase of water temperature

gave a false reading to the sensors. In order to overcome this problem, the temperature of the water was observed from time to time using the thermocouple and infrared thermometer.

Chapter 3: Methodology

For the current work, two parts of experimentations are conducted; the flow pattern investigation and void fraction measurement. Both of the experiments require a complete set of information of two-phase flow system and are conducted based on various flow conditions.

For the flow pattern, the investigation is focused on the experimental works which are based on systematic observation and measurements by using a high speed camera and a few measuring apparatus. In order to carry out this purpose, the two-phase flow loop is constructed using a specific experimental apparatus and components. The flow channels are constructed using three pipes with three different inner diameters of 21.0-mm, 47.0-mm and 95.0-mm. The directions of the flow are vertical upward and horizontal co-current flow with liquid superficial velocity range from 0.025 m/s to 3.0 m/s and gas superficial velocity from 0.025 m/s to 3.0 m/s depending on the size of the pipes.

For the void fraction measurement, the CECM sensor used to measured void fraction was integrated into the two-phase flow system with constant electric current running in the pipe and data acquisition system controlled by virtual experimentation via LabVIEW software. The constant current power source is used to supply the constant electric current via the power electrode and any voltage fluctuation due to gas existence in the channel will be captured by the sensor electrode. At the same time, the data acquisition system recorded the voltage output and the data was analyzed using the LabView software.

Since the experimentation is with the purpose to show the actual situation of two-phase flow, thus it is vital to collect as much information from previous studies and

compared with current experiments. This report should consists of every details of information acquired from literature studies to show appreciation for the researchers who have contributed their efforts in this field.

An experiment procedure is proposed in order to achieve the objectives of this research. Figure 3.1 and 3.3 shows the schematic diagram of two-phase flow experiments set-up and arrangement. The working fluids used are air and filtered water from a reservoir at ambient environment temperature and atmospheric pressure.

3.1 Two Phase Flow System

As mentioned in the previous section, the experimental setup consists of three transparent acrylic pipes with different inner diameters 21.0-mm, 47.0-mm and 95.0-mm with 3.0-m length. This pipes diameter size is choose based on the usual size that used in the industry. The purpose of using transparent acrylic pipes is to observe the actual flow patterns of the two-phase flow inside the pipe. A high speed camera is used to capture the flow patterns such as bubble, slug, churn, and annular flow for vertical upward flow.

3.1.1 Upward Vertical Flow

The pipes are placed vertically for upward vertical arrangement shown in Figure 3.1 and 3.2. The experiment is an adiabatic co-current two phase flow. The working fluids of the two-phase flow are water and air. Water is circulated in the flow loop by a motor pump and air is supplied to this system by using an air compressor and it flows into the test section at the water-air mixing section, just before entering the channel. The two-phase gas-liquid mixture flows through to the outlet of the channel and the air is released into the atmosphere via the separator. This is to ensure that only water (one-

phase) flowed back into the water reservoir. In addition, a separator is designed to release a high pressure of the two-phase of air-water flow when flowing from a test experiment pipe into the outlet piping system. The experiment is performed at room temperature (27 °C) and at atmospheric pressure (101.3 kPa).

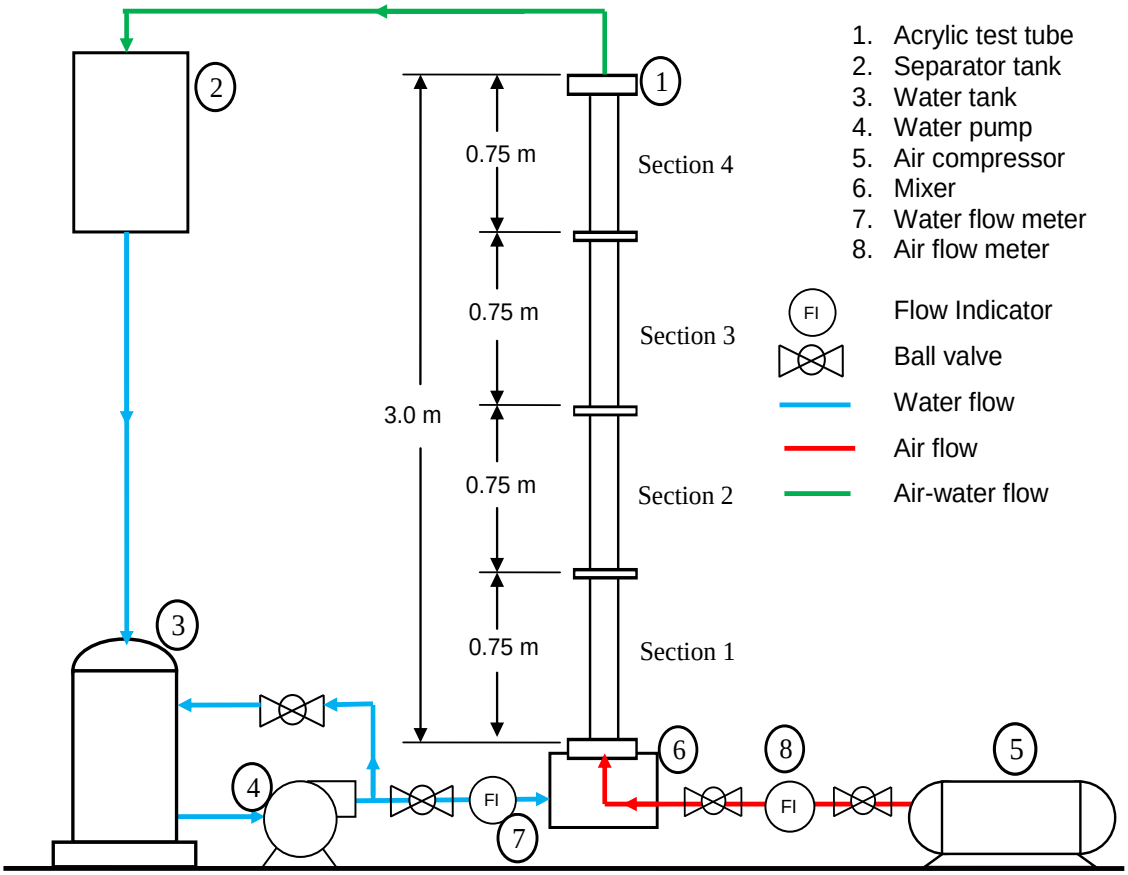

Figure 3.1: The schematic diagram of the two-phase upward vertical flow experimental loop

In this experiment, the air flow rate is measured from 0.83 to 229.04 L/min while the water flow rate is measured from 2.55 to 106.34 L/min. The superficial velocities of air and water are obtained by dividing the volumetric flow rate with the cross-sectional area of the pipe. Superficial velocities are used instead of flow rate because different pipe diameters give different superficial velocities. The ranges of superficial velocities used are as shown in Table 3.1.

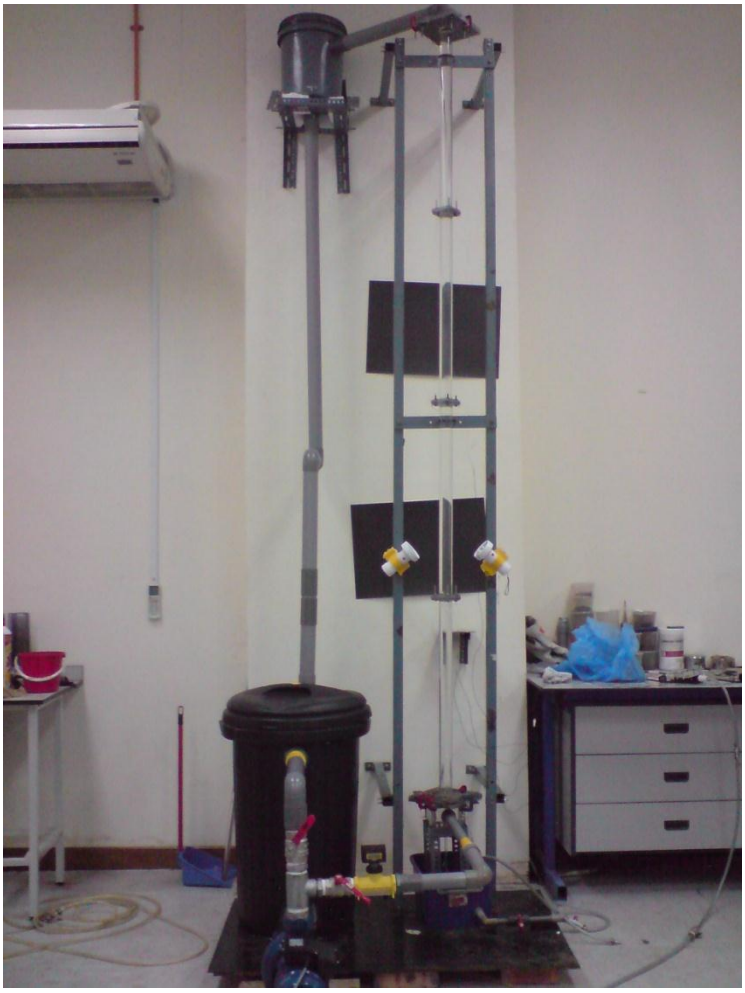

Figure 3.2: The experimental setup for the two-phase flow loop upward vertical flow

Table 3.1: Range of superficial velocities for upward vertical liquid and gas flow according to pipe inner diameter

Pipe inner diameter (mm)	**Superficial liquid velocity, j_L (m/s)**	**Superficial gas velocity, j_G (m/s)**
21.0	0.025 – 3.00	0.025 – 3.00
47.0	0.025 – 2.00	0.025 – 2.00
95.0	0.025 – 0.60	0.025 – 0.60

3.1.2 Horizontal Flow

The horizontal experimental setup also consists of three transparent acrylic pipes with different inner diameters 21.0-mm, 47.0-mm and 95.0-mm with 3.0-m length. The pipes are placed horizontally for horizontal flows that are shown in Figure 3.3 and 3.4. A high speed camera is used to capture the flow patterns to observe the bubble, plug, stratified, wavy, slug and annular for horizontal flow.

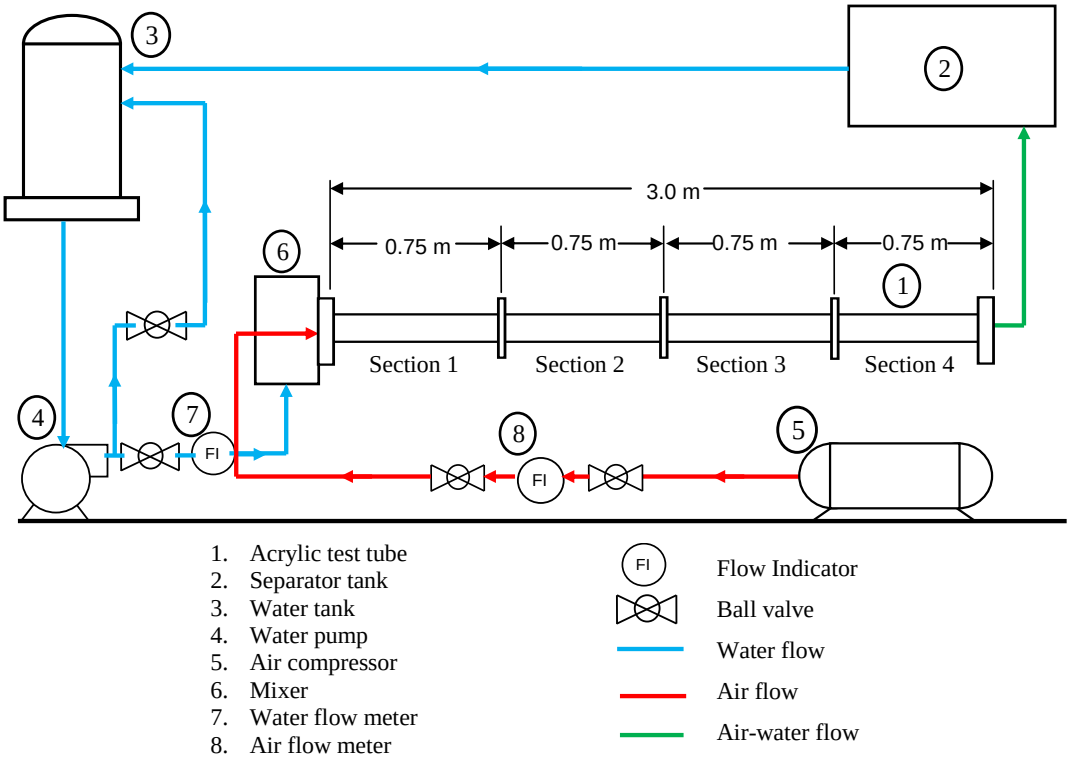

Figure 3.3: The schematic diagram of the two-phase horizontal flow experimental loop.

Repeatedly the same procedure as for the vertical flow, water is pumped into the test acrylic pipes from a water tank. In order to control the flow rates, a valve is attached right after the water pump to control and avoid pressure losses and the flow meter is installed just before the mixer to determine the flow rates of the water. The water in the tank was maintained at room temperature and atmospheric pressure. The water is mixed together with air from the air compressor. The air-water two-phase flow is flown through the pipe to the separator and the air will separate and released into atmospheric

while the water flows from the separator to the water tank in order to release high pressure of two-phase flow. All the water will return back to the tank, making a full loop.

Figure 3.4: The experimental setup for the two-phase flow loop horizontal flow.

Table 3.2: Range of superficial velocities for horizontal liquid and gas flow according to pipe inner diameter.

Pipe inner diameter (mm)	**Superficial liquid velocity, j_L (m/s)**	**Superficial gas velocity, j_G (m/s)**
21.0	0.025 – 3.00	0.025 – 3.00
47.0	0.025 – 2.00	0.025 – 2.00
95.0	0.025 – 0.60	0.025 – 0.60

3.2 Equipment Setup

3.2.1 Two-Phase Flow Experimental Rig

The two-phase flow experimental rig is constructed in three difference pipes sizes. The two-phase flow system apparatus consisted of equipment such as water pump, three different sizes of acrylic tube, PVC pipe, water tank, valves and separator.

- Acrylic pipe

  Three pipes with different inner diameters (21.0, 47.0 and 95.0-mm) were used. The length of each pipe is 3.0-m.

- Water Pump

  The motor pump used in this work is Foras SD200/2 with power 2.2 HP / 1.65 kW and single phase (240V/50Hz/10A). The range of the volumetric flow rate is set between 200-900 L/min.

- Air Compressor

  The Dancomair-Elgi CLISBY Series S air compressor is used in this work. The power of the air compressor is 4 kW. The maximum size/volume of the air receiver is 180 litres and can supply air up to 8 bars. The air compressor is used to supply air into the pipe test section.

- Water tank

  The water tank for this experimentation is made of a plastic material that is chemically stable to the water. The capacity of water tank has been calculated and referred to the water usage and plus an extra space and the maximum load can be up to 70 liters of water.

- Valve

  Two different types of valves are used separately for air and water. The valve size and types of valve depended on the pipe size and the applicability to the system.

- Mixer

  A simple mixer is constructed using the acrylic board to mix up the air and water before enter the experiment pipe.

- Separator

  A simple separator is used to calculate and separate the gas from the water at the end of the pipe. It has been installed to meet the capacity of water flowing from the pipe and the capacity of water flowing to the water tank.

- Piping

  The pipes used for the system are made from PVC pipes and galvanize pipes. The types of pipe are chosen depending on the application. For critical parts with high pressure water, galvanize pipes are used and normal condition with the PVC pipes.

- Support Frame

  Support frame is fabricated based on the design of the system. The support frame is made from mild steel and attached to the wall to stabilize the frame. The frame attached to the wall uses the wall plug.

3.2.2 Imaging Facilities

In order to have an accurate evaluation of observations for the flow patterns and behavior, a specific image facility is required. In this work, a high speed video

camera is applied for this purpose with some aided equipment such as the halogen lamps installed for a better lighting. Data storage equipment is also prepared for later analyses of the images for better observation.

- Camera

  The camera for this particular work is Olympus DSLR E-420 Live View with the resolution of 10 megapixels and it also includes an electronic flash, Olympus Electronic Flash FL-36R. The range of the shutter speed is 2 – 1/4000s.

  For motions of bubbles in the experiments, a high speed video camera is used. The current video camera facility is Casio EX-F1 with capability of 1200 frame per second. The camera can capture a still image for high speed purpose up to 60 frames per second.

- Lighting System

  The lighting system is used based on requirement of the camera. The lighting equipment like LED light, halogen light and camera flash are used to get a better picture during the flow pattern recording. The halogens are located at a specific location and angle to get a good lighting support for the experiment.

3.2.3 Measurement Apparatus

A few measurement apparatus and controller are installed in this experiment. Flow meters are used to determine the flow rate of the liquid with flow rate in the range of the flow condition, in order to get the correct reading with high accuracy. The simple valve control manages the amount of the flow into the system.

- Water Flow Meter

  The liquid flow meter model is Blue White Industries Flow rate meter F-1000-RB (Paddlewheel flow meter). The flow rate of the liquid can be measured up to 600 L/min using this flow meter.

- Air Flow Meter

  Four air flow rate meters are used according to the range of the air flow rate. For low range air flow rate, Kofloc flow rate meters are used. The range of the two flow rate meters are 0.2 – 2.0 L/min and 3 – 30 L/min respectively. For high range air flow rate, McMillan Company 100 Flo-sensor is used with range of 100 – 1000 L/min. MBLD Instrument Company flow meter with range of 12 – 120 L/min was used for the medium range of the flow rate.

- Thermometer

  The model of the thermometer is the Autonics temperature indicator T4Y1 with the thermocouple type K. It is used to measure the temperature of water in the water reservoir.

- Pressure Gauge

  A pressure gauge is used to measure the pressure for the air supplied to the system.

3.2.4 Sensors

In order to have an accurate reading of volumetric gas rate (void fraction) in the system, a sensor based on Constant Electric Current method (CECM) as explained in the previous section is employed in the experiment. The sensor has an ability to measure the void fraction regardless of the portion of gas in the flow

channel. Since, the sensor is mounted flush to the inner wall of the channel; it does not contribute to any possible effect on the two-phase flow in the pipe. The numerical data provided by this sensor will predict some possible flow patterns based on mass flow rate of gas and liquid. It can also be used to measure the velocity of the bubble in the flow system by measuring time elapsed via numerous sensor placed along the flow channel that will be transferred directly to the computer. Figure 3.6 shows the sensor's equipment setup for the void fraction measurement.

- USB Data Aquistion System (DAQ)

  The Instruments NI USB-6215 is used as data acquisition system with 16 analog inputs (16-bit, 250 kS/s), 2 analog outputs, 4 digital inputs, 4 digital outputs and two 32-bit counters. The maximum voltage can be detected by the DAQ is 10 V. In this work, it is used to process the signal (voltage drop) from the sensors. The data from the signal is displayed on waveform charts and numerical displays using LabVIEW software.

- Laptop

  The model of the computer is ASUS X59SR. The processor is CPU Intel Core 2 Duo P8400 and running on Windows Vista operating system. The computer is used to run the LabVIEW software to calculate the void fraction and for output display.

- 3.3.4.3 Power Supply

  The model of the power supply is GW GPS3030D. The range of the electric current is 0.001 – 0.01A and the range of the output voltage is 0 – 40 V. This power supply is used to supply constant electric current to the power electrodes in the test pipe.

- Copper Ring

  The electrodes both for power supply and sensors are made from copper. The thickness of the electrode is 2.0-mm and the inner diameters are the same as the inner diameters of the acrylic pipe (21.0, 47.0 and 95.0-mm). The sensor electrode is used to detect the voltage drop of the void fraction in the test pipe section and the power electrode is used to supply constant electric current. The electrodes are flush mounted with the inner diameter of the pipe to avoid disturbance to the two-phase flow.

- Copper Wire

  A small diameter single copper wire is used in this experiment. The copper wire is properly connected to minimize the noise to the system.

- LabVIEW Software

  LabVIEW 8.6 is used in this experiment. The software gives good features and is suitable for this experiment. The experiment results are obtained via data acquisition device and analyze using LabVIEW software and the output display the output in the front panel of the LabVIEW software.

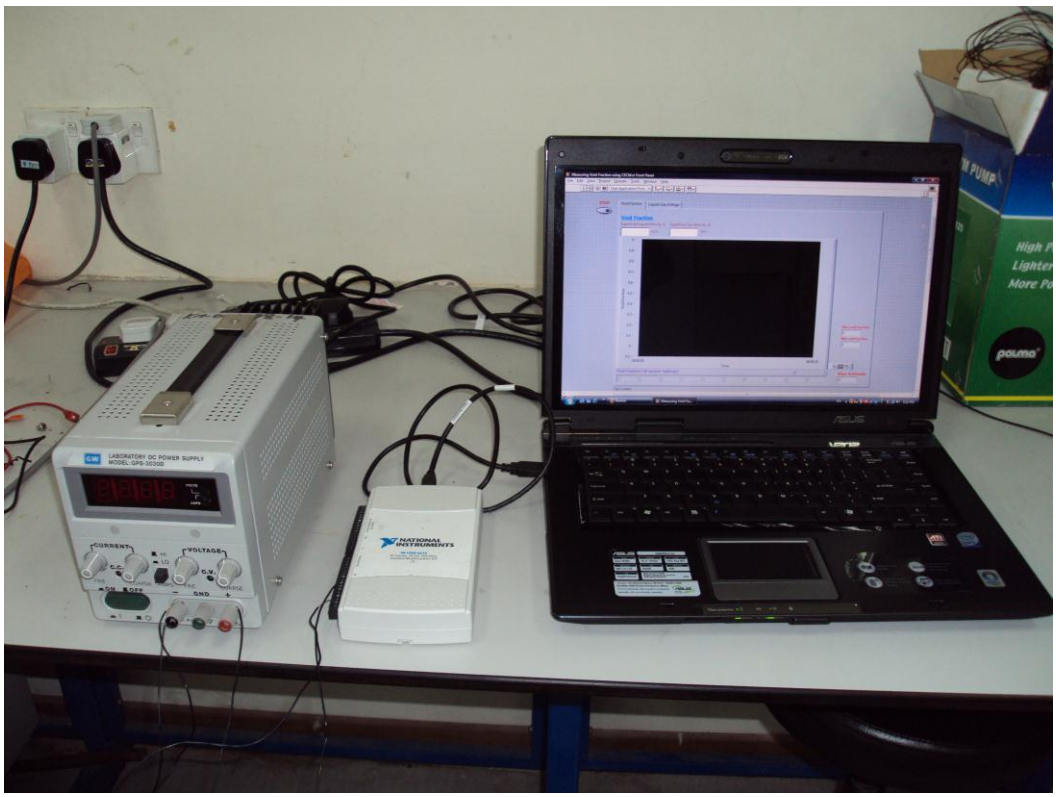

Figure 3.5: The sensor's equipment setup

3.3 Flow Pattern Experiment

3.3.1 Photography Method

The flow patterns information of the two-phase flow is usually attained by visual observation of the flow. The photographic method is one of the visual observation methods for the two-phase flow patterns investigation.

For this work, a digital single lens reflex (DSLR) camera is used to capture the flow patterns images throughout the test section (test pipe) while the high speed video camera are used to capture the slow motion video of the flow pattern for the further analysis. An electronic flash is used to add extra brightness to the test section during the images capturing process as the amount of light is a vital aspect in the photography method.

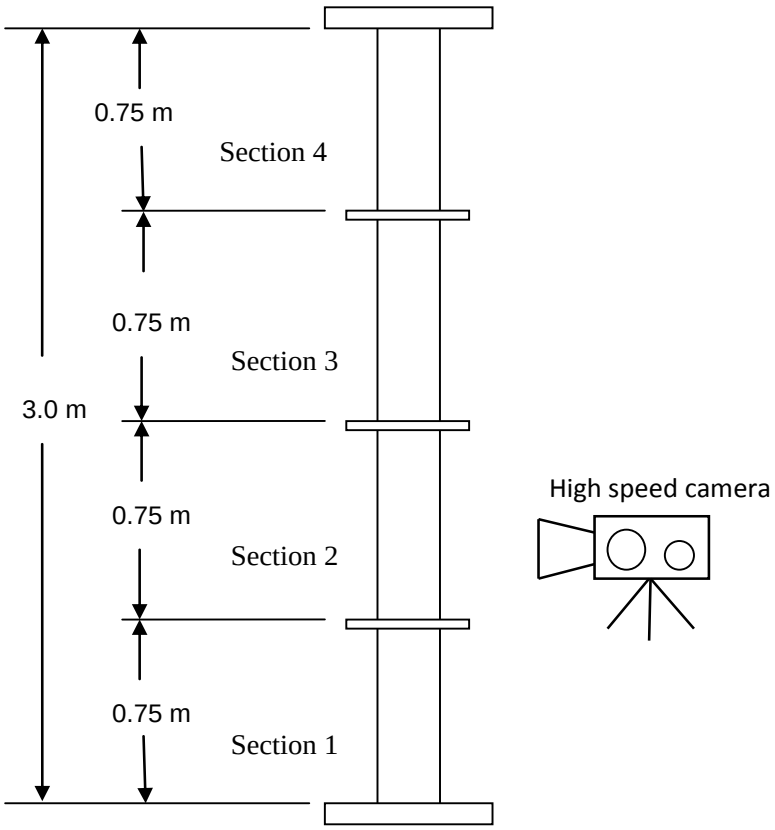

Figure 3.6: Test pipe section and point of observation

In the experiment, each of the 3 m length pipe has been divided into four sections and the end of each section has been identified as the point of observation of the flow patterns. Figure 3.6 shows the test pipe sections and points of observation. Each section has 0.75-m length and the height from the pipe inlet for point 1, point 2, point 3 and point 4 are 0.75-m, 1.5-m, 2.25-m and 3m, respectively. Figure 3.7 shows the flow diagram of the flow pattern experimentation.

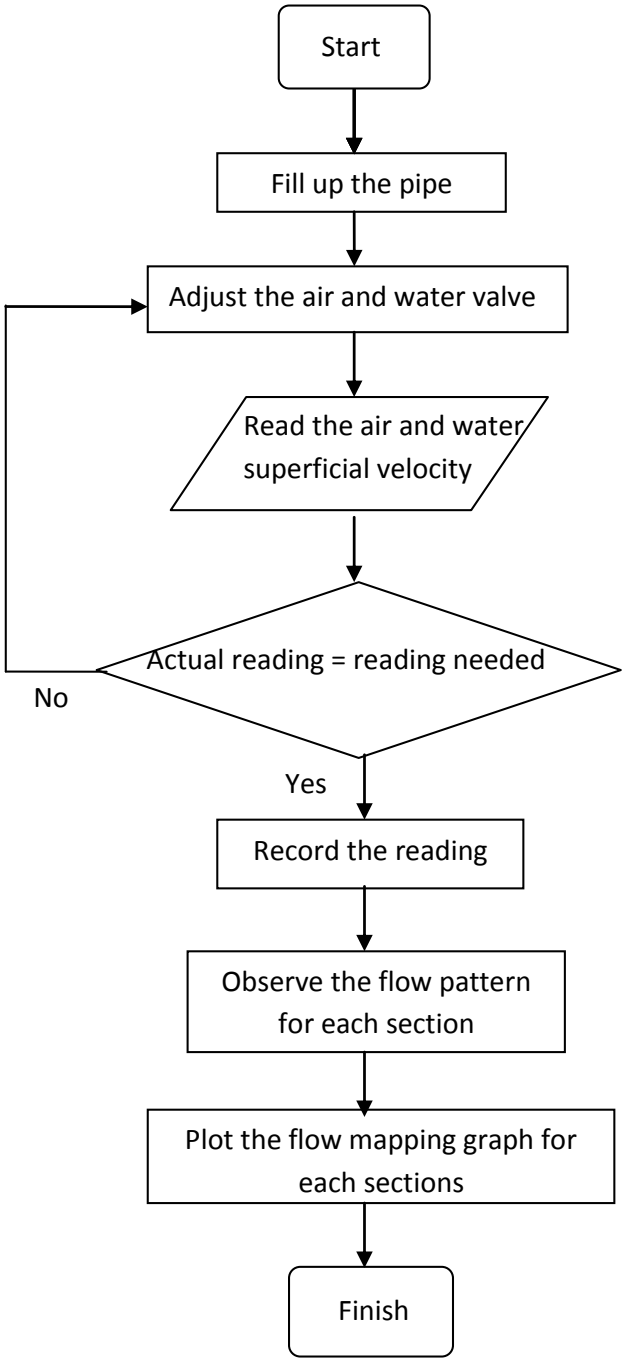

Figure 3.7: Flow diagram of flow pattern experiment

The flow patterns of the two-phase flow throughout the test section are observed and the flow pattern images at each section are captured by using the DSLR camera on shutter mode from range 1/1000s to 1/4000s as the nature of the flow patterns required a high-speed photography technique. Even by using the high-speed photography, the

major disadvantage is that the light is subjected to a complex series of refractions as it passes through the flow and the resultant images of the flow patterns captured are sometimes often difficult to interpret. Therefore, the images captured are subsequently processed using proper image processing software in order to refine the images captured and remove any defects from it. The processed images are then analyzed and their type of flow pattern at each section is recorded.

The high speed video camera is an additional method to determine the actual flow of the flow pattern by viewing the pattern in a slow motion video recording. The high speed video camera can capture the image up to 1200 frames per second which can slowdown the video playing up to 40 times if the video play is in the rate of 30 frames per second.

3.4 Constant Electric Current Method Experiment

3.4.1 Constant Electric Current Method (CECM) System

For this research, all the three test pipes are customized in order to install three pairs of sensor electrodes at three fixed positions which are at point 1, point 2 and point 3 as shown in Figure 3.8 with two power electrodes at each of the pipe end. Each of the 3m length pipe is then cut to four sections with each section that has 0.75-m length as shown in Figure 3.6. Each of the pipe sections is then connected using three flanges. The sensor electrodes pairs are installed in these flanges while the power electrodes are installed at the inlet and the outlet of each pipe.

Copper wires connect all the electrodes to a data acquisition (DAQ) module that is connected to a computer installed with DAQ software (LabVIEW). The computer and the DAQ software are employed to observe, analyze and store the resultant data.

At the beginning of the experiments only the water flow is pumped into the test section and the voltage during liquid phase is taken. Then, for each superficial velocity varied, the voltage readings of the gas-liquid phase voltage are recorded. The void fraction value at all points of observation is then obtained from the basic liquid thickness equation introduced by Fukano (1998) the void fraction can be measured using the following relationship:

The electric resistance of two-phase flow, R_{TP} in unit length of the channel

$$\frac{1}{R_{TP}} = \frac{1-\eta}{R_G} + \frac{\eta}{R_L} \tag{3.1}$$

The hold-up show in voltage drop, with constant current I_0 is supplied

$$\eta = \frac{R_L}{R_{TP}} = \frac{I_0 R_L}{I_0 R_{TP}} = \frac{V_L}{V_{TP}} \tag{3.2}$$

The relationship of hold up and void fraction

$$\eta = \frac{V_L}{V_{TP}} \tag{3.3}$$

$$\alpha = 1-\eta \tag{3.4}$$

$$\alpha = 1-\frac{V_L}{V_{TP}} \tag{3.5}$$

Two power electrodes and two sensor electrodes are installed according to the location shown in Figure 3.15. The void fraction measurement section covered about 0.75-m of the pipe length with the power electrodes located at a distance of 2.25-m. The sampling frequency of the output is at 2 kHz and was processed by a computer.

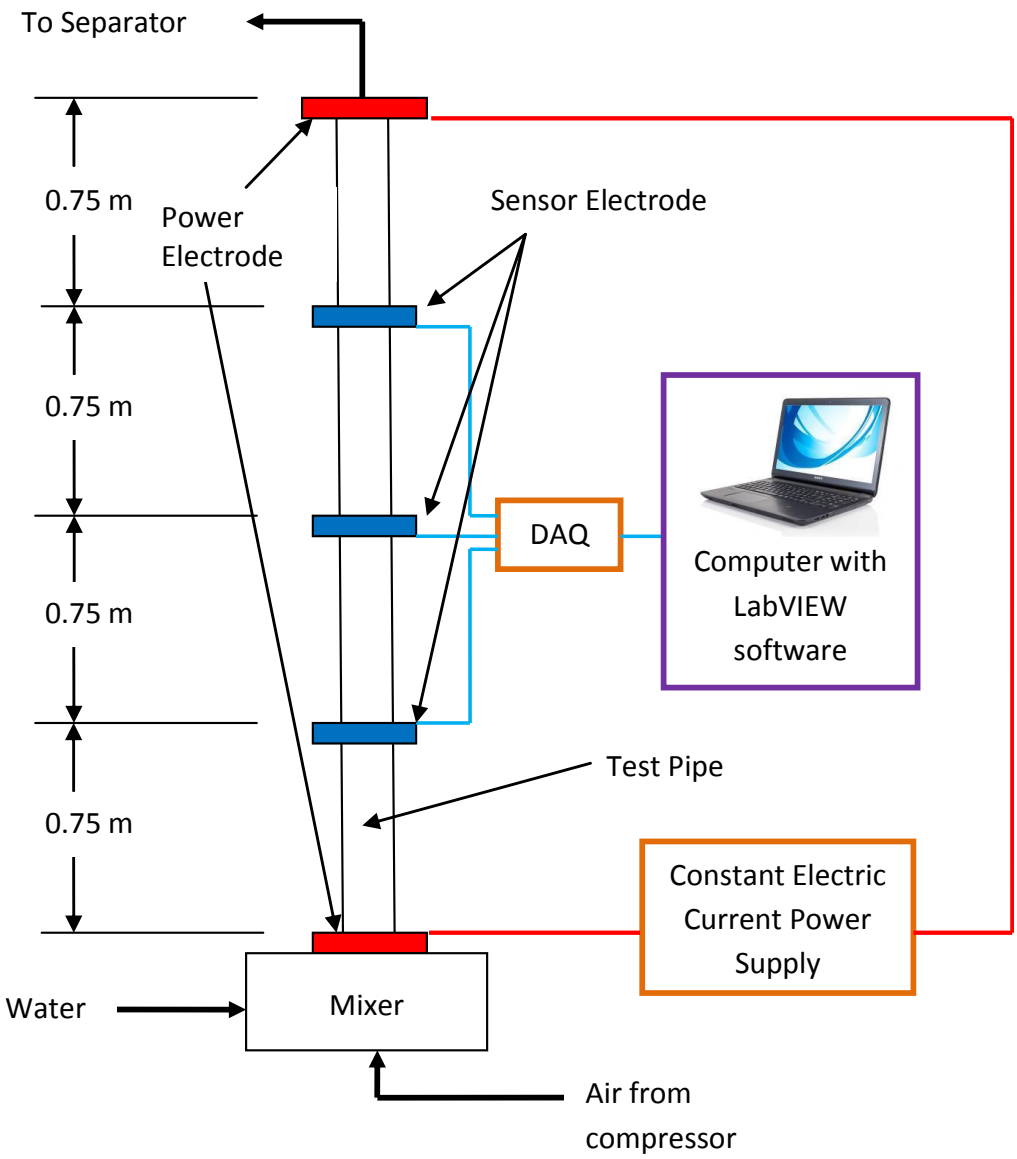

Figure 3.8: Schematic view of the experimental apparatus for void fraction measurement using CECM

3.4.1 CECM Calibration Method

The calibration process is an important procedure before starting the two-phase flow measurement using the CECM method. Below is the step for the calibration process.

1. Firstly, the signal input range is set between 0 and 10V.
2. Next, the experimental pipe section is flown with gas only and the reading must record 0V.

3. Then, the experimental pipe is flown with liquid only and the voltage output is recorded.
4. A low gas and liquid superficial velocity is supplied to the experimental pipe at the same flow rate to get half gas and half liquid. The calculation of the area is based on the visual image captured by high speed camera Figure 3.9. Then, voltage output is recorded.
5. The voltage output get from step 1 to 3 are then converted to the void fraction range of 0 to 1. The gas only reading is set to 1 and the liquid only is set to 0 void fraction. The half gas and half liquid two-phase flown in experimental pipe are set at 0.5 void fraction reading.
6. All the calibration that used to set the void fraction reading is calculated by a mathematical formula in the statistic block in the LabVIEW software (Figure 3.11).

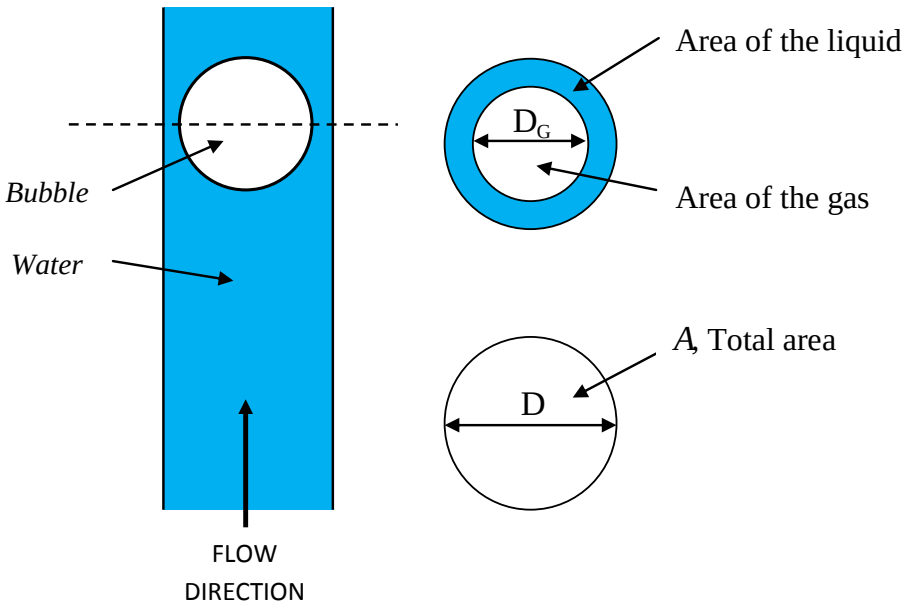

Figure 3.9: Calculation of void area and void fraction

3.4.3 Data Processing Using LabVIEW Program

The data collection and processing in this experiment is carry out using a LabVIEW 8.6 version virtual instrument software and data acquisition module (DAQ) model NI USB-6215 both products from National Instruments Company. The electric current from the sensor converted to signal by DAQ, than analyzed by using the LabVIEW software.

Next, the voltage signal from the DAQ is process through a few programming block within LabVIEW for signal analysis. All the calculations and signal processing for the void fraction are also computed using the formula function blocks in LabVIEW. The output from the sensors electrode is displayed as waveform charts and numerically displayed in the LabVIEW front panel. The value of maximum, minimum and mean void fraction will be recorded and displayed. The graph of void fraction versus time and voltage versus time will also be displayed as output. The flow diagram of the programming for measuring the void fraction is shown in Figure 3.10.

The water and gas superficial velocity will be adjusted and fixed at the required speed before starting to run the CECM experiment.

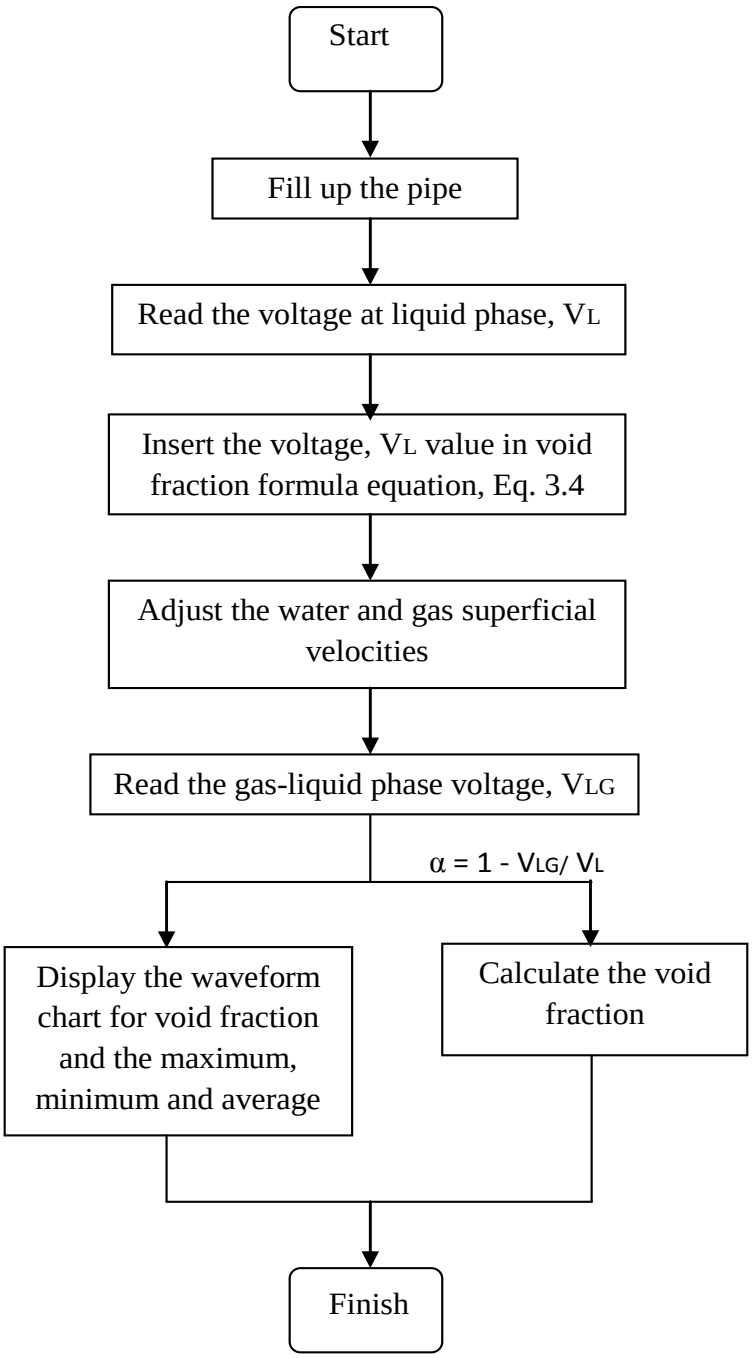

Figure 3.10: Flow diagram for void fraction measurement program

Based on the flow diagram, a program is developed using the blocks concept in LabVIEW software. Loop method is employed in the program so that the program will continue running until the stop button is pressed. The block diagram and the front panel of the program are shown in Figure 3.11 and Figure 3.12.

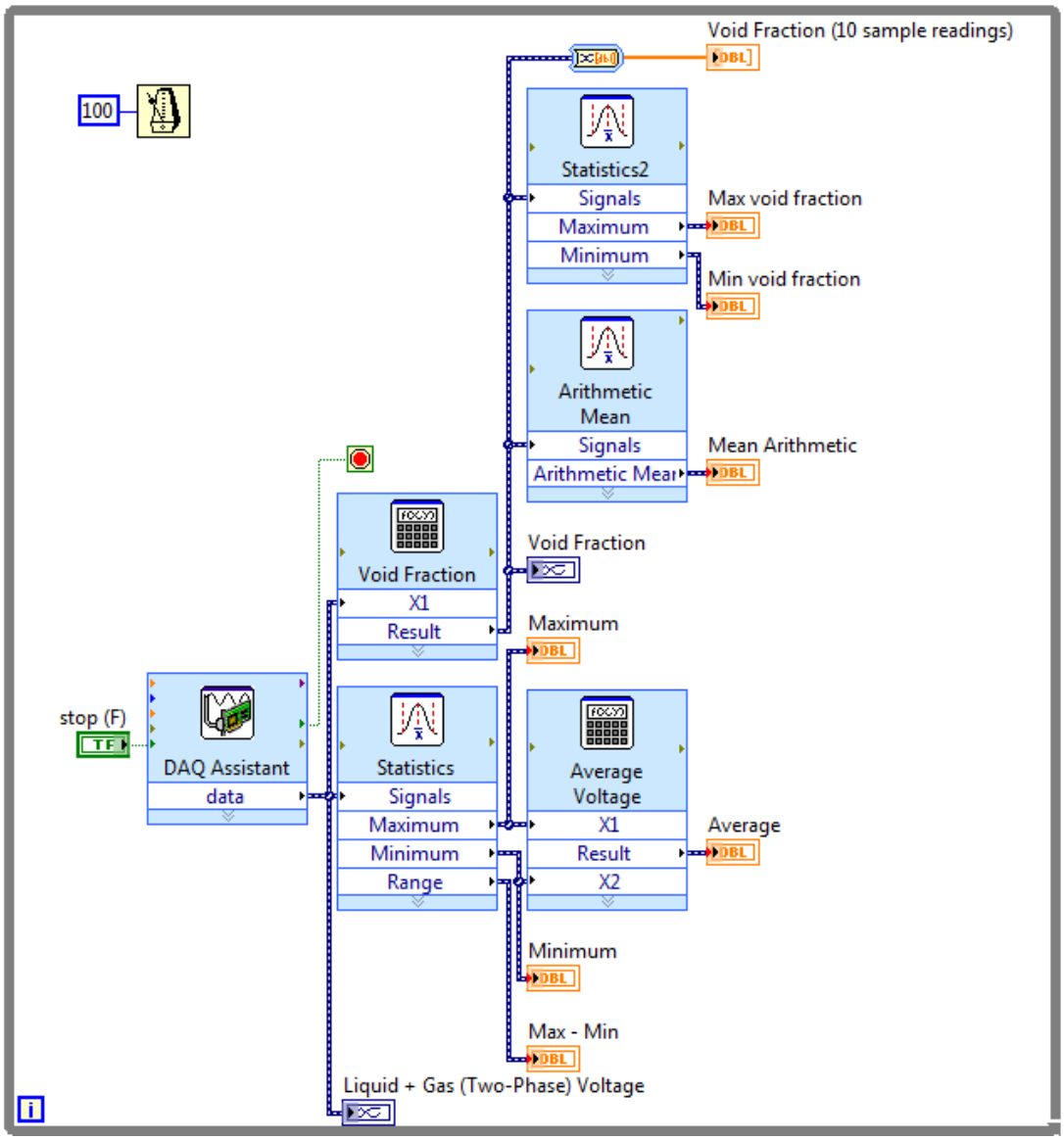

Figure 3.11: The block diagram of the void fraction measurement program

The blocks used in the program are:

i. DAQ Assistant

The signal input range is between 0 and 10 V. For the timing settings, the acquisition mode is set to continuous sample. The sampling rate is selected at 2 kHz.

ii. Statistics

The statistics block is used to generate maximum and minimum value and arithmetic mean of the signal input.

iii. Formula

The formula block is used to compute the void fraction and the average voltage formula.

iv. Wait until next ms multiple

This function is to control the execution rate of the program. The program will wait until the value of the millisecond timer becomes a multiple of the specified millisecond multiple. In this program, the timer was set to 100 ms.

v. Waveform chart

The waveform chart function is to display the fluctuation of the input signal with time. Two waveform charts constructed in this program to display the void fraction and the voltage drop. The waveform charts are shown on the front panel.

vi. Numerical display

Numerical display purpose is to display the value of the signal input. In the program, numerical display is used to display the maximum and minimum value, samples of readings and average value. The numerical displays are shown on the front panel.

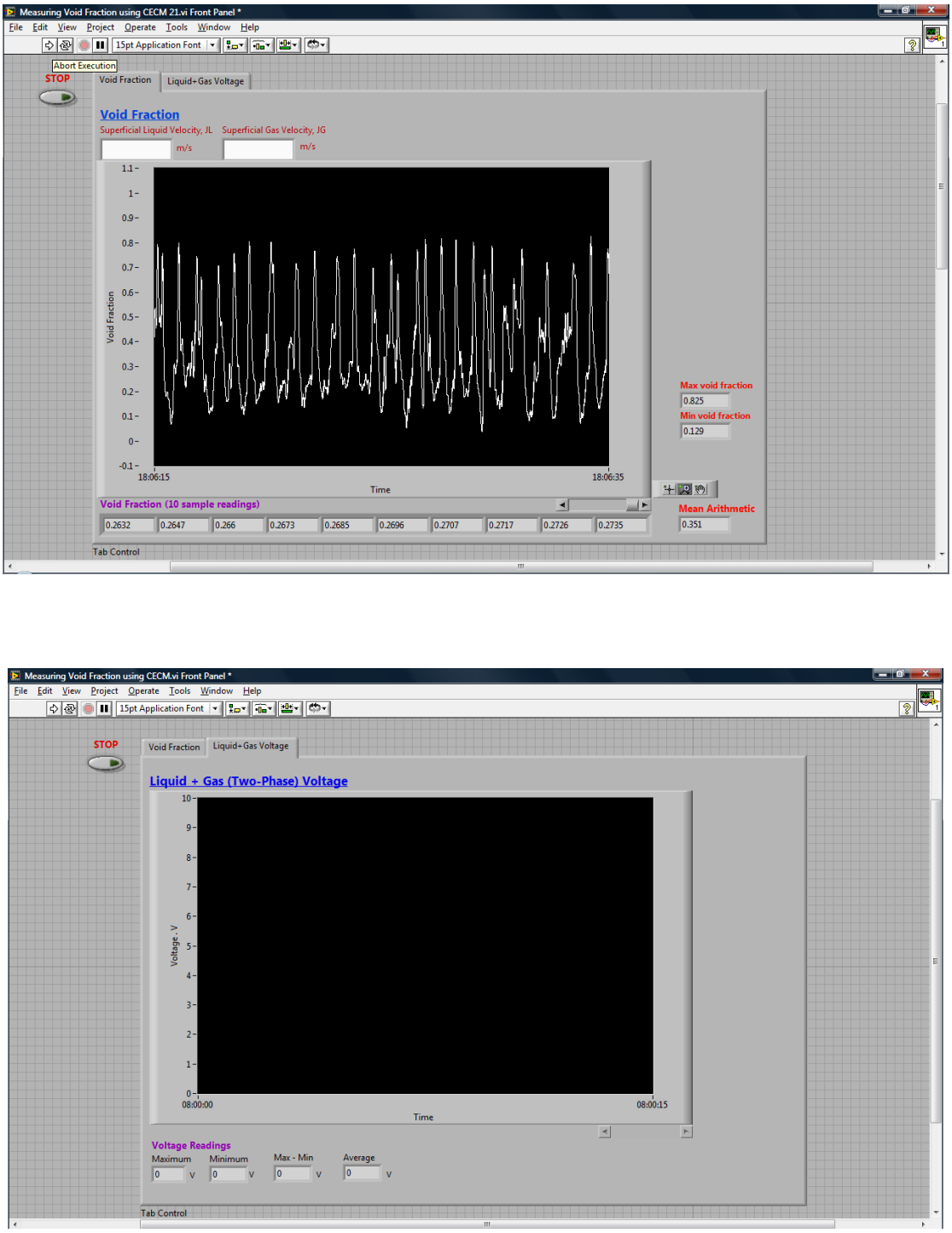

Figure 3.12: The front panel of the void fraction and voltage measurement program

3.5 Data Analysis

3.5.1 Data Collection

The systematic data collection is very important in order to display out all the data without missing and can be interpreted in a correct way and make it easy to understand. For the flow pattern experiment, the data are tabulated manually using a spreadsheet program such as Microsoft Excel and displayed out in form of tables and graphs. The pictures and videos of flow pattern are recorded and saved and tagged referring to their size and gas-liquid velocity. This process is very important to avoid a wrong data collection for the experiment.

In the void fraction measurement, the data are obtained directly from the reading in the LabVIEW front panel after analysis. The result from the reading will then be tabulated in table and displayed out in a graph format. The display data will then be saved in picture format for a further analysis on void fraction experiment and to make sure the originality of the data are well kept for future reference.

3.5.2 Measurement of Uncertainties

The errors that occurred during the experiment were determined and thus gave some impact on the measurement readings and the final results. The most uncertainties that affected the experiment are:

i. Volumetric flow rate

Some difficulties were faced while controlling the valves in order to get the desired volumetric flow rate for air and water. The volumetric flow rate does not stay at one reading for long which caused difficulty in achieving a specific value. The only way to reduce this error is by trying to maintain the volumetric flow rate as close as possible to the desired value.

ii. Water temperature

Conductivity is affected by temperature since water becomes less viscous and ions can move more easily at higher temperatures. In the experiment, the water temperature is maintained at 27 °C. An increase in the water temperature can cause a significant difference in the voltage readings. The temperature increase of the water is caused by the frictional force of the water flowing along the long pipes from the separator which is about 3.0 m above the water reservoir. In addition to that, the dissipation of the heat generated by the pump is also the factor for the increase in water temperature. In order to overcome this problem, the temperature of the water was observed from time to time using thermocouple and also infrared thermometer. If the water temperature increased, the experiment has to be stopped immediately to let the water cool down.

iii. Voltage Drop

Voltage drop is a serious problem in void fraction experiment and can give a big impact to the void fraction result. Furthermore, a small difference will give significant change in a void fraction reading and may get an imprecise result during tabulating data. In order to overcome this problem, the voltage value needs to be observed each time in a single running of the experiment for different velocities.

Chapter 4: Results

4.1 Observation of Two-Phase Flow in Pipes

4.1.1 Vertical Pipes

i. Flow Patterns in 21.0-mm ID Pipe

Figure 4.1 shows the patterns of two-phase flow in 21.0-mm inner diameter pipe size with flow orientation of upward vertical. The patterns were investigated using a high speed camera. In this experiment, all the flow patterns were observed at the section II at position L/D = 53.57 of the pipe. At section 2, the mixture of gas and liquid were completely stable and the bubbles did not coalesce to develop a new pattern. The liquid superficial velocities of two-phase flow in Figures 4.1 (a) - 4.1 (d) are as described.

(a) (b) (c) (d)

Figure 4.1: Flow pattern in 21.0-mm ID vertical pipe
(a) Bubbly flow (j_L = 0.16m/s, j_G = 0.06m/s)
(b) Bubbly-slug flow (j_L = 0.16m/s, j_G = 0.17m/s)
(c) Slug flow (j_L = 0.16m/s, j_G = 0.25m/s);
(d) Churn flow (j_L = 0.16m/s, j_G = 1.0m/s)

As a natural phenomenon, the air was moving faster than water inside the pipe due to the differences of density. From the basic observation of two-phase upward vertical flow with constant liquid superficial velocity, the flow pattern changed with the increase of gas superficial velocity.

At low flow rate of gas and liquid, gas bubbles flowed smoothly inside the liquid and as described in section II, the flow is called the bubbly flow illustrated in Figure 4.1 (a). By increasing the gas flow rate, the number of gas bubbles has increased and the small bubbles then coalesced with each other and occurred in the part of high bubble concentration forming a spherically capped bubble (Figure 4.1 (b)). After increasing the gas flow rate to j_G = 0.25m/s, the percentage of the bubbles that collided and coalesce is really high. The bubbles form a larger bubble, which the bubble diameter is similar to the pipe diameter, the flow is called the bubbly flow (Figure 4.1 (c)).

Lastly, the churn flow was present at high liquid and gas superficial velocity after the breakdown of liquid film in slug flow. The churn flow has an unstable pattern where the liquid motion move oscillatory up and down but still in an upward flow (Figure 4.1 (d)).

ii. Flow Patterns in 47.0-mm ID Pipe

Figure 4.2 showed transition of flow patterns in 47.0-mm inner diameter pipe. The image of flow pattern in Figure 4.2 (a) and 4.2 (b) were captured at the second section of the pipe. Meanwhile, image in Figure 4.2 (c) and 4.2 (d) were located at the section III of the pipe. This was due to the slug and the churn flow were still not developed at the section II and III at fixed liquid superficial velocity. The liquid superficial velocities in Figure 4.2 (a) - 4.2 (d) were fixed to show the effect of gas

superficial velocity to the flow pattern. The gas superficial velocity, j_G were increased from lowest velocity in Figure 4.2 (a) to highest velocity in Figure 4.2 (d) at range of 0.06 m/s -2.20 m/s.

(a) (b) (c) (d)

Figure 4.2: Flow pattern in 47.0-mm ID vertical pipe
(a) The Bubbly flow (j_L = 0.16m/s, j_G = 0.06m/s)
(b) The bubbly-slug flow (j_L = 0.16m/s, j_G = 0.17m/s)
(c) The slug flow (j_L = 0.16m/s, j_G = 0.40m/s)
(d) The churn flow (j_L = 0.16m/s, j_G = 2.20m/s)

In some cases of fixed gas and liquid superficial velocity, various flow patterns could be observed along the pipe and the patterns changed at the different sections inside the pipe. Usually, flow pattern was developed from bubbly flow at the lower part to slug or churn flow at the upper part of the channel. In larger pipe such as in the 47.0-mm ID pipe, the flow pattern was easy to observe rather than the flow pattern inside 21.0-mm pipe. The bigger pipe size allows the bubbles to distribute and spread evenly in all parts of the channel.

By comparing to the 21-mm ID pipe, the maximum length of slug was shorter. The possibility of slug flow liquid film to breakdown in larger pipe was higher compared to the small pipe. As shown in Figure 4.2 (a) the bubbles were much difficult to coalesce inside the 47.0-mm pipe rather than 21.0-mm pipe to develop a bubbly slug flow. At higher gas superficial velocities, slug flow developed slowly in a 47.0-mm ID pipe as shown in Figure 4.2 (b), to form bubbly-slug flow. Then a clear slug flow developed as a result of bubbles coalescences that form bubbles at the size which is the same diameter of the channel (Figure 4.2 (c)).

The characteristic of each flow patterns were examined and tabulated in a table as flow pattern maps in Chapter 4.2. Churn flow in this pipe was presented at the upper part of the pipe with the high gas superficial velocity because of the effect of L/D ratio of the pipe (Figure 4.2 (d)).

iii. Flow Patterns in 95.0-mm ID Pipe

The flow pattern of two-phase flow inside the 95.0-mm ID pipe was difficult to observe in the upward vertical flow inside the pipe. The flow pattern transition was fuzzy to observe with the naked eyes. In this experiment, the gas bubbles were difficult to merge up caused by the rate of coalescences that was low. Another reason might be because of the liquid film was easy to break down inside a large diameter pipe. This situation makes the slug flow pattern difficult to develop and to observe. The observation of the flow pattern needs help from a high speed camera to determine the existence of the exact flow patterns.

(a) (b) (c) (d)

Figure 4.3: Flow pattern in 95.0-mm ID vertical pipe
(a) The bubbly flow (j_L = 0.16m/s, j_G = 0.02m/s);
(b) The bubbly-slug flow (j_L = 0.16m/s, j_G = 0.09m/s);
(c) The slug flow (j_L = 0.16m/s, j_G = 0.15m/s);
(d) The churn flow (j_L = 0.16m/s, j_G = 0.50m/s)

Figure 4.3 shows the transition of flow patterns inside the 95.0-mm ID pipe at a constant liquid superficial velocity with a slow increase of the air superficial velocities. All the images of two-phase flow were captured at the section II, L/D = 23.94 of pipe. The bubbly flow appeared in almost spherical shape at low superficial velocity profile shown at Figure 4.3 (a).

The increase of air superficial velocity resulted an overall high flow velocity. The dense of the bubble packed around together and the pattern was stated to change and forming bubbly-slug flow (Figure 4.3 (b)). The bubbly-slug transition pattern was difficult to observe by normal DSLR camera, however the aid of a high speed video camera helped in determining the flow pattern.

At higher gas superficial velocities, a clear slug flow developed as a result of bubbles coalescences that form bubble at size of the same diameter of the channel. The

slug flow was hard to detect in 95.0-mm ID pipe. It formed a short length slug and easily broke down to form churn flow. The slug flow is in Figure 4.3 (c). Churn flow consisted of oscillating bubble and turbulent wave was observed after increasing the gas superficial velocity as shown in figure 4.3 (d). In a real industrial application, the slug and churn flow were extremely undesirable patterns, because of their unsteadiness and those rapid changes influenced many processes.

4.1.2 Horizontal Pipes

i. Flow Patterns in 21.0-mm ID Pipe

The flow pattern experiment for the 21.0-mm ID pipe showed a few types of the flow pattern. The flow pattern was depend largely on the liquid and gas superficial velocity flowed through the pipe. By comparing with the upward vertical two phase flow, the horizontal flow had some differences that was caused by the gravitational effect. Since water is heavier than air, it will flow at the bottom of the pipe while the air flow at the top of the pipe.

The mixture of the two phase air-water flow mostly occurred at the beginning of the pipe at the section I (L/D = 17.86). At this point, the pattern was in dispersed bubbly flow. After some time, the bubbles started flowing up to the top of the pipe to develop a new pattern either bubbly, plug, slug, wavy or stratified flow. The bubbles began to coalesce with each other to develop a new pattern and then fully separated from the water at the top of the pipe.

Figure 4.4 showed the entire patterns that occurred during the experimentation inside the 21.0-mm ID horizontal flow. Figure 4.4 (a) illustrated the stratified flow inside the pipe. This type of flow pattern obtained at the low liquid and gas superficial velocity where there was a clear separated line between the liquid and gas phases. The

wavy flows occurred when increasing a gas superficial velocity at a low liquid superficial velocity. The wavy flow is shown in Figure 4.4 (b). At this point, the flowing gas flow is faster than above water inside the pipe and developed the wavy pattern at the surface of the water.

Figure 4.4 (c) showed the dispersed bubbly flow. The flows mostly happen at the section I (L/D = 17.86) of the pipe. The liquid superficial velocity was high enough and the gas superficial velocity was low and lead to development of a small dispersed bubble inside the pipe. The small bubble coalesced with each other and moved up to the top of the pipe and developed a bubbly flow after some time (Figure 4.4 (d)). Small bubbles can be seen flowing at the top of the flow channel.

Small bubbles merged with each other and developed a bigger bubble that is called a plug flow. The plug flow is shown in Figure 4.4 (e). The plug flow can easily be seen with slightly higher gas and liquid superficial velocity at section II (L/D = 53.57), III (L/D = 89.29) and IV (L/D = 125.0). A further increase of gas and liquid superficial velocity caused the plug flow to become bigger enough to touch the bottom of the flow channel. This pattern is called the slug flow and it is shown in Figure 4.4 (f). This phenomenon can be called the water hammer effect. The flow was rough and turbulence flow occurred at the tail of each slug. This flow pattern mostly happened at section III (L/D = 89.29) and IV (L/D = 125.0) of the pipe.

Figure 4.4 (g) shows an annular flow inside the 21.0-mm ID horizontal pipe. The annular flow can be achieved at high gas superficial velocity and out of the range of the experimental limit, where minimum gas superficial velocity was at 43.0 m/s to obtain the annular flow. Therefore, if the liquid superficial velocity increases, the gas

superficial velocity also needed to be increased to obtain this pattern. To get this pattern, the L/D ratio must high enough and just can be achieved in the 21.0-mm ID pipe in this experiment.

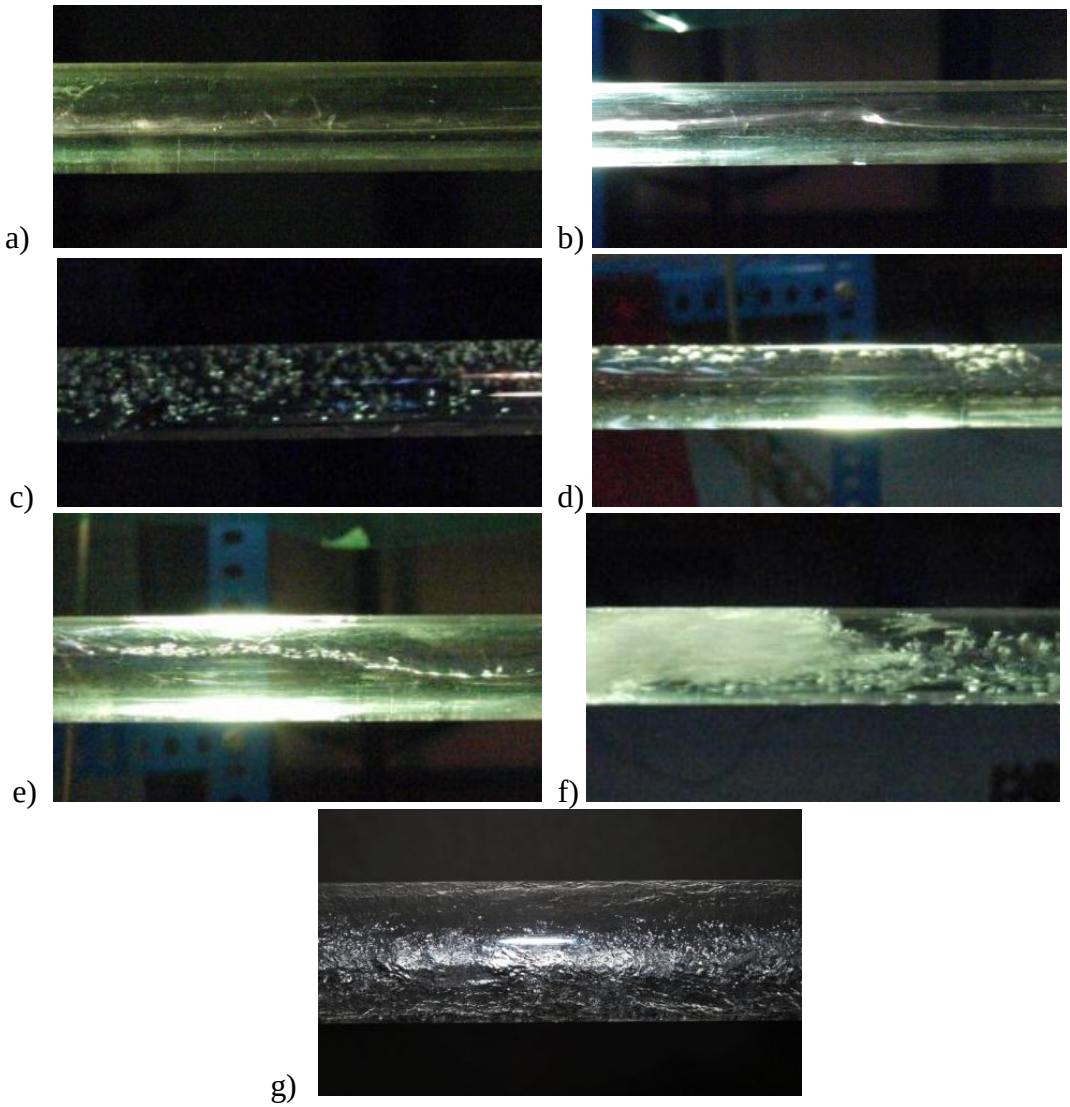

Figure 4.4: Flow pattern in 21.0-mm ID horizontal pipe
(a) The stratified flow (j_L = 0.4m/s, j_G = 0.05m/s),
(b) The wavy flow (j_L = 0.2m/s, j_G = 1.2m/s),
(c) Dispersed Bubble (j_L = 2.0m/s, j_G = 0.05m/s),
(d) The bubbly flow (j_L = 2.0m/s, j_G = 0.05m/s),
(e) The plug flow (j_L = 1.0m/s, j_G = 0.4m/s),
(f)The slug flow (j_L = 2.0m/s, j_G = 2.0m/s),
(g) The annular flow (j_L = 0.4m/s, j_G = 43.0m/s)

ii. Flow Patterns in 47.0-mm ID Pipe

The total length of the 47.0-mm ID pipe horizontal flow experiment is 3 meters is the same as the 21.0-mm ID pipe. Therefore, the difference of the L/D ratio for the 47.0-mm pipe is smaller than the ratio L/D for the 21.0-mm pipe. The flow pattern for the 47.0-mm ID pipe showed some differences from the 21.0-mm pipe where the 47.0-mm ID pipe needed longer distance to develop a new pattern. Furthermore the limitation of the experimentation equipment limited the flow rate of the water and air supply.

Figure 4.5 showed the flow pattern of two-phase horizontal flow inside the 47.0-mm ID pipe. The flow pattern inside the 47.0-mm pipe was much easier to observe compared to 21.0-mm pipe. The coalescences of the bubble were clearer to observe inside the larger pipe, with less coalescences frequency. As a result, the pattern transition was difficult to happen since more length is needed for the bubble to coalesce and develop a new pattern.

Figure 4.5 (a) showed the wavy flow pattern inside the 47.0-mm ID pipe. The wavy flow happened when the gas velocity was higher than the water velocity inside the pipe. Inside the larger pipe, the separation of the wavy flow was clearer than in a smaller pipe. Figure 4.5 (b) showed the slug flow inside the 47.0-mm pipe. Both gas and liquid superficial velocity was high enough to develop the slug flow pattern.

The stratified flows in Figure 4.5 (c), occurred when both the gas and liquid superficial velocity was low. The flow was smooth and has a clear separated line between liquid and gas phases. The dispersed bubble only happened at the section I of the pipe when the liquid superficial was high enough and a small quantity of air spray inside the pipe. The small bubbles were moving fast before coalescing with each other

and developing a bigger bubble. After a few periods in section II (L/D = 23.94), III (L/D = 39.89) and IV (L/D = 55.85), the bubbles moved to the top of the pipe and developed a new flow pattern such as a bubbly flow.

The bubbly pattern inside the 47.0-mm pipe can be observed when the small bubble moved to the top of the pipe caused by gravity. The bubbly flow is shown in figure 4.5 (d) with high liquid superficial velocity and low gas superficial velocity. However, the annular flow cannot be achieved during the experiment of 47.0-mm ID pipe two-phase horizontal flow.

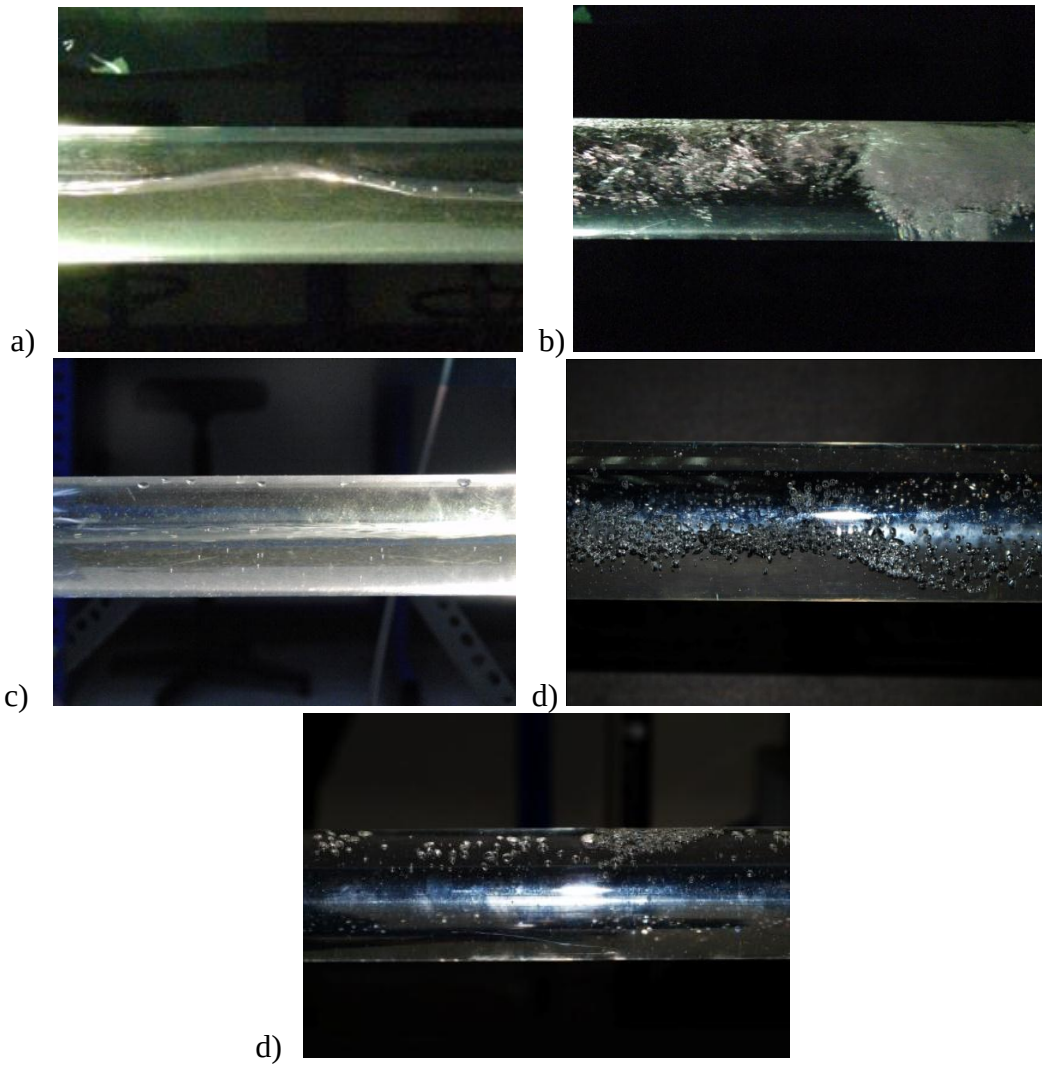

Figure 4.5: Flow pattern in 47.0-mm ID horizontal pipe
(a) The wavy flow (j_L = 0.2m/s, j_G = 0.8m/s);
(b) The slug flow (j_L = 1.0m/s, j_G = 1.2m/s);
(c) The stratified flow (j_L = 0.2m/s, j_G = 0.4m/s);
(d) The dispersed bubbly flow (j_L = 1.6m/s, j_G = 0.1m/s);
(e) The bubbly flow (j_L = 1.4m/s, j_G = 0.5m/s)

iii. Flow Patterns in 95.0-mm ID Pipe

Figure 4.6 depicted the flow patterns inside the 95.0-mm ID pipe. The patterns observed inside the 95.0-mm ID pipe were only the stratified and wavy flow. The experiment could not observe other patterns inside the 95.0-mm ID pipe. The maximum flow rate was the same inside as the 47.0-mm and 21.0-mm ID pipe but the superficial velocity was different.

At low liquid superficial velocity below 0.3 m/s the flow was in the stratified pattern (Figure 4.6 (a)). The flow was smooth and stable and has no disturbance. After an increased of the liquid and gas superficial velocity, the flow pattern changed to the wavy flow. The smooth stratified flow was disturbed by the flow of the gas and formed the wavy flow and it is shown in Figure 4.6.

a) 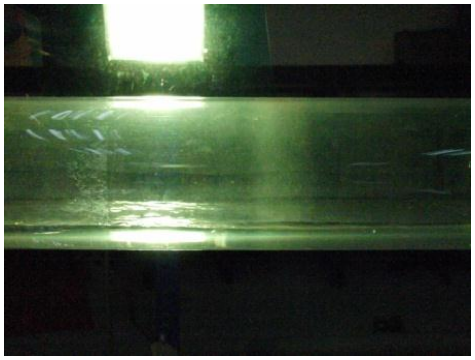 b) 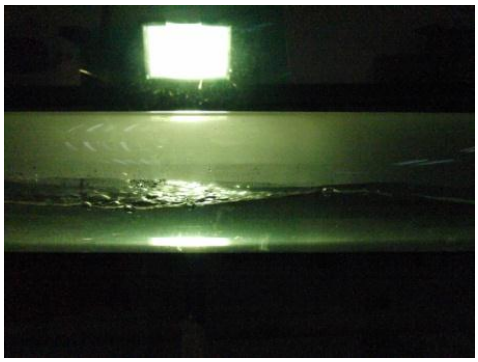

Figure 4.6: Flow pattern in 95.0-mm ID horizontal pipe
(a) The stratified flow (j_L = 0.14m/s, j_G = 0.1m/s)
(b) The wavy flow (j_L = 0.35m/s, j_G = 0.1m/s)

In the 95.0-mm ID pipe, two-phase horizontal flow experiment, the maximum liquid and gas superficial velocity were too low and the L/D ratio was also very small. This limitation was due to the low pumping and compression power that resulted in very low gas and liquid volume in the pipe. From the Figure 4.7, it can be seen that inside the 95.0-mm ID pipe was not fully filled up by the water, and the level of water was dropped after a few centimeters from the mixer.

Figure 4.7: The 95.0-mm ID pipe was not fully filled up

4.2 Flow Pattern Maps in Pipes

4.2.1 Flow Maps inside the Vertical Pipes

i. Flow maps inside 21.0-mm ID pipe

In this experiment, the flow patterns were observed in 21.0-mm ID pipe. The flow type was upward vertical flow. The water superficial velocities, j_L range were set from 0.08 m/s – 1.0 m/s and the air superficial velocities, j_G range were set from 0.06 m/s – 2 m/s respectively. The flow patterns were observed using the DSLR still camera and high speed video camera with a proper lighting system. The observations were made at each section from section I to section IV.

Figure 4.8 to figure 4.11 shows the flow pattern map inside the 21.0-mm ID pipe, upward vertical flow. In these figures, the flow pattern differed at every section inside the pipe. At low gas superficial velocities, the collision frequency of the bubble was very low and the bubbly pattern stayed for a few periods until merging up to form bigger bubbles. The bubbles in this pipe were almost uniformly distributed and the shapes were small and near spherical as shown in Figures 4.1(a). This situation mostly happened at the early section of the pipe. In this experiment, the bubbly flow mostly happened at sections I (L/D = 17.86) of the pipe and the bubbly pattern stayed at this section until the gas superficial velocity reached 0.5 m/s. Bubbly flow formed at all sections at low gas superficial velocity below 0.04 m/s with all range of liquid superficial velocities.

Figure 4.8 showed the flow pattern at section I (L/D = 17.86) inside the 21.0-mm ID pipe. From the flow map, it can be observed that the bubbly flow emerged when the gas superficial velocity was below 0.5 m/s. As the gas superficial velocity increased, the bubbles concentration in the bubbly flow became higher. The distribution of the

bubbles were not uniform anymore and easy to coalesce. Spherically capped bubbles were formed as the coalescence of small bubbles occurring irregularly in the high bubble concentration area. This bubbly-slug flow can be found at all sections inside the 21.0-mm pipe at specific liquid and gas superficial velocity. This pattern can be observed clearly at section I (L/D = 17.86) and section II (L/D = 53.57) during the experiment and almost completely end after increasing the liquid and gas superficial velocity. The area of the bubbly-slug flow was small inside the flow pattern map because the bubbly slug flow is the transition pattern between the bubbly and slug flow.

With the increasing gas superficial velocity, the bubble coalescence happened rapidly until the diameter of the bubble becomes as big as the pipe. This pattern shaped like a large bullet bubble namely slug flow as shown in Figure 4.1 (c). For this experimentation, inside 21.0-mm ID pipe, the slug flow started to develop at section IV (L/D = 125.0) of the pipe when the liquid superficial velocity j_L = 0.16 m/s and gas superficial velocity is j_G = 0.06 m/s. It fully occupied sections 2 (L/D = 53.57) to section IV (L/D = 125.0) when the gas superficial velocity reached 0.5 m/s. The slug flow appeared at all sections inside the pipe at specific gas and liquid superficial velocity.

The churn flow was the last flow pattern that observed during this experiment inside the 21.0-mm ID pipe. As the gas superficial velocity became very high, the structure of the two-phase flow became unstable with the liquid travelling up and down in oscillatory manner. The churn flow pattern was one of the phenomena that should be avoided in the two-phase industrial application because of the destructive consequences on the piping system made by the mass of the slugs. In this experiment, the churn flow can be observed at all sections with specific gas and liquid superficial velocity. The churn flow pattern mostly occurred in the flow maps when the gas superficial velocity

was high. From the Figure 4.10 and 4.11, the flow map at section III (L/D = 89.29) and section IV (L/D = 125.0) were similar because the two-phase flow started to be stable inside the pipe.

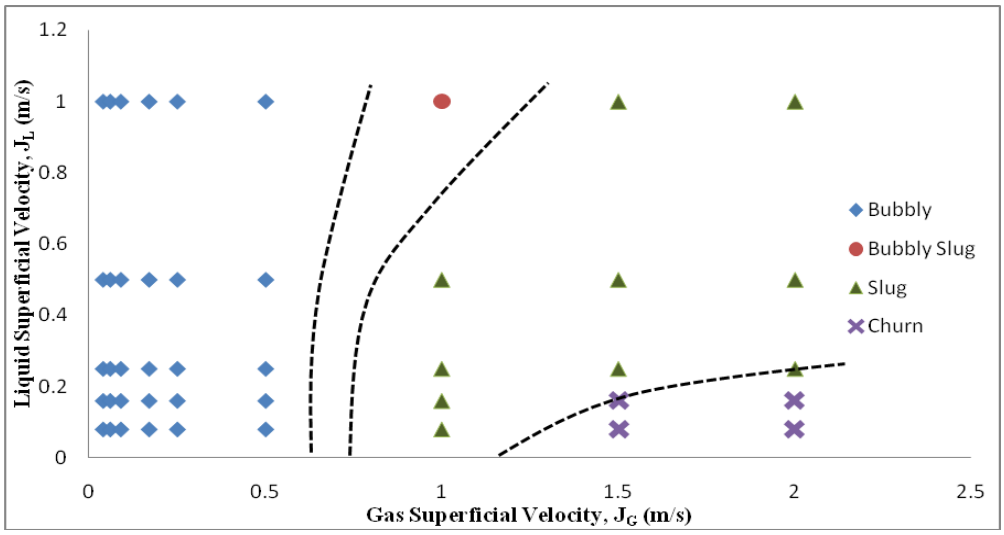

Figure 4.8 : Flow pattern map for section I (L/D = 17.86) of 21.0-mm ID pipe

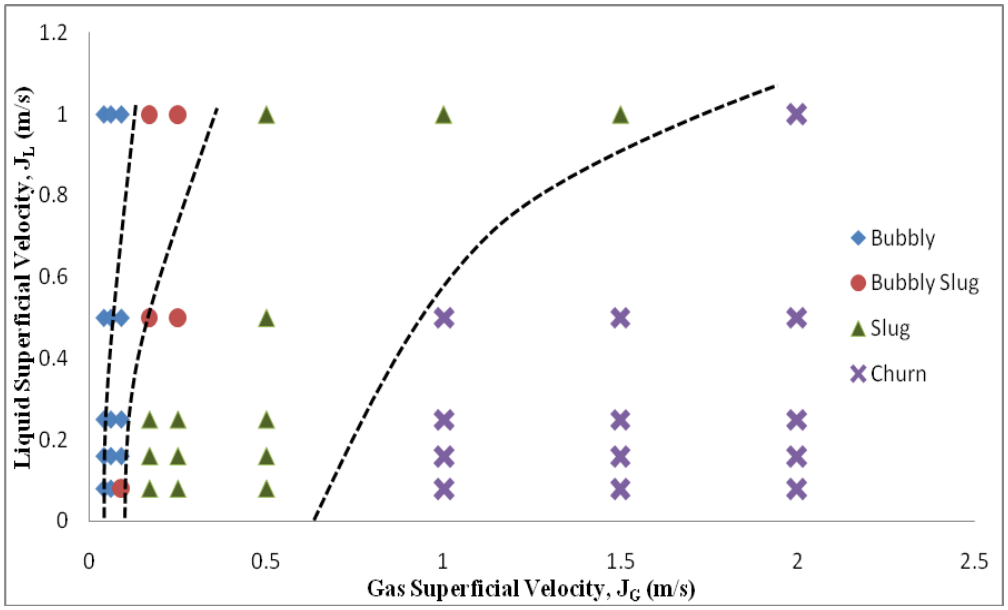

Figure 4.9 : Flow pattern map for section II (L/D = 53.57) of 21.0-mm ID pipe

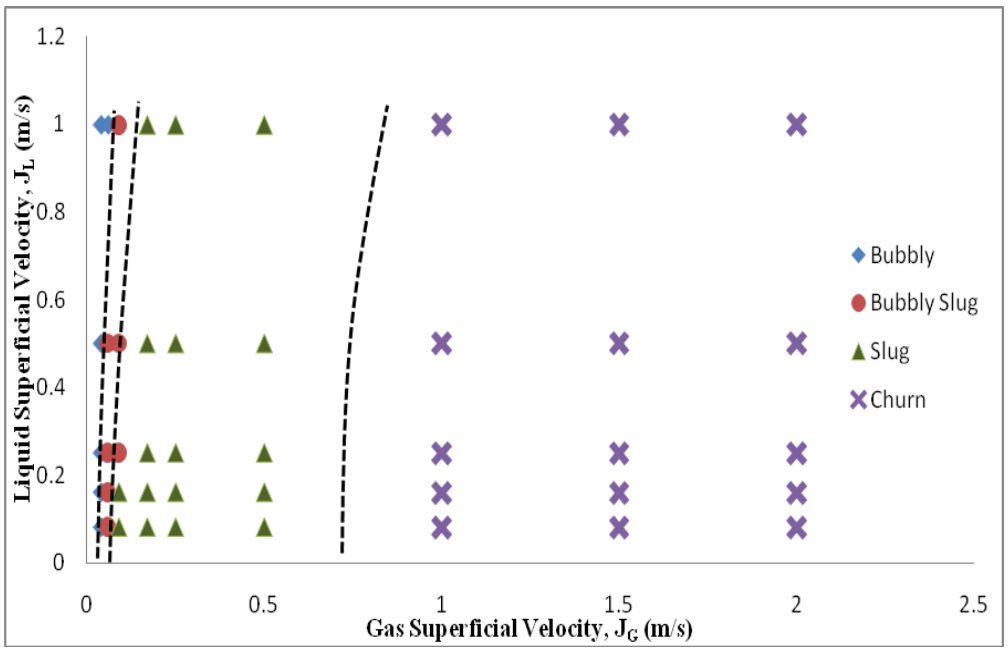

Figure 4.10 : Flow pattern map for section III (L/D = 89.29) of 21.0-mm ID pipe

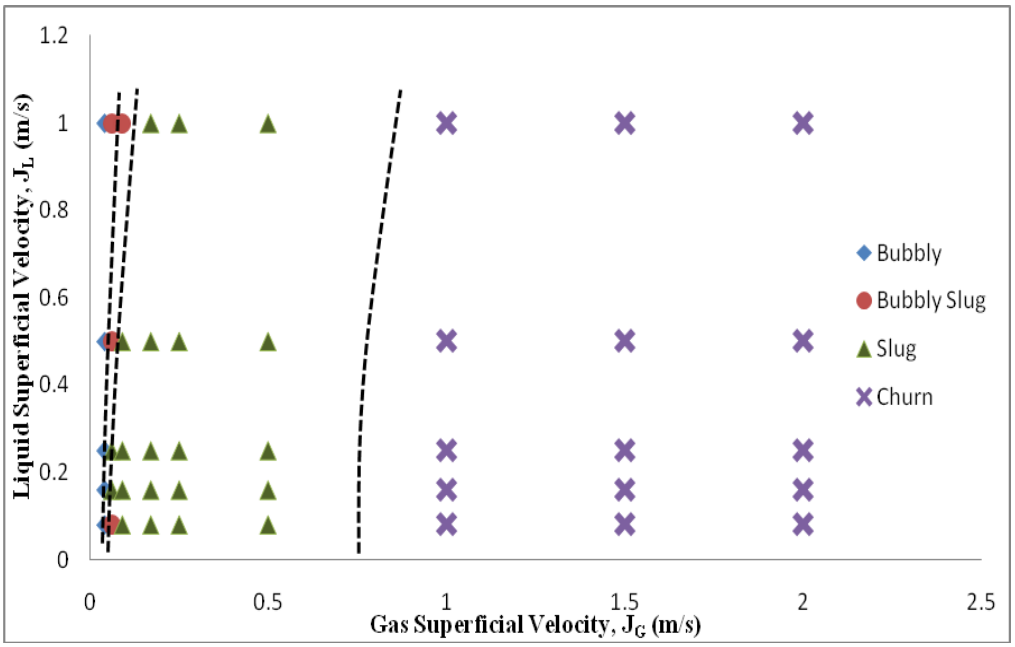

Figure 4.11 : Flow pattern map for section IV (L/D = 125.0) of 21.0-mm ID pipe

ii. Flow maps inside 47.0-mm ID pipe

In the experiment of flow mapping for the upward vertical flow inside the 47.0-mm ID pipe, the water superficial velocities, j_L range were set between 0.08 m/s and 1.0 m/s and the air superficial velocities, j_G range are set from 0.04 m/s and 2.0 m/s respectively. The observation was clearer than the observation inside the 21.0-mm pipe by visual and photographic method. Figures 4.12 - 4.15 show the flow mapping at each section, from section I (L/D = 7.98) to section IV (L/D = 55.58) inside the 47.0-mm ID pipe.

From these figures, the flow patterns have shown small differences due to minor changes in L/D ratio at each section. The bubbles in this pipe were small in shape and uniformly distributed upward as shown in Figure 4.2 (a). Most of the bubbles inside the 47.0-mm ID pipe were smaller than the one inside the 21.0-mm ID pipe. This flow pattern mostly occurred at high liquid superficial velocity and low gas superficial velocities. The percentage of bubbles coalesced inside the 21.0-mm pipe was higher than inside the 47.0-mm pipe and therefore the size of the bubbles became bigger after the coalescence. On the other hand, at low gas superficial velocity below than 0.1 m/s, the bubbly pattern took place at all sections of the pipe at any liquid superficial velocity. At this range, as the collision frequency of the bubble is very low and this pattern would stay, until the bubble started to collide and coalesce.

A spherically capped bubble formed as the coalescence of the small bubbles occurred irregularly in the high bubble concentration area as the gas superficial velocity increased. This bubbly-slug pattern occurred at all sections of the 47.0-mm ID pipe when the gas superficial velocity was low and starts to develop at other sections as the

gas superficial velocity increased. From the flow mapping, it can be observed that this pattern took part at a small range of the gas superficial velocities

With the increasing of the gas superficial velocity, the bubble concentration became higher and the bubbles collided rapidly and the bubbles diameter gradually increased close to the size pipe diameter. Referring to Figures 4.12 - 4.15, the slug flow took part at all sections. The slug flow first appeared at section III (L/D = 39.89) and section IV (L/D = 55.85) of this pipe when the gas velocity was still low and began to occur at other sections as the gas superficial velocity increased. The slug flow took place at all sections when the gas superficial velocity reached 0.5 m/s.

The churn flow was also observed inside this 47.0-mm pipe during the experiment and it occurred at a high range of gas superficial velocity. From Figures 4.12 - 4.15, the churn flow pattern appeared after the gas superficial velocity exceeding 0.8 m/s at all sections inside the pipe with a liquid superficial velocity below 0.4 m/s. At the high range of gas superficial velocities which was at 1.1 m/s to 2.0 m/s the churn flow pattern occurred at all sections at any liquid superficial velocity

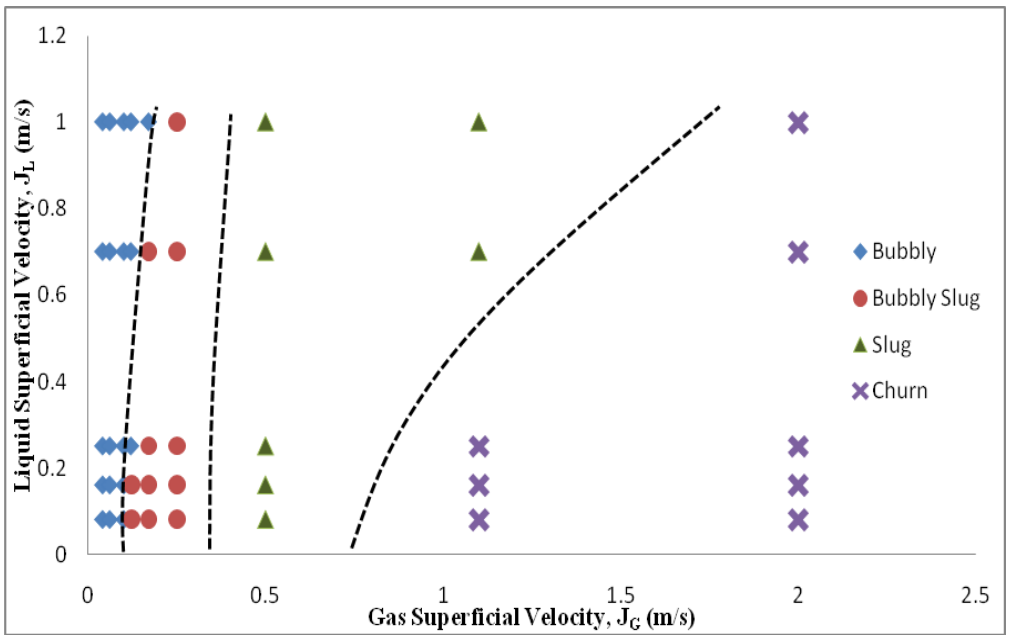

Figure 4.12 : Flow pattern map for section I (L/D = 7.98) of 47.0-mm ID pipe

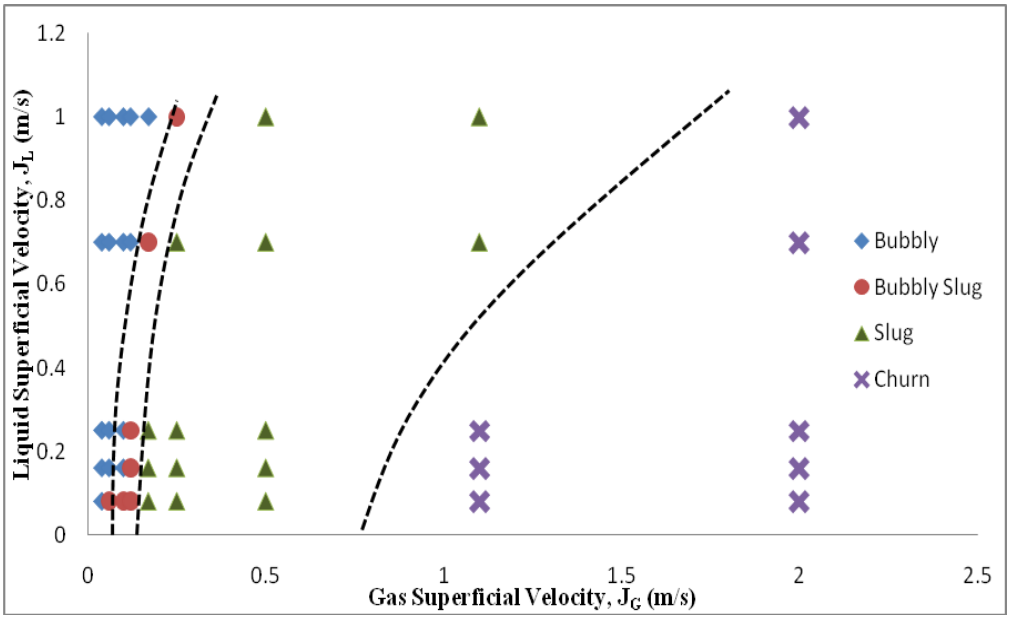

Figure 4.13 : Flow pattern map for section II (L/D = 23.94) of 47.0-mm ID pipe

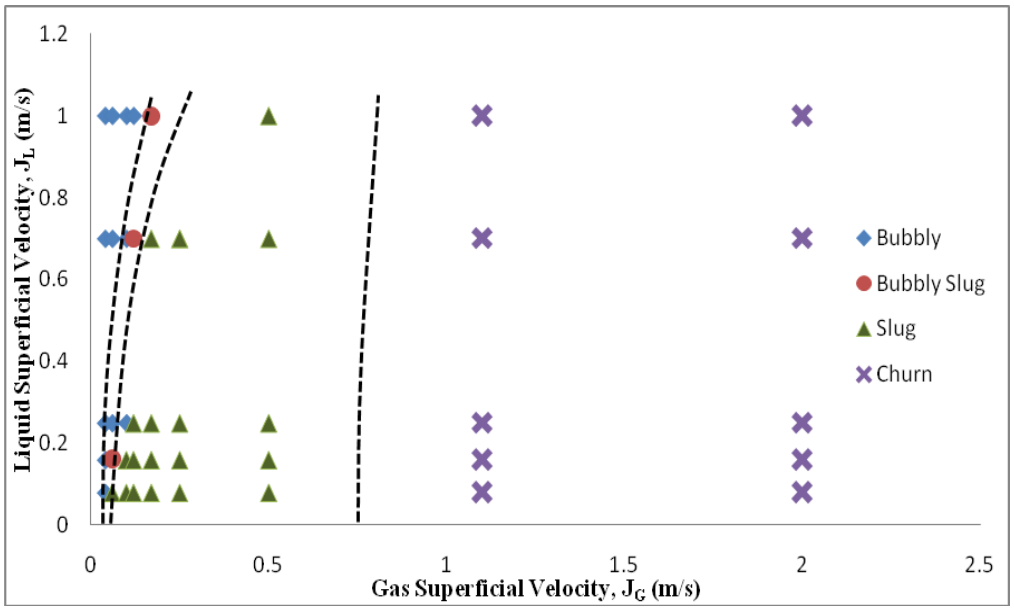

Figure 4.14 : Flow pattern map for section III (L/D = 39.89) of 47.0-mm ID pipe

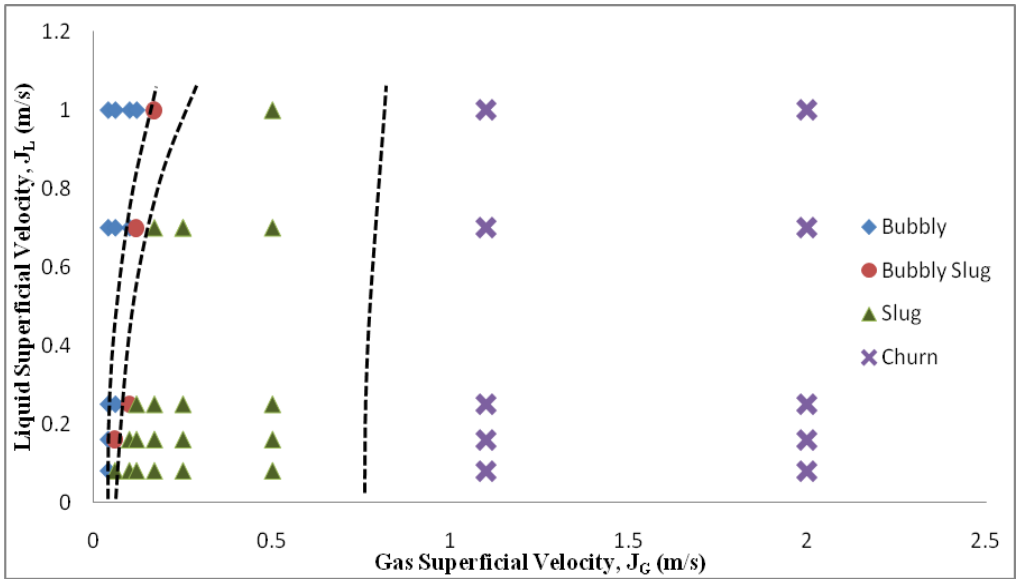

Figure 4.15 : Flow pattern map for section IV (L/D = 55.85) of 47.0-mm ID pipe

iii. Flow maps inside 95.0-mm ID pipe

The next upward vertical flow experiment was the flow mapping for the flow pattern observation inside the 95.0-mm ID pipe. The water superficial velocities, j_L range was set from 0.006 m/s – 0.25 m/s and the air superficial velocities, j_G range was set from 0.006 m/s – 0.5 m/s. The gas and liquid superficial velocities range were small because of the limitation of the equipment to supply the higher rate of gas and liquid flow that were needed for the experimentation. The flow pattern transition inside the 95.0-mm pipe was difficult to observe compared to the flow pattern inside the 21.0-mm and 47.0-mm pipes. Figures 4.16 - 4.19 showed the flow mapping of the upward vertical flow inside the 95.0-mm ID pipe at section I (L/D = 3.95) to section IV (L/D = 27.63).

The bubble in this pipe was very small compared to the previous 21.0-mm and 47.0-mm pipes. The bubbles were also very uniformly distributed and flowing upward as shown in Figure 4.3 (a). This bubbly flow pattern occurred when the liquid superficial velocity was high and at low gas superficial velocities. From Figures 4.16 - 4.19, it can be observed that the bubbly flow took part at every section when the gas superficial velocity below 0.04 m/s and the liquid superficial velocity, j_L range from 0.006 m/s to 0.25 m/s. The bubbly flow pattern was dissolved when the gas superficial velocity was increased.

With the increasing gas superficial velocity, the number of bubbles also grew. The distribution of bubbles was not uniform anymore and as a result some areas might have high concentration of bubbles. The spherically capped bubble was formed when the small bubbles in the high bubble concentration areas coalesced. This bubbly-slug flow pattern occurred at section I (L/D = 3.95) and section II (L/D = 11.84) mainly

when the gas superficial velocity, j_G were in the range of 0.17 m/s to 0.25 m/s. At section III (L/D = 19.74) and section IV (L/D = 27.63), the bubbly-slug flow occurred mainly when the gas superficial velocity, j_G range from 0.06 m/s to 0.09 m/s.

With the gas superficial velocity kept increasing, the bubbles concentrations also grew higher. The rates of coalescence of the bubbles were high and developed a bigger bubbly until the diameter of the bubble became as big as the diameter of the pipe. From this experiment, it can be observed that the length of the slug pattern was shorter compared to the previous 21.0-mm and 47.0-mm pipes with lower gas superficial velocity. This phenomenon happened because the slug flow pattern was easily break down and developed the churn flow pattern inside the larger pipe. The slug flow occurred at all sections with a specific gas and liquid superficial velocity. At section I (L/D = 3.95) and section II (L/D = 11.84), the slug flow pattern only occurred after the gas superficial velocity more than 0.15 m/s and at section III (L/D = 19.74) and section IV (L/D = 27.63) the slug flow pattern occurred after the gas superficial velocity was more than 0.08 m/s.

As the gas superficial velocity became very high, the structure of the two-phase flow became unstable inside the pipe. The churn flow took part at all sections after the breakdown of the slug flow inside the pipe. The liquid flow moved in oscillatory fashion upward down but the overall flow were moving upward .The transition from the slug flow to the churn flow inside the 95.0-mm pipe was very fast compared to the previous 21.0-mm and 47.0-mm pipes, as churn flow was often occurred in wide-bore pipe. Normally, the churn flow develops at high gas superficial velocity with low liquid superficial velocity. From the observation, the churn flow started to occur at section III (L/D = 19.74) and section IV (L/D = 27.63) after the gas superficial velocity, j_G was

more than 0.17 m/s and the liquid superficial velocities, j_L range was from 0.006 m/s to 0.03 m/s. The churn flow started to take place at sections I (L/D = 3.95) and section II (L/D = 11.84) when increasing the gas superficial velocity more than 0.5 m/s.

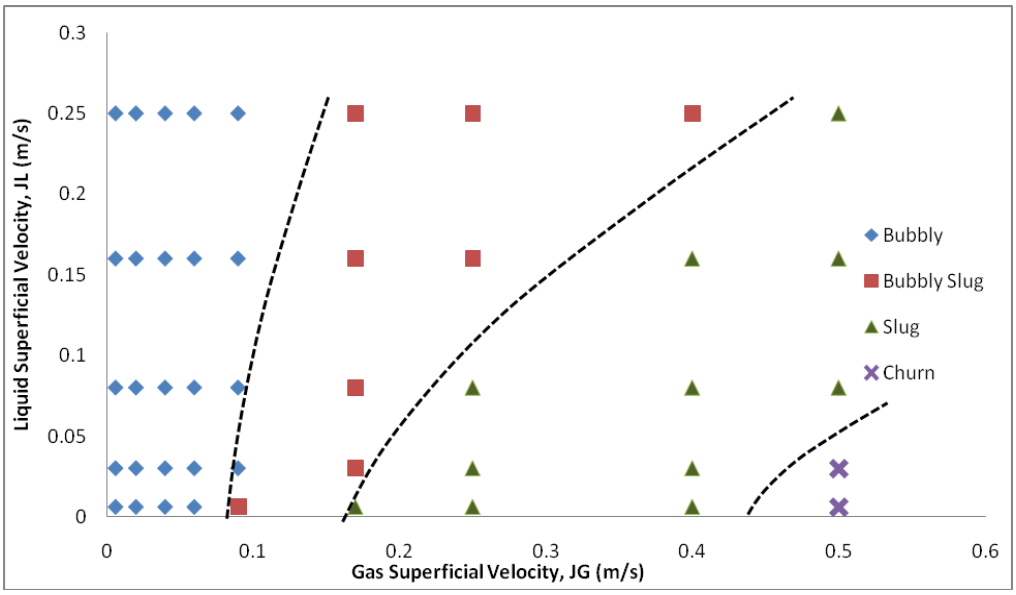

Figure 4.16 : Flow pattern map for section I (L/D = 3.95) of 95.0-mm ID pipe

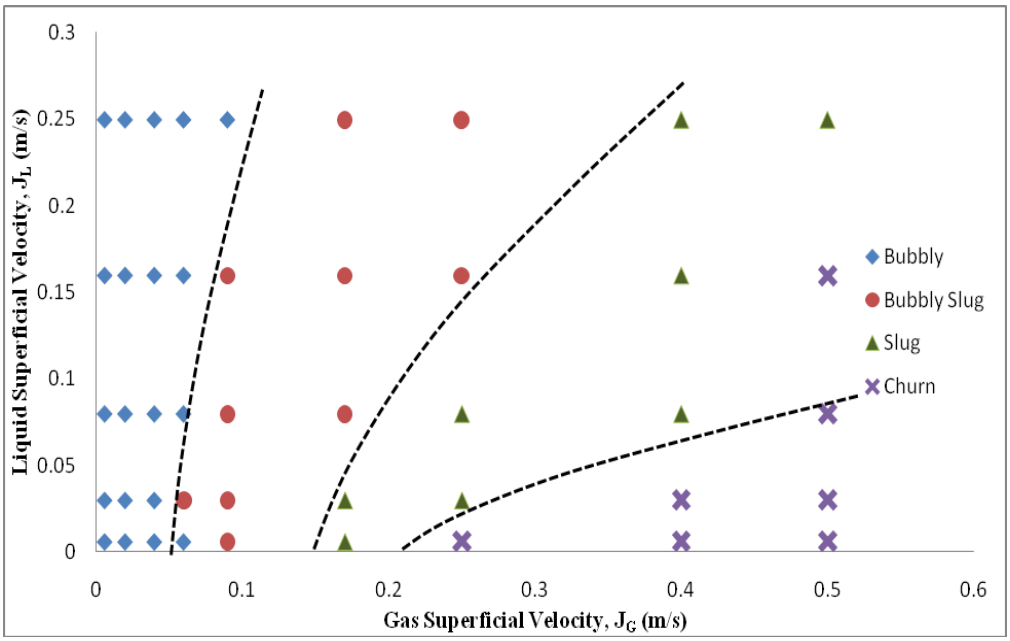

Figure 4.17 : Flow pattern map for section II (L/D = 11.84) of 95.0-mm ID pipe

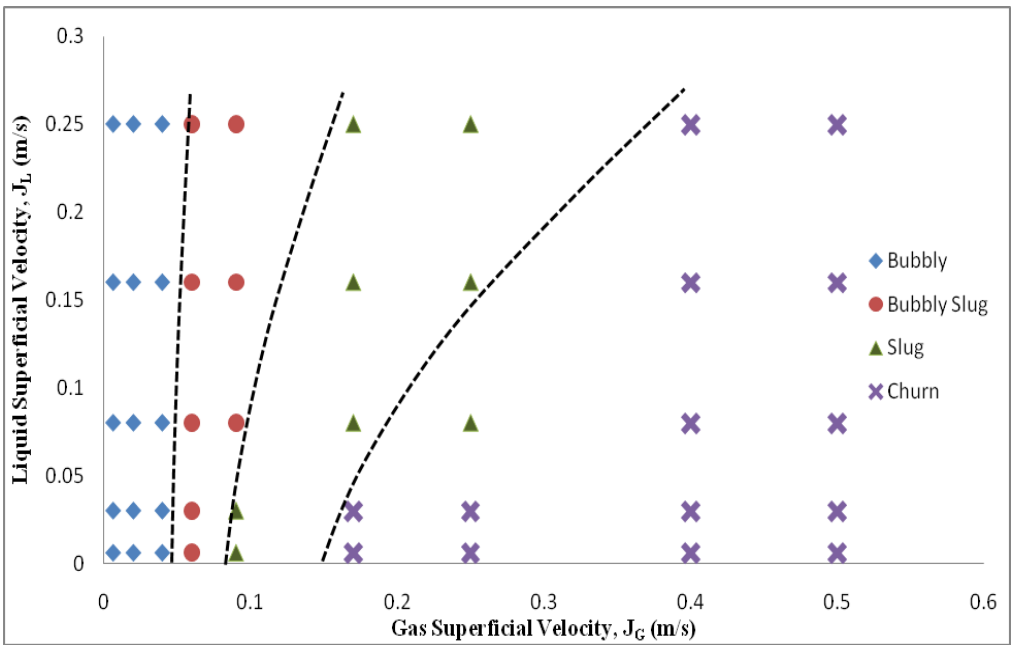

Figure 4.18 : Flow pattern map for section III (L/D = 19.74) of 95.0-mm ID pipe

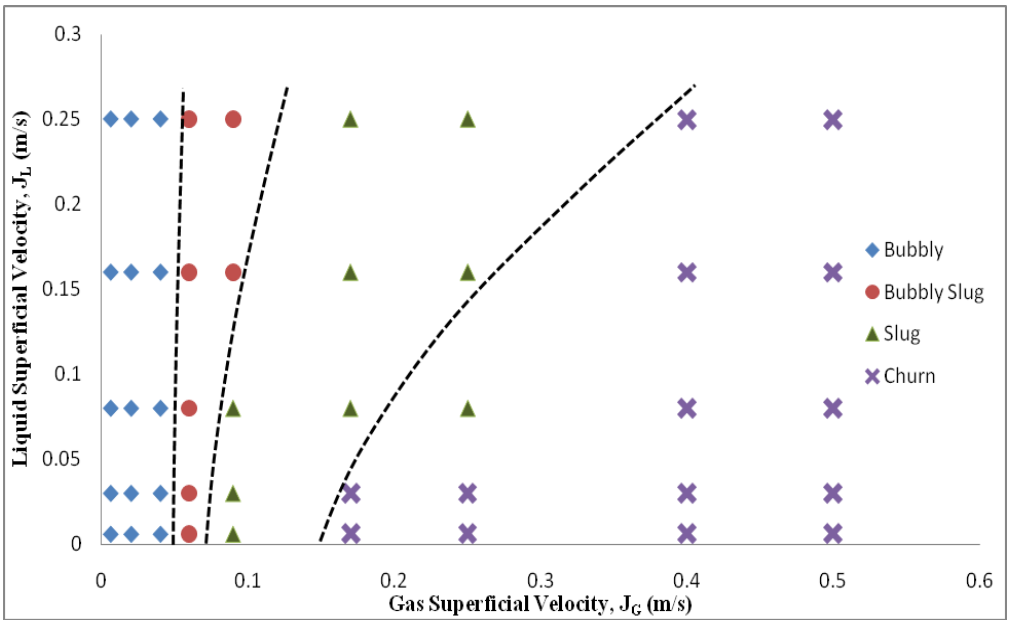

Figure 4.19 : Flow pattern map for section IV (L/D = 27.63) of 95.0-mm ID pipe

4.2.2 Flow Maps inside the Horizontal Pipes

i. Flow maps inside 21.0-mm ID pipe

In this research, works were also being carried out to investigate the flow pattern mapping for the horizontal pipes. The experiment was similar to the previous upward vertical flow, with 4 sections and repeated for 3 difference pipes of 21.0-mm, 47.0-mm and 95.0-mm inner diameter pipes. The horizontal flow differed from the upward vertical flow due to gravitational effect. Therefore, the type of flow patterns for the horizontal flow should have different patterns compared to the upward vertical flow experiment.

Figures 4.20 - 4.23 showed the flow mapping for the two-phase horizontal flow inside the 21.0-mm ID pipe. Each figure showed each section of the pipe from section I (L/D = 17.86) to section IV (L/D = 125.0). The range of gas superficial velocity was at 0.05 m/s to 2.0 m/s while for the liquid superficial velocity was from 0.05 m/s to 3.0 m/s. From Figures 4.20 - 4.23, at every section, the stratified flow occurred at a low gas and liquid superficial velocity as the gravitational separation was completed and the liquid flowed along the bottom of the pipe whereas the air flowed along the top part of the pipe.

With increasing gas superficial velocity and fixed liquid superficial velocity, the wavy flow pattern was formed after the transition from the stratified flow. From the flow mapping in Figures 4.20 - 4.23, wavy flow can be observed at all sections of the 21.0-mm pipe. However, after increasing of liquid superficial velocity and fixed gas superficial velocity it resulted in transition of stratified flow to the bubbly flow pattern. The bubbly flow appeared at all section of the pipe at low gas superficial velocity and high liquid superficial velocity.

The dispersed bubble just appeared at the section I (L/D = 17.86) during the experiment inside the 21.0-mm inner diameter pipe. The dispersed bubble needed a high liquid superficial velocity. At section II (L/D = 53.57), III (L/D = 89.29) and IV (L/D = 125.0), the dispersed bubble already changed the pattern to develop either bubbly, slug or plug flow because of the effect of gravity. The bubbles at the dispersed bubble flow moving upward to the top of the pipe and coalesced with each other. By increasing the gas superficial velocity, the bubbly flow pattern developed the plug flow pattern at all sections. The transition of the bubbly flow to plug flow can be observed in the figures 4.20 - 4.23 below. The bubbles started to merge up by moving upward and coalesced with each other at the top of the pipe and developed a bigger and long shape bubbles.

From these observations, the slug flow just appeared at the section II (L/D = 53.57), III (L/D = 89.29) and IV (L/D = 125.0) only. The slug flow did not appear at section I (L/D = 17.86) because the bubbles did not have enough time to coalesce and merge up to develop a slug pattern. The two-phase flow needs a high amount of gas inside the pipe to form the slug flow pattern. During the experiment of the two-phase flow inside the 21.0-mm ID pipe, the L/D ratio of the pipe was large enough and the range of slug flow rose. The number of bubbly and wavy flow pattern were reduced by developing slug flow and it is easy to achieve even at low gas superficial velocity.

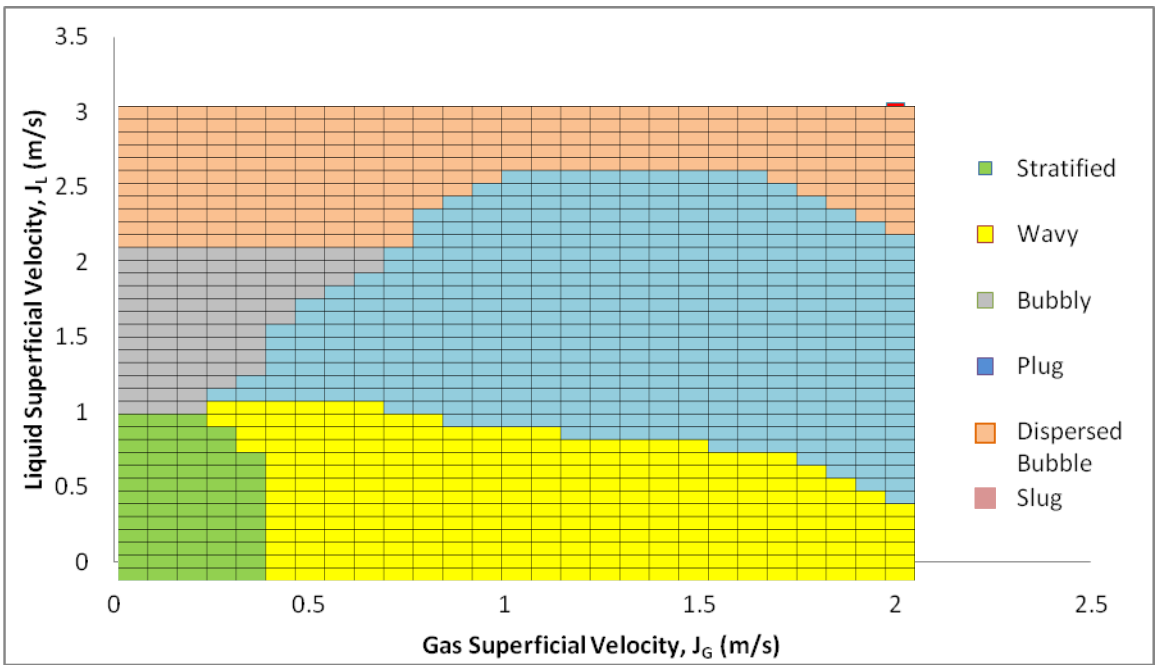

Figure 4.20 : Flow pattern map for section I (L/D = 17.86) of 21.0-mm ID pipe

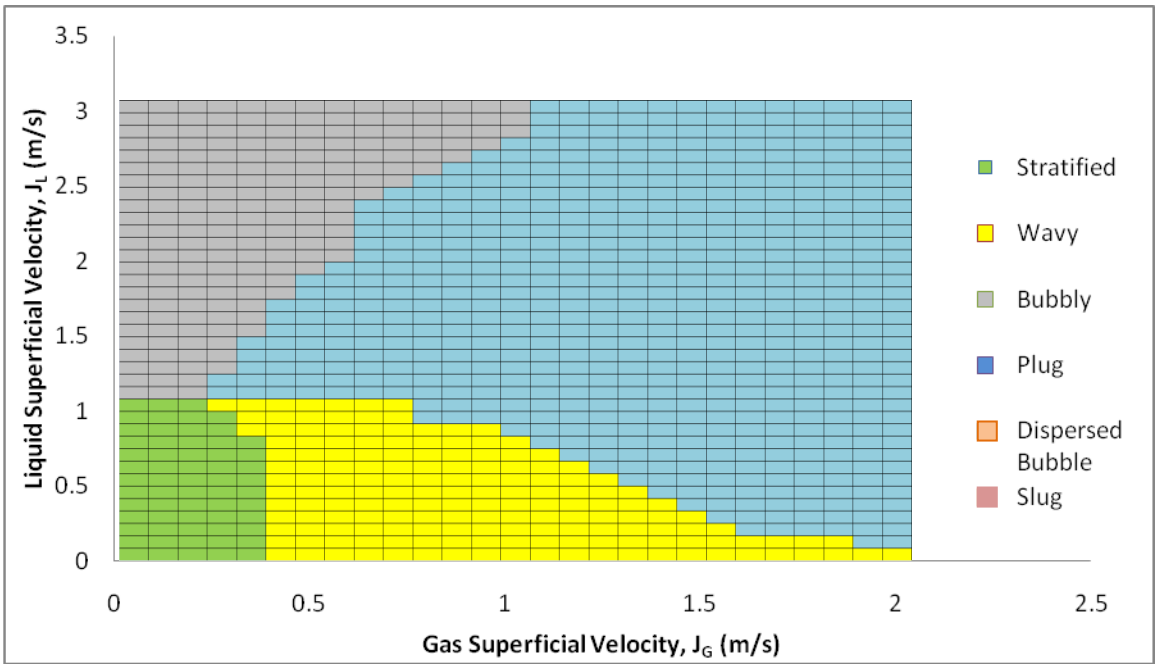

Figure 4.21 : Flow pattern map for section II (L/D = 53.57) of 21.0-mm ID pipe

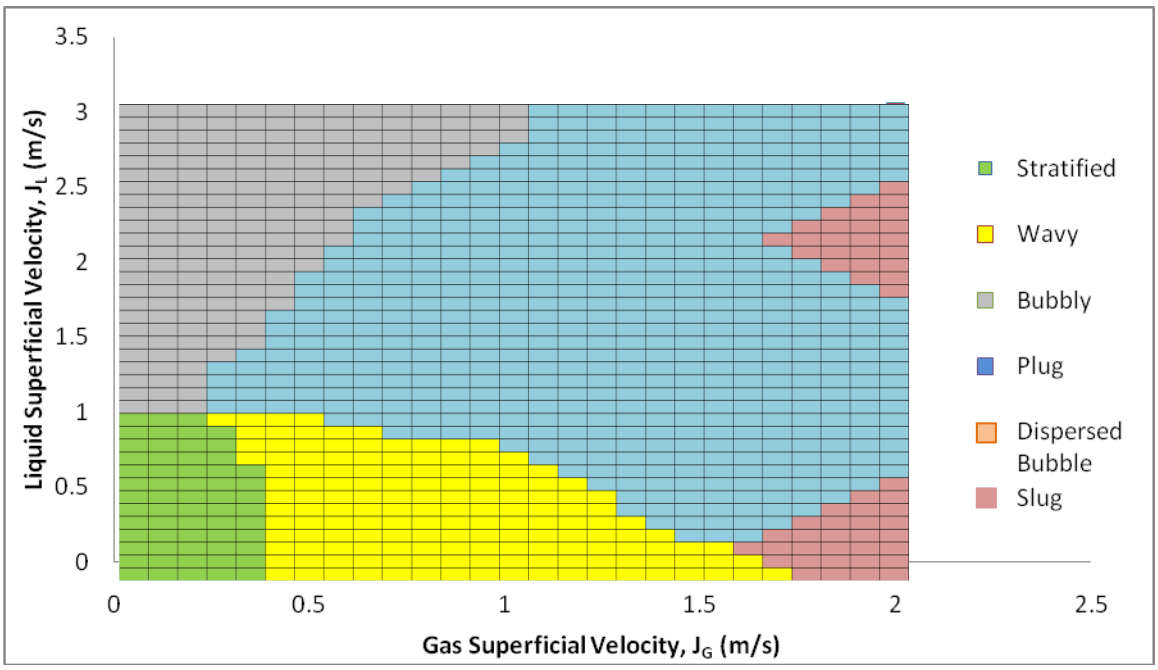

Figure 4.22 : Flow pattern map for section III (L/D = 89.29) of 21.0-mm ID pipe

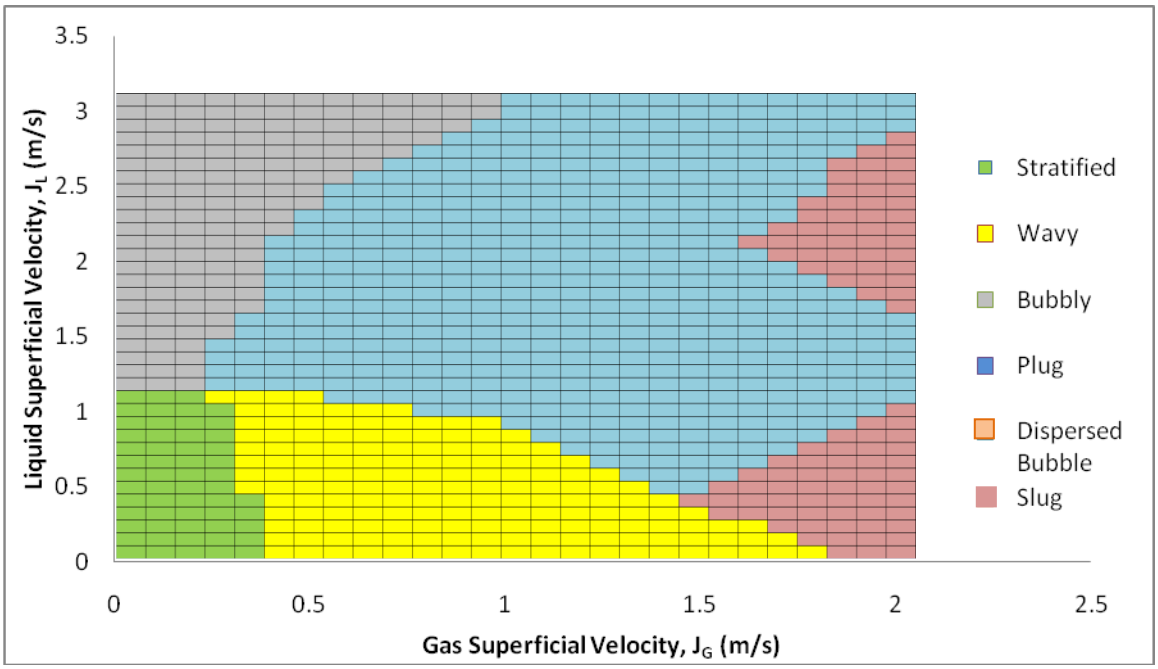

Figure 4.23 : Flow pattern map for section IV (L/D = 125.0) of 21.0-mm ID pipe

ii. Flow maps inside 47.0-mm ID pipe

Figures 4.24 - 4.27 showed the flow mapping for the horizontal flow inside the 47.0 mm ID pipe. Each figure showed the flow mapping at section I (L/D = 7.98) to section IV (L/D = 55.85). The range of the gas superficial velocity, j_G was from 0.05 m/s to 2.0 m/s and the range of liquid superficial velocity, j_L was from 0.05 to 2.0 m/s. There were 4 different fixed points selected to observe the flow patterns. The observation of the flow pattern was carried out by using the visual observation via the DSLR camera and high speed video camera.

At low gas and liquid superficial velocity, the stratified flow pattern took part at all sections. From the figure, it clearly showed that the stratified flow occurred at the gas and liquid superficial velocities, j_L below 1.0 m/s at all sections, depending on the length of the pipe. The two-phase flow has a clear separated line between the gas and liquid caused by the gravitational effect. With the increasing gas superficial velocity, the stratified flow changed to the wavy flow at all sections inside the pipe. The gas and liquid phase were still separated where the surface of the liquid film has disturbance from the gas to develop the wavy flow.

The dispersed bubbly flow just appeared at section I (L/D = 7.98) as shown in Figure 4.24. The dispersed bubbly flow required a high liquid superficial velocity higher than 1.4 m/s and at low gas superficial velocity. At section I (L/D = 7.98), the dispersed bubble still did not merge up and flow uniformly inside the pipe. After a few periods at section II (L/D = 23.94), III (L/D = 39.89) and IV (L/D = 55.85) the bubbles have enough time to coalesce with each other and moved to the top of the pipe. The wavy flow pattern appeared after the gas and liquid superficial velocities were increased inside the pipe. The wavy flow pattern occurred at all sections during the experiment.

By further increasing of the liquid superficial velocity, the wavy pattern changed to develop a plug flow inside the pipe. It happened when the wavy flow grew bigger enough to touch the top of the pipe. In this experiment, the plug flow just appeared at section II (L/D = 23.94), III (L/D = 39.89) and IV (L/D = 55.85). From the observation, the plug flow pattern started to develop when the liquid superficial velocity was higher than 0.8 m/s. At section I (L/D = 7.98), the flow was still in a bubbly form because the bubbles did not reach the top of the pipe and merge up to form plug flow. The plug flow size also depended on the volume of the gas inside the pipe.

The slug flow pattern occurred at section III (L/D = 39.89) and section IV (L/D = 55.85) inside the 47.0-mm ID pipe during the experiment at high gas and liquid superficial velocity. From the observation, the slug flow pattern developed from the bubble flow to plug flow when the waves were big enough to touch the bottom part of the pipe. The transition from plug flow to slug flow pattern happened by larger increase of the gas superficial velocity, where the two-phase flow has high volume of gas flowing inside the pipe. The development of slug flow also required enough length of the pipe, to have time for the bubbles to merge up and that is the reason why the slug flow just existed only at section III (L/D = 39.89) and section IV (L/D = 55.85).

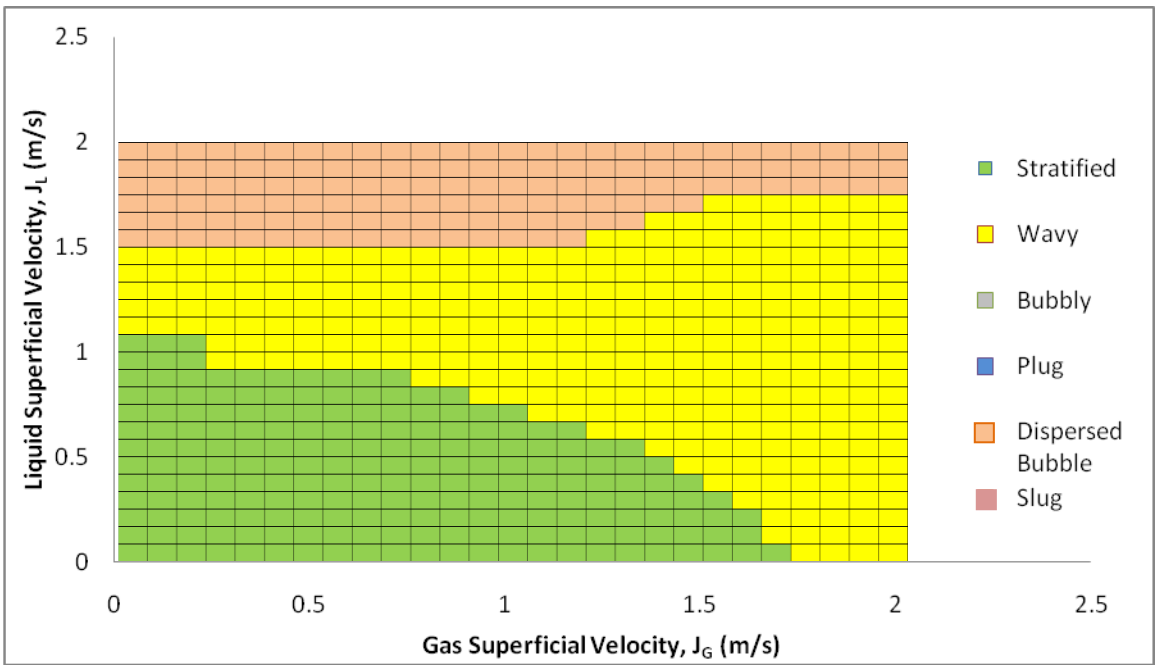

Figure 4.24 : Flow pattern map for section I (L/D = 7.98) of 47.0-mm ID pipe

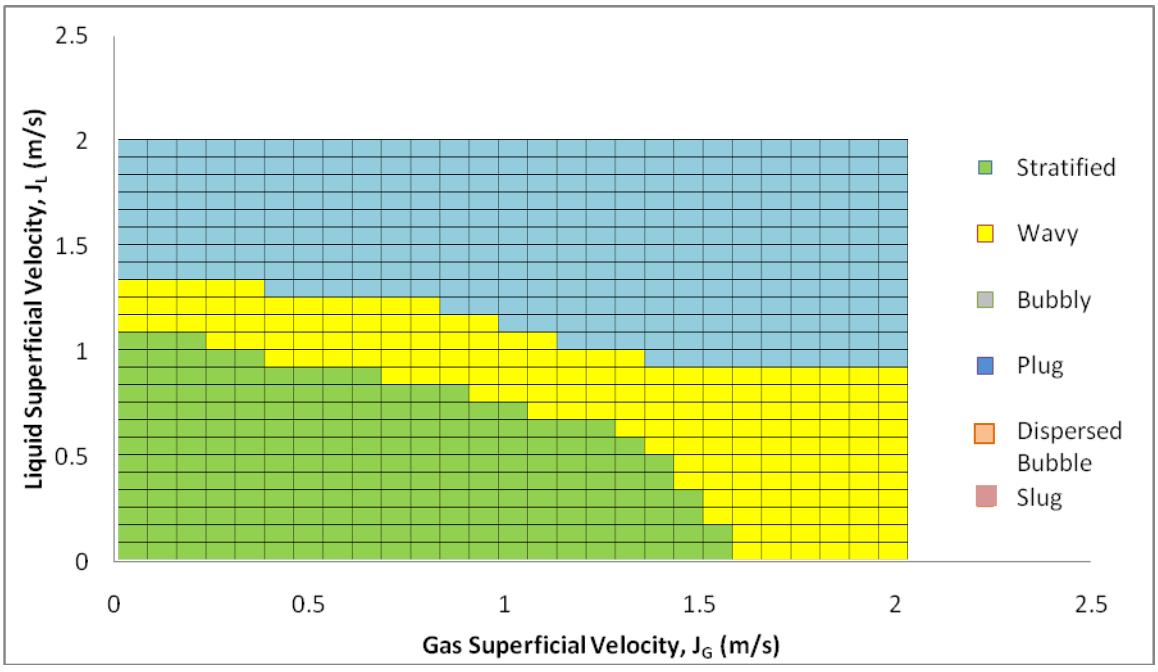

Figure 4.25 : Flow pattern map for section II (L/D = 23.94) of 47.0-mm ID pipe

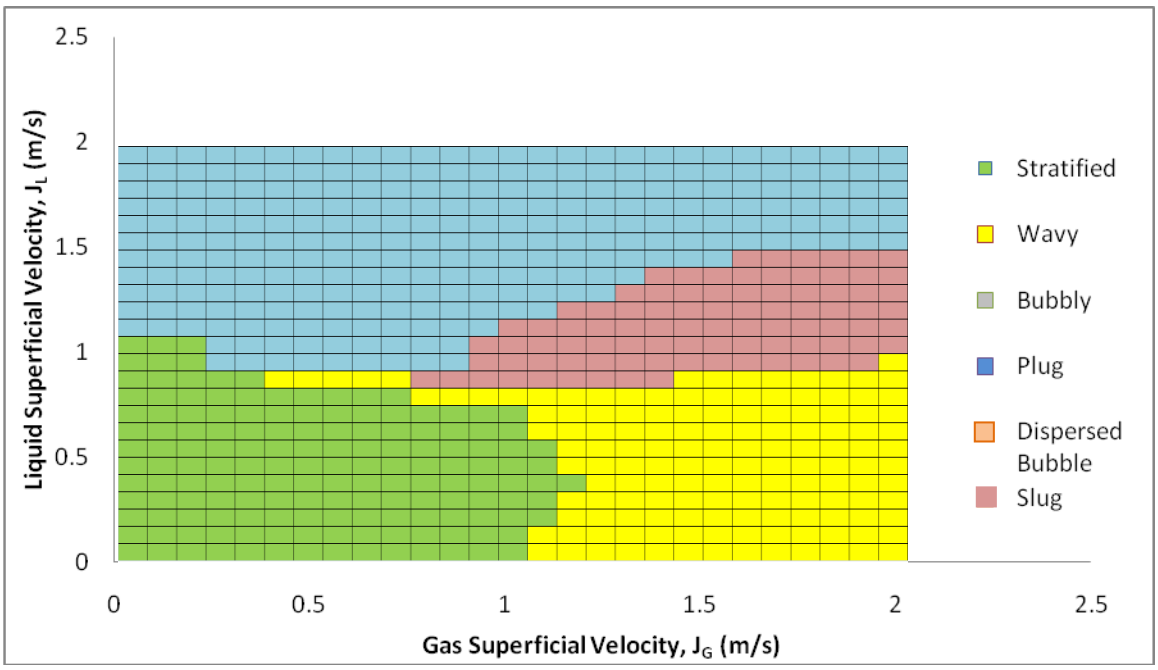

Figure 4.26 : Flow pattern map for section III (L/D = 39.89) of 47.0-mm ID pipe

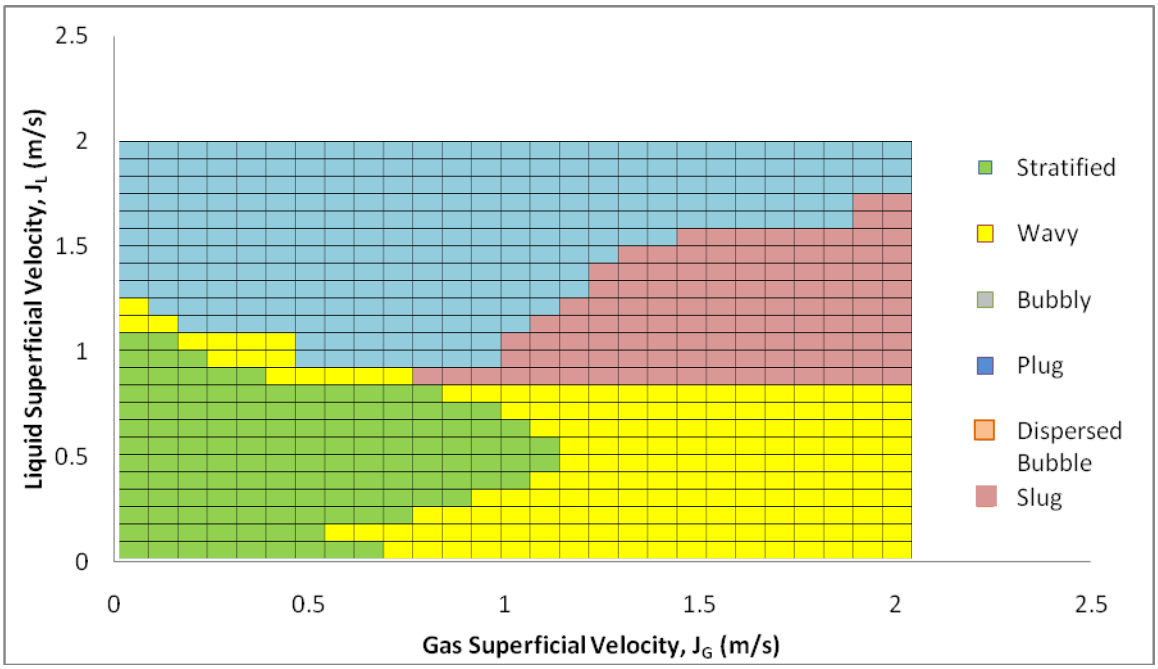

Figure 4.27 : Flow pattern map for section IV (L/D = 55.85) of 47.0-mm ID pipe

iii. Flow maps inside 95.0-mm ID pipe

Figures 4.28 - 4.31 showed the flow mapping for the horizontal two-phase flow inside a 95.0-mm inner diameter pipe. The figures showed the flow mapping for each section of the pipe from section I (L/D = 3.95) to section IV (L/D = 27.63). The current experiments have limitation on the range of gas and liquid superficial velocity due to small pumping and compression pressure. They were run at low gas and liquid superficial velocity. The range of the gas superficial velocity, j_G was from 0.05 m/s to 0.6 m/s while for the liquid superficial velocity, j_L was from 0.05 m/s to 0.4 m/s.

From the figures, there were just two types of flow patterns that can be observed in these experiments, the stratified and wavy flow. Both of the patterns occurred at low gas and liquid superficial velocity. At low liquid superficial velocity, the two-phase flow pattern was in a stratified flow and in steady state. When the liquid superficial velocity was increased, the stratified flow changes to the wavy flow and it happened because the gas-liquid rate was too high and with naked eyes it can be seen that water just fill up less than half of the pipe diameter.

Besides the two patterns described above, there was no other patterns developed on the 95.0-mm ID pipe. The gas and liquid superficial velocity was too low and the L/D ratio of the pipe was too small. Even with maximum flow rate, the liquid still cannot fill up the whole pipe.

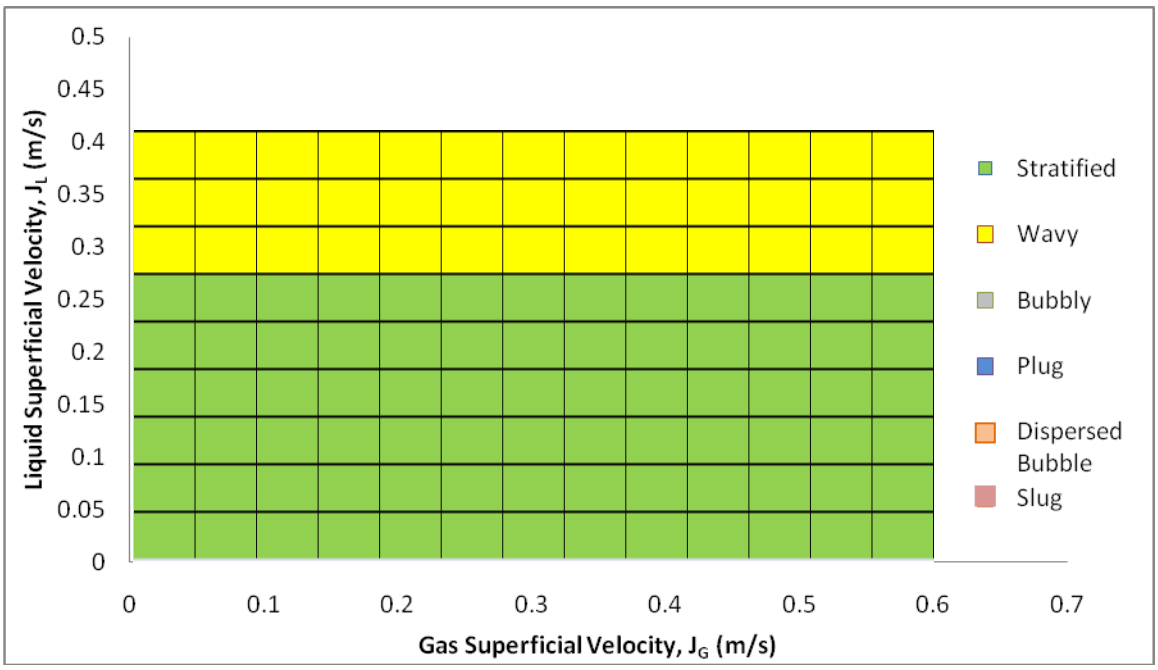

Figure 4.28 : Flow pattern map for section I (L/D = 3.95) of 95.0-mm ID pipe

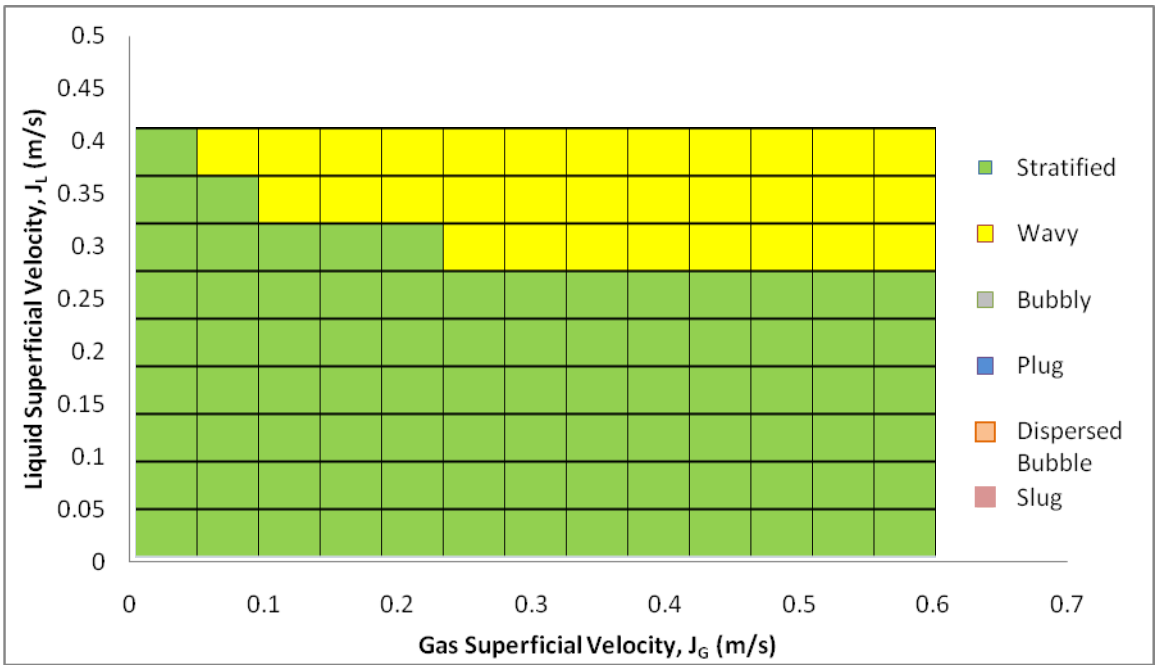

Figure 4.29 : Flow pattern map for section II (L/D = 11.84) of 95.0-mm ID pipe

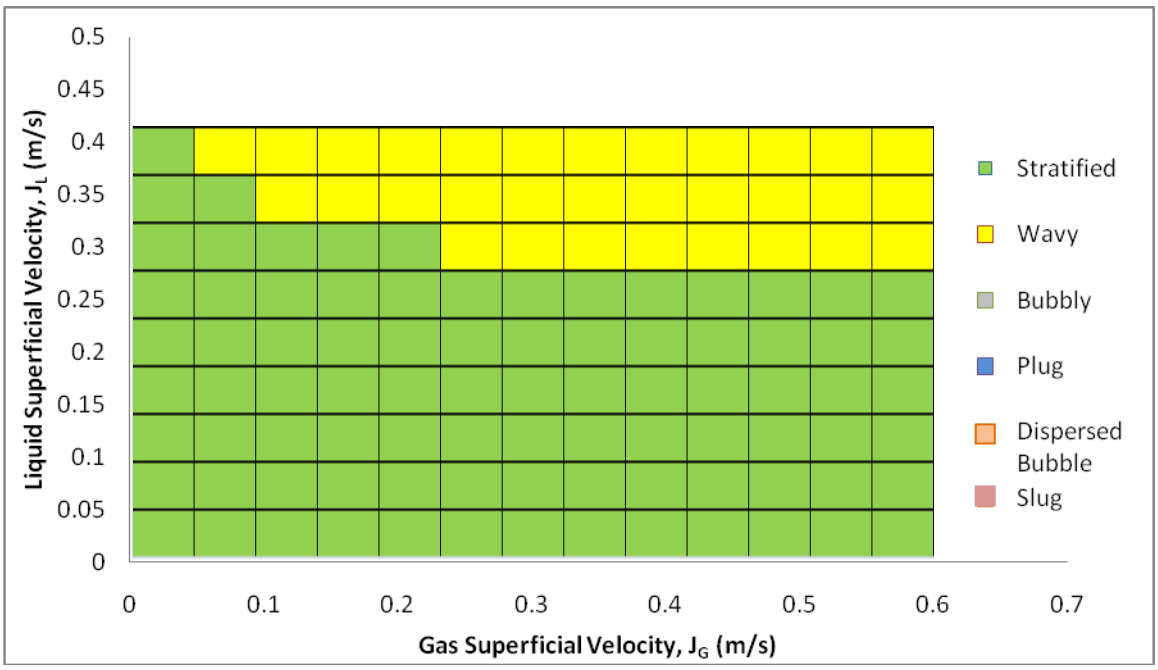

Figure 4.30 : Flow pattern map for section III (L/D = 19.74) of 95.0-mm ID pipe

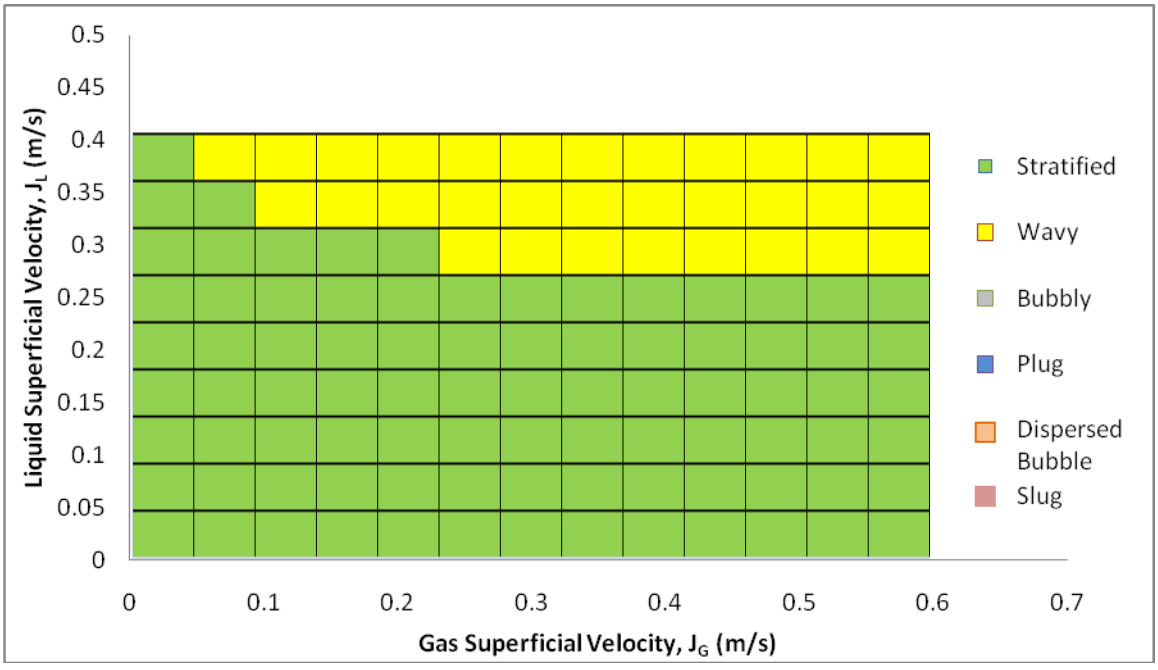

Figure 4.31 : Flow pattern map for section IV (L/D = 27.63) of 95.0-mm ID pipe

All the flow mappings above were agree well with the Taitel and Dukler (1976) shown in Chapter 2.2. The boundary transitions of the flow pattern are based on physical concepts and predictive in that no flow regime transition used.

4.3 Measurement of Void fraction

4.3.1 Vertical Pipes

i. 21.0-mm ID pipe

Void fraction is the ratio of the gas phase (the voids) volume to the total volume of the pipe. From the void fraction value, the ratio or percentage of the gas inside the pipe can be determined. The type of flow pattern can also be determined through the graph of the void fraction based on the time domain. Besides, the graph can showed how the movement of the two-phase flow and the behavior of the gas liquid mixture inside the pipe.

In this void fraction experimentation, the data were obtained from the Constant Electric Current Method (CECM) experiment as explained in section 2.4. Figure 4.32 showed the void fraction time domain graph at various gas superficial velocities inside the 21.0-mm ID for vertical upward flow pipe. The liquid superficial velocity was fixed at j_L = 0.16 m/s, while the gas superficial velocity were changed from a range of j_G = 0.04 m/s to j_G = 2.00 m/s.

At low gas superficial velocity, the value of void fraction was very low. Figure 4.32(a) shows the void fraction, $\alpha = 0.0133$, for the j_G = 0.04 m/s and j_L = 0.16 m/s and the flow pattern was a bubbly flow. The type of flow pattern can be easily determined from the graph rather than visual inspection inside the pipe. Figure 4.32 (a) - 4.32 (b) showed the bubbly flow pattern that can be analyzed from the graph. The figures showed a uniform wavy pattern all the time that revealed the bubble flowing upward inside the pipe. The reading of void fraction will increase if the size of the bubbles increases during the actual time in the two-phase flow experiment.

(a)

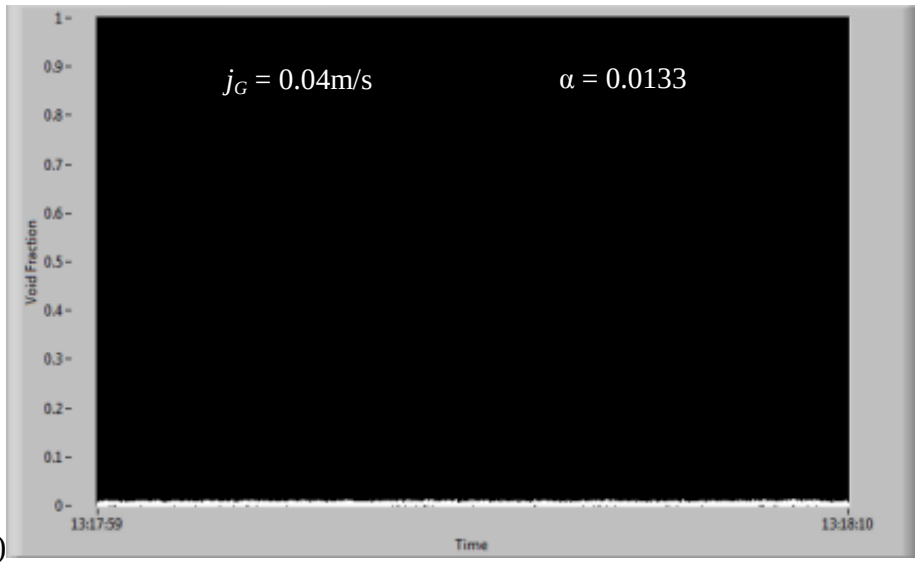
j_G = 0.04m/s
α = 0.0133
Void Fraction
1
0.9
0.8
0.7
0.6
0.5
0.4
0.3
0.2
0.1
0
13:17:59
13:18:10
Time

(b)

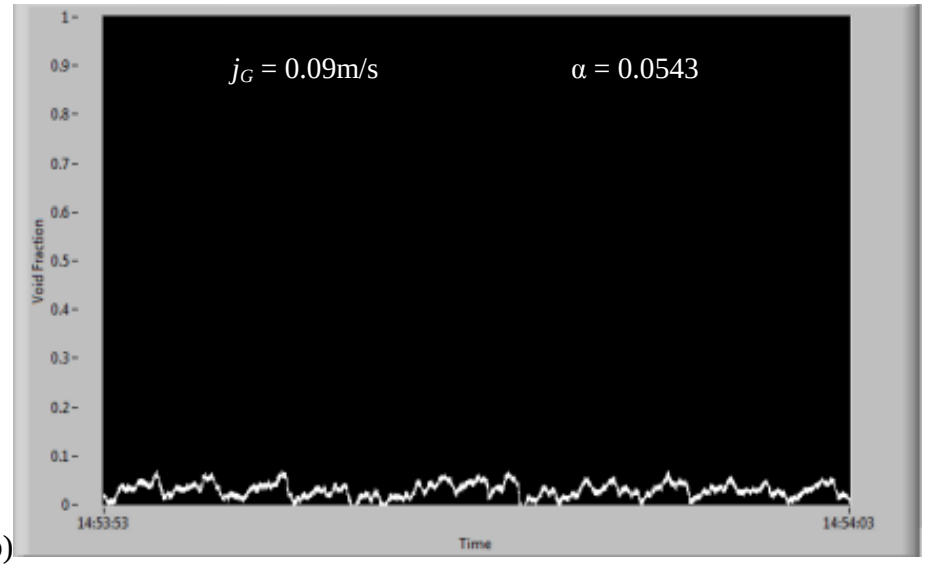
j_G = 0.09m/s
α = 0.0543
Void Fraction
1
0.9
0.8
0.7
0.6
0.5
0.4
0.3
0.2
0.1
0
14:53:53
14:54:03
Time

(c)

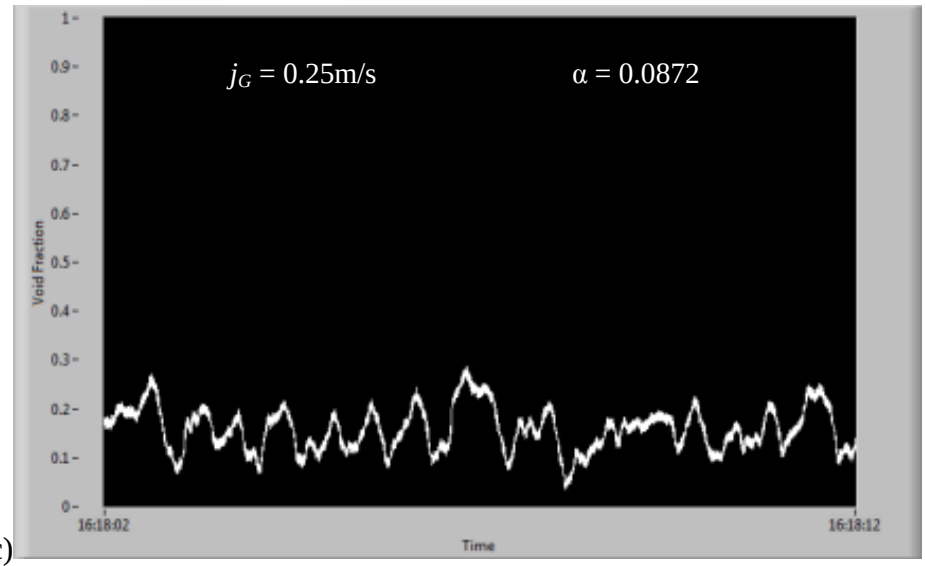
j_G = 0.25m/s
α = 0.0872
Void Fraction
1
0.9
0.8
0.7
0.6
0.5
0.4
0.3
0.2
0.1
0
16:18:02
16:18:12
Time

(d)

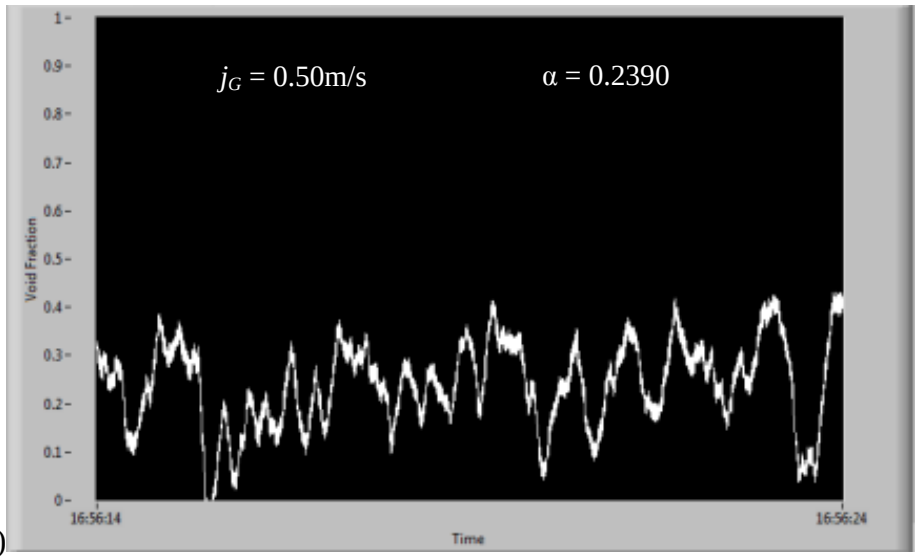

(e)

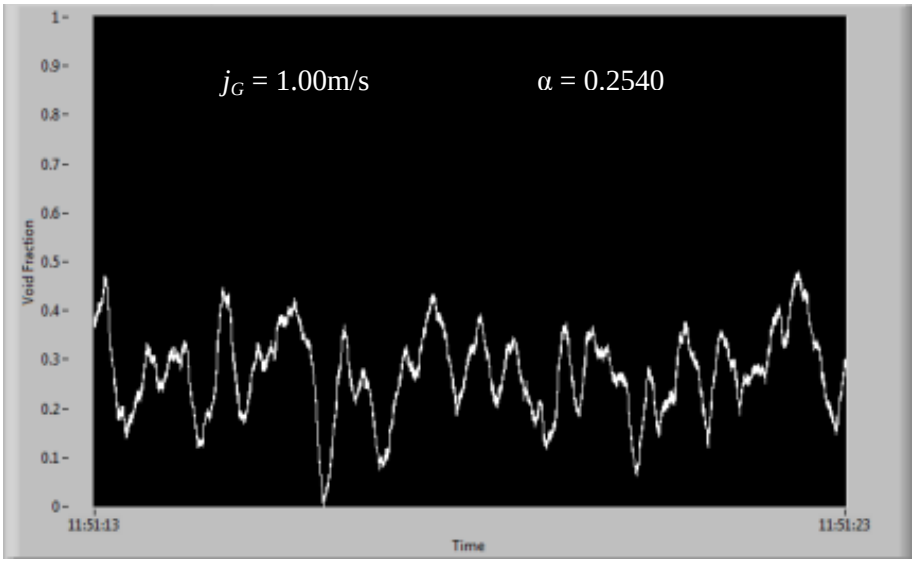

(f)

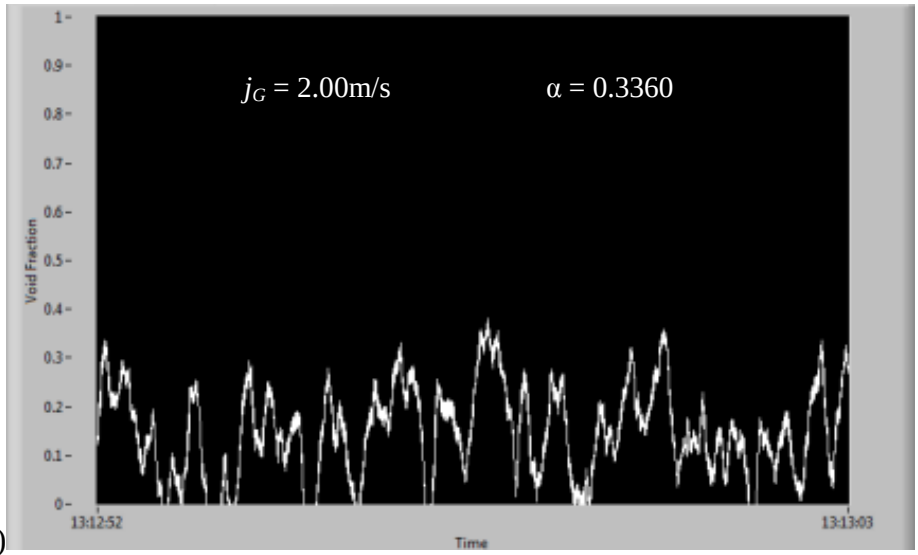

Figure 4.32: Void fraction at j_L = 0.16 m/s in 21.0-mm ID pipe. (a)-(b) Bubbly flow, (c) Slug flow, (d)-(f) Churn flow

The slug flow shown in Figure 4.32 (c) at j_G = 0.25 m/s and j_L = 0.16 m/s and the void fraction was obtained at α = 0.0872. Figures 4.32 (d) - 4.32 (f) showed a void fraction, α = 0.02390 to α = 0.03360 for the churn flow. From these figures, it can be observed that the waves were not stable and they were striking up and down rapidly. This situation appeared at a high gas superficial velocity that was higher than j_G = 0.50 m/s. The churn flow has a behavior of destructive consequences on the piping system by the mass of the slugs. By the CECM method, the churn flow pattern can be controlled with continuous observation from the graph. Any unstable two-phase flow behavior can be detected through the graph.

Figure 4.33 illustrated the void fraction graph for the two-phase flow for the liquid superficial velocity at j_L = 0.25 m/s and the range of gas superficial velocity at j_G = 0.04 m/s to j_G = 2.00 m/s. The liquid superficial was increased from j_L = 0.16 m/s to j_L = 0.25 m/s and the void fraction value were changing due to the same gas superficial velocity. Figures 4.33 (a) - (b) showed a void fraction, α = 0.0091 to α = 0.0393 for the bubbly flow pattern at j_L = 0.25 m/s. At void fraction α = 0.0627, slug flow pattern appeared at gas and liquid superficial velocity j_G = 0.25 m/s and j_L = 0.25 m/s that was shown in figure 4.33 (c). The churn flow at void fraction, α = 0.2060 to α = 0.3280 appeared when the gas superficial velocity was higher than j_G = 0.50 m/s.

(a)

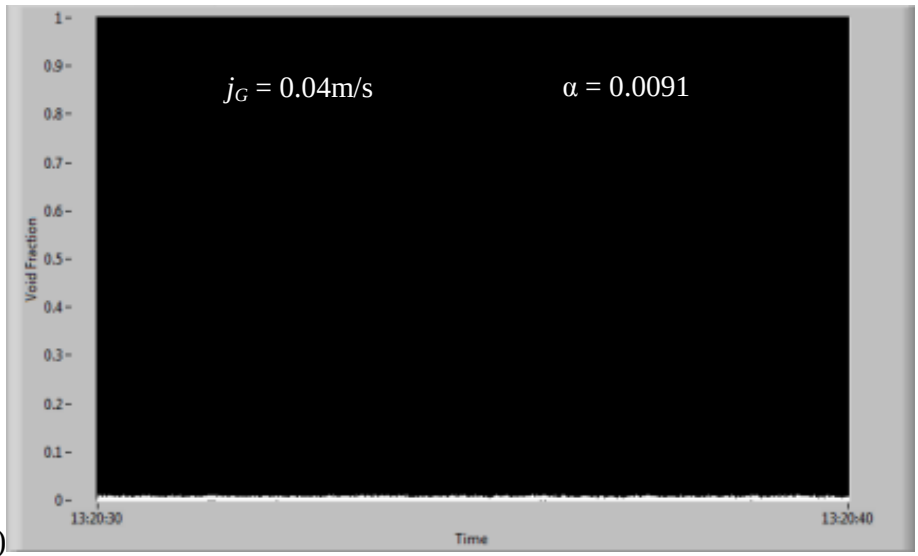
j_G = 0.04m/s
α = 0.0091
Void Fraction
1
0.9
0.8
0.7
0.6
0.5
0.4
0.3
0.2
0.1
0
13:20:30
13:20:40
Time

(b)

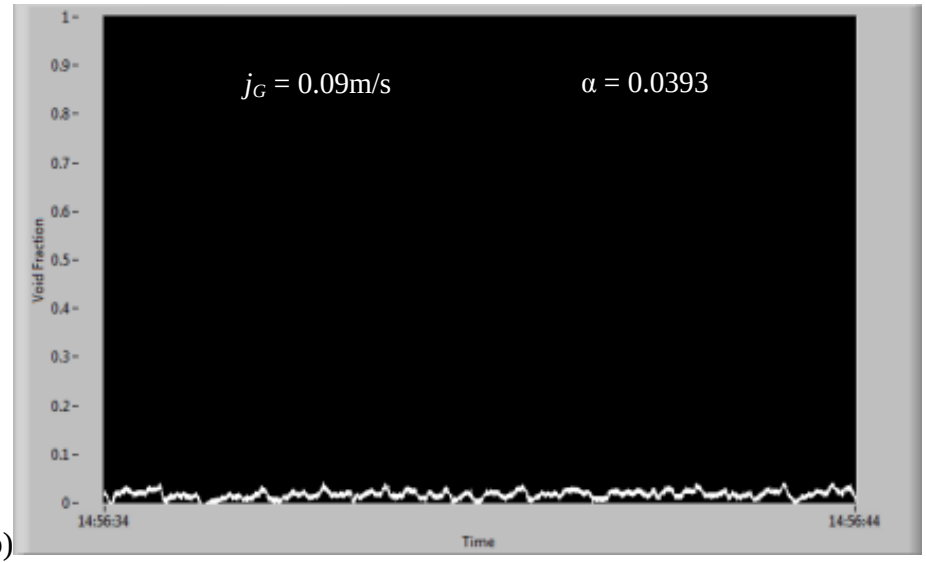
j_G = 0.09m/s
α = 0.0393
Void Fraction
1
0.9
0.8
0.7
0.6
0.5
0.4
0.3
0.2
0.1
0
14:56:34
14:56:44
Time

(c)

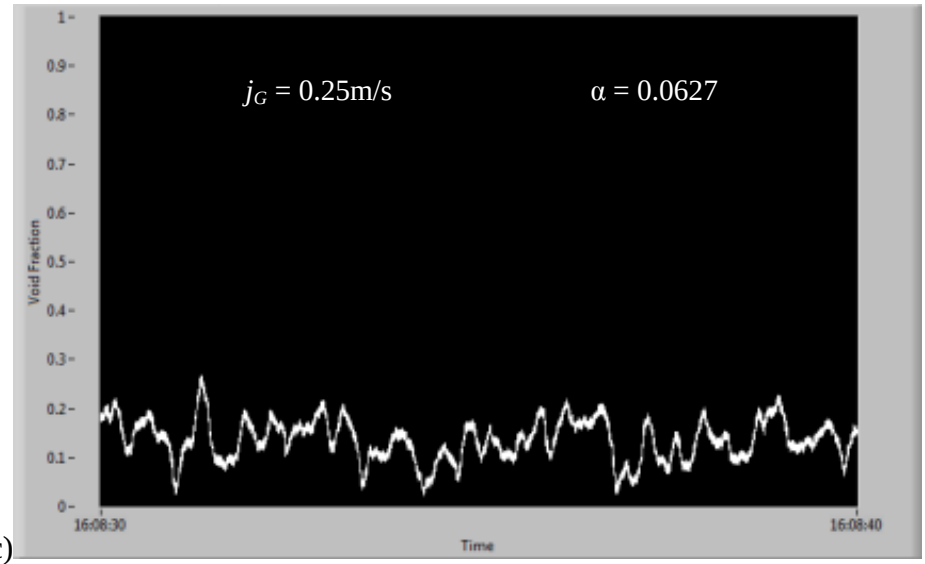
j_G = 0.25m/s
α = 0.0627
Void Fraction
1
0.9
0.8
0.7
0.6
0.5
0.4
0.3
0.2
0.1
0
16:08:30
16:08:40
Time

(d)

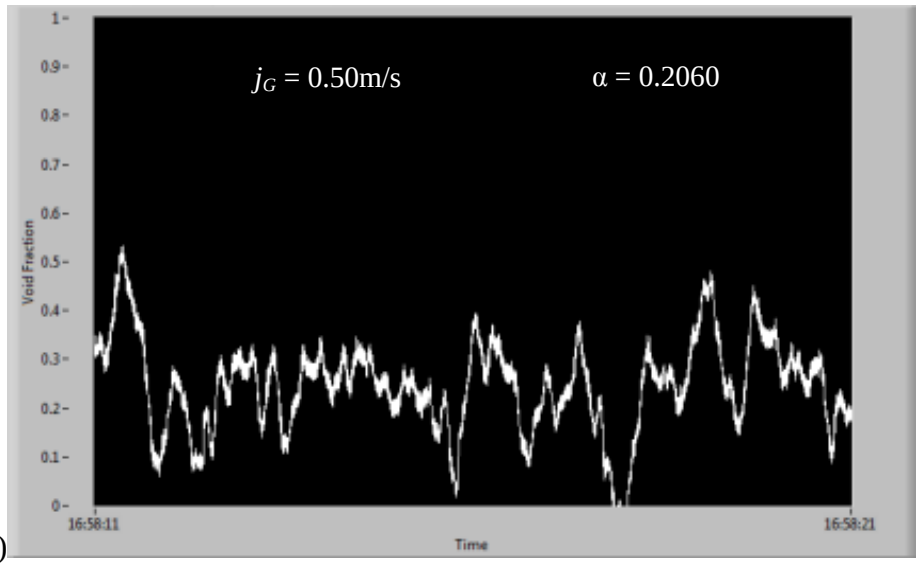

(e)

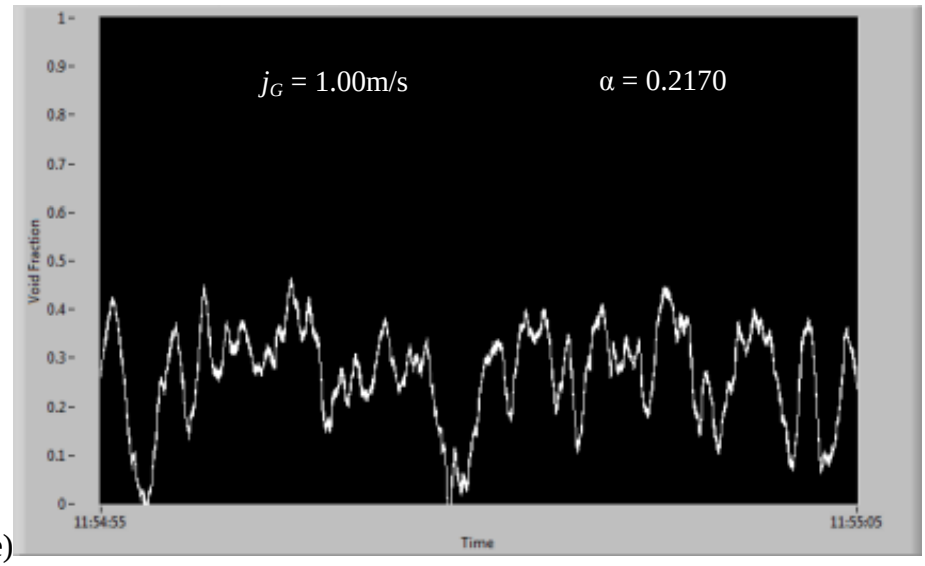

(f)

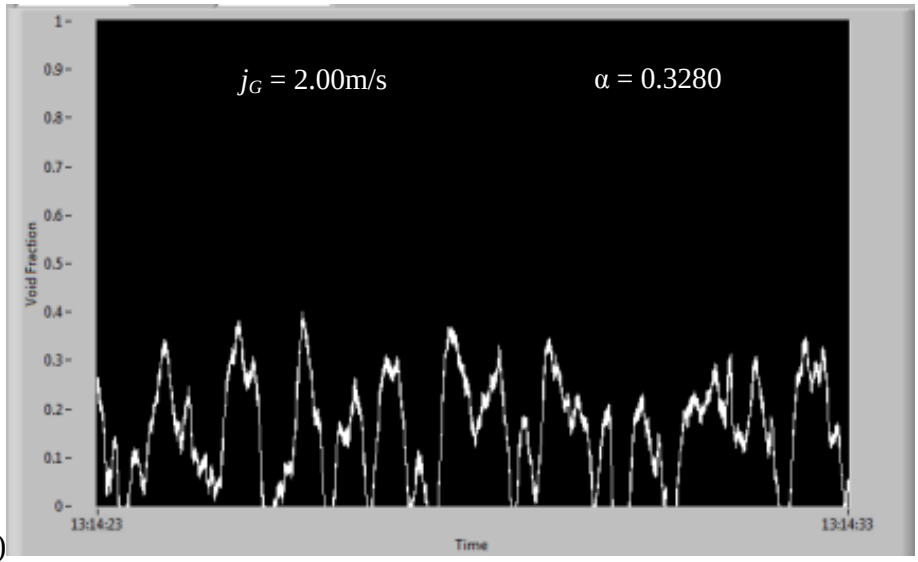

Figure 4.33: Void fraction at j_L = 0.25 m/s in 21.0-mm ID pipe. (a)-(b) Bubbly flow, (c) Slug flow, (e)-(f) Churn flow

ii. 47.0-mm ID pipe

The void fraction experimentation for the 47.0-mm ID pipe were done at fixed liquid superficial velocity j_L = 0.16 m/s and j_L = 0.25 m/s. Figure 4.34 showed the void fraction for the fixed liquid superficial velocity at j_L = 0.16 m/s, while figure 4.35 showed the void fraction for the fixed liquid superficial velocity at j_L = 0.25 m/s. For both liquid superficial velocity, the range of gas superficial velocity was from j_G = 0.04 m/s to j_G = 2.20 m/s. The value of void fraction can be observed directly through the void fraction result and the type of flow pattern can be determined by the value of void fraction.

From these results, at fixed liquid superficial velocity j_L = 0.16 m/s, the void fraction reading were α = 0.0166 to α = 0.0300 at the low gas superficial velocity from range of j_G = 0.04 m/s to j_G = 0.10 m/s and bubbly flow pattern appeared as shown in Figure 4.34 (a) and 4.34 (b). The value of void fraction was small for the bubbly flow. The void fraction, α = 0.0784 for the bubbly slug flow pattern shown in Figure 4.34 (c) appeared after increasing the gas superficial velocity of j_G = 0.25 m/s. Figure 4.34 (d) and (e) shows the void fraction at α = 0.1620 and α = 0.2510 for the slug flow inside the 47.0-mm ID pipe. From the graph, the bubbly slug flow has small surging on the wave of void fraction. The slug flow pattern appeared at this flow rate and the graphs have more spikes than before. The churn flow appeared at void fraction α = 0.3590 at maximum flow rate during the experimentation that was shown in Figure 4.34 (f).

At fixed liquid superficial velocity j_L = 0.25 m/s, at low superficial velocity, the void fraction, α = 0.0132 to α = 0.0262 and the bubbly flow appeared as shown in Figure 4.35 (a) and (b). At void fraction α = 0.0873, the bubbly slug flow appeared at the medium gas superficial velocity that illustrated in figure 4.35 (c). By increasing the

gas superficial velocity the void fraction value increased at α = 0.1750 and the pattern changed to the slug flow that shows in figure 4.35 (d). The churn flow appeared at the maximum gas flow rate at void fraction α = 0.1880 and α = 0.2370 that was shown in figure 4.35 (e) - (f).

(a)

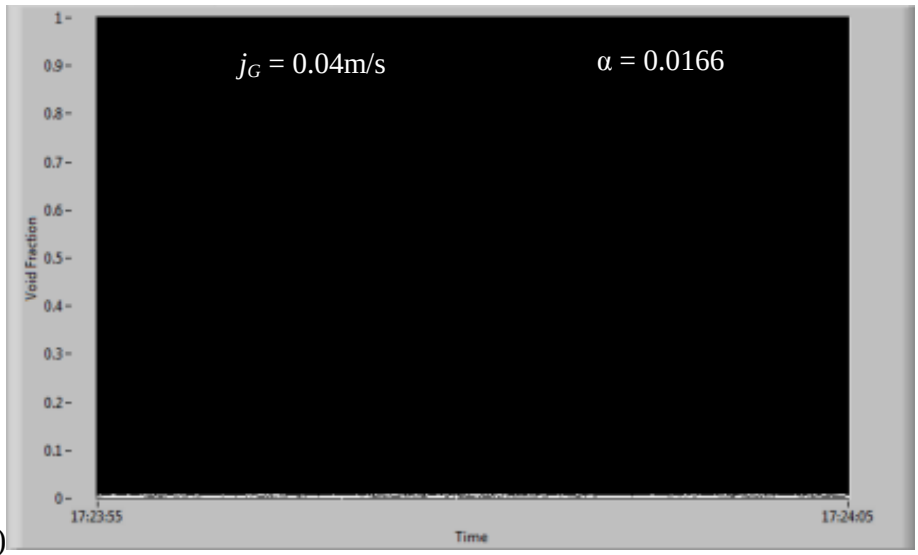

(b)

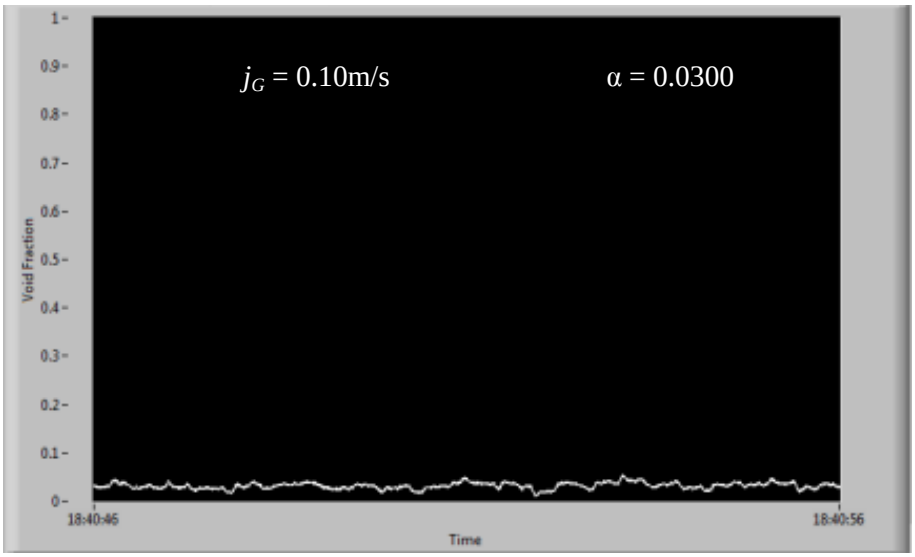

(c)

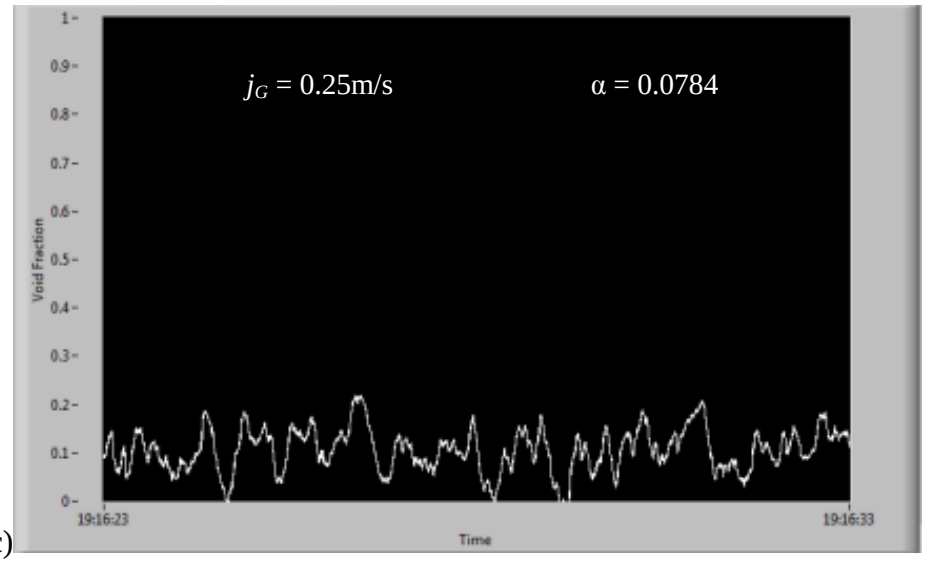
j_G = 0.25m/s
α = 0.0784
Void Fraction
1
0.9
0.8
0.7
0.6
0.5
0.4
0.3
0.2
0.1
0
19:16:23
19:16:33
Time

(d)

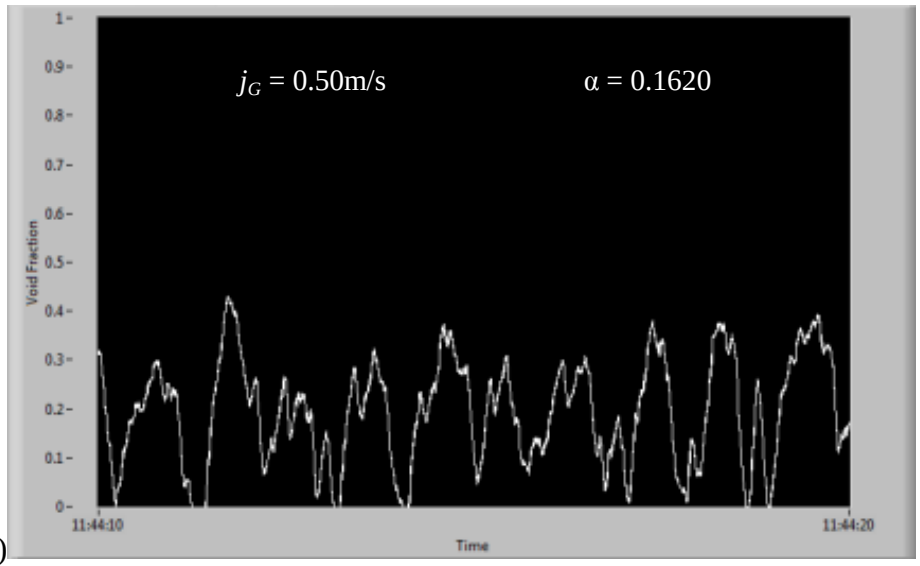
j_G = 0.50m/s
α = 0.1620
Void Fraction
1
0.9
0.8
0.7
0.6
0.5
0.4
0.3
0.2
0.1
0
11:44:10
11:44:20
Time

(e)

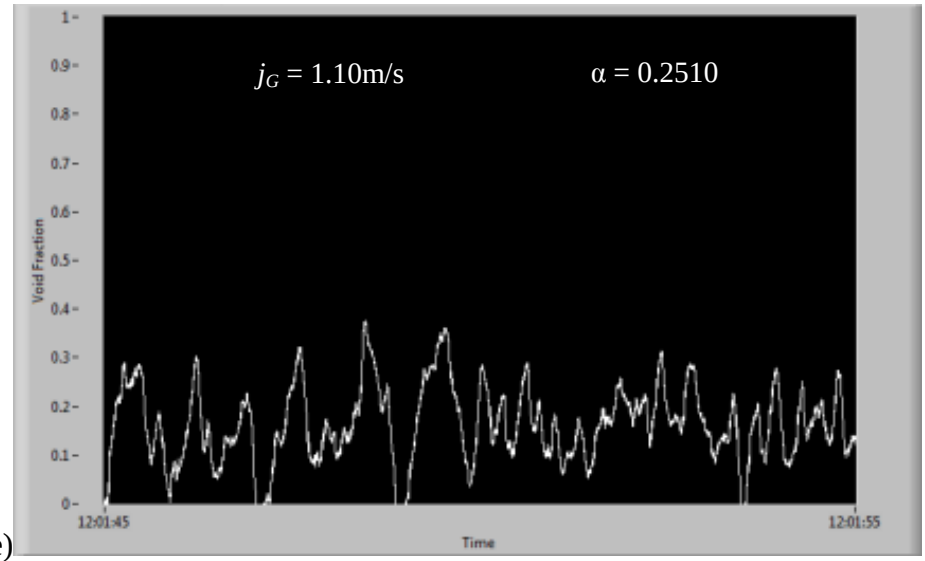
j_G = 1.10m/s
α = 0.2510
Void Fraction
1
0.9
0.8
0.7
0.6
0.5
0.4
0.3
0.2
0.1
0
12:01:45
12:01:55
Time

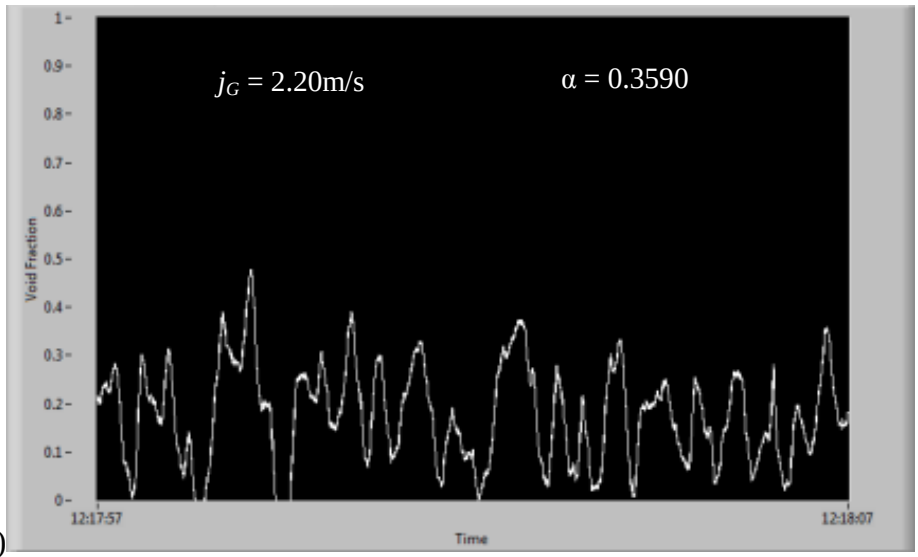

(f)

Figure 4.34: Void fraction at J_L = 0.16 m/s in 47.0-mm ID pipe. (a)-(b) Bubbly flow, (c) Bubbly-slug flow, (d)-(e) Slug flow, (f) Churn flow

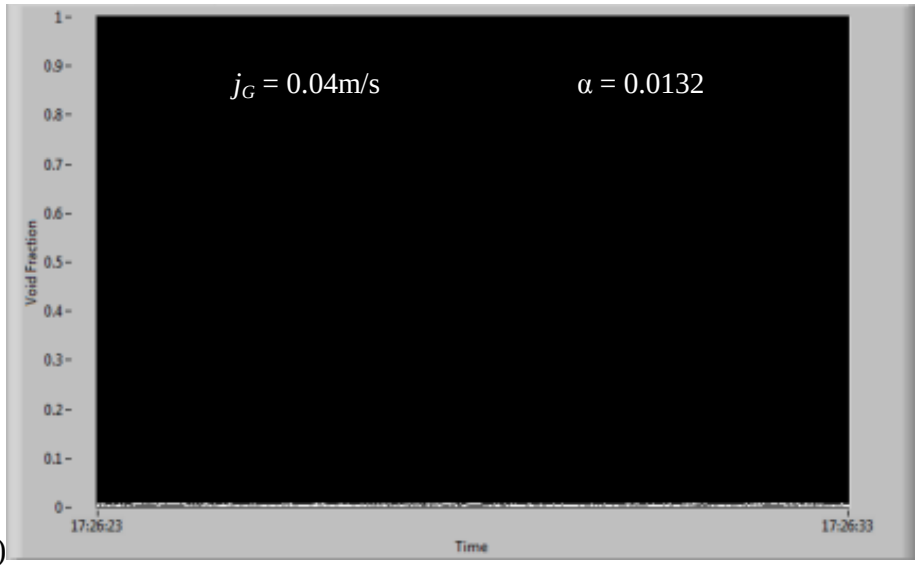

(a)

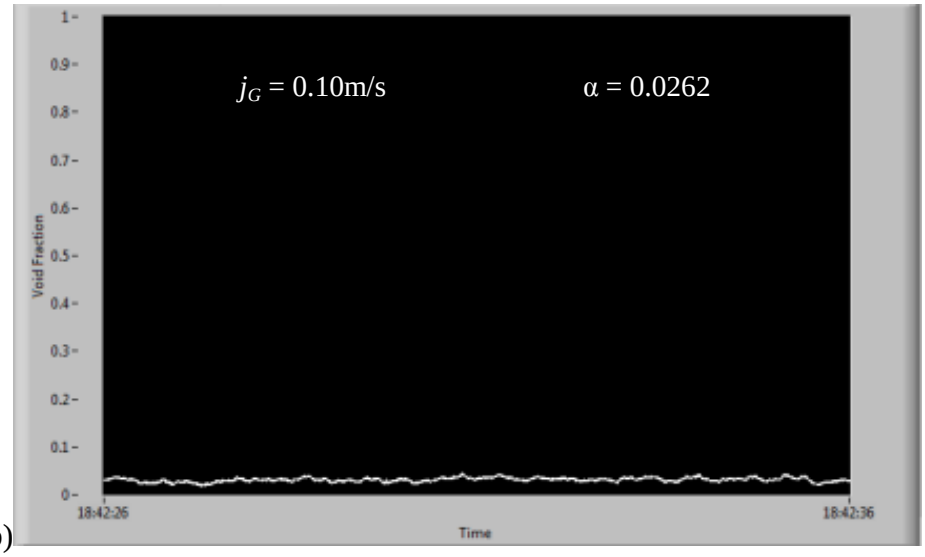

(b)

(c)

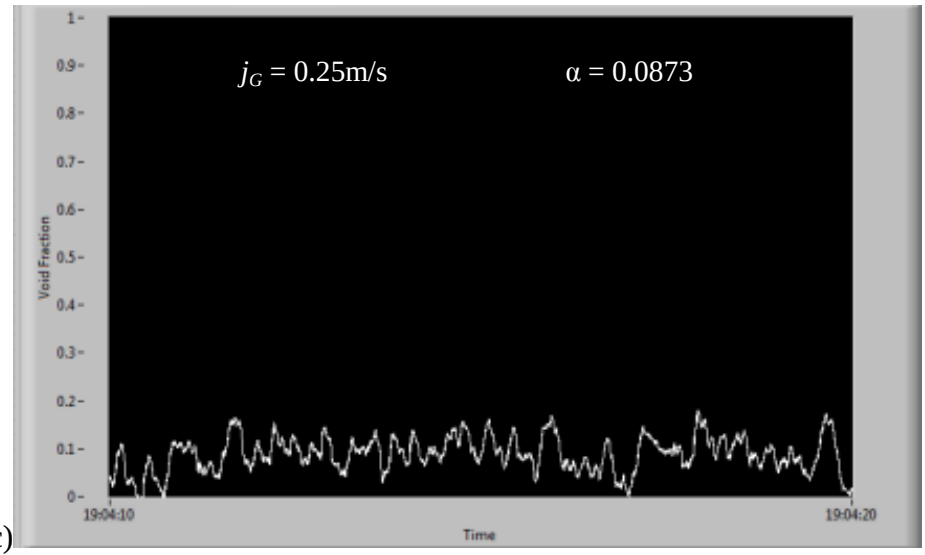
j_G = 0.25m/s
α = 0.0873
Void Fraction
1
0.9
0.8
0.7
0.6
0.5
0.4
0.3
0.2
0.1
0
19:04:10
19:04:20
Time

(d)

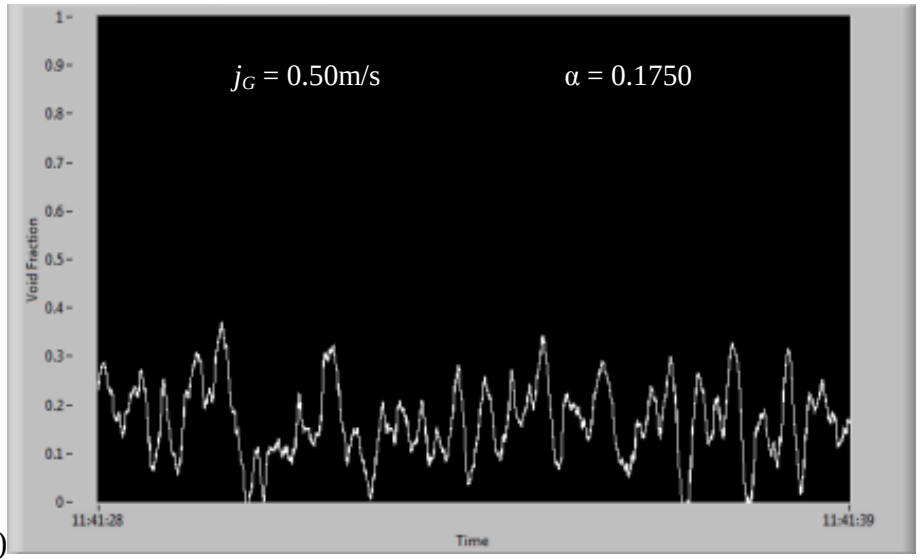
j_G = 0.50m/s
α = 0.1750
Void Fraction
1
0.9
0.8
0.7
0.6
0.5
0.4
0.3
0.2
0.1
0
11:41:28
11:41:39
Time

(e)

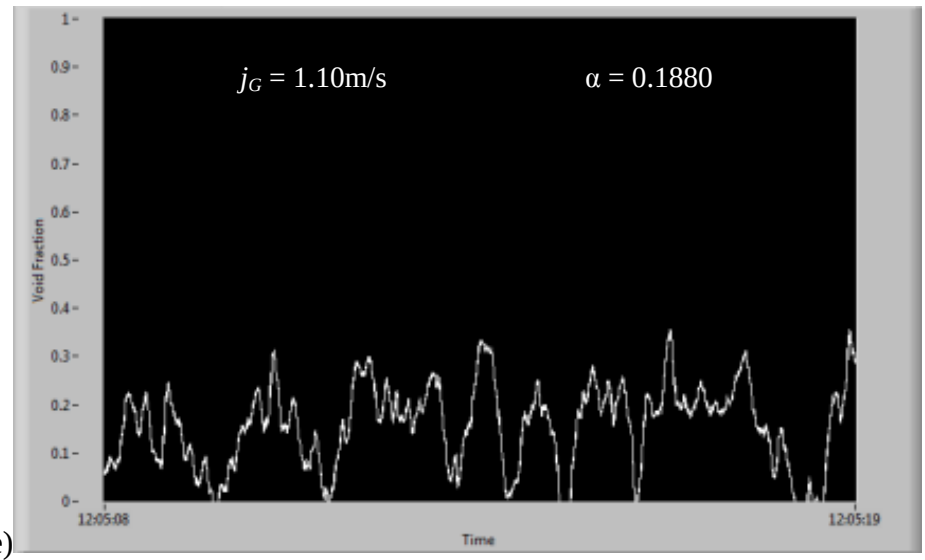
j_G = 1.10m/s
α = 0.1880
Void Fraction
1
0.9
0.8
0.7
0.6
0.5
0.4
0.3
0.2
0.1
0
12:05:08
12:05:19
Time

(f) 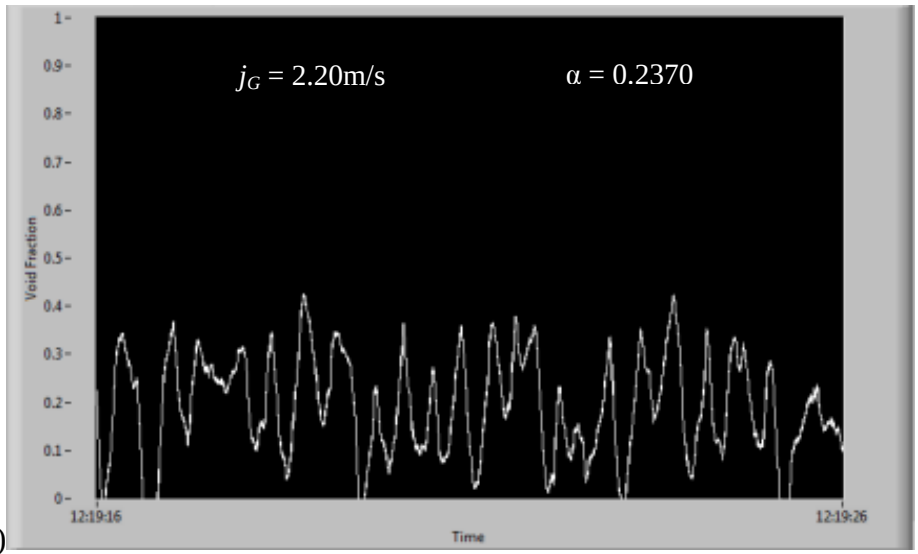

Figure 4.35: Void fraction at J_L = 0.25 m/s in 47.0-mm ID pipe. (a)-(b) Bubbly flow, (c) Bubbly-slug flow, (d) Slug flow, (e)-(f) Churn flow

iii. 95.0-mm ID pipe

Figures 4.36 - 4.37 show the void fraction for the two-phase flow inside the 95.0-mm ID vertical upward flow. The void fraction experimentation for the 95.0-mm ID pipe were done at fixed liquid superficial velocity j_L = 0.16 m/s to j_L = 0.25 m/s. Figure 4.34 illustrated the void fraction graph for the fixed liquid superficial velocity at j_L = 0.16 m/s and the gas superficial velocity flow at range from j_G = 0.006 m/s to j_G = 0.50 m/s while Figure 4.35 illustrated the void fraction graph for the fixed liquid superficial velocity and the range of gas superficial velocity was j_G = 0.006 m/s to j_G = 0.50 m/s. The range of the gas superficial velocity was small due to the limitation of the experimental equipment. The value of void fraction can be observed directly from the figure and the type of flow pattern can be determined by value of void fraction.

From the Figure 4.36, the liquid superficial velocity was set at a low flow rate. Figure 4.36 (a) - (b) at void fraction α = 0.0142 and α = 0.0292, showed the bubbly flow pattern developed inside the pipe. By increasing the gas superficial velocity at void fraction α = 0.0575, the small slugs occurred inside the pipe and a few strikes can be

observed from the graph that indicated in figure 4.36 (c). The slug flow pattern was shown in figure 4.36 (d) at void fraction $\alpha = 0.1070$. The churn flow occurred by increasing the gas superficial velocity at maximum gas flow rate at void fraction $\alpha = 0.1130$ to $\alpha = 0.1180$ that was shown in figure 4.36 (e)-(f).

By increasing the liquid superficial velocity to $j_L = 0.25$ m/s, the void fraction and flow patterns changed with a small effect. With the same gas superficial velocity, the flow patterns did not change compared to the value of liquid superficial velocity $j_L = 0.16$ m/s. These situations happened due to the small differences of flow velocity between both gas and liquid phases.

(a)

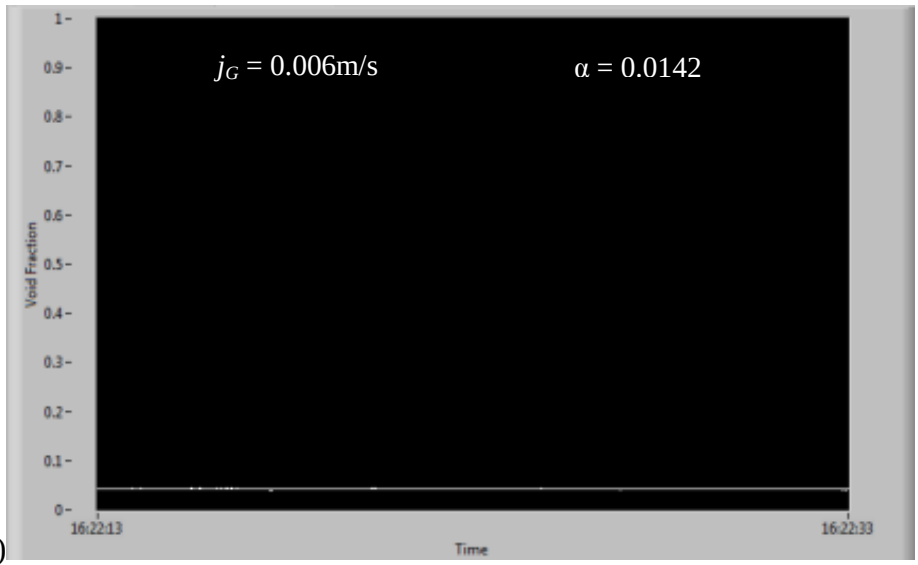
j_G = 0.006m/s
α = 0.0142
Void Fraction
1
0.9
0.8
0.7
0.6
0.5
0.4
0.3
0.2
0.1
0
16:22:13
16:22:33
Time

(b)

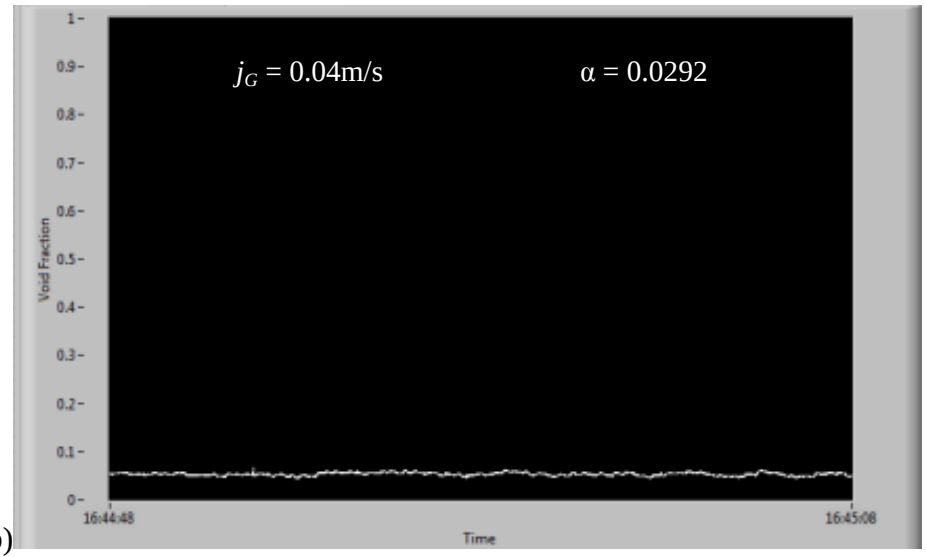
j_G = 0.04m/s
α = 0.0292
Void Fraction
1
0.9
0.8
0.7
0.6
0.5
0.4
0.3
0.2
0.1
0
16:44:48
16:45:08
Time

(c)

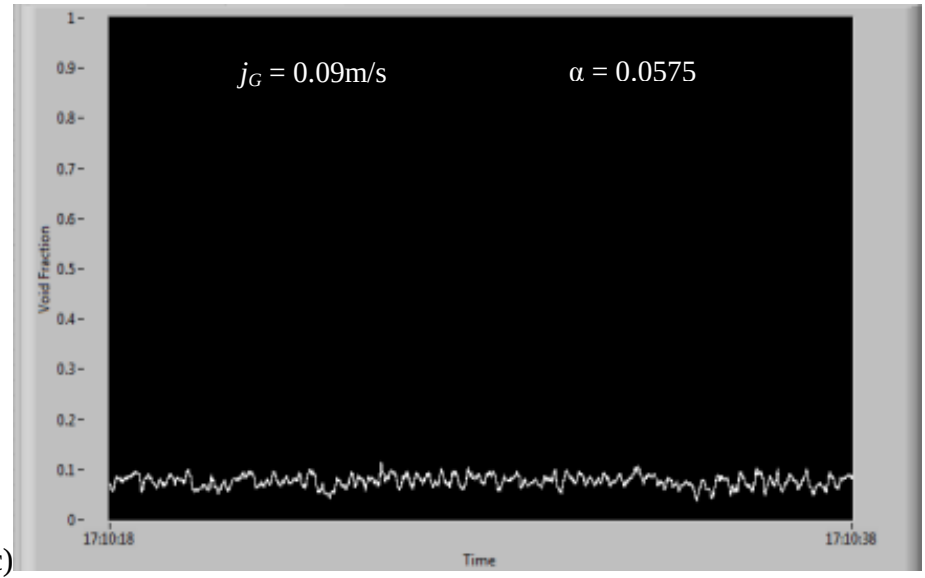
j_G = 0.09m/s
α = 0.0575
Void Fraction
1
0.9
0.8
0.7
0.6
0.5
0.4
0.3
0.2
0.1
0
17:10:18
17:10:38
Time

(d)

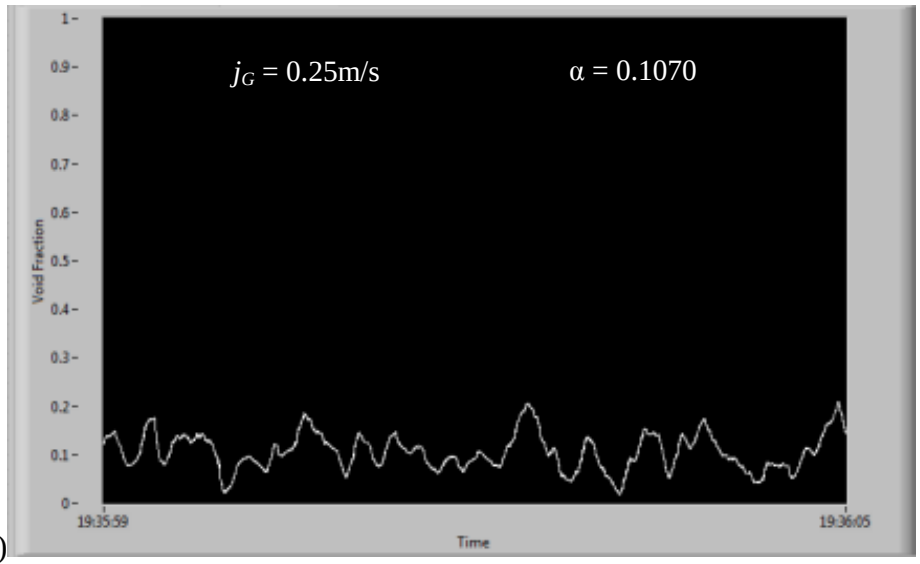

(e)

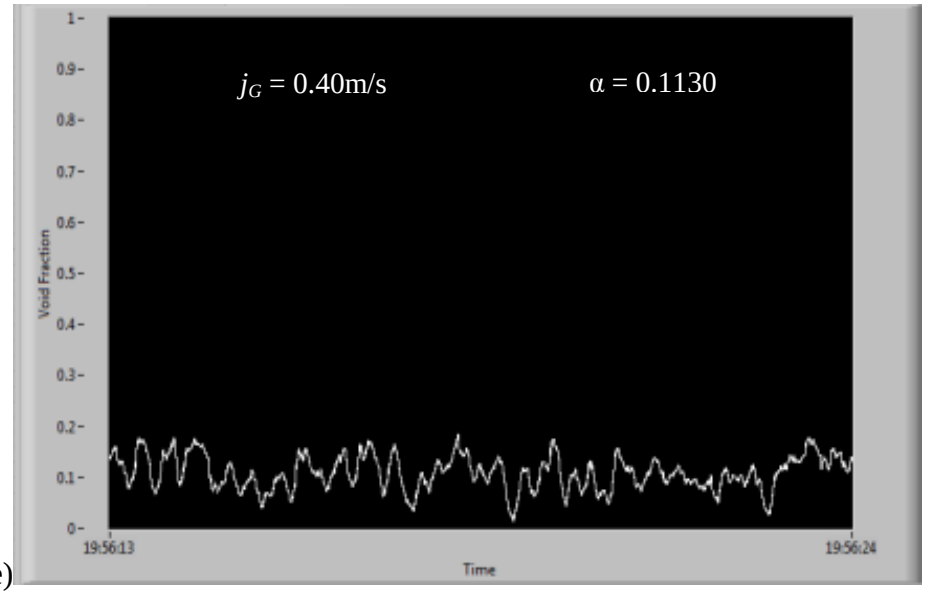

(f)

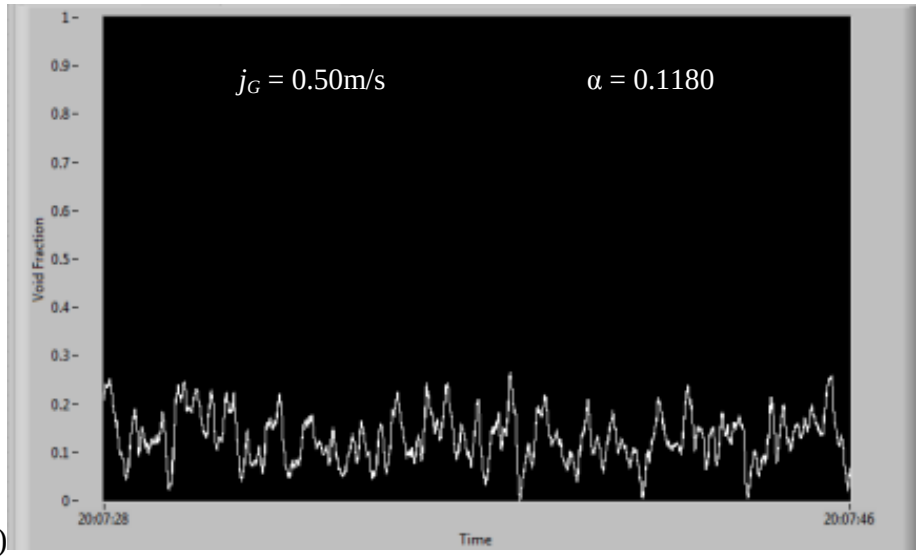

Figure 4.36: Void fraction at j_L = 0.16 m/s in 95.0-mm ID pipe. (a)-(b) Bubbly flow, (c) Bubbly-slug flow, (d) Slug flow, (e)-(f) Churn flow

(a)

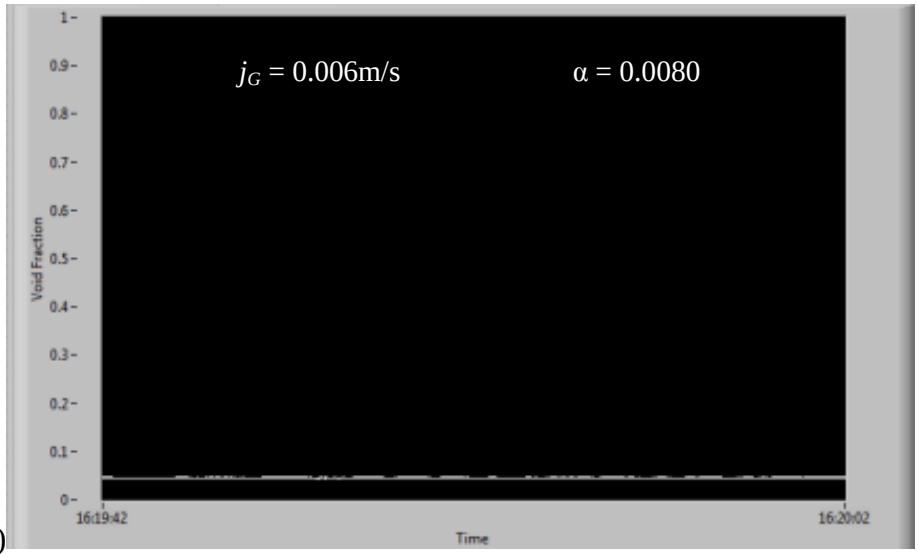
j_G = 0.006m/s
α = 0.0080
Void Fraction
1
0.9
0.8
0.7
0.6
0.5
0.4
0.3
0.2
0.1
0
16:19:42
16:20:02
Time

(b)

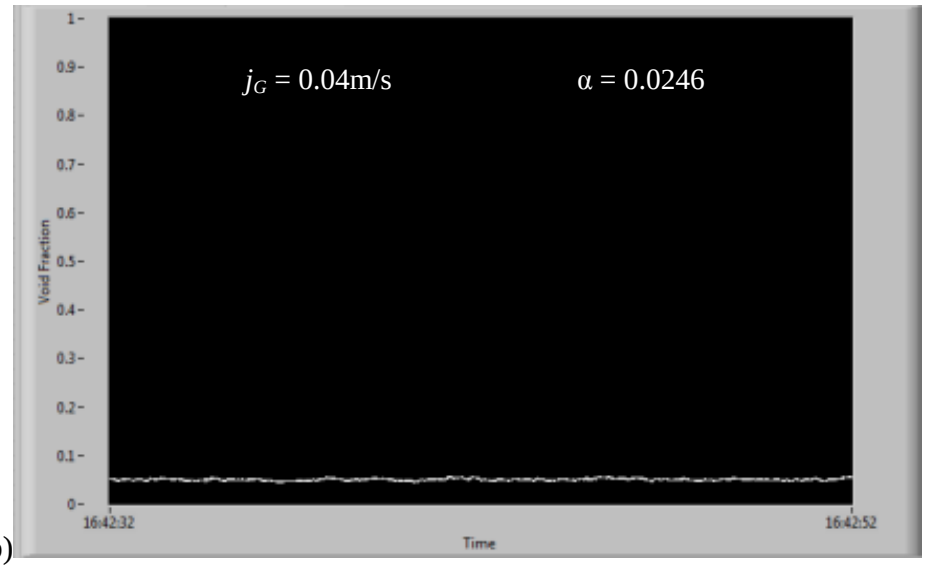
j_G = 0.04m/s
α = 0.0246
Void Fraction
1
0.9
0.8
0.7
0.6
0.5
0.4
0.3
0.2
0.1
0
16:42:32
16:42:52
Time

(c)

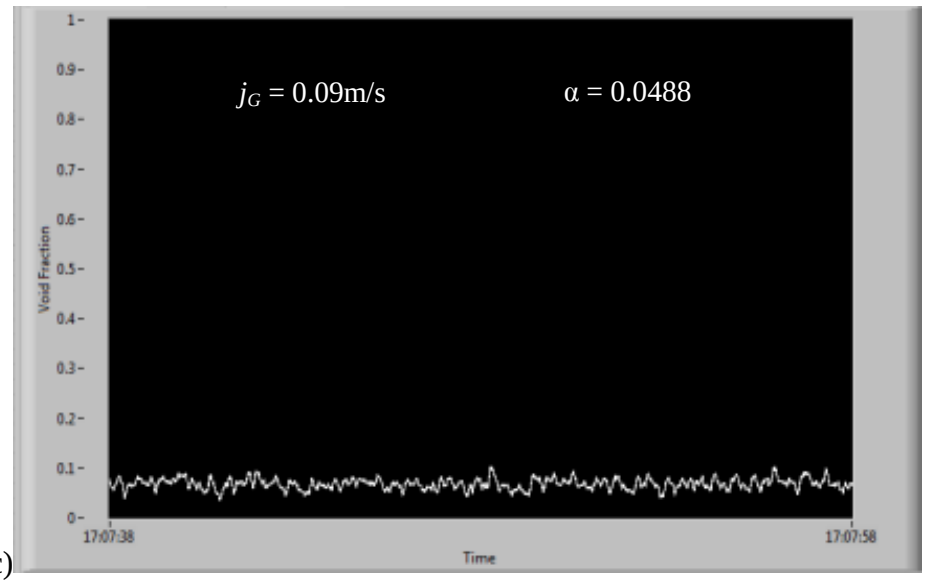
j_G = 0.09m/s
α = 0.0488
Void Fraction
1
0.9
0.8
0.7
0.6
0.5
0.4
0.3
0.2
0.1
0
17:07:38
17:07:58
Time

(d)

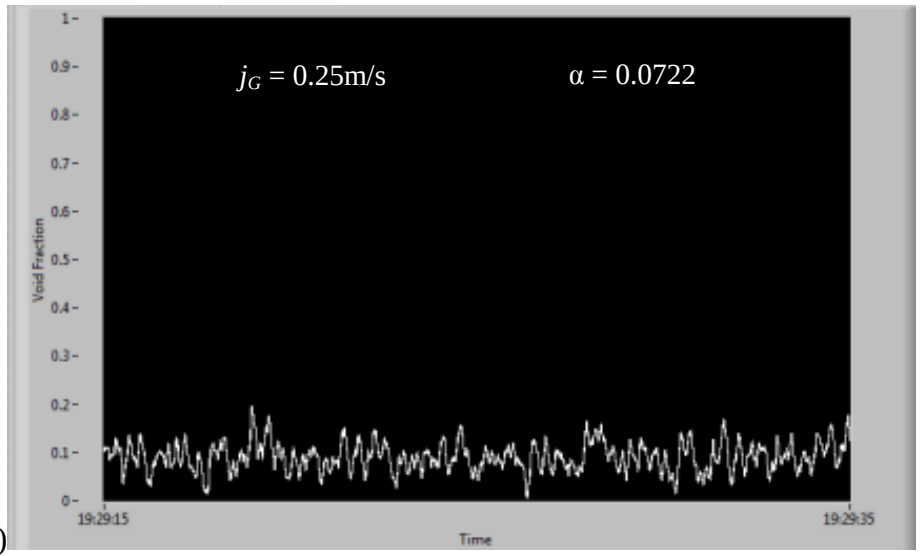

(e)

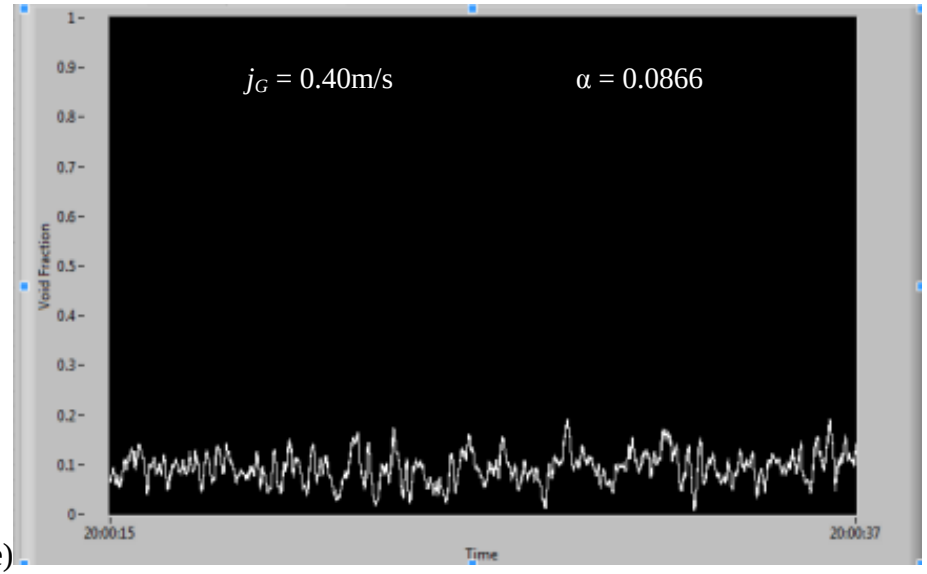

(f)

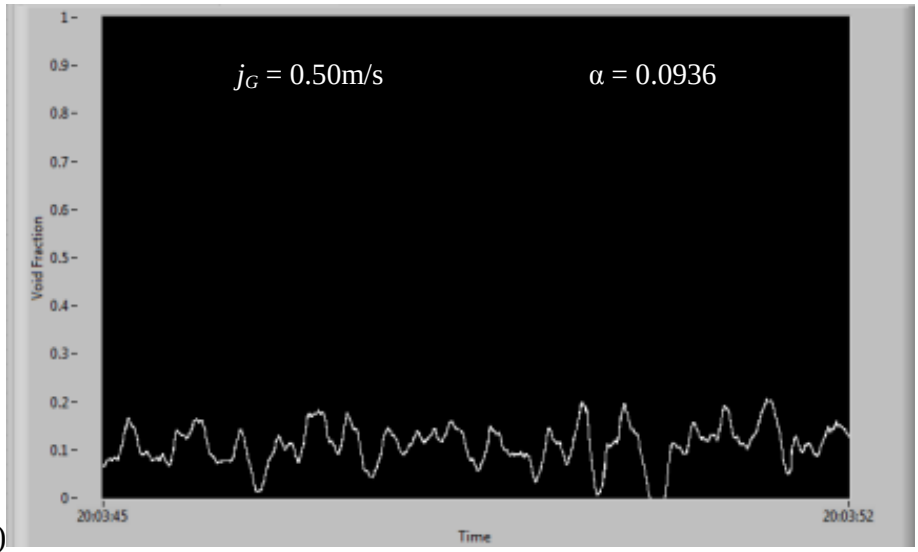

Figure 4.37: Void fraction at j_L = 0.25 m/s in 95.0-mm ID pipe. (a)-(b) Bubbly flow, (c) Bubbly-slug flow, (d) Slug flow, (e)-(f) Churn flow

4.3.2 Horizontal Pipes

i. 21.0-mm ID pipe

The void fraction experiment for the horizontal pipes was different from the upward vertical flow void fraction experiment. The horizontal experiment was a bit complicated compared to the upward vertical experiment. At low liquid superficial velocity, the pipe was not fully filled up with water, but the wetness of the pipe gave an effect to the sensor that affected the reading of the void fraction. With a careful calibration before the experiment, the problem can be solved.

Figure 4.38 showed the void fraction for the horizontal two-phase flow inside 21.0-mm ID pipe. The liquid superficial velocity was set up at j_L = 0.20 m/s and the gas superficial velocity was varied at range from j_G = 0.1 m/s to j_G = 2.0 m/s. Figure 4.38 (a) at void fraction α = 0.318 indicated the stratified flow at low gas superficial velocity. By increasing the gas superficial velocity, the void faction increase at α = 0.346 to α = 0.407 and the pattern changed to wavy flow that was shown in figure 4.38 (b) and (c) while the Figure 4.38 (d) at void fraction α = 0.474, the slug flow was appeared.

By increasing the liquid superficial velocity, the void fraction value decreased and changed the flow pattern. Figure 4.39 showed the void fraction at liquid superficial velocity j_L = 1.00 m/s and the range of gas superficial velocity from j_G = 0.1 m/s to j_G = 2.0 m/s. From the figure can be observed that the amplitude of the graph waves was increased compared to at j_L = 0.20 m/s. There were only two patterns observed during the experimentation, that was bubbly flow at void fraction α = 0.238 shows in figure 4.39 (a) and plug flow at void fraction α = 0.313 to α = 0.415 shown in Figure 4.39 (b) to (d).

At liquid superficial velocity j_L = 2.00 m/s, the void fraction value decreased compared to the previous result. The graph gave a different void fraction result that presented a difference flow pattern. Figure 4.40 (a) at void fraction α = 0.223 showed the bubbly flow at j_G = 0.1 m/s. The plug flow pattern appeared at void fraction α = 0.298 to α = 0.354 after increasing the gas superficial velocity shown in figure 4.40 (b) and (c). At gas superficial velocity j_G = 2.0 m/s and void fraction at α = 0.382, the slug flow taking part inside the pipe was shown in Figure 4.40 (d).

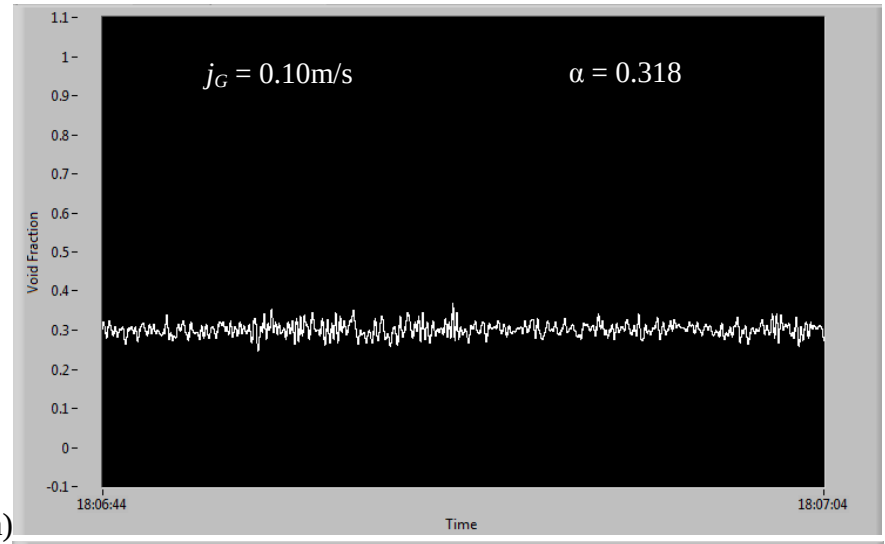

(a)

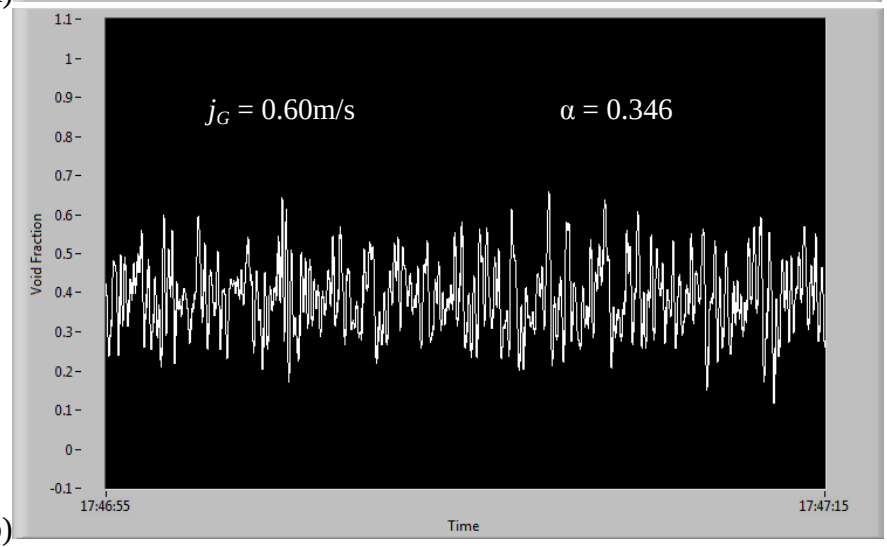

(b)

(c)

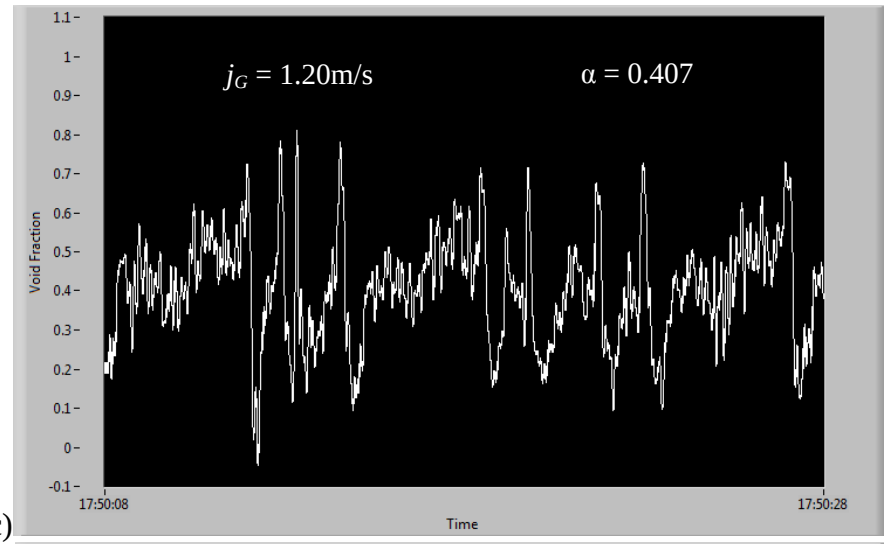

(d)

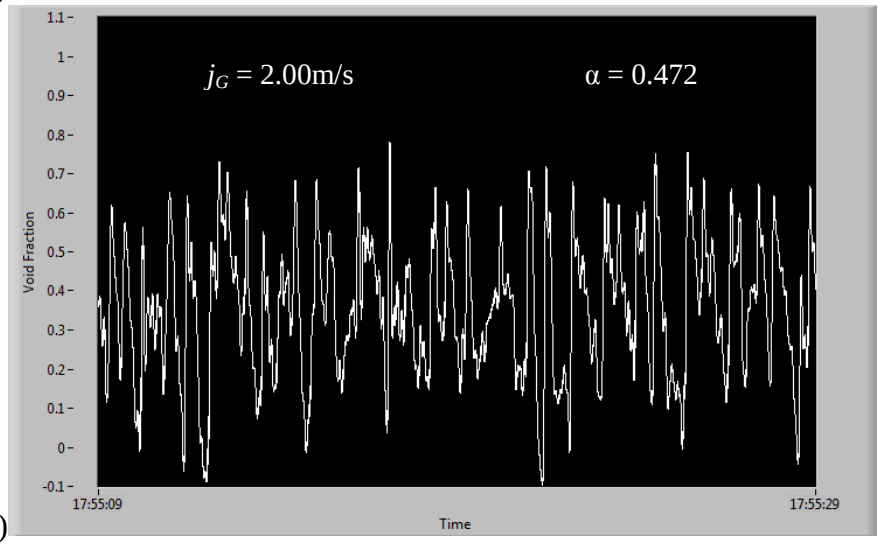

Figure 4.38: Void fraction at j_L = 0.20 m/s in 21.0-mm ID pipe. (a) Stratified flow, (b)-(c) Wavy flow, (d) Slug flow

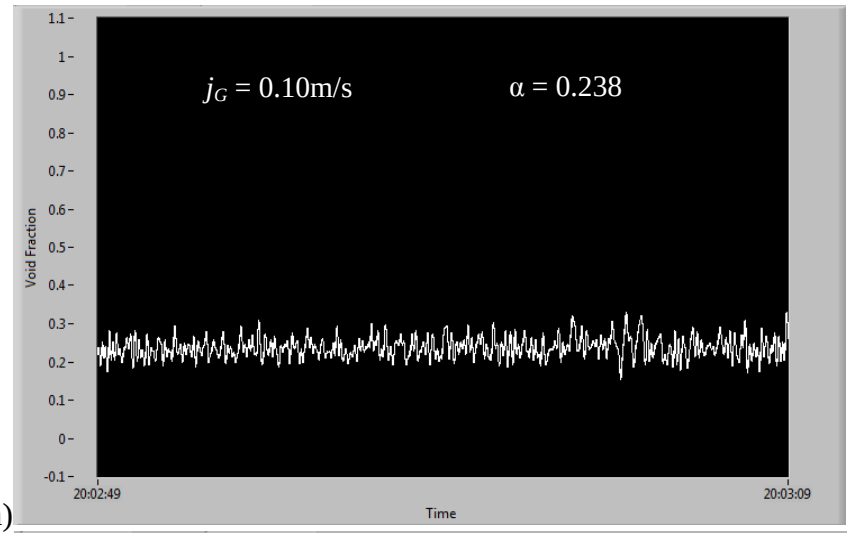
j_G = 0.10m/s
α = 0.238
Void Fraction
1.1
1
0.9
0.8
0.7
0.6
0.5
0.4
0.3
0.2
0.1
0
-0.1
20:02:49
20:03:09
Time

(a)

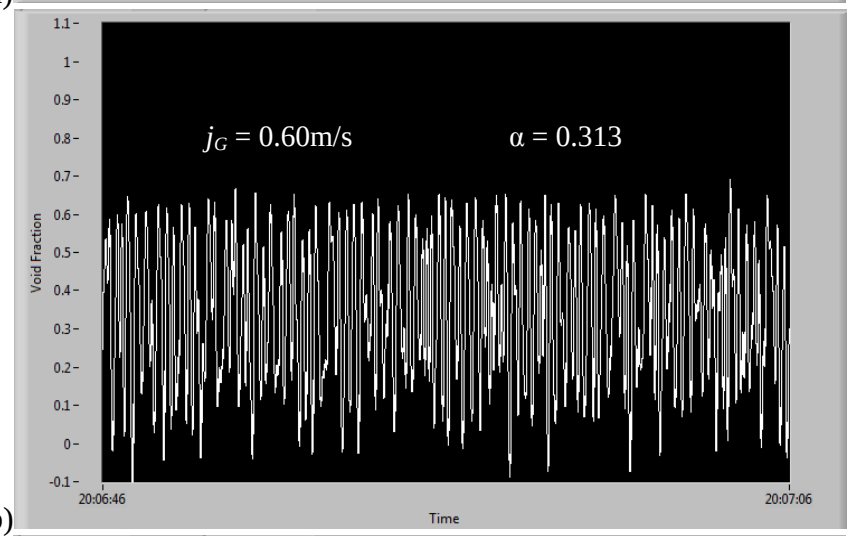
j_G = 0.60m/s
α = 0.313
Void Fraction
1.1
1
0.9
0.8
0.7
0.6
0.5
0.4
0.3
0.2
0.1
0
-0.1
20:06:46
20:07:06
Time

(b)

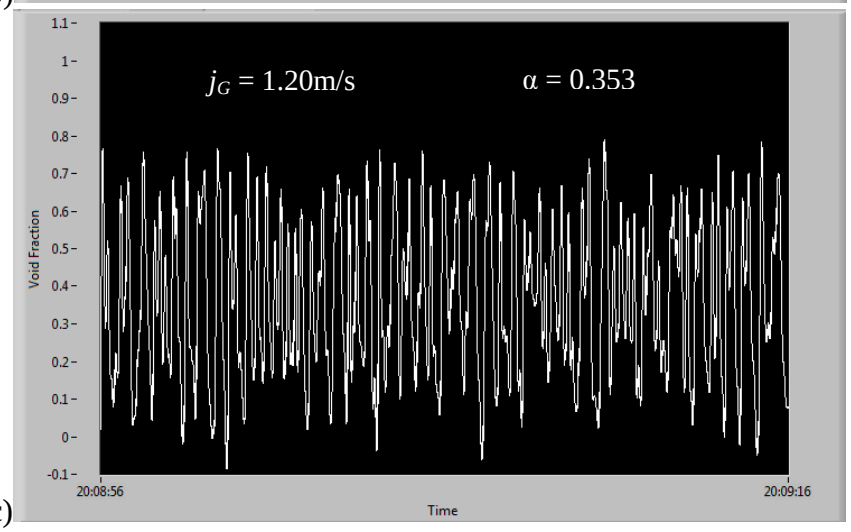
j_G = 1.20m/s
α = 0.353
Void Fraction
1.1
1
0.9
0.8
0.7
0.6
0.5
0.4
0.3
0.2
0.1
0
-0.1
20:08:56
20:09:16
Time

(c)

(d)

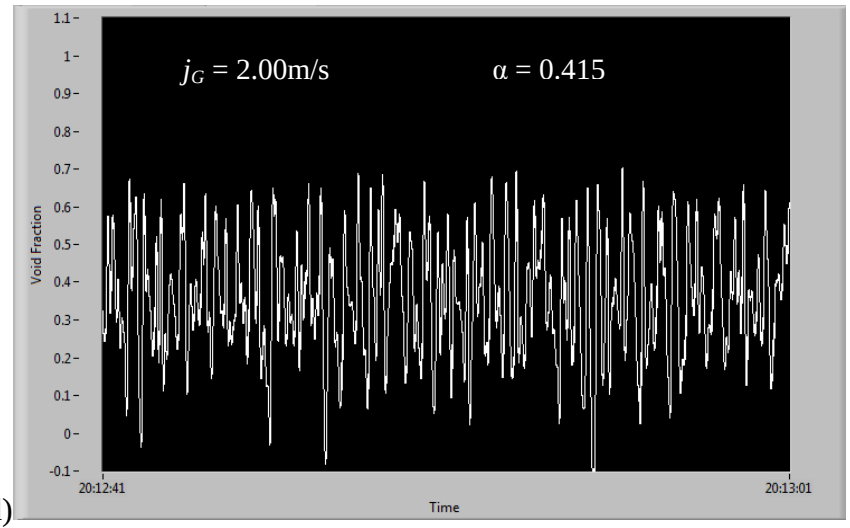

Figure 4.39: Void fraction at j_L = 1.0 m/s in 21.0-mm ID pipe. (a) Bubbly flow, (b)-(d) Plug flow

(a)

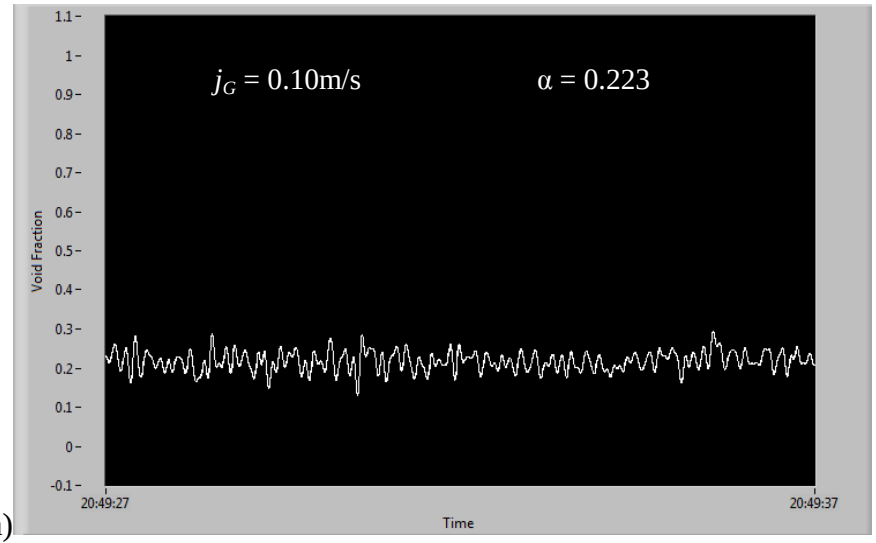

(b)

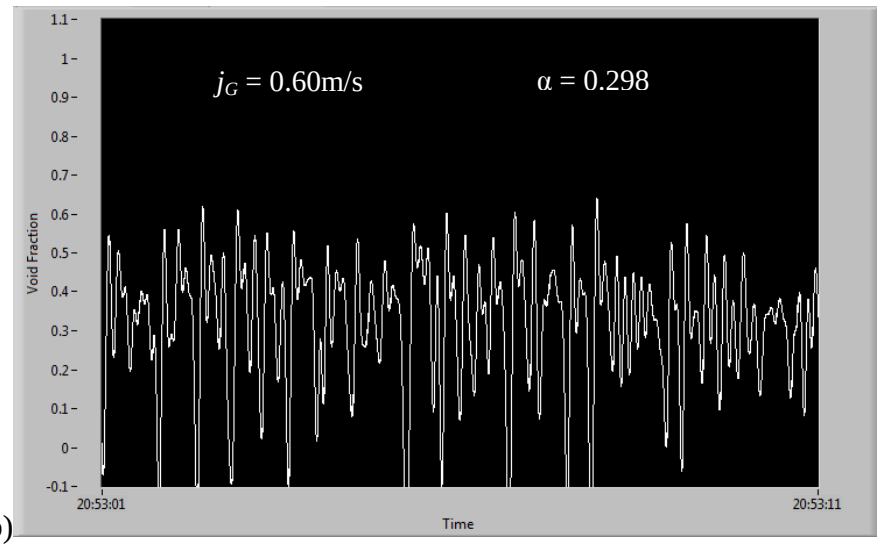

(c)

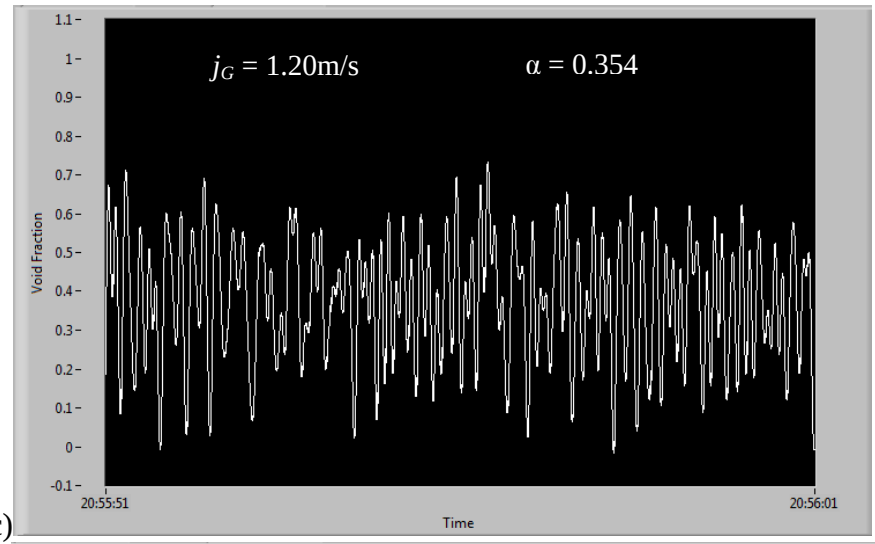

(d)

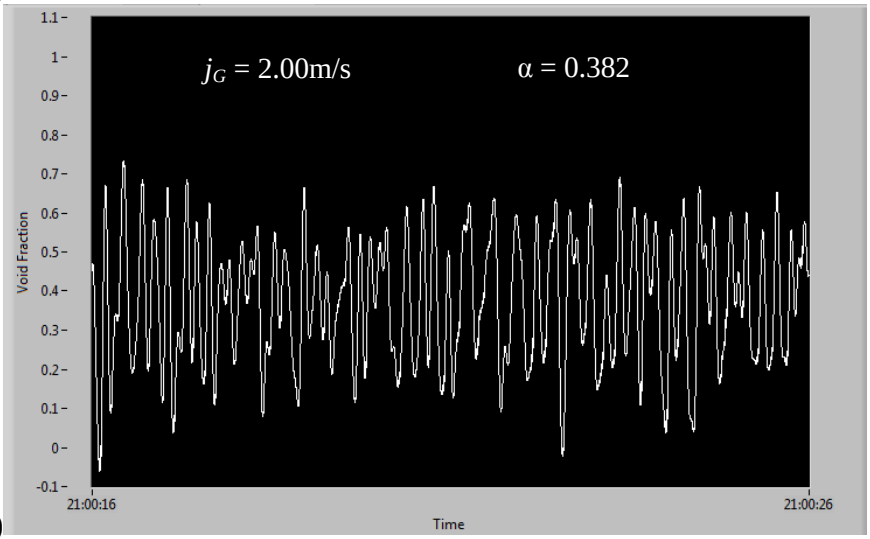

Figure 4.40: Void fraction at j_L = 2.0 m/s in 21.0-mm ID pipe. (a) Bubbly flow, (b)-(c) Plug flow, (d) Slug flow.

ii. 47.0-mm ID pipe

Figures 4.41 - 4.43 showed the void fraction for the two-phase flow inside the 47.0-mm ID pipe horizontal flow. The void fraction data were taken at the second section L/D = 23.94. The pipe has more difficulty to fill up with water compared to the 21.0-mm pipe. At low liquid superficial velocity, the void fraction value was high and by increasing the gas superficial velocity, the void fraction reading will further increase.

Figures 4.41 (a) - (c) at void fraction $\alpha = 0.354$ to $\alpha = 0.571$ indicated the stratified flow at liquid superficial velocity of $j_L = 0.20$ m/s and the gas superficial range from $j_G = 0.1$ m/s to $j_G = 1.2$ m/s. By increasing the gas superficial velocity to $j_G = 2.0$ m/s, the void fraction value increased to $\alpha = 0.668$ and the pattern changed to wavy flow.

Figure 4.42 illustrated the void fraction graph for the liquid superficial velocity at $j_L = 1.00$ m/s and the range of gas superficial velocity from $j_G = 0.1$ m/s to $j_G = 2.0$ m/s. The void fraction values were from $\alpha = 0.152$ to $\alpha = 0.351$ and the plug flow was appeared for all graphs. By further increasing of the liquid superficial velocity to $j_L = 1.6$ m/s the value of void fraction was decreased. From Figures 4.43 (a) to (d) showed that at range of gas superficial velocity from $j_G = 0.1$ m/s to $j_G = 2.0$ m/s the void fraction value were from $\alpha = 0.116$ to $\alpha = 0.248$ and the plug flow appeared at that range.

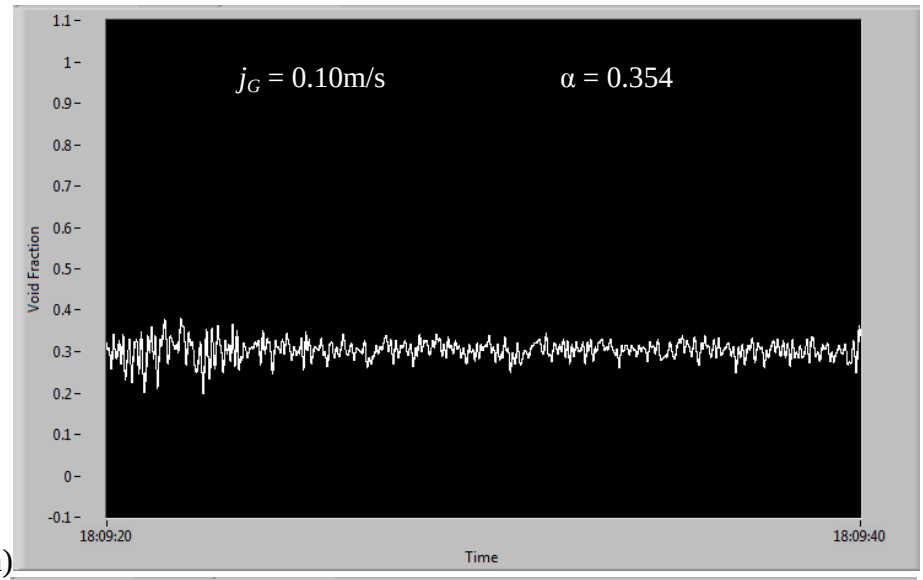
j_G = 0.10m/s
α = 0.354
Void Fraction
1.1
1
0.9
0.8
0.7
0.6
0.5
0.4
0.3
0.2
0.1
0
-0.1
18:09:20
18:09:40
Time

(a)

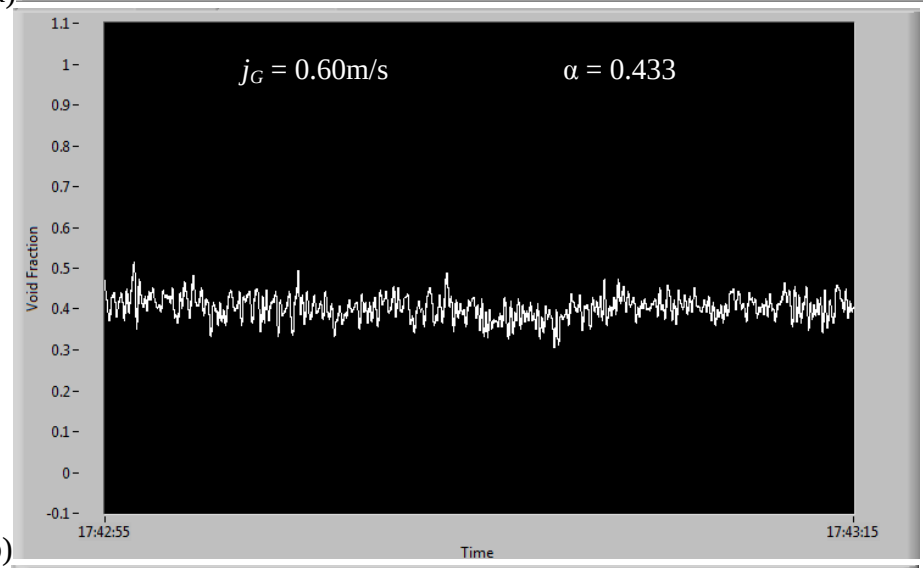
j_G = 0.60m/s
α = 0.433
Void Fraction
1.1
1
0.9
0.8
0.7
0.6
0.5
0.4
0.3
0.2
0.1
0
-0.1
17:42:55
17:43:15
Time

(b)

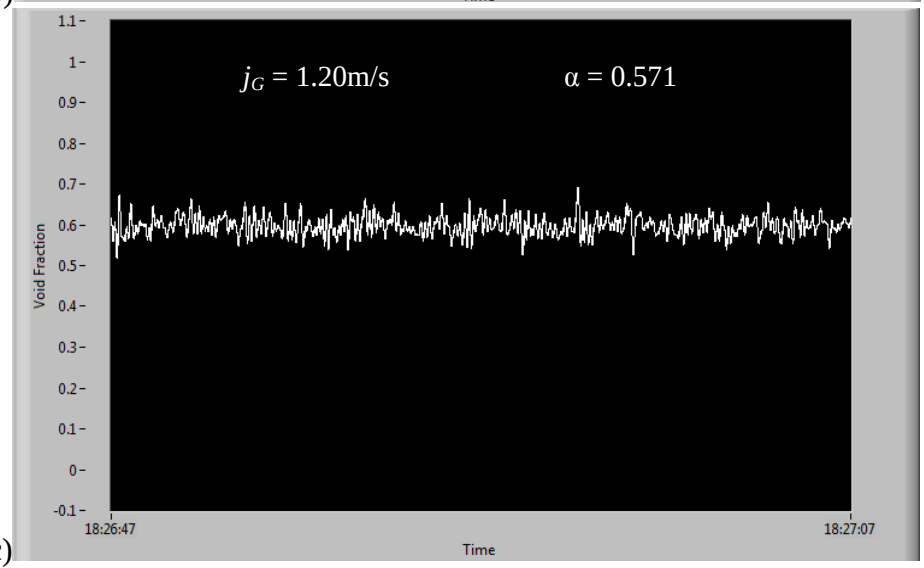
j_G = 1.20m/s
α = 0.571
Void Fraction
1.1
1
0.9
0.8
0.7
0.6
0.5
0.4
0.3
0.2
0.1
0
-0.1
18:26:47
18:27:07
Time

(c)

(d)

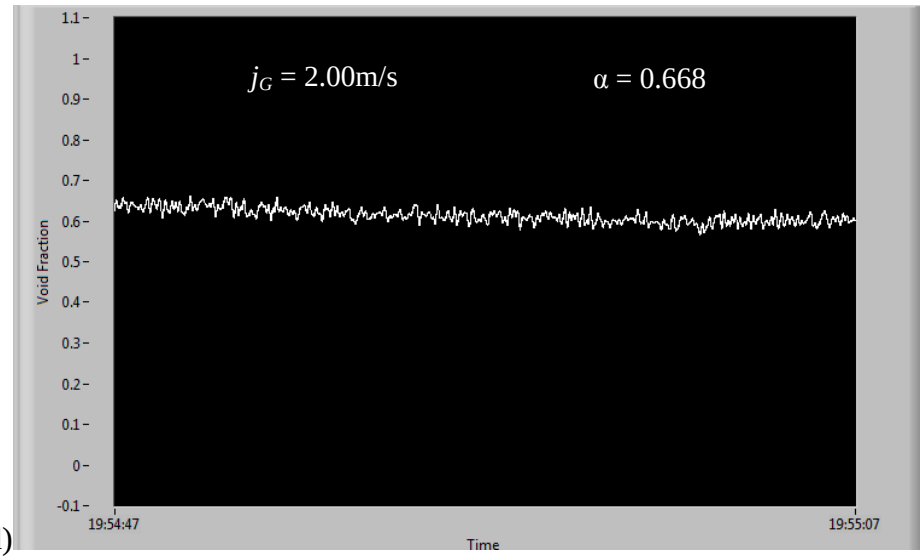

Figure 4.41: Void fraction at j_L = 0.20 m/s in 47.0-mm ID pipe. (a)-(c) Stratified flow, (d)Wavy flow

(a)

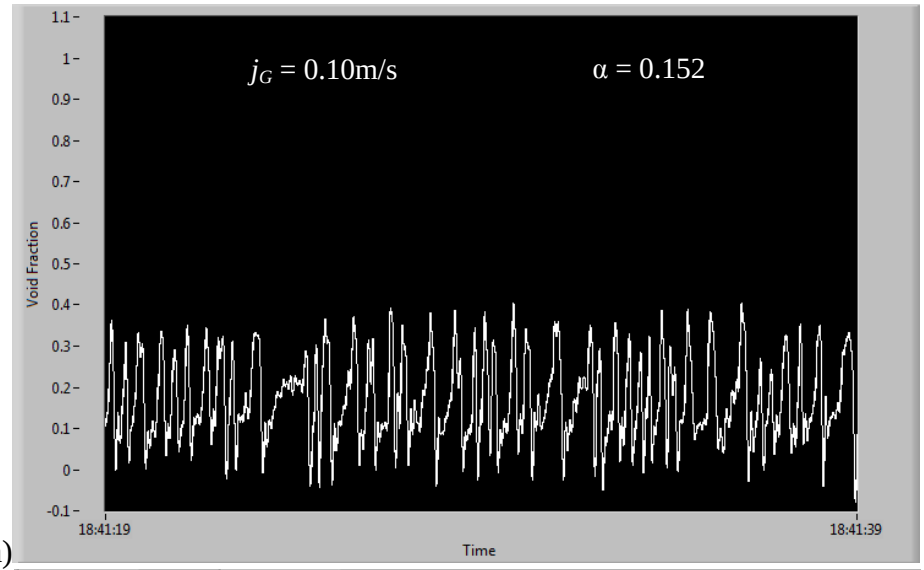

(b)

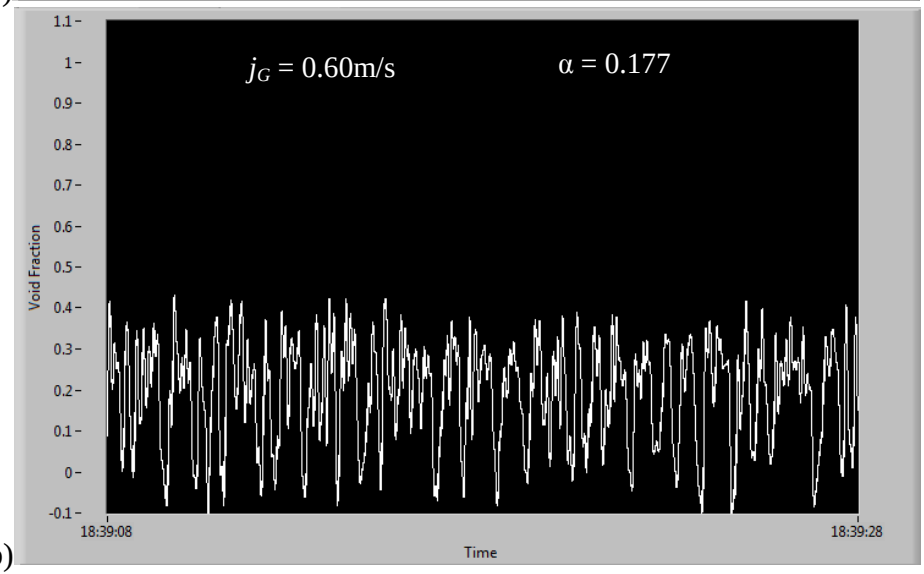

(c)

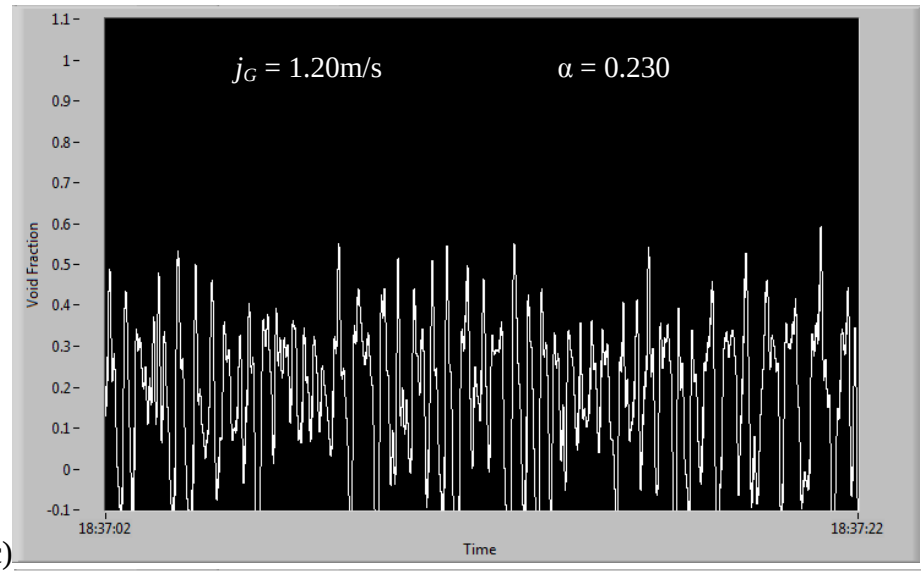

(d)

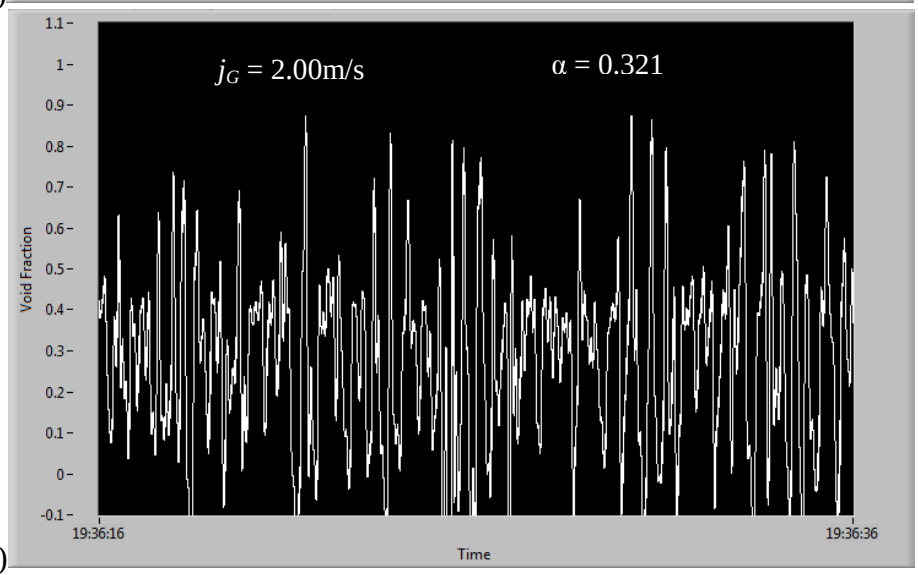

Figure 4.42: Void fraction at j_L = 1.0 m/s in 47.0-mm ID pipe. (a)-(d) Plug flow

(a)

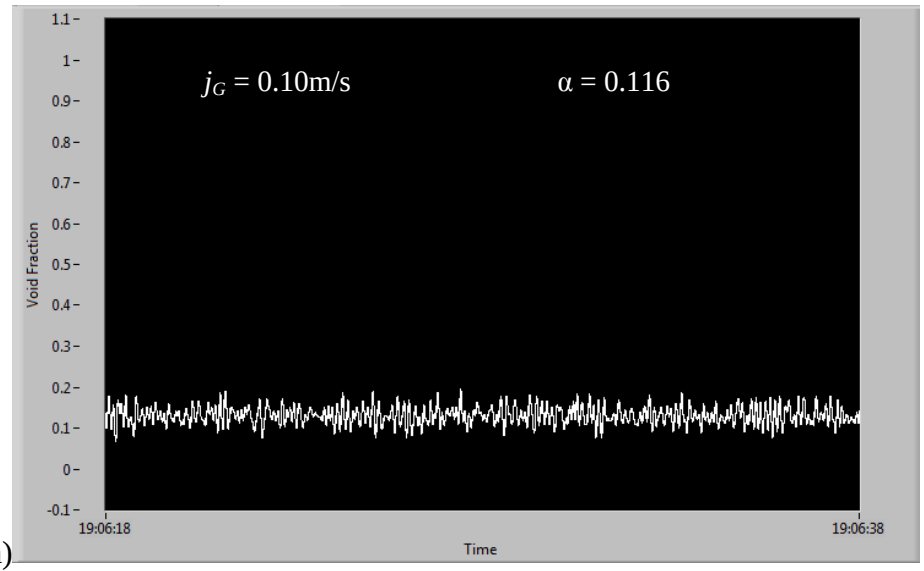

(b)

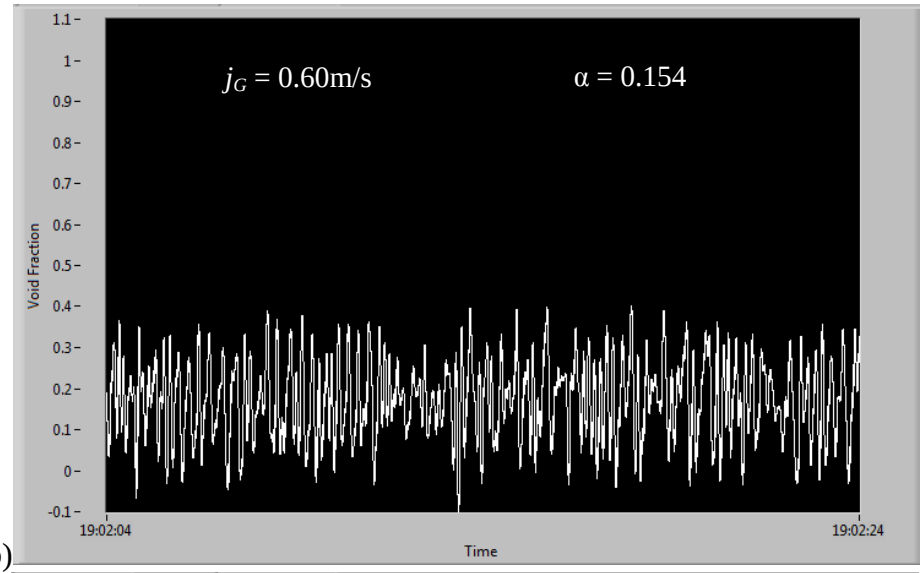

(c)

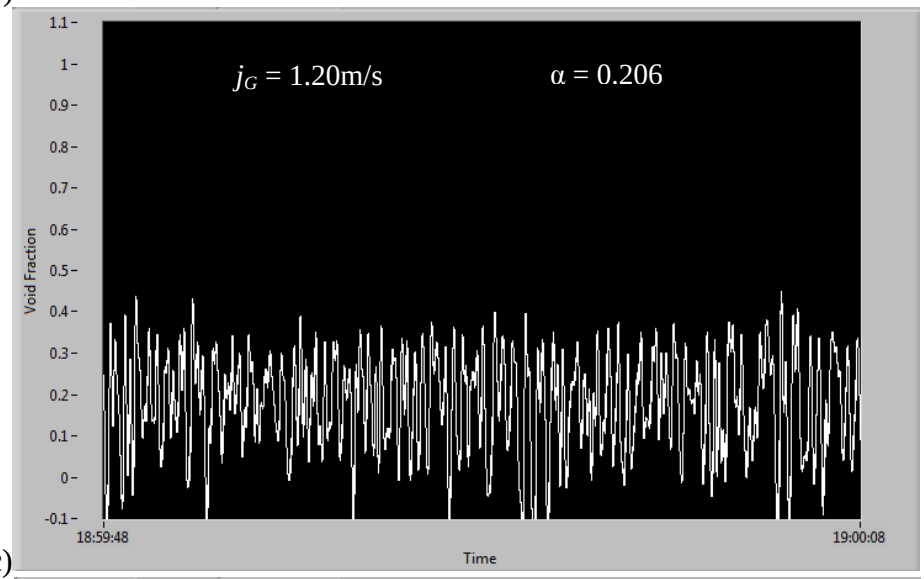

(d)

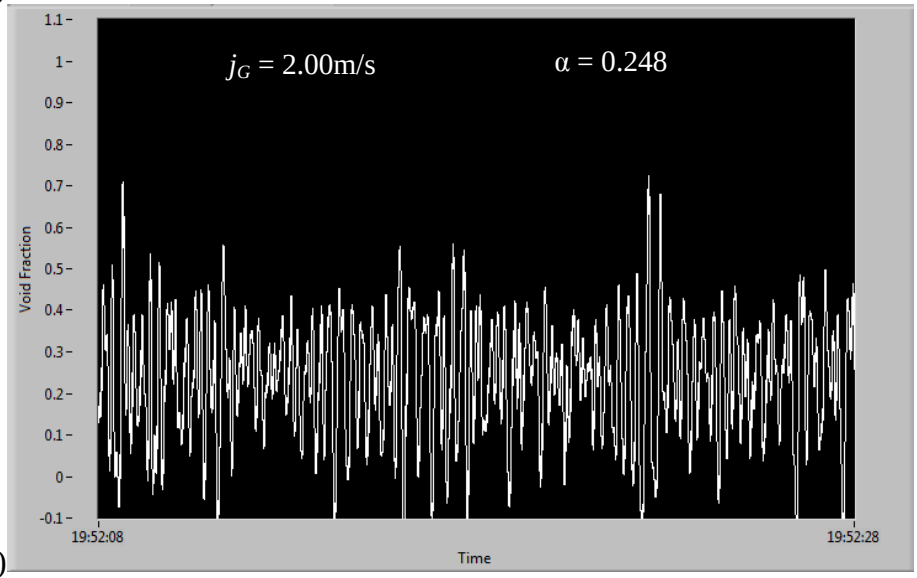

Figure 4.43: Void fraction at j_L = 1.6 m/s in 47.0-mm ID pipe. (a)-(d) Plug flow

iii. 95.0-mm ID pipe

The void fraction experimentations inside the 95.0-mm ID horizontal flow pipe were carried out at a low gas and liquid superficial velocity due to the limitation as mentioned in the previous section. Figures 4.44 - 4.46 showed the void fraction for the two-phase flow inside the 95.0-mm ID horizontal pipe. The liquid superficial velocity was set up at a few different points and the range of gas superficial velocity was set up j_G = 0.1 m/s to j_G = 0.4 m/s. At low liquid superficial velocity, the pipe was never fully filled up with water and as a result, only a few flow patterns can be observed during the experiment.

Figure 4.44 (a) – (d) illustrated the void fraction for the fixed liquid superficial velocity at j_L = 0.05 m/s. The range of gas superficial velocity was from j_G = 0.1 m/s to j_G = 0.4 m/s. From the observation, the wave was stable in all graphs. The void fraction values were at α = 0.364 to α = 0.372 and the flow pattern was a stratified flow pattern. By increasing the liquid superficial velocity to j_L = 0.2 m/s and at the same range of gas superficial velocity, the void fraction values were decreased slightly that was shown in figure 4.45. Figures 4.45 (a) – (d) indiceted the value of void fraction from α = 0.362 to α = 0.367 and the stratified flow pattern appeared at all figures.

The void fraction values were decreased after increasing the liquid superficial velocity to j_L = 0.4 m/s at the same range of gas superficial velocity that was shown in figure 4.46. The graph wave fluctuated more compared to at j_L = 0.05 m/s and j_L = 0.2 m/s. Figures 4.46 (a) – (d) show the void fraction values at α = 0.355 to α = 0.367 and the pattern was a wavy flow.

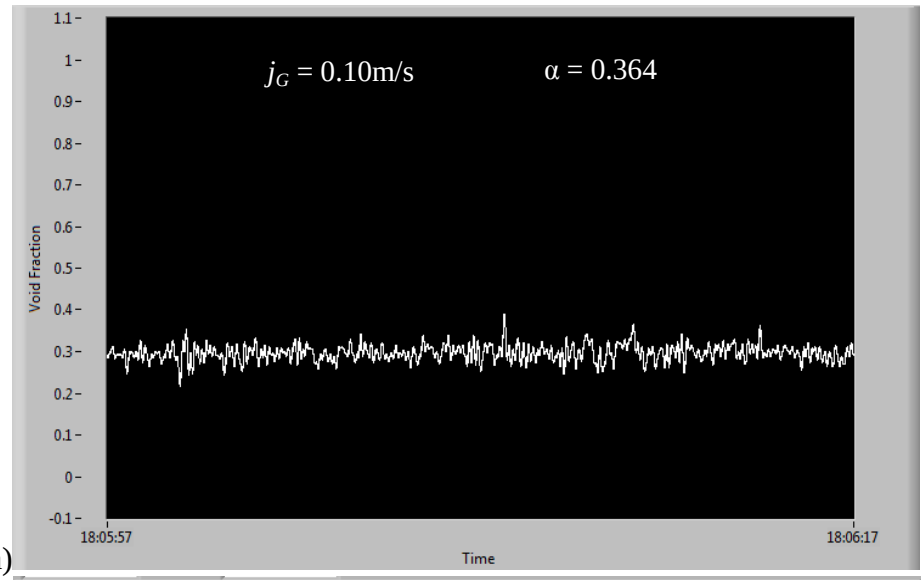
j_G = 0.10m/s
α = 0.364
Void Fraction
1.1
1
0.9
0.8
0.7
0.6
0.5
0.4
0.3
0.2
0.1
0
-0.1
18:05:57
18:06:17
Time

a)

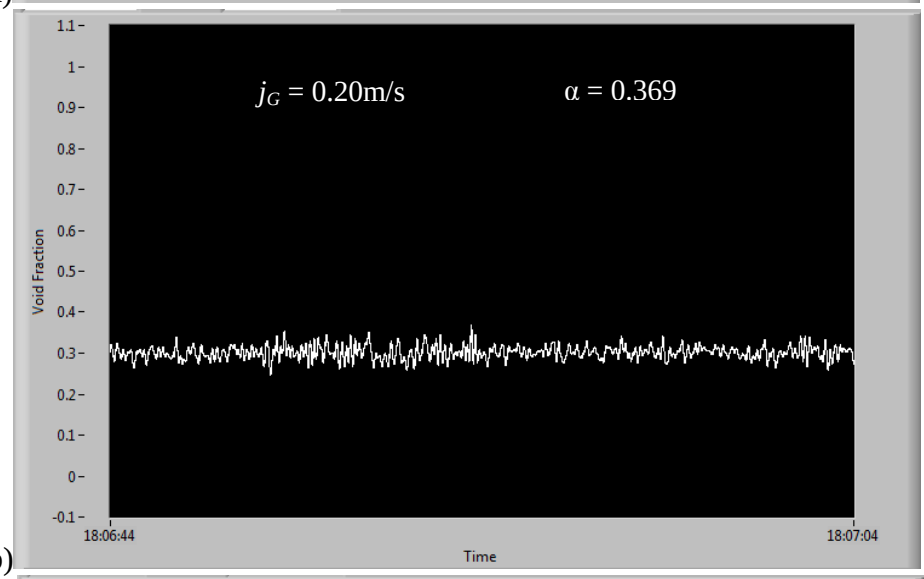
j_G = 0.20m/s
α = 0.369
Void Fraction
1.1
1
0.9
0.8
0.7
0.6
0.5
0.4
0.3
0.2
0.1
0
-0.1
18:06:44
18:07:04
Time

b)

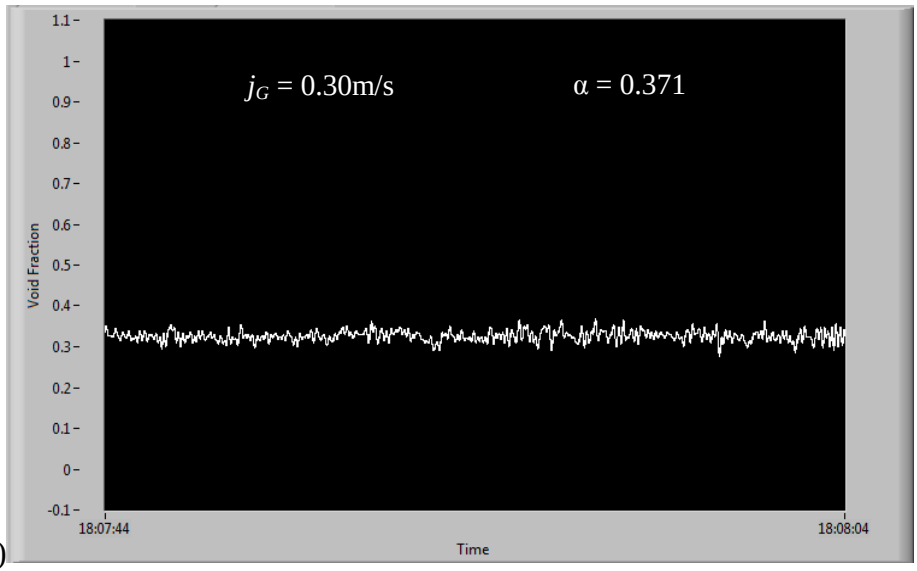
j_G = 0.30m/s
α = 0.371
Void Fraction
1.1
1
0.9
0.8
0.7
0.6
0.5
0.4
0.3
0.2
0.1
0
-0.1
18:07:44
18:08:04
Time

(c)

(d)

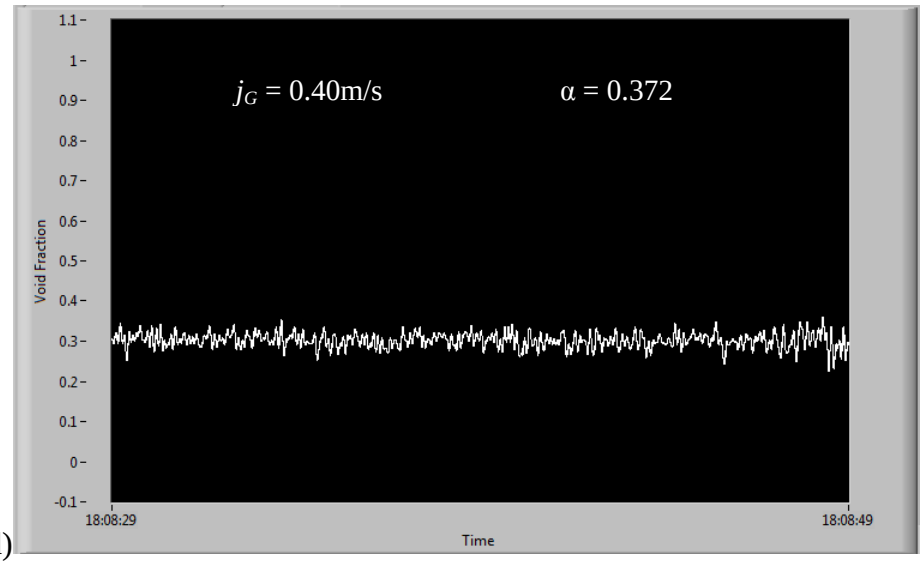

Figure 4.44: Void fraction at j_L = 0.05 m/s in 95.0-mm ID pipe. (a)-(d) Stratified flow

(a)

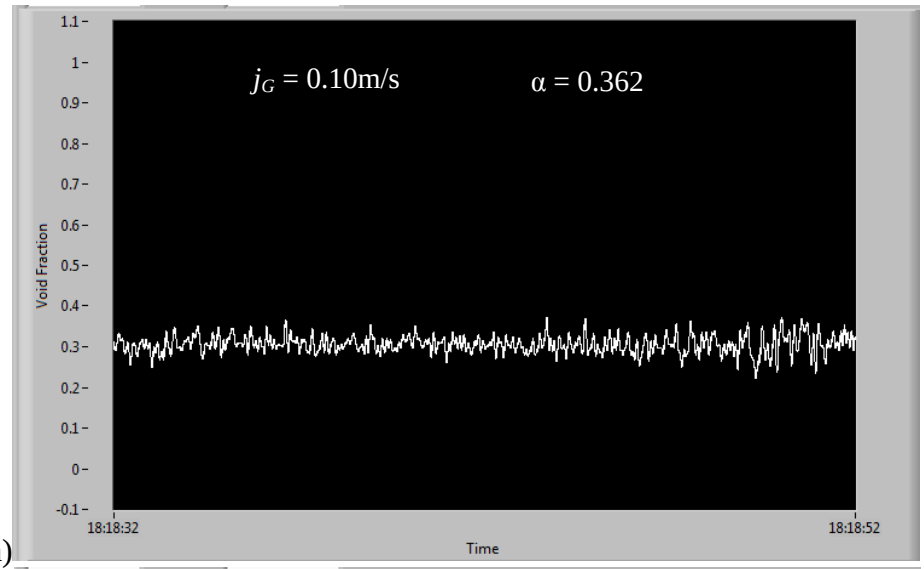

(b)

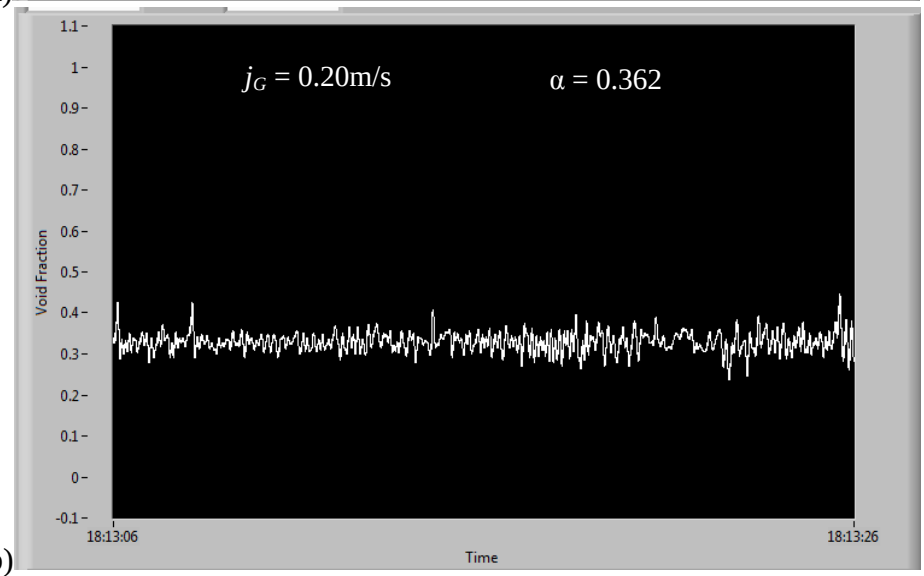

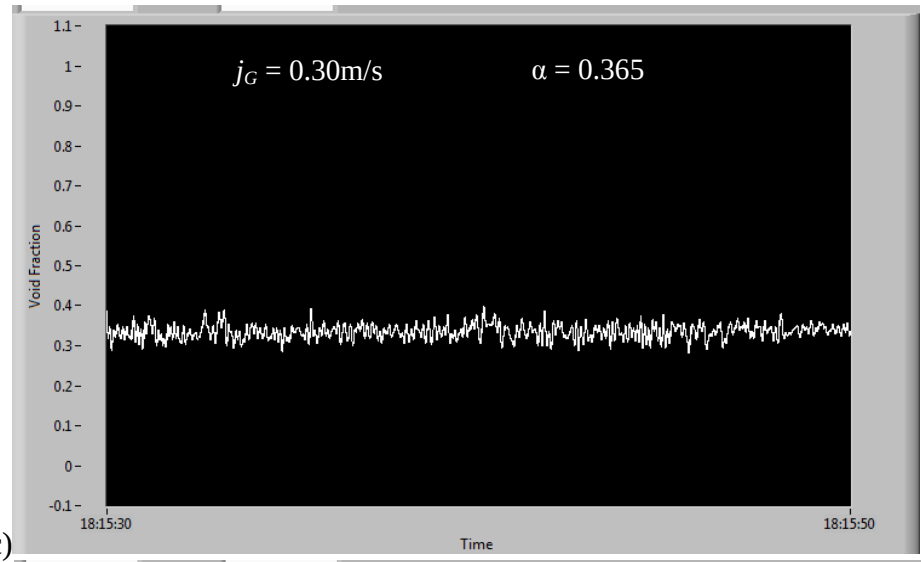

(c)

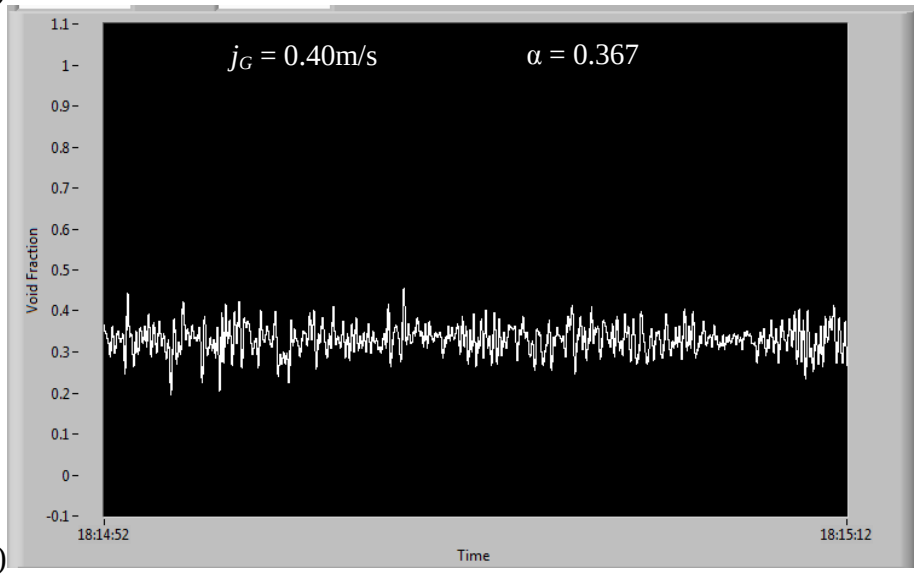

(d)

Figure 4.45: Void fraction at j_L = 0.20 m/s in 95.0-mm ID pipe. (a)-(d) Stratified flow

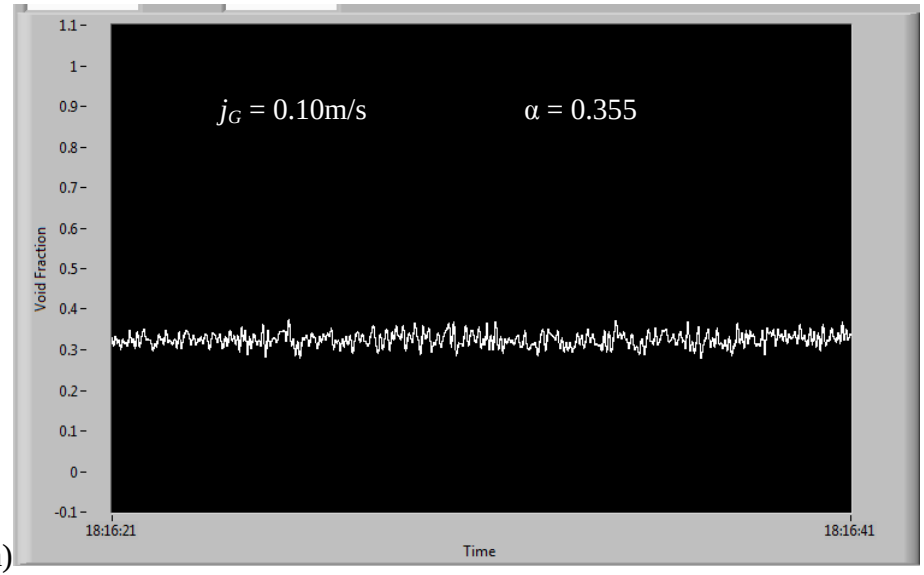

(a)

(b)

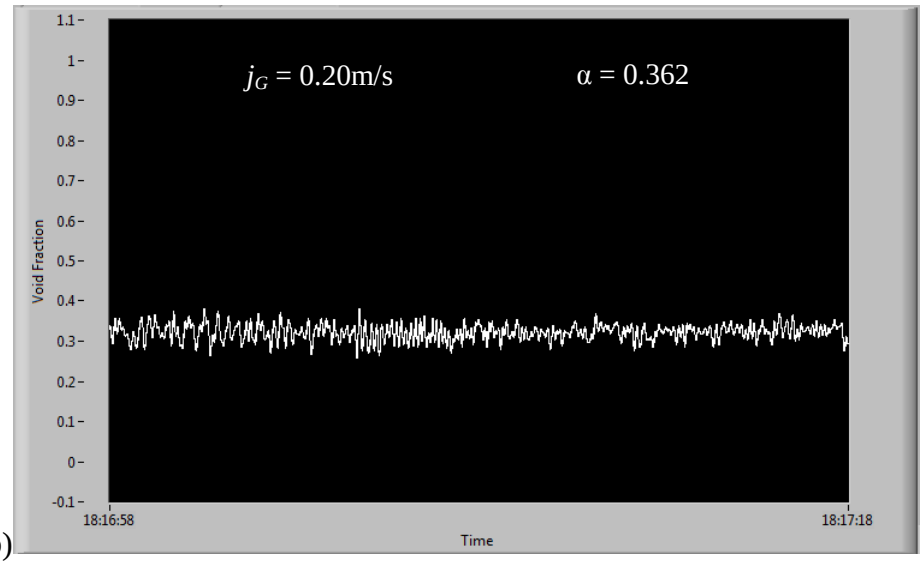

(c)

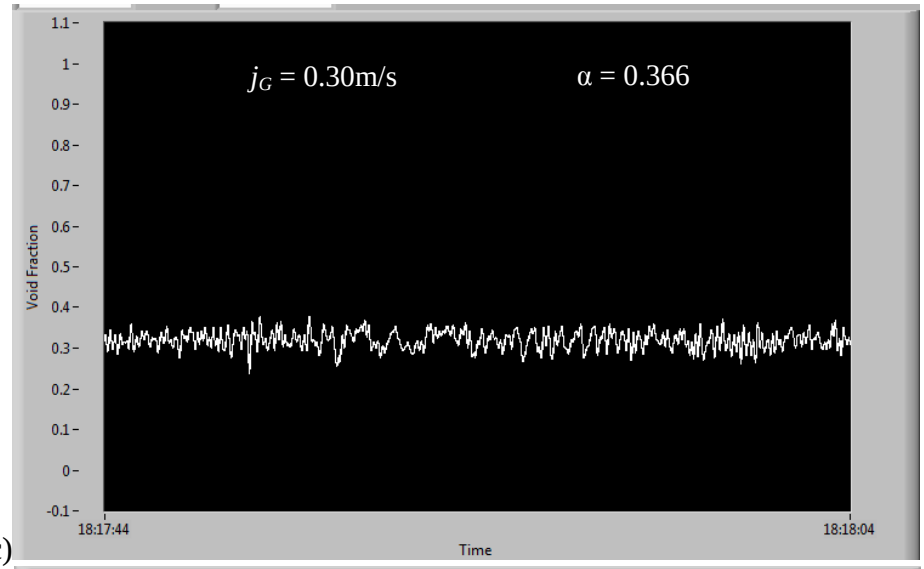

(d)

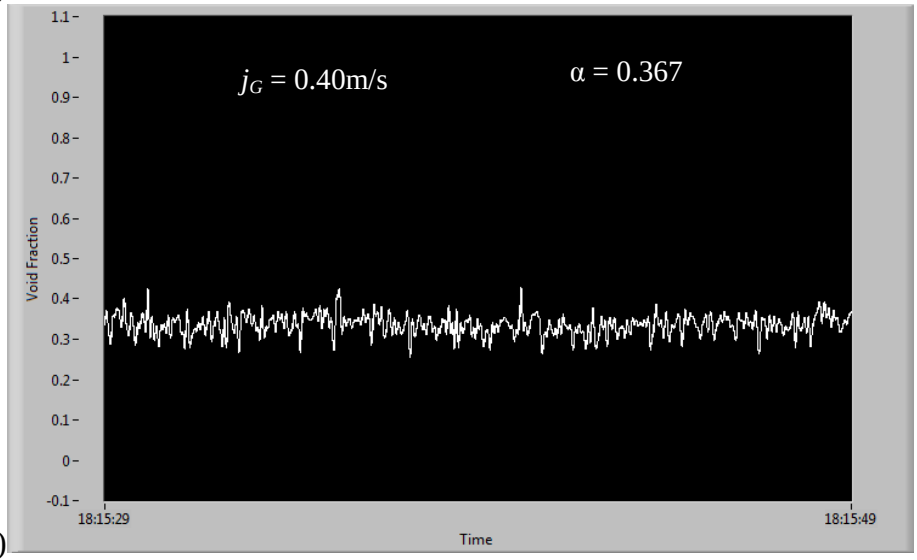

Figure 4.46: Void fraction at j_L = 0.40 m/s in 95.0-mm ID pipe. (a)-(d) Wavy flow

The measurement of void fraction using the CECM method was successful. Every flow patterns of two-phase flow gave a different and unique pattern in CECM result that shows the type and characteristic of the flow. The flow pattern and void fraction can be easily determined from the void fraction plot.

Overall, the increase of void fraction was proportionate to gas superficial velocity, j_G at constant liquid superficial velocity, j_L and decreased with the increasing liquid superficial velocity, j_L at constant gas superficial velocity, j_G in all pipes. This experiment gave a same conclusion and agrees well the experiment done by Triplett et al. (1999). The void values recorded in these experiments were found to be directly proportional with the amount of gas and liquid percentage inside the pipe. However, slight error of the reading during the experimentation can be neglected. The overall reading and result can be accepted to measure the void fraction of two-phase flow by using the CECM method.

4.4. Void Fraction Relationship

4.4.1 Vertical Pipes

Since, the gas and liquid superficial velocity gave an effect to the value of void fraction of two-phase flow inside the pipe, overall void fraction relationship between the gas and liquid superficial velocity can be analyzed to pursuit any possible consequences in the two-phase flow channel.

i. 21.0-mm ID pipe

Figure 4.47 showed the relationship between the gas and liquid superficial velocity and the void fraction value of two-phase upward vertical flow inside the 21.0-mm ID pipe. The gas superficial velocity range for this experiment was from j_G = 0.04 m/s to j_G = 2.00 m/s and the liquid superficial velocity was set up at j_L = 0.08 m/s, j_L = 0.16 m/s, j_L = 0.25 m/s, j_L = 0.5 m/s, and j_L = 0.10 m/s. The values of void fraction were nearly linear until the increase of the gas superficial velocity at fixed gas superficial velocity.

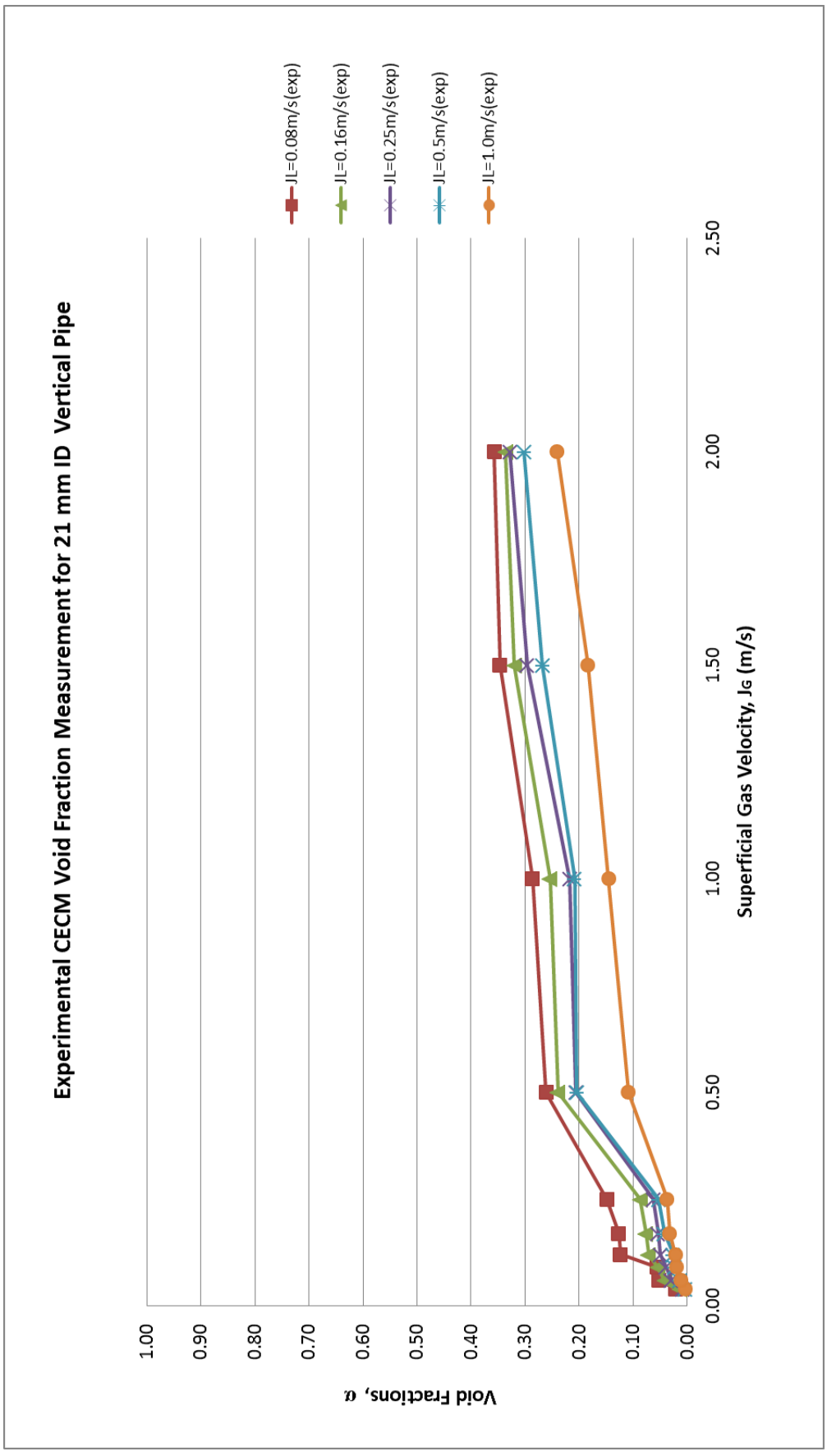

Figure 4.47: Void fraction relationship for 21.0-mm ID vertical upward flow pipe

ii. 47.0-mm ID pipe

Figure 4.48 illustrated the relationship between the gas and liquid superficial velocity and the merged void fraction value of two-phase upward vertical flow inside the 47.0-mm ID pipe. It had the same pattern as for the 21.0-mm ID pipe. The gas superficial velocity ranged from j_G = 0.04 m/s to j_G = 2.00 m/s and the liquid superficial velocity was fixed at j_L = 0.08 m/s, j_L = 0.16 m/s, j_L = 0.25 m/s, j_L = 0.7 m/s, and j_L = 0.10 m/s. The plotted data were not very much linear compared to the 21.0-mm pipe because of some measurement uncertainties during the experiment.

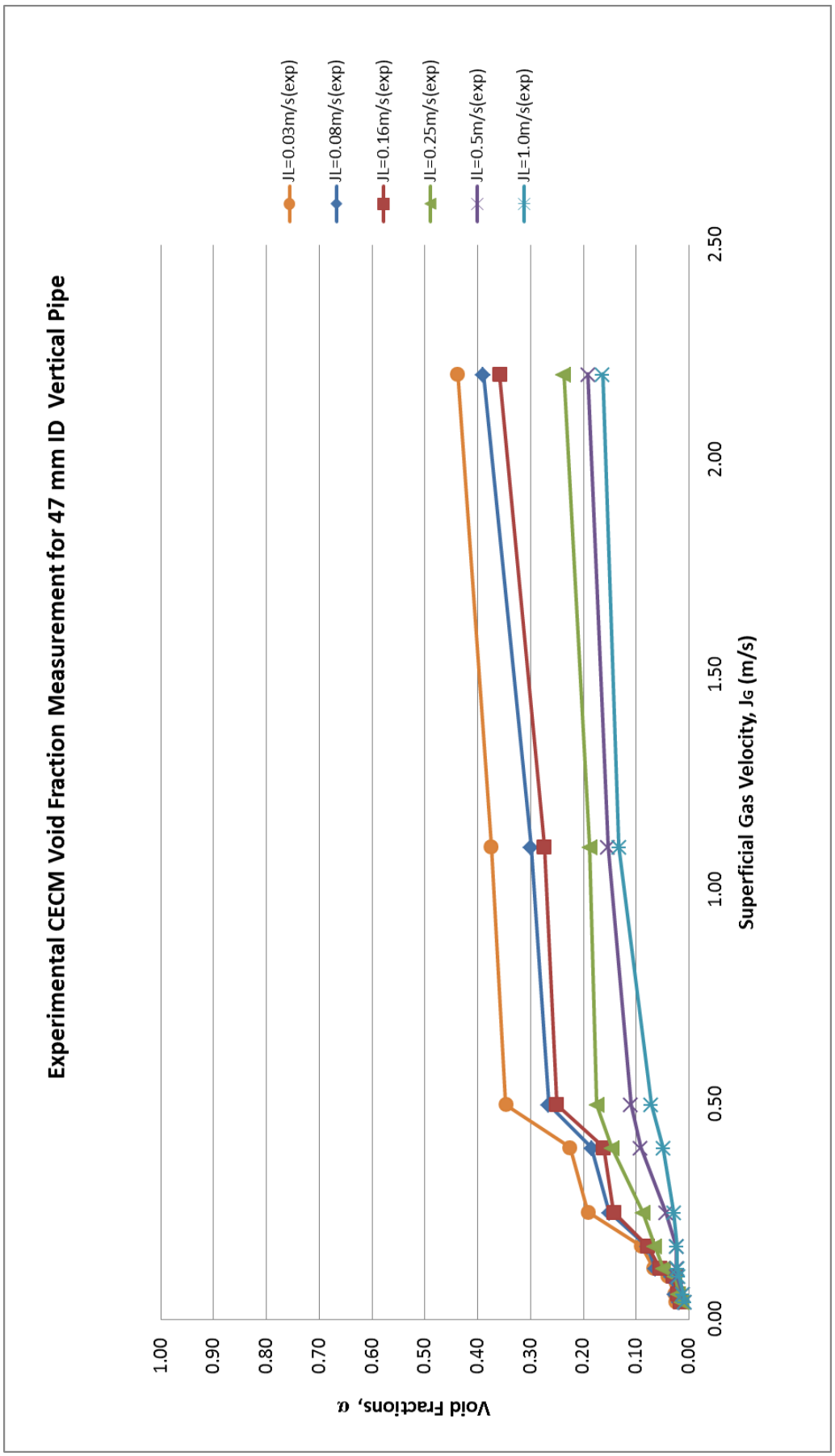

Figure 4.48: Void fraction relationship for 47.0-mm ID vertical upward flow pipe

iii. 95.0-mm ID pipe

Figure 4.49 showed the relationship between the gas and liquid superficial velocity and the void fraction value of two-phase vertical upward flow inside the 95.0-mm inner diameter pipe. The experiments were conducted at low gas and liquid superficial velocity due to the limitation of the experiment equipment. The gas superficial velocity ranged from $j_G = 0.006$ m/s to $j_G = 0.50$ m/s and the liquid superficial velocity were fixed at $j_L = 0.006$ m/s, $j_L = 0.03$ m/s, $j_L = 0.08$ m/s, $j_L = 0.16$ m/s, and $j_L = 0.25$ m/s. From the figure, the lines were smooth and have better results compared to the 21.0-mm and 47.0-mm pipes. This result also arises from the low value of gas and liquid superficial velocity during the experiment.

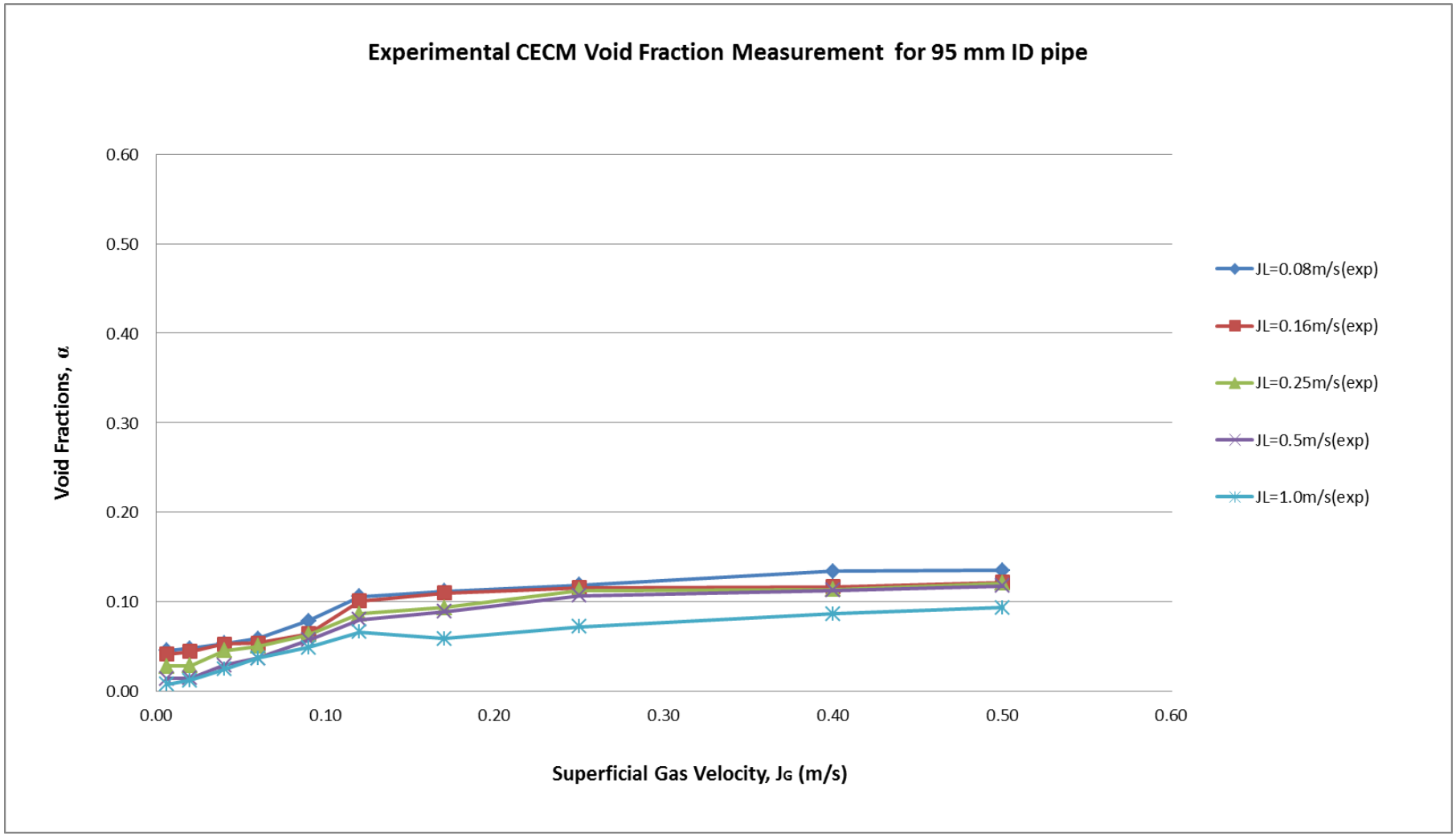

Figure 4.49: Void fraction relationship for 95.0-mm ID vertical upward flow pipe

The patterns in all three pipes, suggested that with the increase in the gas superficial velocity with decreasing the liquid superficial velocity, the value of void fraction will also increase. The effect of both gas and liquid superficial velocity gave very significant changes to the value of void fraction for the two-phase flow inside the pipe.

4.4.2 Horizontal Pipes

i. 21.0-mm ID pipe

The void fraction of two-phase flow inside the horizontal pipe has nearly the same value for the upward vertical flow. Figure 4.50 showed the relationship between the gas and liquid superficial velocity and the void fraction for two-phase horizontal flow inside the 21.0-mm ID pipe. The range of gas superficial velocity was from j_G = 0.1 m/s to j_G = 2.00 m/s and the liquid superficial velocity were fix at j_L = 0.05, m/s j_L = 0.1 m/s, j_L = 0.4 m/s, j_L = 0.8 m/s, j_L = 1.2 m/s, j_L = 1.6 m/s and j_L = 2.0 m/s.

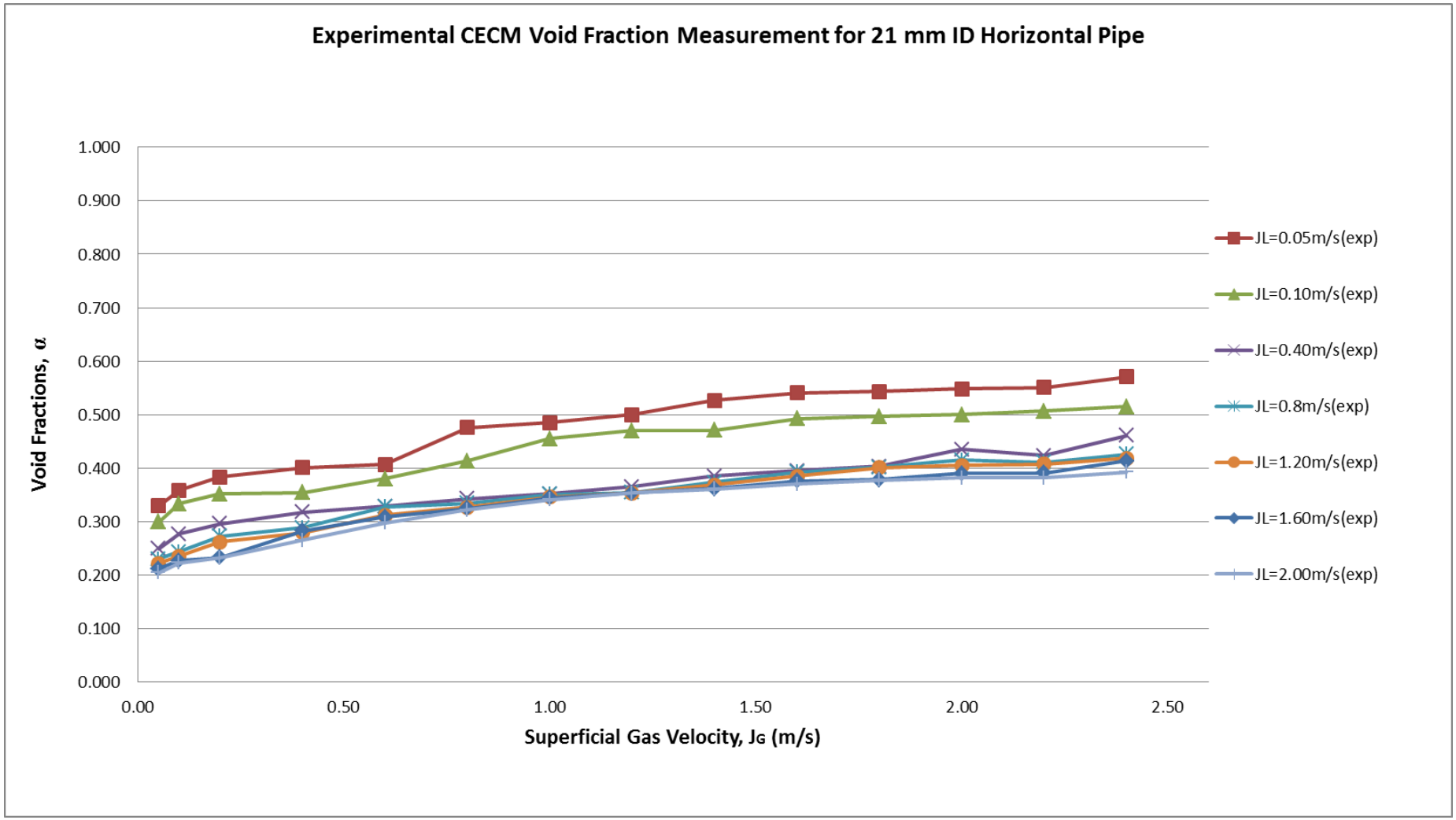

Figure 4.50: Void fraction relationship for 21.0-mm ID horizontal pipe

ii. 47.0-mm ID pipe

Figure 4.51 showed the relationship between the gas and liquid superficial velocity and the void fraction for two-phase horizontal flow inside the 47.0-mm ID pipe. The gas superficial velocity ranged from $j_G = 0.1$ m/s to $j_G = 2.0$ m/s and the liquid superficial velocity were fixed at $j_L = 0.05$, $j_L = 0.1$ m/s, $j_L = 0.4$ m/s, $j_L = 0.8$ m/s, $j_L = 1.2$ m/s, and $j_L = 1.6$ m/s.

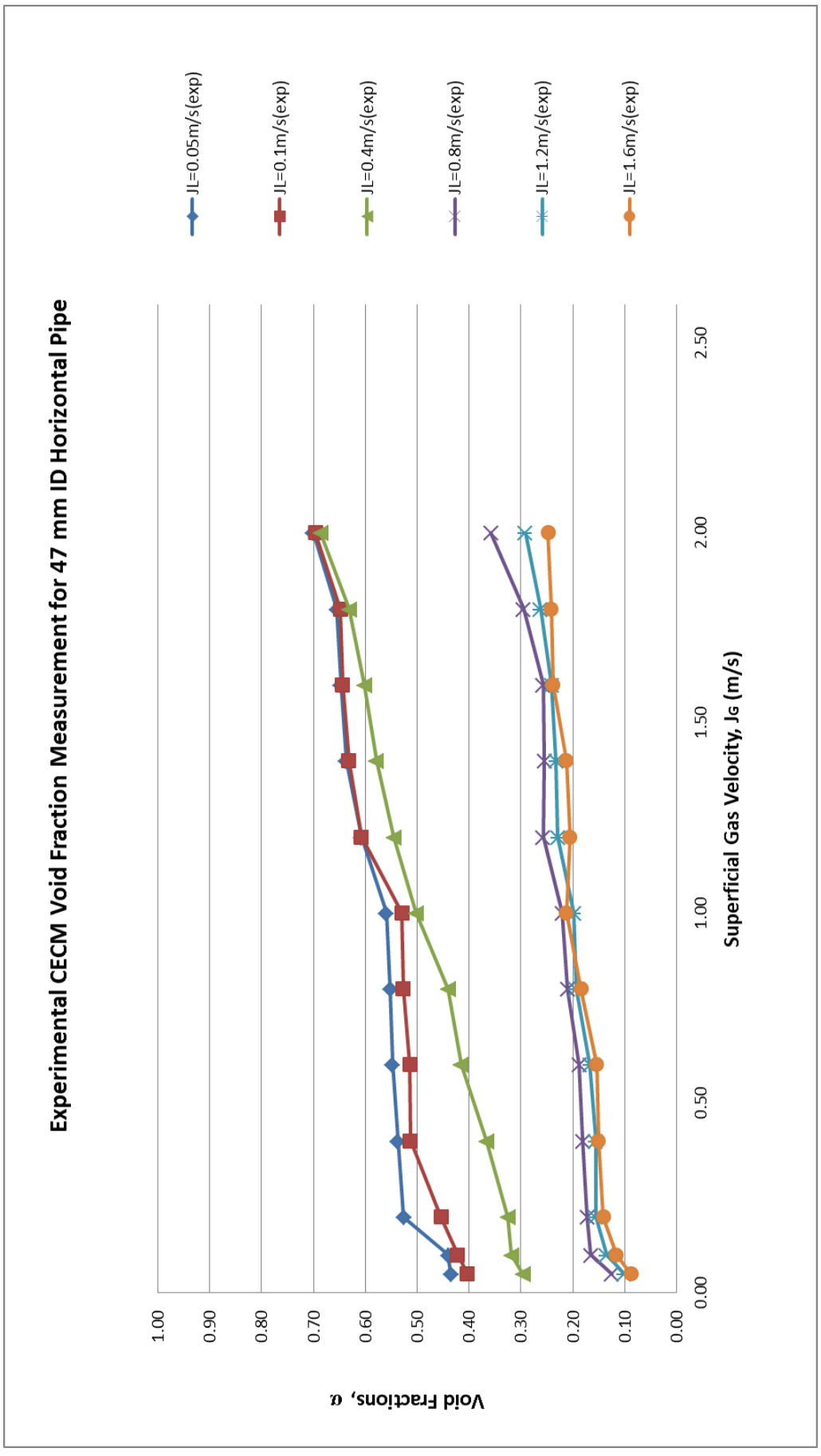

Figure 4.51: Void fraction relationship for 47.0-mm ID horizontal pipe

iii. 95.0-mm ID pipe

Figure 4.52 showed the relationship between the gas and liquid superficial velocity and the void fraction for two-phase horizontal flow inside the 95.0-mm ID pipe. The range of gas superficial velocity was from $j_G = 0.1$ m/s to $j_G = 0.4$ m/s and the liquid superficial velocity were fixed at $j_L = 0.05$, $j_L = 0.1$ m/s, $j_L = 0.2$ m/s, $j_L = 0.3$ m/s, and $J_L = 0.4$ m/s.

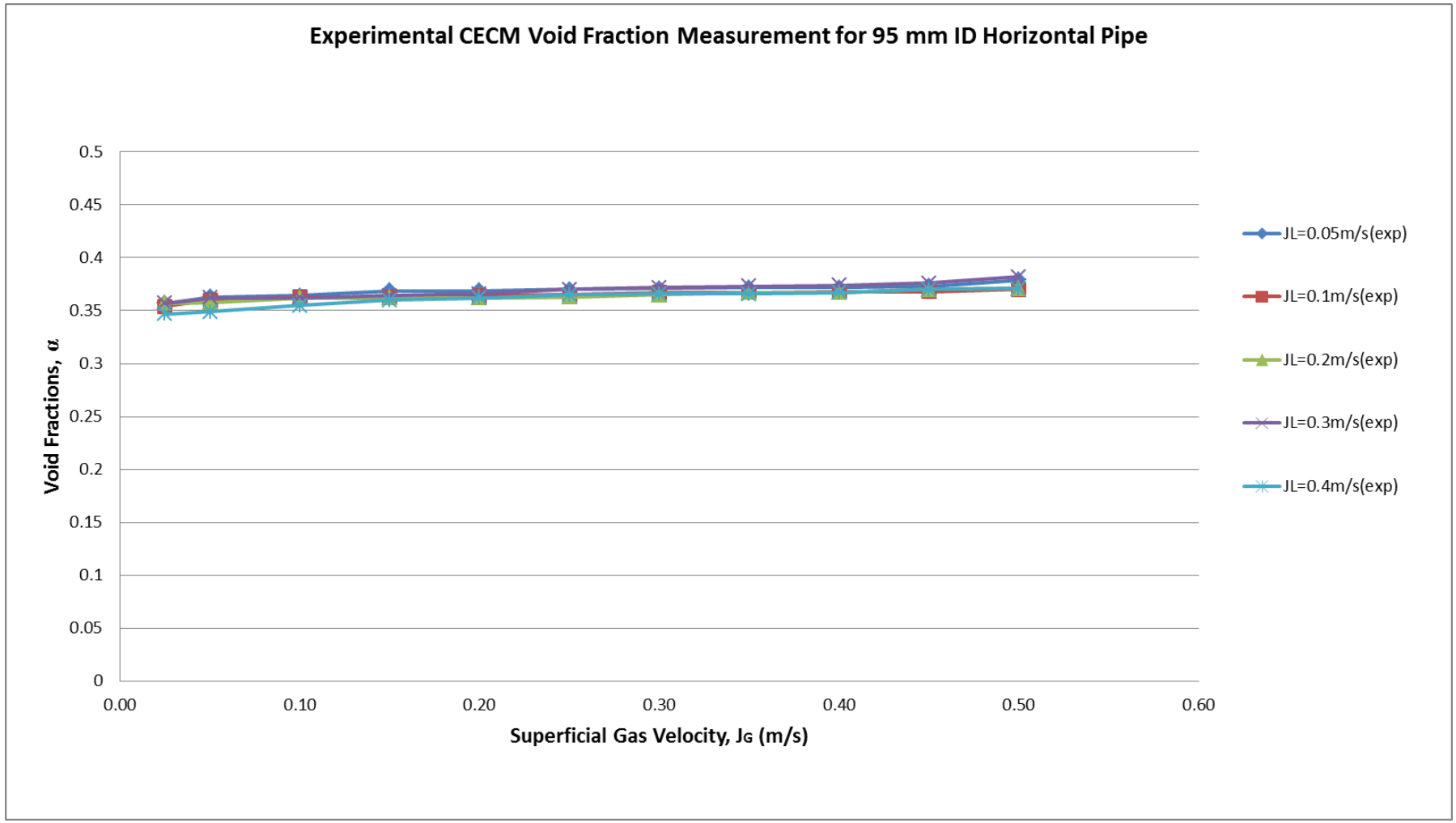

Figure 4.52: Void fraction relationship for 95.0-mm ID horizontal pipe

From the result, it clearly indicated that the void fraction relationship of two-phase flow between the upward vertical flow and the horizontal flow has a same trend. Both vertical upward flow and horizontal flow revealed that by increasing the gas superficial velocity and decreasing the liquid superficial velocity, value of void fraction of two-phase flow inside the pipe will increase.

4.5. Comparison with Other Equation

In order to measure the quality and the reliability of the Constant Electric Current Method (CECM) experiment to measure the void fraction inside the pipe, the results of the void fraction measurement were compared with the Bestion and Toshiba drift-flux model of correlation. The Bestion correlation as shown in Eq. 2.14 was chosen according to the study of the performance of void fraction correlations based on the Findlay-Zuber drift-flux model conducted by Coddington and Macian, (2002). The Toshiba correlation as shown in Eq. 2.17 is the other best correlation to predict the performance of void fraction as reported by Melkamu et al, (2006). Toshiba correlation showed a best correlation prediction capability in the inclined and vertical flow, and among the top correlation for the horizontal flow.

4.5.1 Vertical Pipes

i. 21.0-mm ID pipe

The void fraction results for the 21.0-mm ID pipe were tabulated in Table A2.1.1 – A2.1.3, Appendix 2.1. Table 4.1 referred to the experimental void fraction measurement result using CECM. Meanwhile, Table 4.2 and 4.3 were the void fraction result calculated from void fraction correlation derived from the drift-flux model of Bestion and Toshiba. Figure 4.53 showed the void fraction plot for all the 3 experimental results.

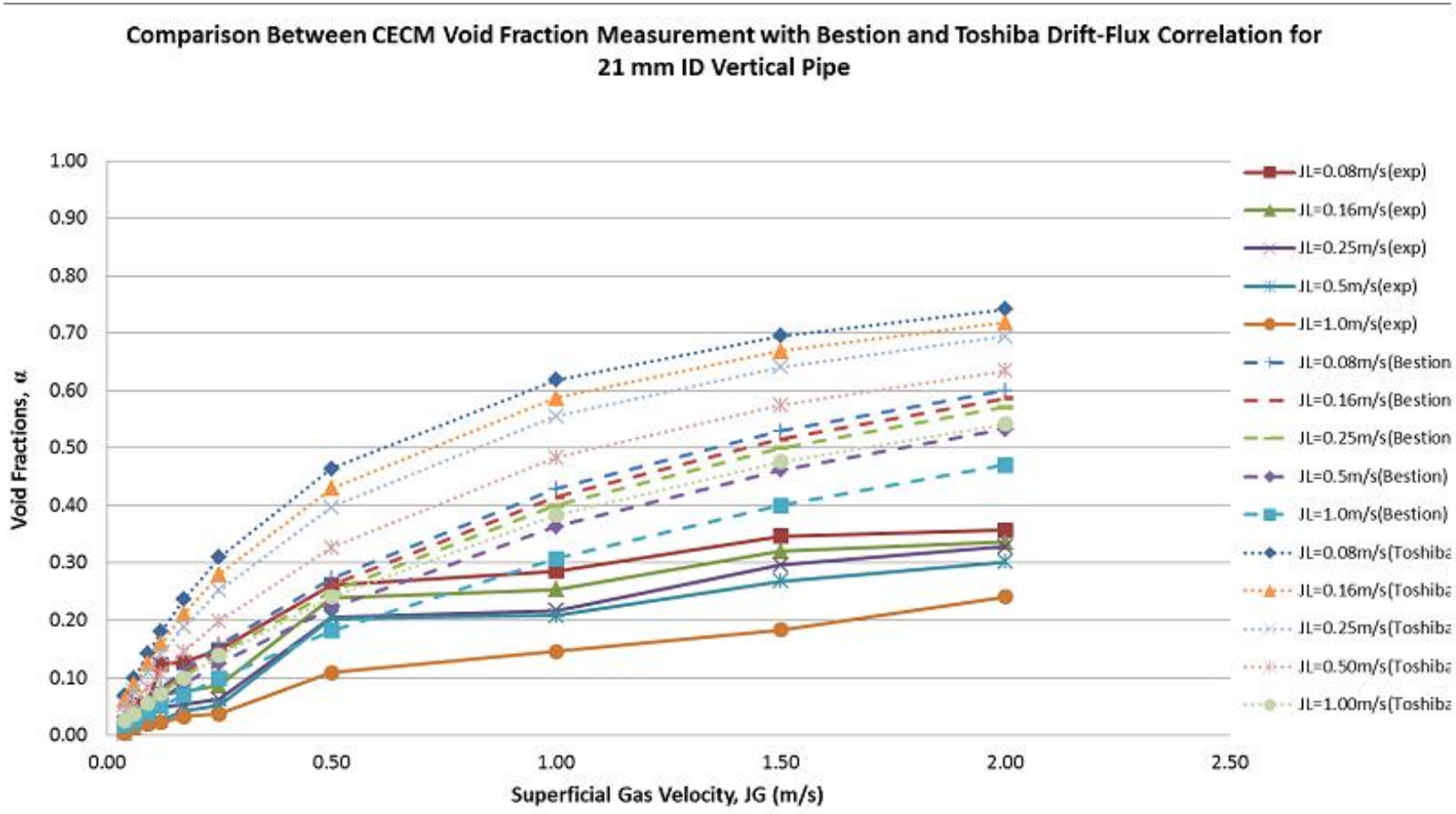

Figure 4.53: Comparison between CECM Void Fraction Measurement with Bestion and Toshiba Drift-Flux Correlation for 21.0-mm ID Vertical Pipe

Table 4.1: Comparison of average error, ε and deviation, s between experimental void fraction and Bestion correlation for 21.0-mm ID vertical pipe

Superficial Liquid Velocity , j_L	0.08	0.16	0.25	0.50	1.00
Deviation	0.0980	0.0921	0.0885	0.0807	0.0846
Average Deviation	0.0888				
Error	-0.0542	-0.0750	-0.0871	-0.0819	-0.0857
Average Error	-0.0768				

Table 4.2: Comparison of average error, ε and deviation, s between experimental void fraction and Toshiba correlation for 21.0-mm ID vertical pipe

Superficial Liquid Velocity , j_L	0.08	0.16	0.25	0.50	1.00
Deviation	0.1329	0.1298	0.1271	0.1126	0.1103
Average Deviation	0.1225				
Error	-0.1776	-0.1834	-0.1818	-0.1505	-0.1266
Average Error	-0.1640				

The experimental result of void fraction using CECM was compared with the Bestion and Toshiba correlation using the average error and average deviation as shown in table 4.4 and 4.5. The comparison of average error and average deviation between experimental result and Bestion correlation gave an average error of -0.0768 and the average deviation of 0.0888. Meanwhile, the comparison between experimental result and the Toshiba correlation gave an average error of -0.1660 and the average deviation of 0.1225. Figure 4.53 illustrated the experimental result have a same trend compared to Bestion and Toshiba correlation. The error and deviation showed the CECM result was most likely to the Bestion correlation compared to Toshiba correlation.

ii. 47.0-mm ID pipe

Table 5.6 showed the experimental void fraction result using the CECM method inside the 47.0-mm ID pipe. Table A2.2.1 and A2.2.3 in Appendix 2.2 showed the void fraction result by using the Bestion and Toshiba drift flux correlation for the 47.0-mm ID meter pipe.

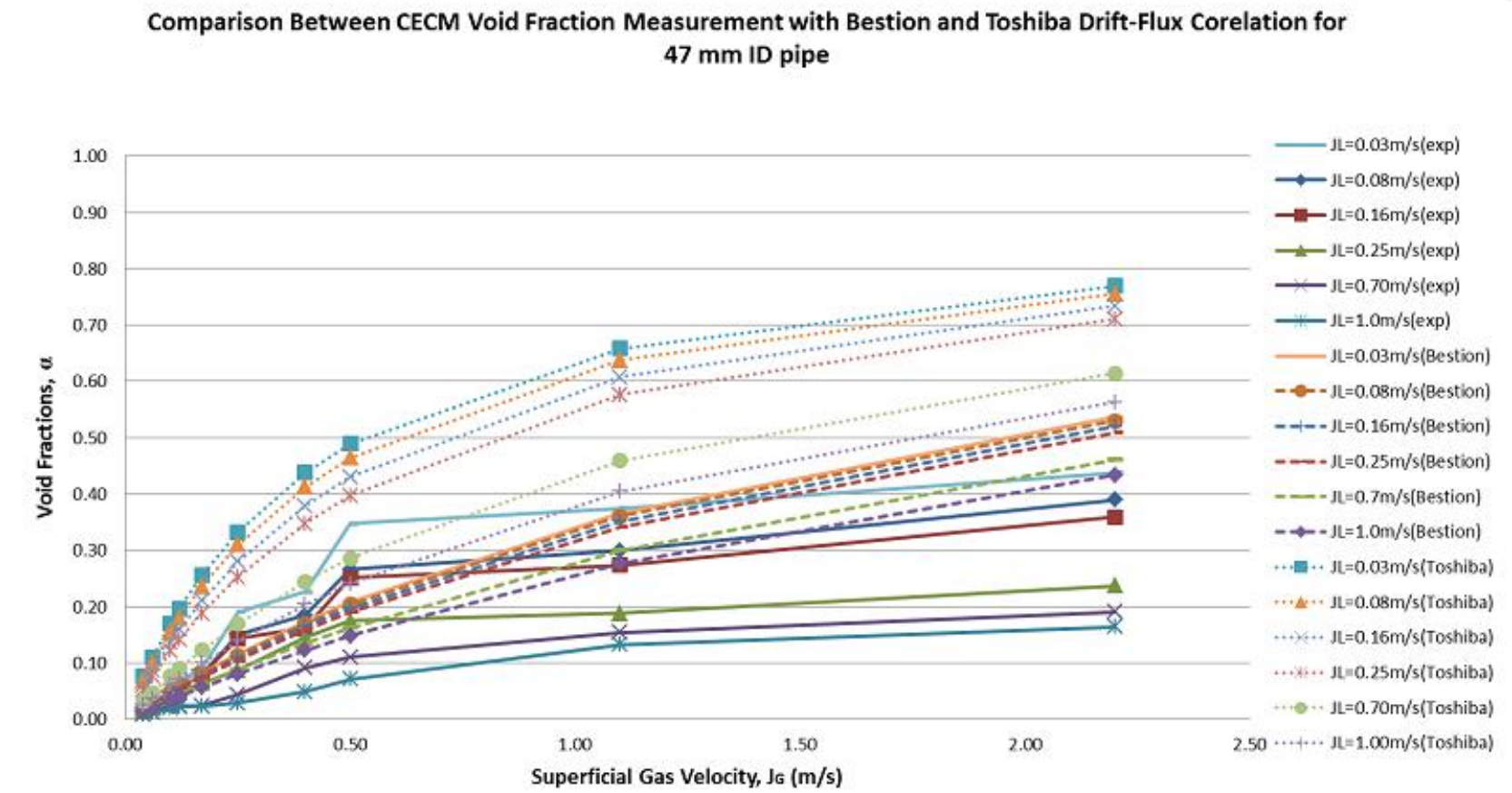

Figure 4.54: Comparison between CECM Void Fraction Measurement with Bestion and Toshiba Drift-Flux Correlation for 47.0-mm ID Vertical Pipe

Table 4.3: Comparison of average error, ε and deviation, s between experimental void fraction and Bestion correlation for 47.0-mm ID vertical pipe

Superficial Liquid Velocity, j_L	**0.03**	**0.08**	**0.16**	**0.25**	**0.7**	**1**
Deviation	0.0616	0.0559	0.0606	0.0895	0.0826	0.0824
Average Deviation	0.0742					
Error	0.0183	-0.0102	-0.0180	-0.0519	-0.0646	-0.0694
Average Error	-0.0428					

Table 4.4: Comparison of average error, ε and deviation, s between experimental void fraction and Toshiba correlation for 47.0-mm ID vertical pipe

Superficial Liquid Velocity, j_L	**0.03**	**0.08**	**0.16**	**0.25**	**0.7**	**1**
Deviation	0.0866	0.1049	0.1099	0.1433	0.1284	0.1229
Average Deviation	0.1160					
Error	-0.1666	-0.1808	-0.1693	-0.1857	-0.1458	-0.1316
Average Error	-0.1633					

An average error and average deviation between experimental result and the Bestion drift flux correlation were summarized in Table 4.9. Table 4.10 recorded the average error and average deviation between experimental result and the Toshiba correlation. The result in Figure 4.54 clearly showed that the error and deviation between the experimental result and Toshiba correlation was higher compared to the error and deviation between experimental result and Bestion correlation. The error and deviation results illustrated by the CECM method for 47.0-mm pipe can displayed a closed result as Bestion correlation even have a same trend for both correlation.

iii. **95.0-mm ID pipe**

Table A2.3.1 in Appendix 2.3 showed the experimental void fraction result of two-phase flow inside the 95.0-mm ID pipe using the CECM method. Meanwhile, table A2.3.2 and A2.3.2 recorded the void fraction of two-phase flow result by using the Bestion and Toshiba drift flux correlation for the 95.0-mm ID pipe.

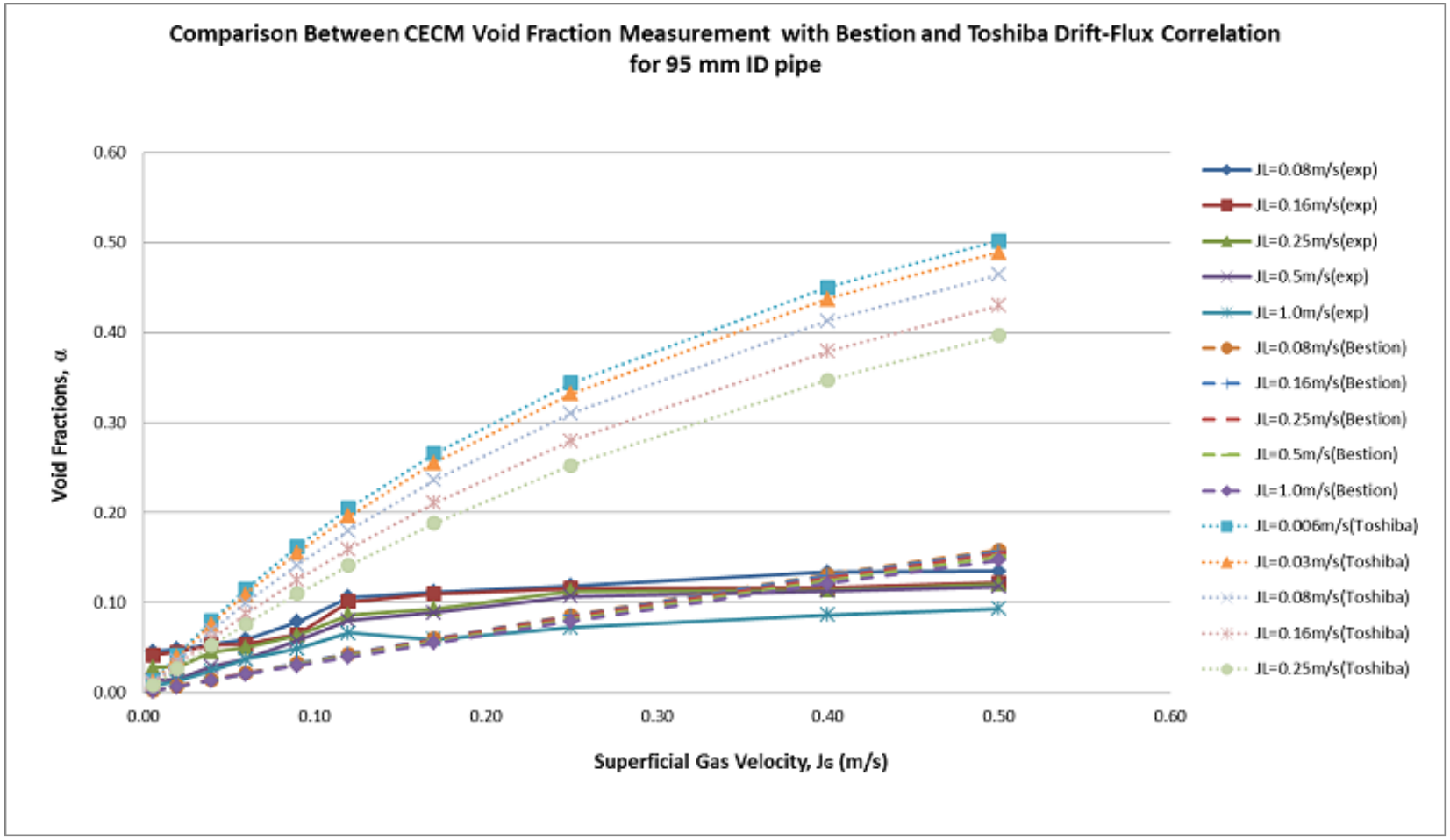

Figure 4.55: Comparison between CECM Void Fraction Measurement with Bestion and Toshiba Drift-Flux Correlation for 95.0-mm ID Vertical Pipe

Table 4.5: Comparison of average error, ε and deviation, s between experimental void fraction and Bestion correlation for 95.0-mm ID vertical pipe

Superficial Liquid Velocity, j_L	**0.006**	**0.03**	**0.08**	**0.16**	**0.25**
Deviation	0.0252	0.0287	0.0243	0.0215	0.0251
Average Deviation	0.0249				
Error	0.0333	0.0270	0.0200	0.0130	-0.0007
Average Error	0.0185				

Table 4.6: Comparison of average error, ε and deviation, s between experimental void fraction and Toshiba correlation for 95.0-mm ID vertical pipe

Superficial Liquid Velocity, j_L	**0.006**	**0.03**	**0.08**	**0.16**	**0.25**
Deviation	0.1353	0.1348	0.1232	0.1074	0.1064
Average Deviation	0.1214				
Error	-0.1288	-0.1279	-0.1217	-0.1112	-0.1091
Average Error	-0.1198				

From the calculation of the average error and deviation between experimental void fraction result and the Bestion correlation, the average error was found to be 0.0185 and the average deviation was calculated at 0.0249. The average error and average deviation between experimental void fraction result and Toshiba correlation is -0.1198 and 0.1214 respectively. From the figure 4.55, can be observed that the result between the experimental result and Bestion correlation has not much difference, compared to Toshiba correlation, the error and deviation is high. The results show that the CECM method for 95.0-mm upward vertical flow can demonstrate a good result if referred to Bestion correlation.

4.5.2 Horizontal Pipes

i. 21.0-mm ID pipe

The experimental void fraction measurement results for horizontal two-phase flow were also compared with the Bestion and Toshiba drift flux correlation. Both of the drift flux correlations are qualified and reliable for the horizontal two-phase flow void fraction measurement that was chosen based on the study of performance. Table 4.16 showed the experimental void fraction measurement result for 21.0-mm ID of horizontal two-phase flow. The void fraction calculated based on the Bestion and Toshiba drift flux correlation to compare with the experimental result and summarizing in Table A2.4.1 - A2.4.1, Appendix 2.4.

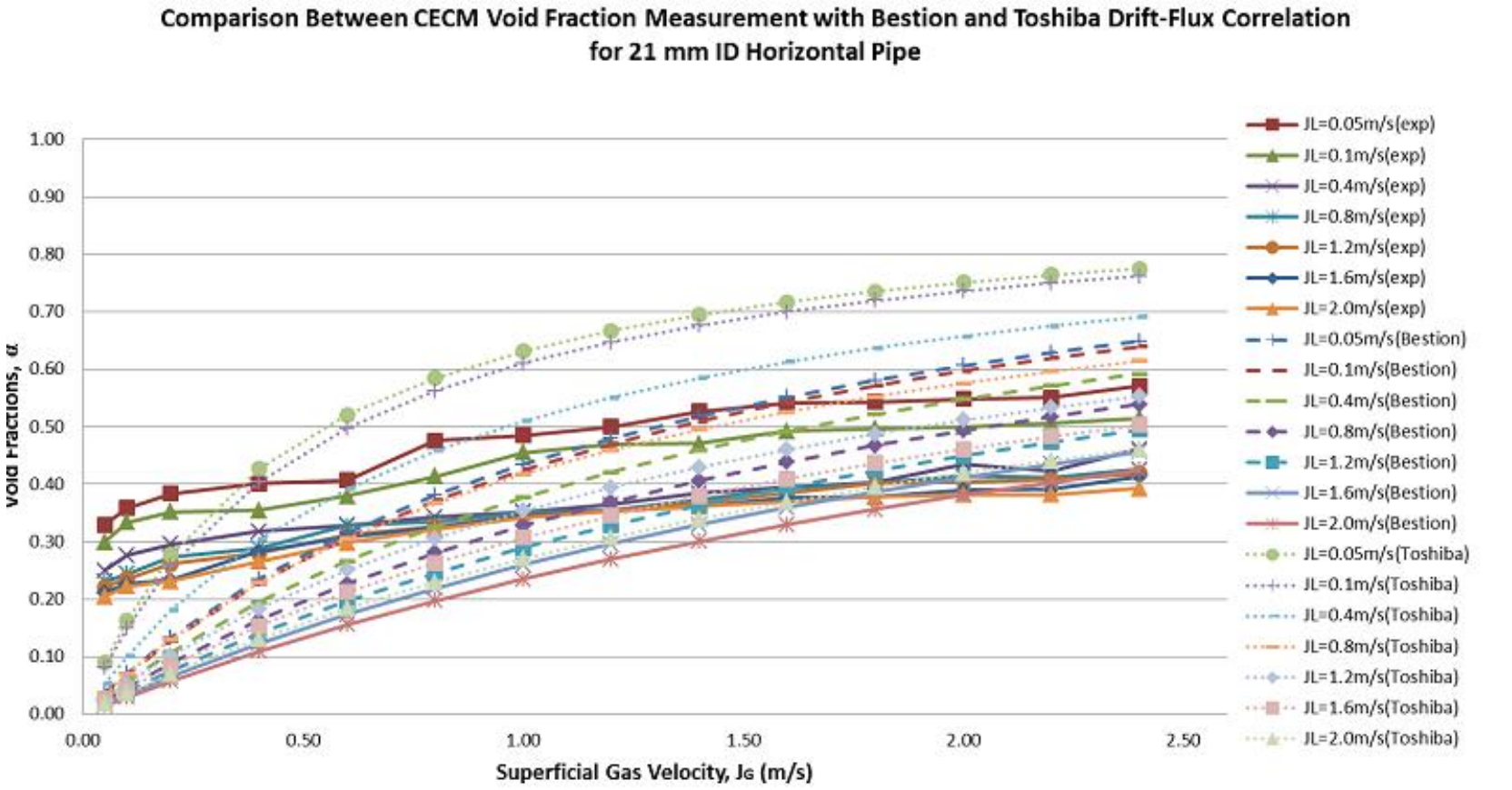

Figure 4.56: Comparison between CECM Void Fraction Measurement with Bestion and Toshiba Drift-Flux Correlation for 21.0-mm ID Horizontal Pipe

Table 4.7: Comparison of average error, ε and deviation, s between experimental void fraction and Bestion correlation for 21.0-mm ID horizontal pipe

Superficial Liquid Velocity, j_L	**0.05**	**0.10**	**0.40**	**0.80**	**1.20**	**1.60**	**2.00**
Deviation	0.0948	0.0984	0.1023	0.0823	0.0699	0.0597	0.0513
Average Deviation	0.0798						
Error	0.1865	0.1530	0.1062	0.1160	0.1271	0.1357	0.1431
Average Error	0.1382						

Table 4.8: Comparison of average error, ε and deviation, s between experimental void fraction and Toshiba correlation for 21.0-mm ID horizontal pipe

Superficial Liquid Velocity, j_L	**0.05**	**0.10**	**0.40**	**0.80**	**1.20**	**1.60**	**2.00**
Deviation	0.1627	0.1657	0.1616	0.1297	0.1082	0.0900	0.0762
Average Deviation	0.1277						
Error	-0.0398	-0.0595	-0.0462	0.0095	0.0484	0.0753	0.0954
Average Error	0.0119						

Figure 4.56 showed the comparison between the Bestion and Toshiba void fraction result for 21.0-mm ID horizontal two-phase flow. The experimental results showed less dispersed flow from the Bestion and Toshiba drift flux correlation.

The average error and average deviation between experimental void fraction measurement result and Bestion drift flux correlation shown in Table 4.19. Table 4.20 showed the average error and average deviation between the experimental void fraction result and Toshiba drift flux correlation. The results were a bit diverged from the correlation results at low gas superficial velocity. The wettability of the pipe affected the CECM result by conducting the unnecessary current.

ii. 47.0-mm ID pipe

Table A2.3.1 in Appendix 2.5 showed the experimental void fraction measurement result using CECM for 47.0-mm ID of horizontal two-phase flow. The result was compared with the Bestion and Toshiba drift flux correlation in Table A2.5.1 and A2.5.1.

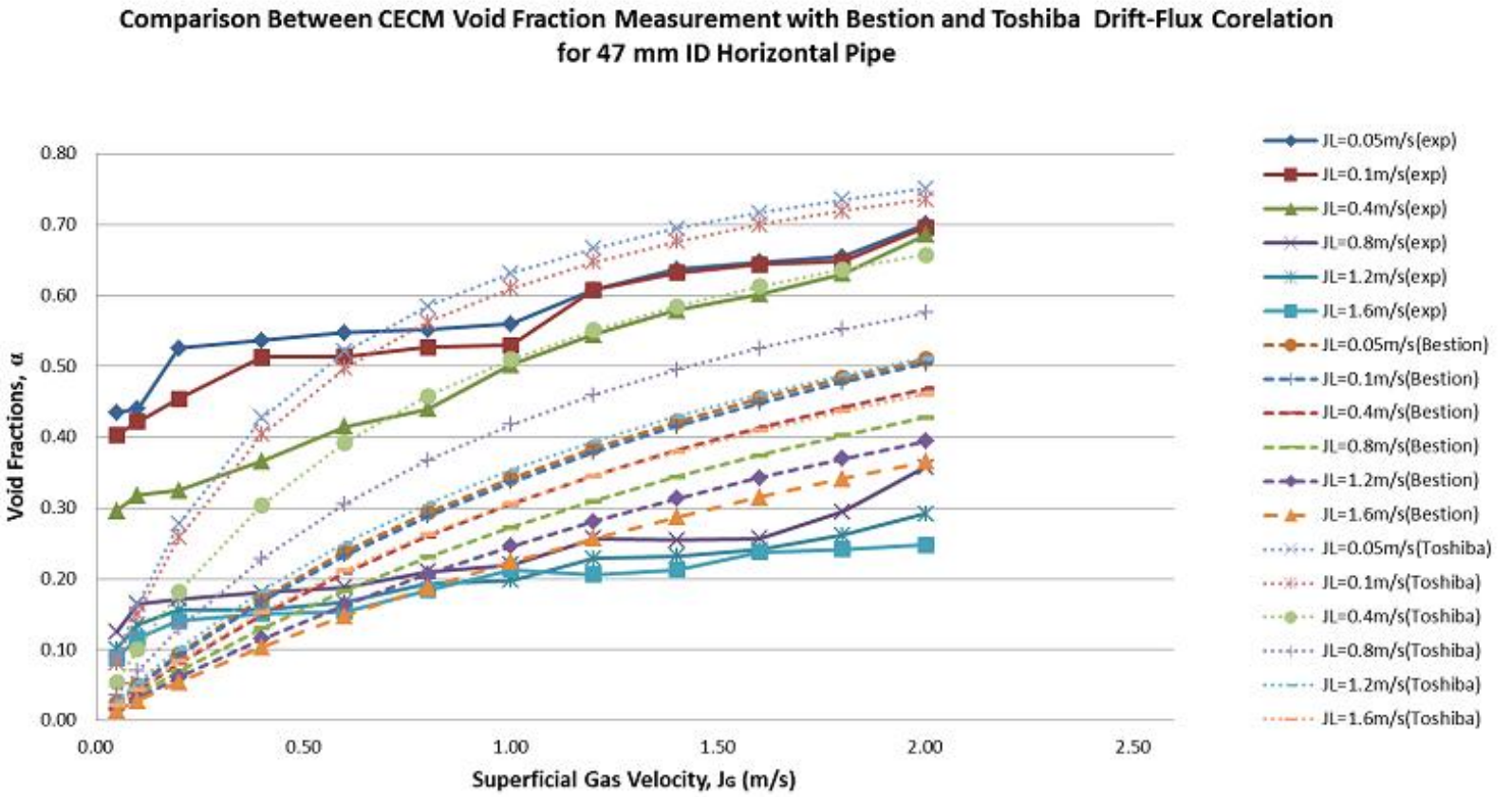

Figure 4.57: Comparison between CECM Void Fraction Measurement with Bestion and Toshiba Drift-Flux Correlation for 47.0-mm ID Horizontal Pipe

Table 4.9: Comparison of average error, ε and deviation, s between experimental void fraction and Bestion correlation for 47.0-mm ID horizontal pipe

Superficial Liquid Velocity, j_L	**0.05**	**0.10**	**0.40**	**0.80**	**1.20**	**1.60**
Deviation	0.0941	0.0788	0.0342	0.0851	0.0779	0.0711
Average Deviation	0.0735					
Error	0.2988	0.2788	0.2197	0.0079	0.0011	0.0043
Average Error	0.1351					

Table 4.10: Comparison of average error, ε and deviation, s between experimental void fraction and Toshiba correlation for 47.0-mm ID horizontal pipe

Superficial Liquid Velocity, j_L	**0.05**	**0.10**	**0.40**	**0.80**	**1.20**	**1.60**
Deviation	0.1615	0.1482	0.0982	0.1342	0.1170	0.1022
Average Deviation	0.1269					
Error	0.0725	0.0663	0.0673	-0.0986	-0.0776	-0.0562
Average Error	-0.0044					

From Figure 4.57 showed that the experimentation void fraction result using CECM method was not smooth and stable compared to the Bestion and Toshiba void fraction drift flux correlation. The average error and average deviation between the experimental void fraction result and void fraction using the Bestion and Toshiba drift flux correlation were showed in Table 4.24 and 4.25. The results show that the CECM for 47.0-mm pipe have a good result at high gas and liquid superficial velocity. At low liquid superficial, the reading of sensor was out of trend due to the wettability of the pipe conducting the electric current.

iii. 95.0-mm ID pipe

The experimentation void fraction measurement result using CECM for 95.0-mm ID pipe is shown in Table A2.6.1, Appendix 2.6. The experimental result then was compared with the void fraction calculated using the Bestion and Toshiba drift flux correlation in Table A2.6.1 and A2.6.1.

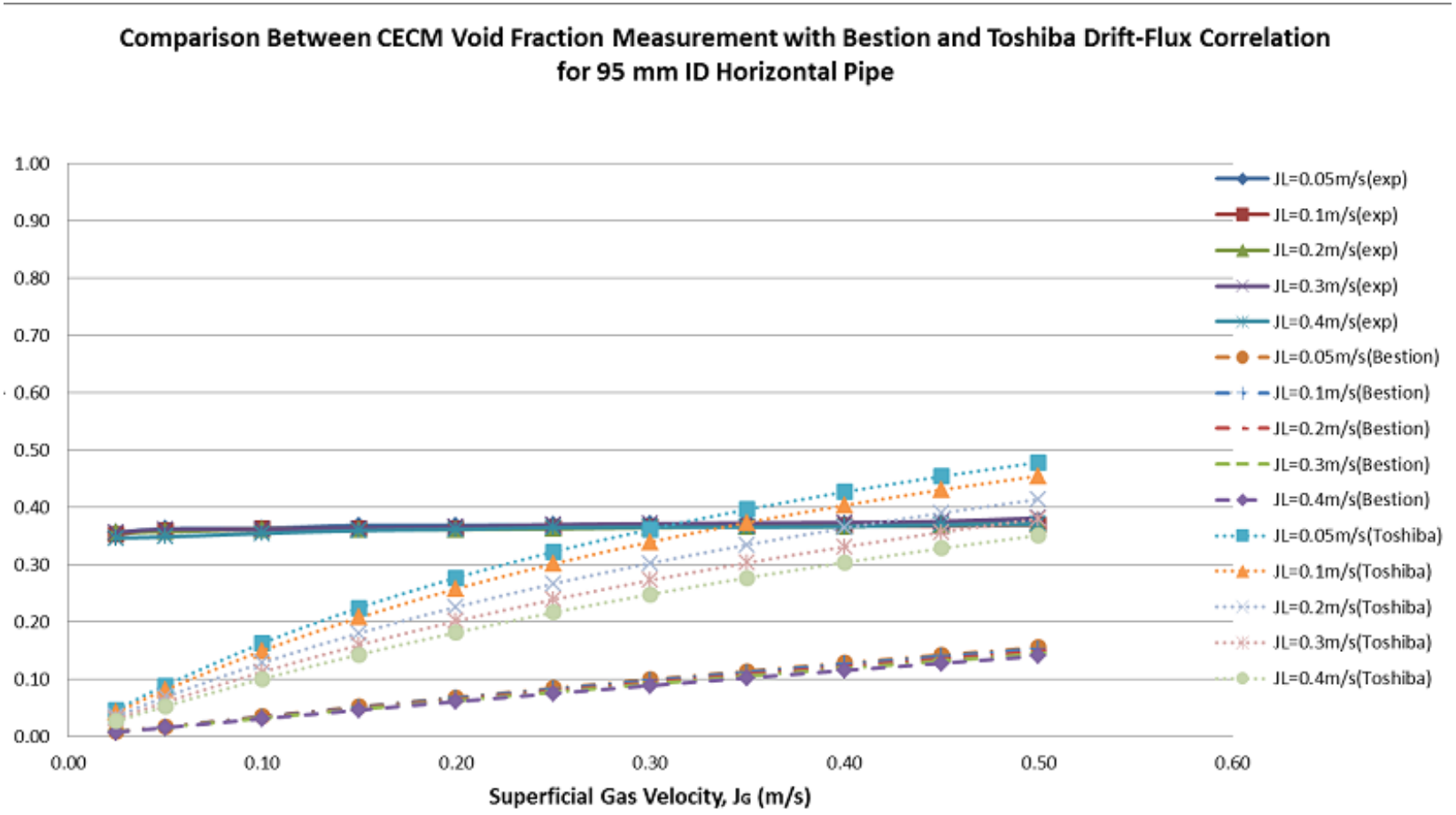

Figure 4.58: Comparison between CECM Void Fraction Measurement with Bestion and Toshiba Drift-Flux Correlation for 95.0-mm ID Horizontal Pipe

Table 4.11: Comparison of average error, ε and deviation, s between experimental void fraction and Bestion correlation for 95.0-mm ID horizontal pipe

Superficial Liquid Velocity, j_L	**0.05**	**0.10**	**0.20**	**0.30**	**0.40**
Deviation	0.0422	0.0428	0.0405	0.0072	0.0355
Average Deviation	0.0336				
Error	0.2799	0.2766	0.2786	-0.0174	0.2891
Average Error	0.2214				

Table 4.12: Comparison of average error, ε and deviation, s between experimental void fraction and Toshiba correlation for 95.0-mm ID horizontal pipe

Superficial Liquid Velocity, j_L	**0.05**	**0.10**	**0.20**	**0.30**	**0.40**
Deviation	0.1353	0.1348	0.1232	0.1074	0.1064
Average Deviation	0.1214				
Error	0.2799	0.2766	0.2786	0.2866	0.2821
Average Error	0.2808				

Figure 4.58 shows the graph of void fraction experimental result using CECM method and the calculated result using Bestion and Toshiba drift flux correlation. Based on Figure 4.58, the experimental void fraction result using CECM method for 95.0-mm ID piped has not achieved the expected result. The patterns of the results were not showed same trend of the Bestion or Toshiba drift flux correlation results patterns. The average error and average deviation between experimental void fraction result and void fraction calculated using Bestion drift flux correlation were 0.2214 and 0.0336. The average error and average deviation between the experimental void fraction result and Toshiba drift flux correlation were 0.2808 and 0.1214 respectively. The result was due to the wettability of the pipe where the balance of water still conducted the electric current at upper part of the sensor ring even the pipe was not fully filled up.

Chapter 5: Conclusion

5.1 Conclusion

The determination of gas-liquid two-phase flow in this research was based on experimental works. Laboratory scale two-phase flow rig was successfully constructed according to industrial specification. The experiments were conducted in an upward vertical and horizontal flow. Three different pipes sizes were used in this experiment, namely 21.0-mm, 47.0-mm and 95.0-mm inner diameter pipes. This experiment has achieved their objective on the basic study of two-phase gas-liquid flow, flow pattern, effect of L/D on the flow pattern and measurement of void fraction.

Flow Pattern and Flow Mapping

From the results, four flow patterns were successfully observed during the upward vertical flow experiment by using the DSLR camera and high speed video camera. The flow patterns are bubble, bubbly-slug, slug and churn flow for a vertical upward flow. They were compared with the flow pattern result by Collier and Thome (1996). From the result, both gas superficial velocity, j_G and liquid superficial velocity, j_L gave an impact to the flow pattern. The liquid superficial velocity j_L has a great impact on the flow pattern transition in the small pipes. The results agree well with the theory by Butterworh et al. (1977). However, the liquid superficial velocity, j_L only contributed small effects on flow pattern transition in large pipe, particularly for the work, for 47.0-mm and 95.0-mm inner diameter pipes.

The bubble flow pattern was easy to develop inside the large diameter pipe compared to the small diameter pipe. The rates of coalescences of the bubbles were reduced inside the large pipe. The transition between bubbly flow and slug flow also know as bubbly slug flow appeared in shape of spherically capped bubble. The bubbly

slug flow pattern was found to be important in larger pipe study, because apparently in smaller pipe, the bubbly-slug flow is not predominant. The slug flow pattern has varied maximum length depending on the diameter size of the pipe. The smaller size of the pipe diameter caused the maximum length of slug increase. From the result, the maximum length for the slug bubble inside the 21.0-mm ID pipe was longest compared with the 47.0-mm and 95.0-mm ID pipes.

From the observation, the churn flow was dominant inside the large vertical upward flow pipe. In the large pipe, the flow transition between slug and churn flow were difficult to observe. The transition range of boundary for the slug flow in the large pipe was small. Churn flow was easily developed inside the 95.0-mm pipe compared to the 47.0-mm and 21.0-mm pipes.

The flow pattern that was observed during the horizontal flow experimentation were dispersed bubble, bubble, plug, stratified, wavy, slug and annular flow. The annular flow was successfully observed inside the 21.0-mm ID pipe at high gas superficial velocity at the first section of the experimental pipe. The dispersed bubble flow occurred at high liquid superficial velocity. From the result, dispersed bubble flow can be observed only at the first section of 21.0-mm and 47.0-mm inner diameter pipe.

The bubble flow pattern appeared when the gas dispersed bubbles flow through the liquid and after some time the bubble will move to the upper half of the pipe caused by buoyancy effect. The stratified flow was observed at low gas and liquid superficial velocity when the gas and liquid phase were completely separated inside the pipe. Meanwhile, the wavy flow pattern occurred by increasing the gas superficial velocity. The waves were observed on the interface between gas and liquid flow in the direction of the flow.

The plug and slug flow pattern were observed inside the 21.0-mm and 47.0-mm ID pipe. The plug flow is when bubbles congregate at the top of the pipe flow and merges after certain distance, became bigger elongated bubble. The slug flow pattern occurred after further increasing the gas superficial velocity and the size of the bubble has about the same diameter of the pipe. The plug and slug flow pattern mostly observed at section 2, 3 and 4 inside the pipe.

Overall, the experiment to determine the flow pattern and flow mapping by using the photography method was successful by using the DSLR camera with a lighting system that can easily capture the image of the flow pattern. The assistance of the high speed video camera made the experiment in advance, by able to view the development, transition and changes of flow pattern during the experimentation.

Effect of Aspect Ratio L/D

The aspect ratio L/D was calculated by the distance from the two-phase mixer to the observation point, L and divided with the diameter of the pipe, D. In this experiment, the pipe was divided into 4 sections. Each pipe has a same length but has a different aspect ratio L/D.

The observation point was set at 0.375-m from the mixer for section I, 1.125-m for section II, 1.875-m for section III and 2.625-m for section IV. From the flow mapping result it showed that the flow patterns vary for each pipe size even if it were observed at the same section for all pipes. This result is valid for both vertical upward and horizontal two-phase flow pattern experiment.

The experimentation results show that the L/D ratio gave an effect to the flow pattern of the pipes even at the same length. This result has a similar conclusion with Akira and Hajime (2000) even at a difference pipe diameter. The diameter of the pipes

gave huge transformation to the flow pattern of two phase flow. The liquid film will easily break down in a large pipe. Besides that, the bubbles have more chances to coalesce and merge up inside the small diameter pipe.

Void Fraction Measurement Using CECM

Void fraction was measured by using the Constant Electric Current Method (CECM) through the voltage drop technique by Fukano (1998). The connections of sensors inside the 21.0-mm, 47.0-mm and 95.0-mm inner diameter pipes were fix to measure the difference of voltage of two-phase flow. The outcome graphs and results from the DAQ system through the computer screen illustrated the reading of void fraction and also determine the flow pattern of two-phase flow by comparing the graph with the observation result. Every flow patterns has a different pattern that will show the type and characteristic of the flow.

Overall, the increase of void fraction was proportionate to superficial gas velocity, j_G at constant superficial liquid velocity, j_L and decreased with the increasing superficial liquid velocity, j_L at constant superficial gas velocity, j_G in all pipes. This experiment gave a same conclusion and agrees well the experiment done by Triplett et al. (1999) in the micro channels tube. The void values recorded in these experiments were found to be directly proportional with the amount of gas and liquid percentage inside the pipe. However, slight error of the reading during the experimentation can be neglected. The overall reading and result can be accepted to measure the void fraction of two-phase flow by using the CECM method.

The comparisons of experimentation result with Bestion and Toshiba drift-flux correlation were made in measuring the void fraction. The average error and average deviation were calculated from the void fraction values for all pipes. Table 5.1 shows the average error and average deviation for the 21.0-mm, 47.0-mm and 95.0-mm inner

diameter pipe vertical upward two-phase flow. On the other hand, table 5.2 shows the average error and average deviation for the 21.0-mm, 47.0-mm and 95.0-mm inner diameter pipe horizontal two-phase flow.

Table 5.1: The summary of comparison for average error and average deviation between the experimental result with Bestion and Toshiba Correlation in vertical upward flow

Correlation	**Bestion Correlation**			**Toshiba Correlation**		
Pipe Size	**21.0 mm**	**47.0 mm**	**95.0 mm**	**21.0 mm**	**47.0 mm**	**95.0 mm**
Average Error	-0.0768	-0.0428	0.0185	-0.1640	-0.1633	-0.1198
Average deviation	0.0888	0.0742	0.0249	0.1225	0.1160	0.1214

Table 5.2: The summary of comparison for average error and average deviation between the experimental result with Bestion and Toshiba Correlation in horizontal flow

Correlation	**Bestion Correlation**			**Toshiba Correlation**		
Pipe Size	**21.0 mm**	**47.0 mm**	**95.0 mm**	**21.0 mm**	**47.0 mm**	**95.0 mm**
Average Error	0.1382	0.1351	0.2214	0.0119	-0.0044	0.2808
Average deviation	0.0798	0.0735	0.0336	0.1277	0.1269	0.1214

From the summary of the average error and average deviation, the comparison between the experimental result and Bestion correlation for the vertical upward flow has small error and deviation. The average error was below 0.08 % for all pipes and the average deviation was below 0.09% for all pipes. The comparison between the experimental results and Toshiba correlation gave an average error below 0.15% for all pipes and average deviation was below 0.13% for all pipes.

Therefore, it can be concluded that measurement void fraction using the CECM method for the 21.0-mm, 47.0-mm and 95.0-mm upward vertical pipes can be accepted by referred to the average error and deviation compared to Bestion and Toshiba correlation. The error and deviation are considered small and the result can be improved by having better experiment and data acquisition setup.

Meanwhile for the horizontal two-phase flow experimental, the average error between the experimental results and Bestion correlation was below 0.23% and average deviation was below 0.08% for all pipes. The comparison between the experimental results and Toshiba correlation gave a reading of average error below 0.29% and average deviation 0.13% for all pipes. The experimental results for the 21.0-mm and 47.0-mm pipes were better compared to 95.0-mm pipe. The experimental result for 95.0 mm pipe was a bit diverged from the two correlations.

The void fraction measurement using the CECM method for horizontal flow was not as good as the upward vertical flow especially for bigger pipe. This matter was due to the effect of pipe wettability where the balance of water at upper part of the sensor ring still conducted the electric current even the pipe was not fully filled up.

Overall, the void fraction measurement using the CECM method for both vertical upward and horizontal two-phase flow were in acceptable range by compared with the Bestion and Toshiba correlation. The value of error and deviation were small for upward vertical flow, however the error and deviation for horizontal flow were quite high especially for bigger pipe. In the conclusion, CECM method is reliable to measure the void fraction inside the pipe for both vertical upward and horizontal two-phase flow.

5.2 Recommendation

The research of flow pattern and void fraction can be developed in wide scope of studies. By using same experiment facilities, difference scope of studies can be achieved. With a few improvement and changes in the experiment facilities, variation and broader research objectives can be carried out. A difference type gas and liquid can be used rather than air and water with difference viscosity and properties. A difference liquid viscosity will give a difference effect, flow pattern and void fraction reading with a same gas and liquid superficial velocities.

By improving the experiment's equipment such the water pump and air compressor, a huge amount of gas and liquid flow rate can be supplied in the experiment. An experiment for a larger pipe can be done. The high gas and liquid superficial velocity experimentation can be performed. For example to study the annular flow pattern and void fraction required high liquid superficial velocities up to 80 m/s.

For flow patterns experimentation, the photographic and video graphic method can be improved to have an accurate experiment results. Miss interpretation of flow pattern due to complex series of refraction to the specific area of pipe during the experiment can be avoided by setting a suitable lighting system for high speed still and video camera.

The improvement to the CECM void fraction measurement method can be made in future in order to have an accurate experiment result. A new design of CECM method on the sensor configuration has more features to be improved such as material selection, sensor dimension and connection of the wire to get a better voltage result and avoided noise to the reading. The amount of current and voltage supply are very crucial to a sensitive CECM sensor and therefore suitable current and voltage supply are also very important.

References

1. Akira Ohnuki, Hjime Akimoto (2000). Experimental study on transition of flow pattern and phase distribution in upward air-water two-phase flow along large vertical pipe. *International Journal of Multiphase Flow 26.* 367-386.

2. Bergles, Lopina and Fiori (1967). Closure to "Discussion of `Critical-Heat-Flux and Flow-Pattern Observations for Low-Pressure Water Flowing in Tubes'. *ASME J. Heat Transfer, 90,* p. 280.

3. Butterworth, D., Hewitt, G. F. (1977) Flow Patterns, in G. F. Hewitt, eds, *Two – Phase Flow and Heat Transfer*. Oxford University Press, Oxford, p. 18-39.

4. Butterworth, D., Hewitt, G. F. (1977) Introduction, in G. L. Shires, eds, *Two-Phase Flow and Heat Transfer*. Oxford University Press, Oxford, p. 1-17.

5. Butterworth, D., Hewitt, G. F. (1977) One-Dimensional Flow, in D. Butterworth, eds, *Two-Phase Flow and Heat Transfer*. Oxford University Press, Oxford, p. 40-57.

6. Chao Tan, Feng Dong and Mengmeng Wu (2007). Identification of gas/liquid two-phase flow regime through ERT-based measurement and feature extraction. *Flow Measurement and Instrumentation*. Volume 18, Issues 5–6, Pages 255–261.

7. Fukano, T. (1998). Measurement of Time Varying Thickness of Liquid Film flowing with High Speed Gas Flow by a Constant Electric Current Method (CECM). *Nuclear Engineering and Design, 184 (199*8), 363-377.

8. H.Y Kim, S. Koyama, W. Matsumoto. (2001). Flow pattern and flow characteristics for counter-current two phase flow in a vertical round tube with wire-coil inserts. *International Journal of Multiphase Flow 27.* 2063-2081

9. Hewitt, G. F., 1978. Measurement of Two Phase Flow Parameters. *Academic Press, New York*, p.111.

10. Hideo Ide, Akira Kariyasaki, Tohru Fukano. (2007). Fundamental data on gas-liquid two-phase flow in minichannels. *International Journal of Thermal Sciences, 46,* 519-530.

11. Hlaing N. D., Sirivat A., Siemanond K., Wilkes J. O. (2006) Vertical Two – Phase Flow Regimes and Pressure Gradients: Effect of Viscosity. *Experimental Thermal and Fluid Science*. 31. 567 – 577.

12. Ho-Joon Lim1, Kuang-An Chang, Chin B. Su, and Chi-Yueh Chen (2008). Bubble velocity, diameter, and void fraction measurements in a multiphase flow using fiber optic reflectometer. *Review of Scientific Instruments*. Volume 79, Issue 12.

13. H. Abdulmouti. (2014) Bubbly Two-Phase Flow: Part I-Characteristics, Structures, Behaviors and Flow Patterns. *American Journal of Fluid Dynamics*, 194-240.

14. J.C. Gamio, J. Castro, L. Rivera and J. Alamilla (2005). Visualisation of gas-oil two-phase flows in pressurised pipes using electrical capacitance tomography. *Flow Measurement and Instrumentation*, Volume 16, Issue 2-3, April 2005, Pages 129-134.

15. John G. Collier, John R. Thome (1996). *Convective Boiling and Condensation*. Oxford University Press, Incorporated.

16. K. Mishima, T. Hibiki and H. Nishihara. (1997). Visualization and measurement of two-phase flow by using neutron radiography. *Nuclear Engineering and Design.* 175. 25-35.

17. Lockhart, R. W.; Martinelli, R. C. (1949). "Proposed correlation data for isothermal two-phase two-component flow in pipes." *Chemical Engineering Progress*, Vol. 45, No. 1, pp. 39-48.

18. M.Fossa. (1998). Design and performance of conductance probe for measuring the liquid fraction in two-phase gas-liquid flows. *Flow Measurement and Instrumentation 9.* 103-109

19. Mariusz R. Rząsa experiment. (2009).The measuring method for tests of horizontal two-phase gas-liquid flows, using optical and capacitance tomography. *Nuclear Engineering and Design.* 239**.** 699-707.

20. Melkamu A, Woldesemayat, and Afshin J. Ghajar. (2007) Comparison of void fraction correlation for different flow patterns in horizontal and upward inclined pipes. *International Journal of Multiphase Flow* 33 (2007) 347-370

21. Mishima, K. And Hibiki, T. (1996). Some characteristics of air-water two-phase flow in small diameter vertical tubes. *International Journal of Multiphase Flow.* 22**.** 703-712.

22. Morooka, S., Ishizuka, T., Iizuka, M., Yoshimura, K. (1989). Experimental study on void fraction in a simulated BWR fuel assembly (evaluation of cross-sectional averaged void fraction). *Nuclear Engineering & Design*, *114*, 91–98.

23. Nan Da Hlaing, Anuvat Sirivat, Kitipat Siemanond, James O. Wilkes. (2007). Vertical two-phase flow regimes and pressure gradients: Effect of viscosity. *Experimental Thermal and Fluid Science, 31***,** 567-577.

24. Owen C. Jones Jr. and Novak Zuber (1975).The interrelation between void fraction fluctuations and flow patterns in two-phase flow. *International Journal of Multiphase Flow*. Volume 2, Issue 3, Pages 273-306

25. Paul Coddington, Rafael Macian. (2002). A study of the performance of void fraction correlations used in the context of drift-flux two-phase flow models. *Nuclear Engineering and Design,* 215. 199-216.

26. Premoli, A., Francesco, D., and Prina, A. (1971). A Dimensional Correlation for Evaluating Two-Phase Mixture Density. *La Termotecnica 25(1),* 17-26.

27. Salamon Levy (1999). *Two-Phase Flow in Complex System*. John Wiley & Son, INC.

28. T Hibiki and M. Ishii (1998). Effect of flow-induced vibration on local flow parameters of two-phase flow. *Nuclear Engineering and Design,* 185 (1998), 113-125

29. Takamasa, T. Hazuku and T. Hibiki (2008). Experimental Study of gas–liquid two-phase flow affected by wall surface wettability. *International Journal of Heat and Fluid Flow*, 29 (2008), 1593-1602.

30. Theodore J. Heindel, Joseph N. Gray and Terrence C. Jensen. (2007). An X-ray system for visualizing fluid flows. *Measurement and Instrumentation 19.* 67-78

31. Triplett, K.A., Ghiaasiaan, S.M., Abdel-Khalik, S.I., LeMouel, A., McCord, B.N. (1999). Gas-liquid two-phase flow in microchannels Part II: void fraction and pressure drop. *International Journal of Multiphase Flow, 25*, 395-410.

32. Wolverine Tube, Inc. (2007), Chapter 12: Two-phase flow patterns. *Engineering Data Book III*. 12-1 – 12-34.

33. Xiuzhong Shen, Kaichiro Mishima, Hideo Nakamura. (2005) Two-phase phase distribution in a vertical large diameter pipe. *International Journal of Heat and Mass Transfer*. Volume 48, Issue 1, , 211-225.

34. Y. Taitel, A.E. Dukler. Effect of pipe length on the transition boundaries for high-viscosity liquids Original Research Article. *International Journal of Multiphase Flow*, Volume 13, Issue 4, July–August 1987, Pages 577-581.

35. Y. Taitel, A.E. Dukler. A model for predicting flow regime transitions in horizontal and near horizontal gas-liquid flow. *AIChE Journal,* Volume 22, Issue 1, pages 47–55.

36. Zuber, N., Findlay, J. A. (1965) Average Volumetric Concentration in Two-Phase Flow System. *Journal of Heat Transfer, 87*, 453-468.

Appendices

Appendix 1.1

Experiment Equipment - Two-Phase Flow Experimental Rig

a) Motor pump - Foras SD200/2, 2.2 HP / 1.65 kW and single phase (240V/50Hz/10A

b) Air Compressor - Dancomair-Elgi CLISBY Series S, 4 kW, 180 litres and up to 8 bars

c) Valve – Water valve

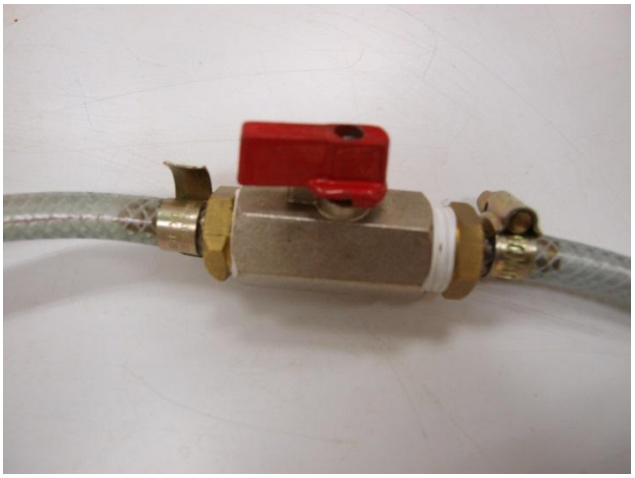

d) Valve – Air valve

d) Acrylic pipe

d) PVC pipe

Appendix 1.2

Experiment Equipment - Imaging Facilities

a) DSLR Camera - Olympus DSLR E-420, 10 megapixels with Olympus Electronic Flash FL-36R

b) High Speed Video Camera - Casio EX-F1 with capability of 1200 frame per second and up to 60 frames per second for still image

c) Light - Halogen light, 500W

Appendix 1.3

Experiment Equipment - Measurement Apparatus

a) Water flow meter - Blue White Industries Flow rate meter F-1000-RB (Paddlewheel flow meter) up to 600 L/min

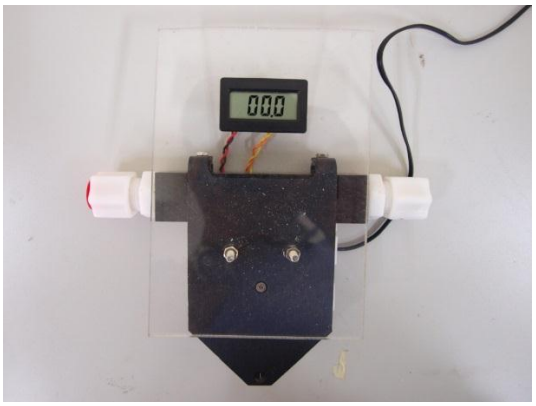

b) High range air flow meter - McMillan Company 100 Flo-sensor with range of 100 – 1000 L/min

c) Low range air flow meter - Kofloc flow rate meters with range of 0.2 – 2.0 L/min and 3 – 30 L/min

Appendix 1.4

Experiment Equipment - Sensors

a) Power Supply - GW GPS3030D with range of electric current 0.001 – 0.01A and the range of the output voltage 0 – 40 V

b) USB Data Aquistion System (DAQ) - NI USB-6215 with 16 analog inputs (16-bit, 250 kS/s), 2 analog outputs, 4 digital inputs, 4 digital outputs and two 32-bit counters

c) Copper Ring - The thickness is 2mm and the inner diameters are the same as the inner diameters of the acrylic pipe (21, 47 and 95 mm)

Appendix 2.1

Void Fraction Measurement Using CECM for 21.0-mm ID Vertical Pipe

Table A2.1.1: Experimental void fraction measurement using CECM for 21.0-mm ID pipe

	QG (LPM)	0.83	1.25	1.87	2.49	3.53	5.20	10.39	20.78	31.18	41.57
	JG(m/s)	**0.04**	**0.06**	**0.09**	**0.12**	**0.17**	**0.25**	**0.50**	**1.00**	**1.50**	**2.00**
QL (LPM)	JL (m/s)										
10.63	0.08	0.022	0.053	0.055	0.124	0.127	0.149	0.261	0.286	0.347	0.357
21.27	0.16	0.013	0.042	0.054	0.071	0.077	0.087	0.239	0.254	0.320	0.336
42.53	0.25	0.009	0.029	0.039	0.050	0.053	0.063	0.206	0.217	0.296	0.328
63.80	0.50	0.004	0.014	0.023	0.026	0.043	0.053	0.204	0.208	0.268	0.302
85.07	1.00	0.003	0.013	0.019	0.022	0.032	0.037	0.109	0.146	0.184	0.241

Table A2.1.2: Bestion correlation void fraction measurement for 21.0-mm ID pipe

	QG (LPM)	0.83	1.25	1.87	2.49	3.53	5.20	10.39	20.78	31.18	41.57
	JG(m/s)	**0.04**	**0.06**	**0.09**	**0.12**	**0.17**	**0.25**	**0.50**	**1.00**	**1.50**	**2.00**
QL (LPM)	JL (m/s)										
10.63	0.08	0.029	0.043	0.063	0.083	0.113	0.158	0.273	0.429	0.530	0.601
21.27	0.16	0.028	0.041	0.060	0.078	0.108	0.151	0.262	0.415	0.515	0.587
42.53	0.25	0.026	0.038	0.057	0.074	0.102	0.143	0.250	0.400	0.500	0.571
63.80	0.50	0.022	0.033	0.049	0.064	0.089	0.125	0.222	0.364	0.462	0.533
85.07	1.00	0.017	0.026	0.038	0.051	0.070	0.100	0.182	0.308	0.400	0.471

Table A2.1.3: Toshiba correlation void fraction measurement for 21.0-mm ID pipe

	QG (LPM)	0.83	1.25	1.87	2.49	3.53	5.20	10.39	20.78	31.18	41.57
	JG(m/s)	**0.04**	**0.06**	**0.09**	**0.12**	**0.17**	**0.25**	**0.50**	**1.00**	**1.50**	**2.00**
QL (LPM)	JL (m/s)										
10.63	0.08	0.069	0.100	0.142	0.180	0.236	0.310	0.465	0.619	0.696	0.742
21.27	0.16	0.060	0.087	0.125	0.159	0.211	0.280	0.430	0.587	0.669	0.719
42.53	0.25	0.052	0.076	0.110	0.141	0.188	0.253	0.397	0.556	0.641	0.694
63.80	0.50	0.039	0.057	0.083	0.107	0.145	0.198	0.327	0.483	0.575	0.635
85.07	1.00	0.025	0.038	0.055	0.072	0.099	0.139	0.242	0.383	0.476	0.542

Appendix 2.2

Void Fraction Measurement Using CECM for 47.0-mm ID Vertical Pipe

Table A2.2.1: Experimental void fraction measurement using CECM for 47.0-mm ID pipe

	QG (LPM)	4.16	6.25	10.41	12.49	17.70	26.03	41.64	52.06	114.52	229.04
	JG(m/s)	**0.04**	**0.06**	**0.10**	**0.12**	**0.17**	**0.25**	**0.40**	**0.50**	**1.10**	**2.20**
QL (LPM)	**JL (m/s)**										
10.63	**0.03**	0.025	0.027	0.041	0.068	0.090	0.191	0.226	0.347	0.375	0.438
21.27	**0.08**	0.019	0.026	0.034	0.064	0.079	0.151	0.185	0.266	0.299	0.390
42.53	**0.16**	0.017	0.022	0.030	0.055	0.078	0.143	0.162	0.251	0.274	0.359
63.80	**0.25**	0.013	0.019	0.026	0.049	0.065	0.087	0.146	0.175	0.188	0.237
85.07	**0.70**	0.009	0.012	0.023	0.024	0.024	0.044	0.092	0.110	0.154	0.191
106.34	**1.00**	0.009	0.011	0.020	0.022	0.023	0.029	0.049	0.071	0.133	0.164

Table A2.2.2: Bestion correlation void fraction measurement for 47.0-mm ID pipe

	QG (LPM)	4.16	6.25	10.41	12.49	17.70	26.03	41.64	52.06	114.52	229.04
	JG(m/s)	**0.04**	**0.06**	**0.10**	**0.12**	**0.17**	**0.25**	**0.40**	**0.50**	**1.10**	**2.20**
QL (LPM)	**JL (m/s)**										
10.63	**0.03**	0.021	0.031	0.050	0.059	0.082	0.116	0.174	0.208	0.367	0.537
21.27	**0.08**	0.020	0.030	0.049	0.058	0.080	0.114	0.170	0.204	0.361	0.530
42.53	**0.16**	0.019	0.029	0.047	0.056	0.077	0.110	0.165	0.198	0.351	0.520
63.80	**0.25**	0.019	0.028	0.045	0.054	0.074	0.105	0.159	0.191	0.342	0.509
85.07	**0.70**	0.015	0.023	0.037	0.045	0.062	0.089	0.135	0.163	0.300	0.461
106.34	**1.00**	0.014	0.020	0.034	0.040	0.056	0.080	0.122	0.148	0.277	0.434

Table A2.2.3: Toshiba correlation void fraction measurement for 47.0-mm ID pipe

	QG (LPM)	4.16	6.25	10.41	12.49	17.70	26.03	41.64	52.06	114.52	229.04
	JG(m/s)	**0.04**	**0.06**	**0.10**	**0.12**	**0.17**	**0.25**	**0.40**	**0.50**	**1.10**	**2.20**
QL (LPM)	JL (m/s)										
10.63	**0.03**	0.076	0.110	0.169	0.196	0.255	0.332	0.437	0.489	0.659	0.770
21.27	**0.08**	0.069	0.100	0.155	0.180	0.236	0.310	0.413	0.465	0.638	0.755
42.53	**0.16**	0.060	0.087	0.137	0.159	0.211	0.280	0.379	0.430	0.607	0.734
63.80	**0.25**	0.052	0.076	0.121	0.141	0.188	0.253	0.347	0.397	0.577	0.711
85.07	**0.70**	0.032	0.047	0.076	0.090	0.122	0.169	0.244	0.286	0.459	0.614
106.34	**1.00**	0.025	0.038	0.061	0.072	0.099	0.139	0.204	0.242	0.405	0.563

Appendix 2.3

Void Fraction Measurement Using CECM for 95.0-mm ID Vertical Pipe

Table A2.3.1: Experimental void fraction measurement using CECM for 95.0-mm ID pipe

	QG (LPM)	2.55	8.51	17.01	25.52	38.28	51.04	72.31	106.34	170.14	212.67
	JG(m/s)	**0.006**	**0.020**	**0.040**	**0.060**	**0.090**	**0.120**	**0.170**	**0.250**	**0.400**	**0.500**
QL (LPM)	JL (m/s)										
10.63	0.006	0.0457	0.0482	0.0537	0.0589	0.0787	0.1060	0.1120	0.1190	0.1340	0.1350
21.27	0.030	0.0418	0.0447	0.0532	0.0538	0.0643	0.1010	0.1100	0.1160	0.1170	0.1220
42.53	0.080	0.0283	0.0285	0.0455	0.0504	0.0635	0.0865	0.0936	0.1130	0.1140	0.1210
63.80	0.160	0.0142	0.0147	0.0292	0.0373	0.0575	0.0802	0.0890	0.1070	0.1130	0.1180
85.07	0.250	0.0080	0.0126	0.0246	0.0371	0.0488	0.0664	0.0591	0.0722	0.0866	0.0936

Table A2.3.2: Bestion correlation void fraction measurement for 95.0-mm ID pipe

	QG (LPM)	2.55	8.51	17.01	25.52	38.28	51.04	72.31	106.34	170.14	212.67
	JG(m/s)	**0.006**	**0.020**	**0.040**	**0.060**	**0.090**	**0.120**	**0.170**	**0.250**	**0.400**	**0.500**
QL (LPM)	JL (m/s)										
10.63	0.006	0.0023	0.0075	0.0148	0.0221	0.0328	0.0432	0.0602	0.0860	0.1309	0.1584
21.27	0.030	0.0022	0.0074	0.0147	0.0219	0.0325	0.0429	0.0596	0.0853	0.1299	0.1572
42.53	0.080	0.0022	0.0073	0.0144	0.0215	0.0319	0.0421	0.0586	0.0839	0.1278	0.1548
63.80	0.160	0.0021	0.0071	0.0140	0.0209	0.0310	0.0410	0.0570	0.0817	0.1246	0.1511
85.07	0.250	0.0021	0.0068	0.0136	0.0203	0.0301	0.0397	0.0554	0.0794	0.1212	0.1471

Table A2.3.3: Toshiba correlation void fraction measurement for 95.0-mm ID pipe

	QG (LPM)	2.55	8.51	17.01	25.52	38.28	51.04	72.31	106.34	170.14	212.67
	JG(m/s)	**0.006**	**0.020**	**0.040**	**0.060**	**0.090**	**0.120**	**0.170**	**0.250**	**0.400**	**0.500**
QL (LPM)	JL (m/s)										
10.63	0.006	0.0130	0.0418	0.0801	0.1151	0.1625	0.2048	0.2656	0.3441	0.4502	0.5018
21.27	0.030	0.0123	0.0397	0.0761	0.1096	0.1553	0.1961	0.2553	0.3323	0.4374	0.4890
42.53	0.080	0.0111	0.0358	0.0690	0.0998	0.1420	0.1802	0.2361	0.3100	0.4131	0.4645
63.80	0.160	0.0095	0.0310	0.0601	0.0873	0.1250	0.1595	0.2108	0.2800	0.3792	0.4300
85.07	0.250	0.0083	0.0270	0.0524	0.0765	0.1101	0.1412	0.1881	0.2525	0.3472	0.3968

Appendix 2.4

Void Fraction Measurement Using CECM for 21.0-mm ID Horizontal Pipe

Table A2.4.1: Experimental void fraction measurement using CECM for 21.0-mm ID pipe

	QG (LPM)	1.04	2.08	4.16	8.31	12.47	16.63	20.78	24.94	29.10	33.26	37.412	41.569	45.726	49.882
	JG(m/s)	0.05	0.10	0.20	0.40	0.60	0.80	1.00	1.20	1.40	1.60	1.80	2.00	2.20	2.40
QL (LPM)	JL (m/s)														
1.039	0.05	0.330	0.359	0.384	0.401	0.407	0.476	0.485	0.500	0.527	0.541	0.543	0.548	0.551	0.571
2.078	0.10	0.300	0.334	0.352	0.355	0.380	0.414	0.455	0.470	0.471	0.493	0.497	0.500	0.507	0.515
8.314	0.40	0.250	0.277	0.296	0.318	0.329	0.343	0.352	0.365	0.385	0.395	0.404	0.435	0.424	0.461
16.627	0.80	0.231	0.244	0.273	0.289	0.328	0.335	0.351	0.355	0.374	0.393	0.402	0.415	0.411	0.426
24.941	1.20	0.222	0.236	0.262	0.280	0.312	0.327	0.346	0.354	0.369	0.385	0.401	0.405	0.408	0.419
33.255	1.60	0.212	0.227	0.233	0.283	0.309	0.325	0.345	0.354	0.362	0.376	0.379	0.390	0.391	0.414
41.569	2.00	0.205	0.223	0.232	0.266	0.298	0.322	0.341	0.354	0.361	0.370	0.378	0.382	0.382	0.393

Table A2.4.2: Bestion correlation void fraction measurement for 21.0-mm ID pipe

	QG (LPM)	1.04	2.08	4.16	8.31	12.47	16.63	20.78	24.94	29.10	33.26	37.412	41.569	45.726	49.882
	JG(m/s)	0.05	0.10	0.20	0.40	0.60	0.80	1.00	1.20	1.40	1.60	1.80	2.00	2.20	2.40
QL (LPM)	JL (m/s)														
1.039	0.05	0.037	0.071	0.133	0.235	0.316	0.381	0.435	0.480	0.519	0.552	0.581	0.606	0.629	0.649
2.078	0.10	0.036	0.069	0.129	0.229	0.308	0.372	0.426	0.471	0.509	0.542	0.571	0.597	0.620	0.640
8.314	0.40	0.029	0.057	0.108	0.195	0.267	0.327	0.377	0.421	0.459	0.492	0.522	0.548	0.571	0.593
16.627	0.80	0.024	0.047	0.089	0.163	0.226	0.281	0.328	0.369	0.406	0.438	0.468	0.494	0.518	0.539
24.941	1.20	0.020	0.039	0.075	0.140	0.197	0.246	0.290	0.329	0.364	0.395	0.424	0.449	0.473	0.495
33.255	1.60	0.017	0.034	0.066	0.123	0.174	0.219	0.260	0.296	0.329	0.360	0.387	0.412	0.436	0.457
41.569	2.00	0.015	0.030	0.058	0.110	0.156	0.198	0.235	0.270	0.301	0.330	0.356	0.381	0.404	0.425

Table A2.4.3: Toshiba correlation void fraction measurement for 21.0-mm ID pipe

	QG (LPM)	1.04	2.08	4.16	8.31	12.47	16.63	20.78	24.94	29.10	33.26	37.412	41.569	45.726	49.882
	JG(m/s)	0.05	0.10	0.20	0.40	0.60	0.80	1.00	1.20	1.40	1.60	1.80	2.00	2.20	2.40
QL (LPM)	JL (m/s)														
1.039	0.05	0.090	0.163	0.278	0.427	0.521	0.585	0.631	0.667	0.694	0.717	0.735	0.751	0.764	0.775
2.078	0.10	0.082	0.150	0.258	0.404	0.498	0.563	0.611	0.647	0.676	0.700	0.719	0.736	0.750	0.762
8.314	0.40	0.053	0.101	0.182	0.304	0.392	0.458	0.510	0.551	0.585	0.613	0.637	0.657	0.675	0.691
16.627	0.80	0.037	0.070	0.131	0.229	0.306	0.367	0.418	0.460	0.495	0.526	0.552	0.576	0.596	0.614
24.941	1.20	0.028	0.054	0.102	0.184	0.251	0.307	0.354	0.394	0.430	0.461	0.488	0.512	0.534	0.553
33.255	1.60	0.022	0.044	0.084	0.153	0.212	0.263	0.307	0.345	0.379	0.410	0.437	0.461	0.483	0.503
41.569	2.00	0.019	0.037	0.071	0.131	0.184	0.230	0.271	0.307	0.340	0.369	0.395	0.419	0.441	0.461

Appendix 2.5

Void Fraction Measurement Using CECM for 47.0-mm ID Horizontal Pipe

Table A2.5.1: Experimental void fraction measurement using CECM for 47.0-mm ID pipe

	QG (LPM)	5.206	10.411	20.822	41.644	62.466	83.288	104.11	124.932	145.754	166.576	187.398	208.22
	JG(m/s)	0.05	0.10	0.20	0.40	0.60	0.80	1.00	1.20	1.40	1.60	1.80	2.00
QL (LPM)	JL (m/s)												
5.205509	0.05	0.435	0.440	0.526	0.537	0.548	0.552	0.560	0.608	0.637	0.647	0.655	0.701
10.41102	0.10	0.403	0.422	0.454	0.513	0.514	0.527	0.530	0.608	0.632	0.644	0.648	0.696
41.64407	0.40	0.296	0.318	0.325	0.366	0.415	0.440	0.502	0.545	0.579	0.602	0.631	0.686
83.28814	0.80	0.125	0.165	0.172	0.181	0.188	0.210	0.220	0.257	0.255	0.257	0.295	0.358
124.9322	1.20	0.101	0.135	0.156	0.156	0.167	0.194	0.198	0.229	0.232	0.241	0.262	0.292
166.5763	1.60	0.088	0.116	0.141	0.151	0.154	0.184	0.213	0.206	0.213	0.238	0.242	0.248

Table A2.5.2: Bestion correlation void fraction measurement for 47.0-mm ID pipe

	QG (LPM)	5.206	10.411	20.822	41.644	62.466	83.288	104.11	124.932	145.754	166.576	187.398	208.22
	JG(m/s)	0.05	0.10	0.20	0.40	0.60	0.80	1.00	1.20	1.40	1.60	1.80	2.00
QL (LPM)	JL (m/s)												
5.205509	0.05	0.025	0.050	0.094	0.172	0.238	0.294	0.342	0.385	0.422	0.455	0.484	0.510
10.41102	0.10	0.025	0.048	0.092	0.169	0.233	0.289	0.337	0.379	0.415	0.448	0.477	0.504
41.64407	0.40	0.022	0.042	0.081	0.150	0.209	0.261	0.306	0.346	0.381	0.413	0.442	0.468
83.28814	0.80	0.018	0.036	0.070	0.130	0.183	0.231	0.272	0.310	0.344	0.375	0.403	0.428
124.9322	1.20	0.016	0.032	0.061	0.115	0.163	0.207	0.246	0.281	0.313	0.343	0.370	0.394
166.5763	1.60	0.014	0.028	0.054	0.103	0.147	0.187	0.224	0.257	0.287	0.316	0.342	0.366

Table A2.5.3: Toshiba correlation void fraction measurement for 47.0-mm ID pipe

	QG (LPM)	5.206	10.411	20.822	41.644	62.466	83.288	104.11	124.932	145.754	166.576	187.398	208.22
	JG(m/s)	0.05	0.10	0.20	0.40	0.60	0.80	1.00	1.20	1.40	1.60	1.80	2.00
QL (LPM)	JL (m/s)												
5.205509	0.05	0.090	0.163	0.278	0.427	0.521	0.585	0.631	0.667	0.694	0.717	0.735	0.751
10.41102	0.10	0.082	0.150	0.258	0.404	0.498	0.563	0.611	0.647	0.676	0.700	0.719	0.736
41.64407	0.40	0.053	0.101	0.182	0.304	0.392	0.458	0.510	0.551	0.585	0.613	0.637	0.657
83.28814	0.80	0.037	0.070	0.131	0.229	0.306	0.367	0.418	0.460	0.495	0.526	0.552	0.576
124.9322	1.20	0.028	0.054	0.102	0.184	0.251	0.307	0.354	0.394	0.430	0.461	0.488	0.512
166.5763	1.60	0.022	0.044	0.084	0.153	0.212	0.263	0.307	0.345	0.379	0.410	0.437	0.461

Appendix 2.6

Void Fraction Measurement Using CECM for 95.0-mm ID Horizontal Pipe

Table A2.6.1: Experimental void fraction measurement using CECM for 95.0-mm ID pipe

	QG (LPM)	10.634	21.267	42.535	63.802	85.07	106.337	127.604	148.872	170.139	191.407	212.674
	JG(m/s)	0.03	0.05	0.10	0.15	0.20	0.25	0.30	0.35	0.40	0.45	0.50
QL (LPM)	JL (m/s)											
21.2674	0.05	0.357	0.363	0.364	0.369	0.369	0.370	0.371	0.372	0.372	0.373	0.379
42.53483	0.10	0.354	0.360	0.363	0.363	0.364	0.365	0.367	0.367	0.368	0.368	0.370
85.06965	0.20	0.357	0.358	0.362	0.362	0.362	0.363	0.365	0.367	0.367	0.370	0.371
127.6045	0.30	0.357	0.362	0.362	0.364	0.366	0.370	0.372	0.373	0.374	0.376	0.382
170.1393	0.40	0.347	0.349	0.355	0.360	0.362	0.365	0.366	0.366	0.367	0.370	0.371

Table A2.6.2: Bestion correlation void fraction measurement for 95.0-mm ID pipe

	QG (LPM)	10.634	21.267	42.535	63.802	85.07	106.337	127.604	148.872	170.139	191.407	212.674
	JG(m/s)	0.03	0.05	0.10	0.15	0.20	0.25	0.30	0.35	0.40	0.45	0.50
QL (LPM)	JL (m/s)											
21.2674	0.05	0.009	0.018	0.036	0.053	0.069	0.085	0.100	0.115	0.129	0.143	0.156
42.53483	0.10	0.009	0.018	0.035	0.052	0.068	0.083	0.098	0.113	0.127	0.141	0.154
85.06965	0.20	0.009	0.017	0.034	0.050	0.066	0.081	0.095	0.109	0.123	0.136	0.149
127.6045	0.30	0.008	0.017	0.033	0.048	0.063	0.078	0.092	0.106	0.119	0.132	0.145
170.1393	0.40	0.008	0.016	0.032	0.047	0.062	0.076	0.090	0.103	0.116	0.129	0.141

Table A2.6.3: Toshiba correlation void fraction measurement for 95.0-mm ID pipe

	QG (LPM)	10.634	21.267	42.535	63.802	85.07	106.337	127.604	148.872	170.139	191.407	212.674
	JG(m/s)	0.03	0.05	0.10	0.15	0.20	0.25	0.30	0.35	0.40	0.45	0.50
QL (LPM)	JL (m/s)											
21.2674	0.05	0.047	0.090	0.163	0.225	0.278	0.323	0.362	0.397	0.427	0.455	0.479
42.53483	0.10	0.043	0.082	0.150	0.208	0.258	0.302	0.340	0.374	0.404	0.431	0.455
85.06965	0.20	0.036	0.069	0.129	0.181	0.227	0.267	0.303	0.335	0.364	0.391	0.415
127.6045	0.30	0.031	0.060	0.113	0.160	0.202	0.239	0.273	0.304	0.332	0.357	0.381
170.1393	0.40	0.028	0.053	0.101	0.144	0.182	0.217	0.249	0.278	0.304	0.329	0.352

List of Publication

1. M.A. Zubir and M.Z. Zainon (2011). Two-Phase Flow Behaviour and Pattern in Vertical Pipes. *Journal of Applied Sciences*, 11(9), 1491-1500.